EPA 600/7-87-008

NTIS PB 87-165270

EVALUATION OF RETORTED OIL SHALE AS A LINER MATERIAL FOR RETORTED SHALE DISPOSAL SITES

By

William J. Culbertson, Jr.
Charles H. Habenicht
James D. Mote
Denver Research Institute
Chemical and Materials Sciences Division
University of Denver
Denver, CO 80208

Cooperative Agreement CR-809233

Project Officer

Edward R. Bates
Air and Energy Engineering Research Laboratory
U.S. Environmental Protection Agency
Research Triangle Park, NC 27711

Prepared for

U.S. Environmental Protection Agency
Office of Research and Development
Washington, DC 20460

NOTICE

The information in this document has been funded wholly or in part by the United States Environmental Protection Agency under Cooperative Agreement CR-809233 to the Denver Research Institute. It has been subject to the Agency's peer and administrative review, and it has been approved for publication as an EPA document.

Mention of trade names or commercial products does not constitute endorsement or recommendation for use.

ABSTRACT

This study has considered the possibility of using a spent oil shale itself as a water barrier or "liner" beneath a spent oil shale waste embankment. Pertinent properties of unburned TOSCO II spent shale and an average mixture of Lurgi spent shale have been measured. Materials consisting of 1, 20, and 30% burned spent Tosco shale admixed into unburned TOSCO II shale have also been considered. Two autoclave mellowed materials admixed into their respective unmellowed spent shales have also been studied.

This work indicates the difficulty of having both easy self healing and low permeability of the unmellowed Tosco materials and mixtures thereof, as well as perhaps the unmellowed Lurgi spent shale. Autoclave mellowing of the burned Tosco material, however, produced a high plasticity index material that may be blended with the silty unburned TOSCO II spent shale to produce a liner having (at least in the short term) both low permeability and good self healing possibilities. A similar attempt with the Lurgi spent shale was not successful due to the high permeability produced in the short term aging experiment.

CONTENTS

		Page
ABSTRACT		iii
LIST OF FIGURES		vi
LIST OF TABLES		xi
SYMBOLS AND ABBREVIATIONS		xii
ACKNOWLEDGEMENTS		xiv
I.	SUMMARY	1
II.	INTRODUCTION AND SCOPE	3
	A. Object	3
	B. Approach	4
	C. Experimental Plan and Independent Variables Used	6
III.	NATURE OF SPENT SHALES USED AND MATERIALS PREPARATION	9
	A. Lurgi, TOSCO II, Spent Shale	9
	B. TOSCO II Spent Shale	9
	C. Burned TOSCO Spent Shale	13
	D. Autoclave Mellowed Burned Tosco Spent Shale	13
	E. Autoclave Mellowed Lurgi Spent Shales	16
	F. Compaction Curves of Starting Mixtures for Spring Oedometers, Brazil Tests and Pneumatic Arm Oedometers	16
	G. Atterberg Limits of Mixtures	19
IV.	APPARATUS AND PROCEDURES	24
	A. Compaction of Specimens in Spring Oedometers and Measurement of Apparent Dry Density	24
	B. Curing and Consolidation in Spring Oedometers and Consolidation Curves	25
	C. Permeability Measurement	25
	D. Torsion Triaxial Machine and Shear Strength Measurement	25
	1. Neutralizing Sample Disturbance by Testing Sample of Known Overconsolidation Ratio and Use of SHANSEP	26
	2. Handling of Cemented Clay (or Spent Oil Shale) in the Same Torsion Triaxial Apparatus as Designed for Soft Clay (or Spent Oil Shale)	27
	3. Advantages of Torsion Shear Strength Over Compressive Triaxial Shear Strength for Study of Cemented and Uncemented Clay-like Spent Oil Shale	29
	4. Data from Torsion Stress Strain Surve	29
	5. Handling Vertical Pressure in Torsion Test	30
	6. Advantages of Membrane Walled Specimen for Torsion Shear Test	32
	E. Drying Oven	32

F. EGA Apparatus for Hydrate Water Determination. 32
G. X-ray Diffractometer 33
H. Brazil Tensile Strength Test 35
I. Pneumatic Loaded Arm Oedometers for Compressibility Coefficient 37

V. RESULTS. 40
A. Results from Compacted Cured Permeatee and Torsion Sheared Specimens of the Spring Oedometers. 40
1. Initial Apparent Dry Density 40
2. Mineral Grain Density of Cured Specimens 49
3. Cured Specimen Void Ratio 49
4. Secondary Compression Index 49
5. Permeability Coefficient 49
6. Shear Modulus During Torsion 49
7. Peak Shear Strength 49
8. Residual Shear Strength. 51
9. Brittleness Index 51
10. Photographs of Sheared Specimens. 54
11. EGA Determined Hydrate Water 54
B. Brazil Test Results 55
C. Pneumatic Arm Oedometer Compressibility Coefficients . . 55

VI. DISCUSSION OF RESULTS 100
A. Permeability. 100
B. Peak Angle of Internal Friction O_p Related to Self Healing and Its Trade Off with Permeability. 105
C. Residual Shear Strength and Critical Void Ratio Related to Slope Stability 111
D. Brittleness Index Related to Cementation and Permeability. 112
E. Relation of Peak Friction Angle O_p and Brittleness Index BI with Initial Torsional Stiffness and Shear Modulus G. 114
F. Relation of Peak Friction Angle with Twist at Peak Strength 117
G. Relation of Peak Friction Angle and Squashiness Index with Cured Void Ratio, ... 117
H. Hydrate Species Determined by EGA. 117
I. Secondary Compression Index C Related to Cementation and Mellowing 122
J. Indirect Tensile Strength (Brazilian) Test. 124
K. Compression Index 127

VII. CONCLUSIONS AND RECOMMENDATIONS 130

VIII. Quality Assurance and Quality Control 132

IX. REFERENCES 135

LIST OF FIGURES

		Page
III 1.	Particles Through 325 Mesh Sieve as a Function of Mineral Carbon Left in Spent Shale.	12
III 2.	X-ray Diffraction Intensities of Dolomite Relative to Albite as Function of Mineral Carbon Found by Calcimeter for Lurgi Spent Shales.	12
III 3.	X-ray Diffraction Intensities Relative to Quartz of Gehienite, Stevensite, Ettringite, and Gypsum and/or Other Species as Function of Autoclaving Pressure for Burned TOSCO Spent Shale	14
III 4.	EGA Ettringite Peak Height: Thermal Conductivity Detector Recorder Trace as Function of Autoclaving Pressure for Burned TOSCO Spent Shale	14
III 5.	Clay Size Fines of Autoclave Mellowed Burned TOSCO Spent Shale as Function of Autoclave Pressure.	15
III 6.	Plasticity Index of Autoclave Mellowed Burned TOSCO Spent Shale as Function of Autoclave Pressure.	15
III 7.	Miniature Compaction Curves for TOSCO II Spent Shale	18
III 8.	Four Inch Mold Compaction Data for TOSCO II Spent Shale. . . .	18
III 9.	Summary of Optimum Moisture Needed to be Added and Wet of Optimum Moisture Needed to be Added to Mixtures of TOSCO II Spent Shale with 10%, 20%, and 30% Contents of Burned TOSCO Spent Shale.	20
III 10.	Disappearance of Water Due to Hydrate Formation for 50% Burned TOSCO Spent Shale With 50% TOSCO II Spent Shale and 100% Burned TOSCO Spent Shale.	20
III 11.	Compaction Curves For Average Lurgi Spent Shale, 30-60 Minutes after Mixing	21
III 12.	Water Disappearance in Average Lurgi Spent Shale	21
III 13.	Compaction Curves for Mixtures of Mellowed and Unmellowed Lurgi Spent Shale	21
III 14.	Compaction Curves for Mixtures of Mellowed Burned TOSCO with Burned TOSCO and Unburned TOSCO II Spent Shale	22
III 15.	Atterberg Limits of Burned TOSCO - TOSCO II Spent Shale Mixtures.	22
IV 1.	Apparatus for Transference of Spring Oedometer Consolidated Specimens to Triaxial Torsion Machine.	28

IV 2. EGA Trace of Blended Mellowed and Unmellowed Burned TOSCO Spent Shale, M4 + TA. 34

V 1. Some Secondary Compression Curves of Spring Oedometer Specimens 50

V 2. Some Torsion Stress-Strain Curves Loadings 32, 33, 42, 64, 92 53

V 3. Torsioned Specimen of Oedometer Loading 33, A Non Brittle Material. 63

V 4. Torsioned Specimen of Loading 64, A Mildly Cemented Specimen. 63

V 5. Torsioned Specimen of Loading 42, A More Strongly Cemented Specimen 64

V 6. Torsioned Specimen of Loading 92, A rather Impermeable Little Cemented Specimen. 64

V 7. Torsioned Specimen of Loading 32, A Low Brittleness Material Showing Shear Plane. 65

V 8. EGA of Loading 30 66

V 9. EGA of Loading 31 67

V 10. EGA of Loading 32 68

V 11. EGA of Loading 33 69

V 12. EGA of Loading 35 70

V 13. EGA of Loading 39 71

V 14. EGA of Loading 40 72

V 15. EGA of Loading 42 73

V 16. EGA of Loading 43 74

V 17. EGA of Loading 46 75

V 18. EGA of Loading 47 76

V 19. EGA of Loading 48 77

V 20. EGA of Loading 49 78

V 21. EGA of Loading 53 79

V 22. EGA of Loading 56 80

V 23. EGA of Loading 57 81

V 24. EGA of Loading 58 82

V 25. EGA of Loading 59 83

V 26. EGA of Loading 62 84

V 27. EGA of Loading 68 85

V 28. EGA of Loading 86 86

V 29. EGA of Loading 88 87

V 30. EGA of Loading 90 88

V 31. EGA of Loading 91 89

V 32. EGA of Loading 92 90

V 33. EGA of Loading 96 91

V 34. EGA of Loading 98 92

V 35. EGA of Loading 100. 93

V 36. EGA of Loading 104. 94

V 37 EGA of Mellowed Lurgi, Run M14. 95

V 38. EGA of Autoclave Mellowed Burned TOSCO Run M 15 96

V 39. EGA of Average Unwetted Lurgi 97

V 40. EGA of Unwetted Burned TOSCO II 98

V 41. EGA of Unwetted Unburned TOSCO II 99

VI 1. Permeability of Mixtures of Burned TOSCO and Unburned TOSCO Spent Shale after Approximately Four Weeks Curing in Spring Oedometers 101

VI 2. Permeability of 100% TOSCO II Spent Shale (TOSCO 100) . . . 102

VI 3. Permeability of 90% TOSCO II - 10% Burned TOSCO Spent Shale (TOSCO 90). 102

VI 4. Permeability of 80% TOSCO II - 20% Burned TOSCO Spent Shale (TOSCO 80). 103

VI 5. Permeability of 70% TOSCO II - 30% Burned TOSCO Spent Shale (TOSCO 70). 103

VI 6. Permeability of Lurgi Spent Shale 103

VI 7. Permeability of Mellowed Lurgi (M14) mixed into Lurgi and Mellowed Burned TOSCO (M-15) Mixed into TOSCO II and into Burned TOSCO Spent Shale. 104

VI 8. Mineral Grain Density vs Time for TOSCO 100 Spent Shale . . 106

VI 9. Mineral Grain Density vs time for TOSCO 90 Spent Shale. . . 106

VI 10. Mineral Grain Density vs Time for TOSCO 80 Spent Shale. . . 107

VI 11. Mineral Grain Density vs Time for TOSCO 70 Spent Shale. . . 107

VI 12. Mineral Grain Density vs time for Lurgi Spent Shale 108

VI 13. Permeability of Spent Shales Correlated with Void Ratio . . 109

VI 14. Permeability Of TOSCO Spent Shale Mixtures Correlated with Peak Friction Angle. 110

VI 15. Permeability of Lurgi Spent Shale Correlated with Peak Friction Angle 110

VI 16. Brittleness Index Correlated with Peak Friction Angle . . . 113

VI 17. Permeability Compared with Brittleness Index. 115

VI 18. Peak Friction Angle Compared with Initial Shear Modulus G 116

VI 19. Brittleness Index Compared with Initial Shear Modulus G 118

VI 20. Extent of Twist at Peak Strength Correlated with Peak Friction Angle. 119

VI 21. Peak Friction Angle of TOSCO 100 vs Void Ratio. 120

VI 22. Peak Friction Angle of TOSCO 90 vs Void Ratio 120

VI 23. Peak Friction Angle of TOSCO 80 vs Void Ratio 120

VI 24. Peak Friction Angle of TOSCO 70 vs Void Ratio 120

VI 25. EGA Hydrate Water Peak of Tobermorite and Ettringite vs Time for TOSCO 100, 90, and 70 Specimens 121

VI 26. Peak Friction Angle vs Time for TOSCO 100, 90, and 70 Specimens 121

VI 27. Initial Torsional Stiffness vs 115 to 135°C EGA Peak Height 123

VI 28. Twist at Peak Strength vs 115 to 135°C EGA Peak Height. . . 123

VI 29. Final C_α at 45° Peak Friction Angle for Oedometer Specimens of Various Spent Shale Mixtures 125

VI 30. Final C_α vs Peak Friction Angle for TOSCO 100 Specimens . . 125

VI 31. Final C_α vs Peak Friction Angle for TOSCO 90 Specimens. . . 125

VI 32. Final C_α vs Peak Friction Angle for TOSCO 80 Specimens. . . 125

VI 33. Final C_α vs Peak Friction Angle for TOSCO 70 Specimens. . . 125

VI 34. Final C_α vs Peak Friction Angle for Lurgi Specimens 125

VI 35. Torsion Test Twist at Peak Strength vs Brazil Tensile Strength. 126

VI 36. Brazil Tensile Strain At Failure vs Torsion Test Twist at Peak Strength. 126

VI 37. Brazil Tensile Strength vs Initial Water Content. 129

VI 38. Compression Index of Fresh Specimens for Loading Increment 155 to 310 PSI. 129

LIST OF TABLES

		Page
II 1.	Experimental Design - TOSCO II. Lurgi, and Mixtures of Mellowed TOSCO and Mellowed Lurgi with Burned and Unburned TOSCO and Unmellowed Lurgi Spent Shale.	8
III 1.	Sieve Analyses of Lurgi and Burned TOSCO Spent Shale.	10
III 2.	Calcimeter Determined Mineral Carbon In Spent Shales Collected.	11
V 1.	K_o Consolidation in Spring Oedometer.	41
V 2.	Starting Materials, Permeability from "In Situ" Spring Oedometer Specimens, and Results from Torsion Tests	43
V 3.	Summary of Brazil Tensile Strength Tests	56
V 4.	Pneumatic Arm Oedometer Results From Fresh Specimens: Void Ratios e and Compression Indices C_c	59
VIII 1.	Quality Assurance Objectives and Performance	134

SYMBOLS AND ABBREVIATIONS

The following symbols have been used in this report.

TA	Fluidized bed burned TOSCO II spent shale from TOSCO Rocky Flats site (from drum number TA).
TOS100 100 TOSCO II	Unburned TOSCO scalped retorted spent shale from a pilot size TOSCO 100%II retort at the TOSCO Rock Flats site.
TOS90 TOSCO 90	A mixture of 90% unburned TOSCO II spent shale with 10% of burned spent shale from a pilot size fluidized bed burner fed TOSCO II spent shale at the TOSCO Rocky Flats site.
TOS80 TOSCO 80	A mixture of 80% unburned TOSCO II spent shale with 20% of the burned spent shale.
TOS70 TOSCO 70	A mixture of 70% unburned TOSCO II spent shale with 30% of the burned spent shale.
MEL	Signified autoclave mellowed material.
△	Triangle data points on graphs are usually for standard proctor specimens.
□	Square data points on graphs are usually for modified proctor specimens.
51	Number by data point on graph signifies oedometer loading number of specimen tested.
24%	Percentage figure by data point on graph signifies percent water dry basis added to spent shale mix before loading oedometer.
psi	Pounds per square inch
Gm or g	Grams mass
cc	Cubic centimeters
lb	Pounds
EGA	Evolved gas analysis
e	Void ratio
°F	Degrees Fahrenheit [°C=5/9(°F-32)]
in.	Inches (1 in.= 2.54 cm)

lbs/Ft^3	Pounds per cubic Foot (1 lb/Ft^3=16.02 Kg/m^3)
in. lbs	Inch pounds (1 in. lb = 1.15 cm Kg)
micron	1 micron = 1 x 10^{-6} meters
C_α	Secondary compression index = $\frac{e}{\log t}$ = slope of void ratio vs logarithm of time plot of secondary compression.
	Normal stress = stress normal to shear plane
σ_v	Vertical stress.
σ_v'	Effective vertical stress = vertical stress less any pore water pressure. Important to the mechanics of the soil skeleton.
τ	Shear stress
τ_p	Peak or failure shear stress
τ_R	Residual shear stress
ϕ_P, ϕ_P'	Angle of internal friction (or friction angle) at peak shear strength - particularly useful for noncohesive or silty soil. ϕ_P = arctan τ/σ.
ϕ_R, ϕ_R'	Same as above but for residual strength.
BI	Brittleness index = $\frac{\tau_P - \tau_R}{\tau_P}$
PL	Plastic limit, % water dry basis
LL	Liquid limit, % water dry basis
PI	Plasticity index = LL - PL
CSH I	One type of tobermorite, CaO SiO_2.nH_2O using cement chemists terminology
K_o	Earth pressure or confining pressure exerted on a specimen buried at depth

Acknowledgments

The following people have contributed particularly to this work:

Russell Nye, Senior Research Technician, DRI
Michael Shaffron, DRI, For Consolidation Data Reduction
Lindsay Patten, Student Chemist, Univ. of Denver
Penny Hudson, Mineralogist, DRI
Dr. Paul Predecki, Some of the X-ray Diffraction, DRI
Dr. Ed Eimutis, Monsanto Research Corp., For aid in Experimental Design
Craig Ruff, Student, University of Denver, X-ray diffraction data display computer programs

I. SUMMARY

This study has considered the possibility of using a spent oil shale itself as a water barrier or "liner" beneath a spent oil shale waste embankment. Pertinent properties of unburned TOSCO II spent shale and an average mixture of Lurgi spent shale have been measured. Materials consisting of 10, 20, and 30% burned spent Tosco shale admixed into unburned Tosco II shale have also been considered. Two autoclave mellowed materials admixed into their respective unmellowed spent shales have also been studied.

This work indicates difficulty of having both easy self healing and low permeability of the unmellowed Tosco materials and mixtures and perhaps also of the unmellowed Lurgi spent shale. Autoclave mellowing of the burned Tosco material, however produced a high plasticity index material that may be blended with the silty unburned TOSCO II spent shale to produce a liner having (at least in the short term) both low permeability and good self healing possibilities. A similar attempt with the Lurgi spent shale was not successful due to the high permeability produced in the short term aging experiments.

The well mixed moistened spent shale batches were compacted by a miniature proctor system to either standard or modified proctor and consolidated under a spring force equivalent to around 280 pounds per square inch vertical pressure. Data for secondary consolidation curves were obtained during curing of the specimens until they were tested (still under the same 280 psi vertical soil skeleton pressure) for permeability under a water pressure of usually 20 psi. Lower water pressures were found to sometimes give unusually low permeation rates or erratic rates. This may have been due to the "oily" hydrophobic nature of some specimens. At 20 psi hydraulic pressure permeabilities seemed internally consistent with each other. Some specimens were not subjected to water permeation for comparison with permeated ones in later shear strength testing.

All specimens were transferred from their individual spring oedometers to a triaxial confining water pressure apparatus in a way to minimize disturbance causing overconsolidation or breaking the bond between specimen and porestones and vanes. After the transfer each one inch high 2½ inch diameter specimen was retained between drained pore stones and its cylindrical surface was covered by a thick gum rubber membrane. Brass vanes embedded in the pore stones aided torsioning the specimen for obtaining peak shear strength "residual" shear strength, initial stiffness, and twist to peak strength. Torsion testing was selected rather than the more usual compressive triaxial test as it allows a long slip displacement to develop which is needed for measurement of residual strength. This is not possible in the triaxial test which is sometimes supplemented by the tedious ring shear torsion test to obtain residual strength. Moreover ring shear would be quite difficult as part of the in-situ like testing program here developed.

Availability of the peak and "residual strength" of a specimen allowed computation of a brittleness index. Since the normal or vertical pressure on the ends of the specimen is known (in some tests this was made equal during torsioning to the prior consolidation pressure) angles of internal friction for peak and residual strengths corresponding to the high overburden load of around 280 psi were calculated.

The specimens from simple mixtures for the most part were of silty nature and sometimes cemented as well. The high drainage rate of the silty specimens allowed use of the internal friction concept. Some more unusual mixtures were more clayish and corresponded to boulder clay in having a low brittleness index and high strength, as well as low permeability. Cemented specimens often had low permeability but produced high peak shear strengths and a high brittleness index. Very little cementation is believed to prevent rapid self healing if a tension crack were to occur. Long term creep closure of a crack has not been directly studied but comparison of secondary consolidation rates suggests creep is also inhibited by cementation.

In general the strengths of the specimens were little affected by water permeation during permeability measurements before torsion testing although the brittleness index of some was reduced.

The course of generation of cementing hydrates in TOSCO spent shale with various fractions of burned TOSCO spent shale showed a maximum in hydrate water at around 30 days curing.

II. INTRODUCTION AND SCOPE

A. Object

This work was undertaken to survey the possibility of use of spent oil shale itself in constructing a deeply buried liner below embankments of spent oil shale. Some possible modification of these spent oil shales were to be tried including the admixing of autoclave mellowed burned spent oil shale with the hope of reducing the cementation tendencies of otherwise rather fine grained material, sometimes of low emplaced permeability, and of reducing the permeability due to hydrothermal generation of clay like species. In general a material was sought which had much of the frictional characteristics and volume stability of silt but the impermeability of clay without a tendency for eventual cementation on the one hand or leachability and partial soil skeleton loss on the other.

One of the important needs of a spent oil shale based "clay" liner is low permeability. Perhaps the next most important is self healing ability if it risks being cracked through subsidence below or geologic faulting. A disadvantage of high strength soil such as can be achieved by cementation, dehydration or compaction is that, "once ruptured, the structure does not readily, if at all, reform. Weak bonds possess a certain capacity for self healing. . ." (Ingles 1968). A third requirement is volume stability or resistance to swelling and shrinking.

The present study has mostly been concerned with 100% standard and 100% modified proctor compacted specimens of spent oil shale although static compaction of some TOSCO II and Lurgi material to some 280 psi was done during torsion shear strength apparatus "shake down." The specimens have often seemed too brittle for good self healing due to high compaction and/or cementation. Their volume stability to consolidation under 280 psi pressure has been good, however.

Any detrimental effect of drying on the spent oil shale liner materials is presently speculation. There seems to be little shrinkage, in general, but the effect on permeability and self healing capability when re-wetted is unknown. The self healing capability while still dry is perhaps nill for some of the more cemented materials but lesser cemented materials such as TOSCO II material may show some ability to flow into tension cracks while dry under say 300 psi overburden vertical pressure.

Fortunately the underground environment of the liner will probably be moist on the country rock side of the liner and can be made moist on the spent shale embankment side.

An important possible hazard to be considered is that of increased pore water pressure in loosely compacted somewhat saturated liner due to shearing, chemical defloculation due to permeate composition, or earthquake liquification. In a <u>too</u> impermeable liner, an increase in pore water pressure may not dissipate rapidly enough so that shear strength would drop due to reduced friction between soil skeleton particles as the effective normal stress is lowered. The liner might then become more like a grease than a liner allowing a spent shale embankment to slide.

Some specimens of the present study have been proctor hammer compacted so well that they apparently begin on the dense side of the critical volume line so they generally dilate at the beginning of shear. This should reduce pore pressure rather than increase it as shear occurs. Standard proctor TOSCO II spent shale cured for a short time shows no peak in the stress/strain curve and must begin above the critical volume line and although probably self healing to some degree might, in spite of its silty nature and high permeability, develop pore pressure during rapid shearing or other disturbance. These considerations have not been directly addressed in this study. Mainly plasticity and self healing problems in the face of cementation have been addressed.

Compressibility coefficients at various normal pressures in conventional oedometers have been determined on compacted specimens of zero age in looking for any collapse of the soil skeleton at higher pressures than even the 280 psi vertical pressure of the torsion tests. Of course the vigorous compaction used in preparing the specimens has reduced any tendency for collapse and pore pressure increase but study of wetting or saturating is also needed. Wetting has been tried for spring oedometer specimens after various aging times before determination of torsion shear strength and accompanied by specimen volume measurement before and after wetting during permeability testing.

B. Approach

The routine testing approach has centered around study of rather highly consolidated specimens of various mixtures of spent oil shale at two moisture contents, one at optimum water content for maximum dry density, the other at a somewhat wetter than optimum water content. Often wetter than optimum material is used for small dam cores and around abutments for increased flexibility and lower brittleness and sometimes lower permeability also results. A vertical consolidation pressure of around 280 psi was produced by spring loaded oedometers.

To simulate a liner placement technique sometimes proposed, the specimens were compacted in spring oedometer sheaths to 100% of standard proctor or 100% of modified proctor. These compactions allowed a small further consolidation in the oedometers. The oedometer consolidation is a sort of model of burial under an embankment of moderate height and allows a standard and somewhat realistic environment for subsequent aging/curing/and or cementation processes in the specimen. There is some unreality in immediate application of the full 280 psi consolidation pressure just after compaction however, as some time is needed for construction of full embankment height.

After permeability testing a specimen, it was transferred from the spring oedometer to a rubber membrane in a triaxial chamber for torsion testing under a confining water pressure generally corresponding to an assumed K_o of 0.5 to 0.7. A K_o of 0.7 is higher than corresponds to a two dimensionally normally consolidated silty material but may be about right for certain specimens. In this way the tendency for swelling in diameter of a specimen as it in effect is extruded from the oedometer sheath to the rubber membrane in the triaxial chamber is mitigated. Such swelling might break cementation of cemented specimens. Without the confining pressure even some stiff somewhat cemented specimens were crushed when only moderate vertical pressures were applied prior to torquing.

It is desirable to perform shear strength tests on undisturbed specimens. Specimens may be disturbed by swelling which softens them, by overconsolidation which during extrusion hardens them or by breaking cementation which softens them or fractures them prematurely. After obtaining the torsion stress/strain curve, the specimens were removed from the triaxial container and their enclosing gum rubber membranes cut away so previously transferred longitudinal acrylic paint stripes on the specimens could be examined and the specimen photographed.

Some physical and chemical properties of the specimens were next determined on dried fragments left from the torsion test. These include EGA analysis for hydrate water of species formed during curing. Some of these species are of a cementing or potentially leachable nature. X-ray diffraction scans for confirmation or identification of these species were also made.

The Atterberg limits of beginning materials and blends of spent shale materials are a parameter important in soil mechanics correlations. These were obtained for some raw material spent shale and mellowed spent shale. Atterberg limits on cemented specimens were not made.

Considerable time was needed to learn how to best operate the specially built triaxial torsion machine. Some specimens from preliminary series were tested under various confining water pressures and with different variations of specimen extrusion methods before the combination of conditions used for most of the specimens prepared for the following experimental plan was standardized. At the beginning it was believed that cured specimens containing much of the burned TOSCO spent shale would be too cemented to be handled by the triaxial torsion apparatus and this material was limited to 30% in mixtures with less cementing TOSCO II material. This fear was validated as tests proceded. Some of the 30% mixtures were strong enough to cause slipping of the piston rod in the torque transmitting collet gripping it. Usually this could be remedied by further tightening of the collet. Also sometimes a little bending over of the brass vanes in the pore stones gripping a well cemented specimen occurred during twisting.

It was also feared that there might be poor contact and gripping of the top of the specimen by the piston pore stone when standard proctor and particularly when modified proctor compaction was used, especially since a 3/32 inch cross section rubber o-ring was being used at the periphery of the piston pore stone between the specimen and stone. Preliminary experiments using a pneumatic loaded oedometer with proctored material seemed to partially support this fear and many of the main series of specimens were loaded in the spring oedometers using the o-rings but with some loose material sprinkled on top of the compacted specimen within the o-ring before insertion of the piston and application of spring pressure. Previous static compactions with the spring alone without proctor compaction had shown attainment of rather high density although not as high as by some standard proctorings and all modified proctorings. For this reason some hope was held that the thin loose layer would bond well enough to the piston pore stone-vane structure. When torsion tests were made, however, it was found that slippage often occurred between specimen top and the piston pore stone without involvement of the interior of the specimen to much extent. Moreover disassembly of the specimen and porestones after torsion testing

revealed that the material at the top of the specimen was much softer than that at the bottom.

Immediately a new procedure of torsion testing was devised wherein the vertical pressure on the specimen was brought up to that originally existing during consolidation in the spring oedometer with the hope that this could dig the vanes into the top of the specimen and secure a good enough grip. This was somewhat successful. The vertical pressure on the specimen during torsion testing should probably be kept at that during consolidation anyway for less likelyhood of disturbance of the specimen. With fixed upper and lower specimen porestones about 1/2 of the vertical pressure is lost during extrusion of the specimen in the triaxial confining chamber and should be replaced before torsion. As this fraction was apparently unaffected by elimination of the loose layer and piston porestone o-rings in a revised specimen loading procedure, some other reasons for the loss have been sought.

Loss of vertical pressure on the soil skeleton during unsheathing is presently believed to be due to (1) some back lash in the pedestal pins and mating sheath holes and (2) some specimen overconsolidation caused by excess piston pressure on the specimen generated by friction drag between the teflon coated sheath and the specimen. As the results of the effect are apparently of little consequence at the present rough stage of development of the method and useful correlations and comparisons between specimens were being made, a further change in methodology was not instituted. One change might be to grease the inside of the oedometer sheath contacted by the specimen but this would make temporary adherence of the acrylic paint marker stripes difficult.

C. Experimental Plan and Independent Variables Used

Table II 1 summarizes the experimental plan. Each box under columns C1 and C2 represents one specimen, compacted in a spring oedometer and consolidated at around 280 psi. Duplicate specimens compacted in a three segment ring mold were also prepared then coated with wax for curing at constant moisture prior to being subjected to the Brazil indirect tensile test. These Brazil test specimens are denoted by "B" in the boxes under columns C1 and C2.

The boxes under the C3 columns which have entries represent specimens prepared by standard proctor compaction and tests by pneumatic arm oedometer at five consolidation pressures up to 310 psi. The water contents chosen were those for optimum moisture for maximum dry density for standard and modified proctor and several water contents including some wetter than optimum for standard proctor, four or five water contents total, for each of the nine spent shale raw material types or mixtures tested by the others methods . The loading number for the spring oedometer experiments is given in the lower left corner of each applicable box in Table II 1. This number is followed by B if Brazil tests specimens were to also be prepared. The water to be added, percent dry basis, in preparing the specimens is entered in the upper area of each box.

C1 represents modified proctor compaction, C2 standard proctor compaction. T1, T2, and T3 represent curing times of nominally 2, 4, and 8 weeks respectively. "Yes" represents that later "saturation" was to be carried out by means of permeability measurement operations, "No" represents

that the spring oedometer specimen was to be torsion tested without saturation after consolidation.

Table II 1. Experimental Design - TOSCO II, Lurgi, and Mixtures of mellowed TOSCO and Mellowed Lurgi With Burned and Unburned TOSCO And Unmellowed Lurgi Spent Shale

Material	Later Satd.?	Spring Oedometer and Triaxial : Torsion Test C1 = Modified Proc. T1	T2	T3	T4	C2 = Standard Proc T1	T2	Pneumatic Arm Oedometer C_3 = Standard Proc. except with * which is Modified Proc.
Unburned TOSCO II	Yes+	22% 54 B	22% 34 B	22% 46 B	22% 27% 32% 94B 95B 96B	25% 71 B	25% 32 B	* 22% 25% 20% 30% H_2O
	No	22% 55**	22% 35	22% 47		25% 91	25% 33	
10% Burned TOSCO, 90% Unburned TOSCO II	Yes+	23 56 B	23% 39 B	23% 48 B	23% 97B	27% 70 B	27% 31 B	* * 23% 28% 22% 27% 33%
	No	23% 57**	23% 49			27% 90	27% 30	
	Ample Moisture+	28% 53 B	28% 62 B					
20% Burned Tosco 80% Unburned TOSCO II	Yes+	24% 75 B	24% 60 B	36 B		24% 80 B	24% 37 B	* * 24% 29% 24% 29% 34%
	No	24% 67	24% 63			24% 81	24% 38	
	Ample Moisture+	29% 66 B	29% 61 B					
30% Burned TOSCO 70% Unburned TOSCO II	Yes+	25% 76 B	25% 58 B	25% 40 B		28% 89 B	28% 41 B	* * 25% 34% 28% 33% 39%
	NO	25% 77	25% 68			28% 88	28% 42	
	Ample Moisture+	34% 74	34% 59					
Ample Moisture 75% Mellowed Burned TOSCO, 25% Burned	Yes+	55% 92 B	55% 8 B					* 55%
50% Mellowed Burned TOSCO, 50% TOSCO II Ample Moisture	Yes+	40% 93 B	40% 87 B		40% 45% 103B 104B			* 40% 45
Lurgi	Yes+	22% 51 B	22% 72 B	22% 43 B	22% 100B	30% 78 B	30% 64 B	* * 22% 27% 30% 35% 40%
	No	22% 50	22% 73	22% 44		30% 79	30% 65	
	Ample Moisture+	27% 52 B	27% 69 B	27% 45 B	27% 32% 101B 102B			
75% Mellowed Lurgi 25% Unmellowed Ample Moisture	Yes+	25% 82 B	25% 83 B					* 25% 25 30 35
50% Mellowed Lurgi 50% Unmellowed	Yes+	25% 84 B	25% 85 B					* 25% 25 30 35

* Modified Proctor

\+ Permeability determined also

**Permeability determined out of order resulting in "yes" instead of "No" later saturation.

III. NATURE OF SPENT SHALES USED AND MATERIALS PREPARATION

Spent shales collected have been in nine 55 gal drums containing Lurgi spent shale, five containing a burned TOSCO spent shale, and four of regular unburned TOSCO II process spent shale.

A. Lurgi Spent Shale

Material from the nine drums of Lurgi spent shale had been separately examined. Equal portions from each drum was screened through 16 mesh to scalp out particles of spent shale, poorly retorted shale, and cracked heat transfer ball fragments. This material passing through the screen from all drums was well mixed. This single average Lurgi material was used for making all Lurgi specimens, blends of Lurgi material, and autoclave mellowing runs starting with Lurgi spent shale.

Sieve analyses of each of the collected drums of Lurgi spent shale are given in Table III 1. Mineral Carbon analyses determined by evolution of CO_2 by dilute hydrochloric acid and its volumetric determination using a calcimeter are given in Table III 2. Mineral carbonates such as calcite, dolomite, nahcolite, dawsonite, kutnahorite, siderite, and ankerite are probably all decomposed by this treatment.

Figure III 1 in which the mineral carbon found in a drum is plotted against the percentage of material passing a 325 mesh sieve for the drum shows a tendency for the more intensely burned material which contains less mineral carbon (or mineral carbonates) because of greater calcination of mineral carbonates to be less finely divided. Hasty conclusions regarding the Lurgi process should not be made from this data, however. Drums L, C, G and J material which is more finely divided may merely be drums of electrostatic precipitator captured material whereas the other drums may be from a cyclone separator. It may be concluded, however, that if necessary some adjustment of properties of Lurgi material for a liner may be possible.

Figure III 2 shows a fair correlation between the dolomite found in the various drums of Lurgi spent shale and the mineral carbon found. The dolomite plotted is the ratio of one of its x-ray diffraction line peak heights to an albite line peak height used as an internal standard. Ettringite, a hydrated species, was found in the x-ray diffraction patterns and also seen in EGA scans in material from several of the drums of Lurgi spent shale. There was no good evidence that water for formation of ettringite came from rain or snow water entering during their storage at Tract CA before collection. Some of these drums contained mostly very large lumps with casts of the drum interiors in mildly cemented material. Possibly enough steam or moisture contacted these spent shales during operation of the Lurgi pilot plant to partly hydrate the spent shale and form ettringite there or perhaps the material had been dumped in the weather before being placed in the drums. This material, although blended into the batch, was a minor fraction.

B. TOSCO II Spent Shale

TOSCO II spent shale is a finely divided material resulting from retorting in a small TOSCO II rotary retort at the TOSCO Rocky Flats site north of Denver. It was supplied by Robert Hall of TOSCO. As a result of

Table III 1

Sieve Analyses of Lurgi and Burned TOSCO Spent Shale

Mesh Size	Lurgi Drum A	Lurgi Drum B	Lurgi Drum B,dup.	Lurgi Drum C	Lurgi Drum D	Lurgi Drum E	Lurgi Drum F	Lurgi Drum G	Lurgi Drum H	Lurgi Drum H,dup.	Lurgi Drum J	Burned TOSCO Drum TA
on 48	0.03%	0.00%	0.00%	0.14%	2.14%	0.13%	0.14%	0.07%	0.00%	0.20%	0.27%	0.82%
on 100	1.37	1.48	1.43	0.00	1.14	1.14	1.03	0.21	1.48	1.41	0.40	3.99
on 150	3.02	2.96	2.51	0.07	1.85	2.03	1.58	0.28	3.12	2.42	0.27	5.28
on 200	4.33	5.59	4.48	0.34	3.28	4.31	3.02	0.41	3.42	4.43	0.54	1.47
on 270	2.13	4.18	3.94	0.14	2.85	4.56	2.40	0.42	3.27	3.63	0.54	3.29
on 325	5.64	7.48	6.09	0.54	4.56	7.10	5.08	1.11	5.94	5.24	0.94	9.33
on pan	81.79 / 98.31	79.2 / 100.89	82.79 / 101.24	95.09 / 96.32	86.04 / 101.86	80.86 / 100.13	87.42 / 100.67	96.80 / 99.30	79.79 / 97.02	80.24 / 97.57	97.04 / 100.00	69.25 / 93.43

Table III 2

Calcimeter Determined Mineral Carbon In Spent Shales Studied

Determination	Lurgi A	Lurgi B	Lurgi C	Lurgi D	Lurgi E	Lurgi F	Lurgi G	Lurgi H	Lurgi J	Lurgi K	Lurgi L	Lurgi M*
No. 1	5.667%	5.140	5.885	5.394	5.162	5.412	6.051	5.691	6.107	5.557	6.012	2.681
No. 2	5.592%	4.976	6.007	5.488	5.142	5.288	6.206	5.570	6.140	5.403	5.844	2.725
No. 3	5.621%	4.980	6.122	5.475	5.101	5.348	6.190	5.691	6.190	5.475	5.905	2.456 2.828
No. 4												
%C. Mean	5.627%	5.032	6.005	5.452	5.135	5.350	6.149	5.651	6.146	5.478	5.920	2.672
Std. Dev.	0.67%	1.86	1.08	0.93	0.61	1.16	1.39	1.23	0.68	1.41	1.44	5.87

% Carbon Determination	Burned TOSCO TA	Burned TOSCO TA	Burned TOSCO T5	Burned TOSCO TC
No. 1	3.013	2.988	3.050	2.746
No. 2	3.097	2.868	3.086	2.953
No. 3	3.185 3.347	2.989	3.037	3.116
No. 4	3.150			2.861
%C. Mean	3.159	2.948	3.058	2.919
Std. Dev. %	3.9	2.36	0.83	5.35

*Note: Sandy Grains present-probably start-up sand. Grab sample was ground with Mortar and Pestle.

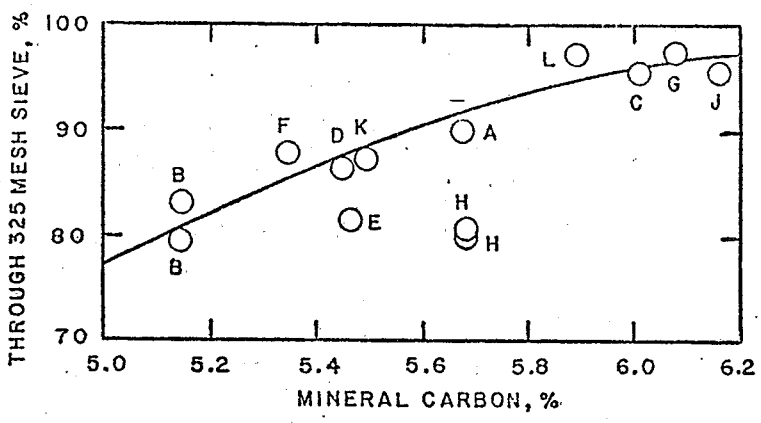

Figure III 1. Particles Through 325 Mesh Sieve as a Function of Mineral Carbon Left in Spent Shale

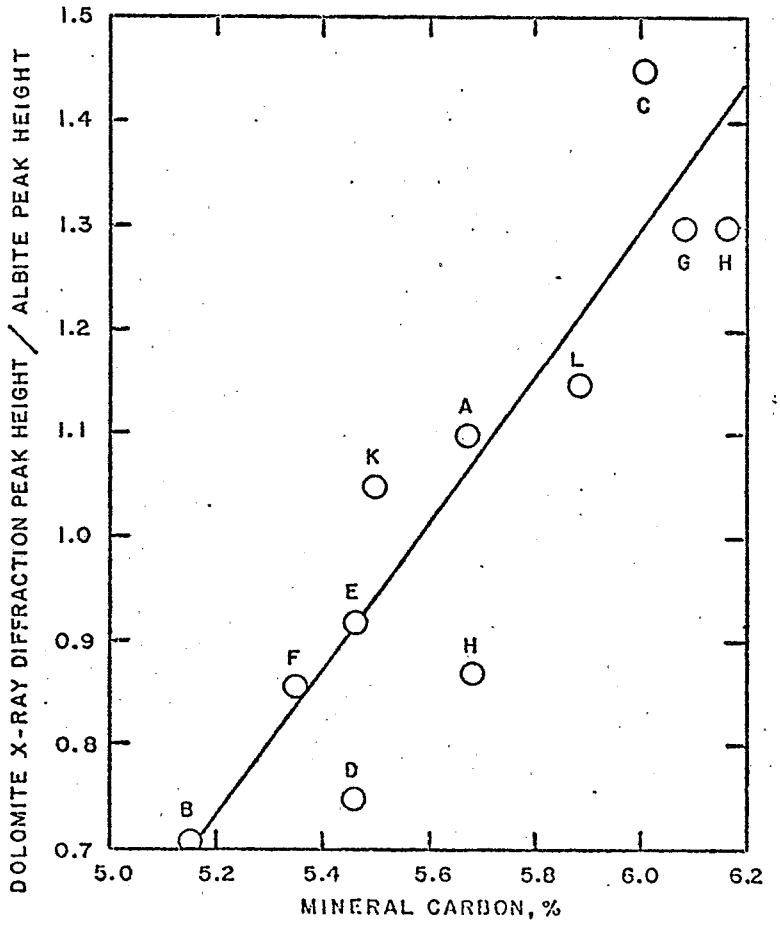

Figure III 2. X-ray Diffraction Intensities of Dolomite Relative to Albite as Function of Mineral Carbon Found by Calcimeter for Lurgi Spent Shales

by passing through the retort some relatively unretorted material was present which had not disintegrated by attrition. This was larger particles which were scalped out by screening through the 16 mesh screen. Equal portions of screened material from each of four drums of material were mixed and used for subsequent tests. The sieve analysis of this material is presented in Table III 1 above.

Although the clay mineral illite is said to be in Piceance Basin oil shale no evidence for it was found in the TOSCO II material analyzed by x-ray diffraction. This may be because the 950°F retorting temperature disrupted the major interlayer structure enough to eliminate the important low angle diffraction line. Illite may have been seen in the poorly retorted large fragments screened out of the material used.

C. Burned TOSCO Spent Shale

Five 55 gallon drums containing this material were also supplied by Robert Hall of TOSCO. These were said to be of identical composition among themselves. This material was said to have been optimized in regard to cementing power and was produced in a TOSCO fluidized spent shale burner at Rocky Flats.

Table III 1 includes a sieve analysis for one of the drums (designated TA) of burned TOSCO spent shale. This material appears to be not quite so finely divided as the Lurgi material. Table III 2 includes several mineral carbon assays by calcimeter of the burned TOSCO material. Less mineral carbon (due to less uncalcined mineral carbonates) is found in the burned TOSCO spent shale than in the Lurgi spent shale signifying more vigorous burning and/or calcination of the former.

D. Autoclave Mellowed Burned TOSCO Spent Shale

Slurry autoclaving of burned TOSCO spent shale had been previously done at various temperatures (and various resulting steam pressures) to "mellow" or reduce its cementation potentalities before placement as a liner. There is a simultaneous increase in the clayish nature of the material as indicated by plasticity index although the amount of clay sized fractions below 2 microns diameter and 5 microns diameter compared to those from unmellowed burned TOSCO material determined by sedimentation jar did not suggest much increase in clay sizes nor a clear conclusion. There is some possibility that otherwise sharp angular particles of certain minerals have been partially dissolved and rounded during autoclaving. This would also tend to reduce the angle of internal friction of the material in a liner and presumably increase the plasticity index.

X-ray diffraction scans of the autoclaved material have shown an increase of a species which is probably gypsum and also of a mineral which seems to be the clay stevensite and decrease of gehlenite up to 250 psi autoclave pressure but decrease of gypsum above 250 psi. See Figure III 3. Ettringite decreased above 200 psi. See Figure III 4 and Figure III 3. It was suspected that the sulfate of ettringite and gypsum was being incorporated into other species, perhaps an ellestadite type of apatite (where sulfate replaces phosphate) or sulfate bearing hydrogarnet.

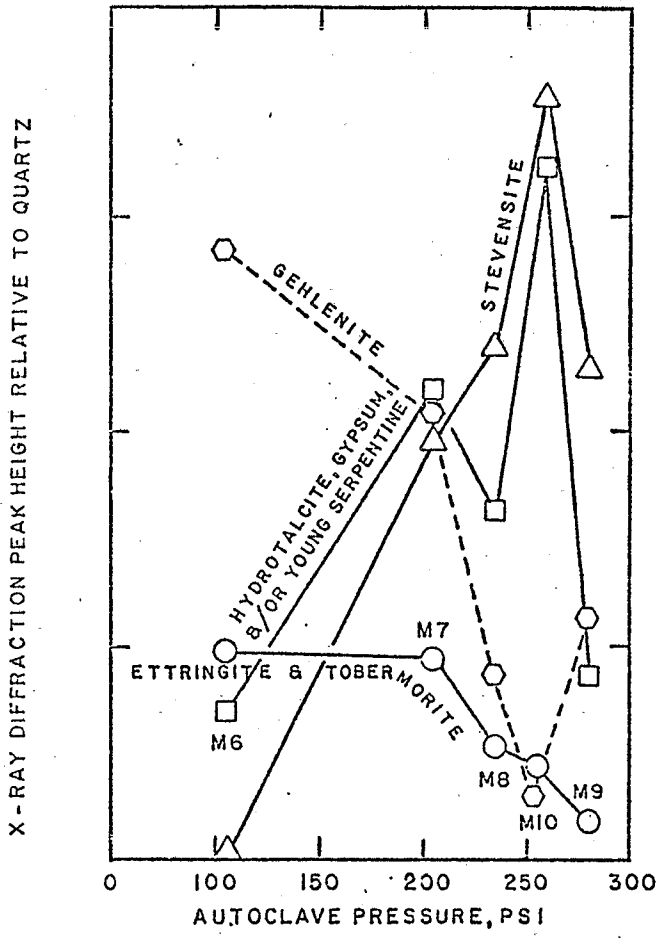

Figure III 3. X-ray Diffraction Intensities Relative to Quartz of Gehenite, Stevensite, Ettringite, and Gypsum and/or Other Species as Function of Autoclaving Pressure for Burned TOSCO Spent Shale.

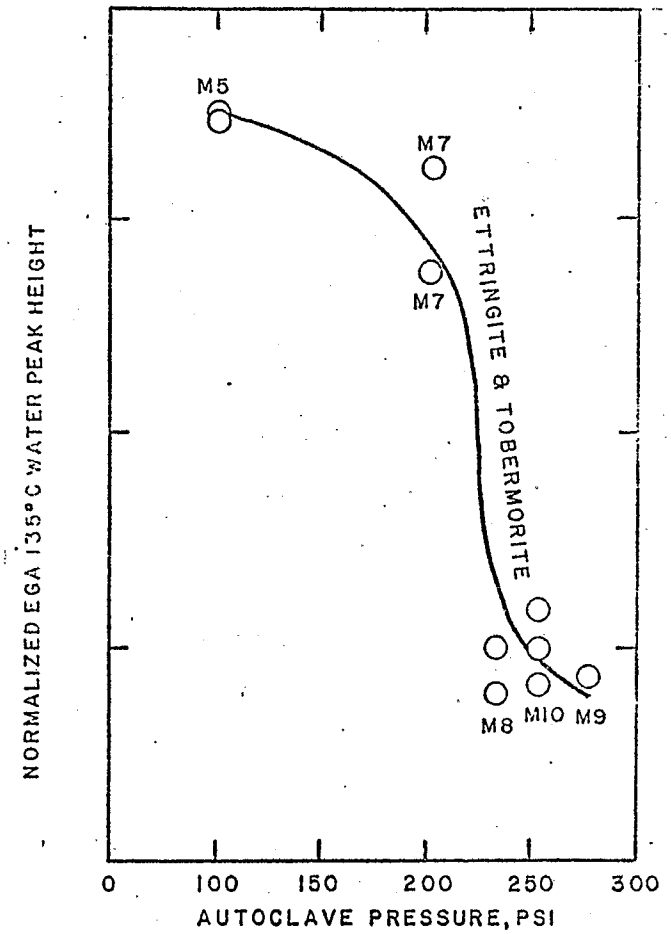

Figure III 4. EGA Ettringite Peak Height: Thermal Conductivity Detector Recorder Trace as Function of Autoclaving Pressure for Burned TOSCO Spent Shale.

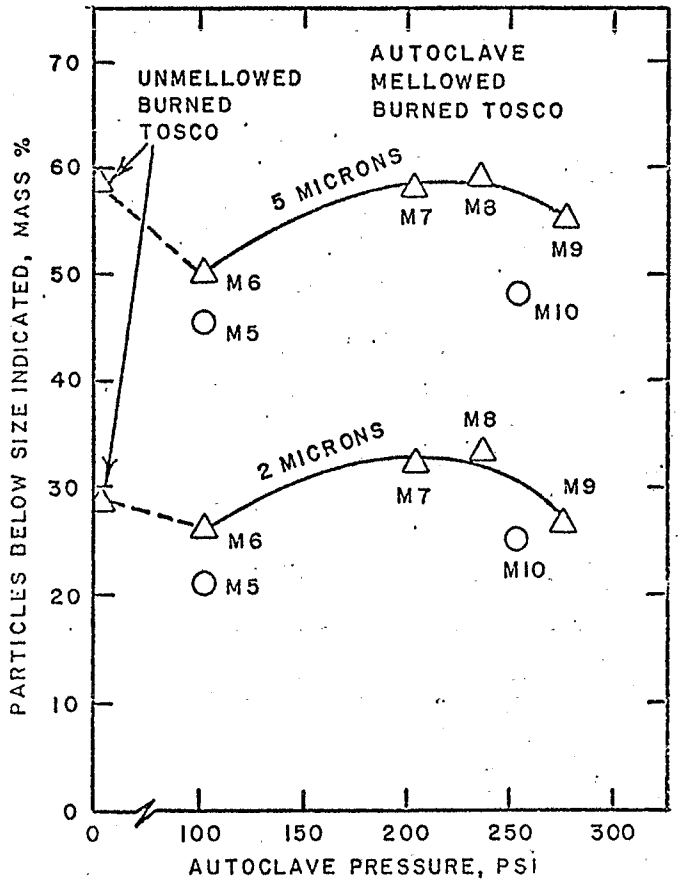

Figure III 5. Clay Size Fines of Autoclave Mellowed Burned TOSCO Spent Shale as Function of Autoclave Pressure.

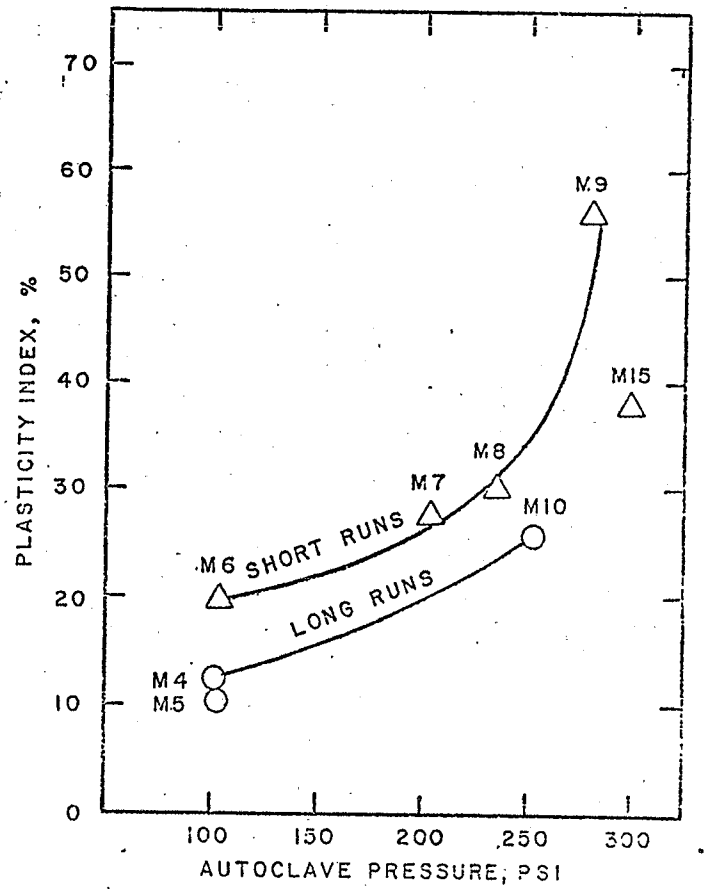

Figure III 6. Plasticity Index of Autoclave Mellowed Burned TOSCO Spent Shale as Function of Autoclave Pressure

In any case another autoclaving mellowing run M15 was made at 298 psig and 382°F to produce material for various mixtures of mellowed burned TOSCO spent shale with unburned TOSCO II spent shale for candidate liner materials.

Figure III 5 shows the clay size particle assay by hydrometer jar sedimentation for similar previous mellowing runs on burned TOSCO spent shale. Run M15 was made without calcium lignosulfonate thinner. The mass in the autoclave became quite stiff towards the end of the run but when dug out was not cemented hard. It was almost powdery in spite of the large amount of water retained in the mass.

Figure III 6 shows the plasticity index of mellowing run M15 material along with this index for material from previous mellowing runs at other autoclave pressures.

E. Autoclave Mellowed Lurgi Spent Shale

Autoclave mellowing at 400°F and 298 psi (Run M14) of the Lurgi Spent Shale did not produce nearly as much change in the material as did that of the burned TOSCO spent shale. Previous autoclavings of the Lurgi material were runs M11, M12 and M13 at 210, 292, and 292 psi pressure respectively. A fair amount of gypsum was formed and no evidence of stevensite was found.

F. Compaction Curves of Mixtures for Spring Oedometers, Brazil Tensile Tests, and Pneumatic Arm Oedometers

The specimen size used in the pneumatic loaded conventional oedometers as well as in the newly built spring oedometer - triaxial torsion test system was one inch high by 2½ inches diameter. As these specimens were to be made by "standard proctor" or "modified proctor" compaction which strictly interpreted requires compaction in four inch diameter molds a modification of the method was made. This involved decrease of the diameter of the proctor hammer to 1¼ inch diameter and a reduction of the lift height so three lifts for a standard proctor compaction and five for a modified proctor compaction for a one inch high specimen were used. The weight of the miniature standard proctor hammer and that of the miniature modified proctor hammer was proportioned so with a certain reduced drop distance an equivalent work input per sample volume was had as for the full sized four inch diameter proctor compactions. As for full sized proctor compaction 25 hammer blows per lift of material was retained.

1. 100% Tosco II Spent Shale

Figure III 7 shows preliminary standard and modified miniature compaction curves for TOSCO II spent shale after the mixes with water had aged about one day in the air tight ziplock freezer bags in which they had been manually mixed. Repeated data points for mixes compacted only 30 to 70 minutes after mixing with water are also shown.

Apparently for the standard proctor compaction, aging the mix for a period of around one day causes some difficulty in densification which is overcome by the heavier hammer and thinner lifts of the modified proctor procedure. There may be some roughening of the particles by some hydrate species formation or needless of some hydrated species may have formed which cause increased particle to particle friction during compaction. Yet

another possibility is that some clumping or floculation of particles to form larger loose clusters (with or without some cementation) occurs after a time.

A fairly good correspondence of the miniature compaction data with some full sized 4 inch mold compaction data shown in Figure III 8 was had. The full sized compactions gave slightly greater densities but the same optimum moisture added contents.

From the miniature compaction curves of Figure III 7 optimum moisture added of 25% for standard proctor and 22% for modified proctor have been determined which have been used in preparing mixes for non-ample moisture 100% Tosco II specimens.

In subsequent mixing and loading of oedometers and preparing Brazil test specimens a time between mixing with water and compacting of 30 minutes to an hour was instituted.

The compaction curves we have obtained for scalped TOSCO II material are somewhat different from those reported by Townsend and Peterson (1979) (Their Fig. 17) for a whole TOSCO II material. Their optimum water contents are about 4% lower than those of Figure III 8 and their optimum dry densities are higher by about 9 pounds per cubic foot for standard proctor and 6 for modified proctor.

This may be due to several possible factors. Scalping (removing) particles larger than 16 mesh may have removed denser lower Fischer assay material which decrepitates less during retorting leaving lower density material for our tests than for theirs. They report however, a solids density of 2.61 whereas we found 2.72 for our dry scalped TOSCO II to as low as 2.62 for material wetted and cured for about 30 days followed by a steady state value of 2.71 for material aged 50 to 73 days or longer. There is also the possibility that the material they used was from a different strata or had been retorted less completely. We have also found that with the unburned TOSCO II spent shale a delay of a day between adding water and proctoring produces a less dense specimen. Possibly further delay would produce a more dense specimen as latent clays begin to become hydrated and plasticity index increases. We do not know if a heap mellowing time was allowed by Towsend and Peterson.

2. Mixtures of TOSCO II Spent Shale with 10%, 20%, and 30% Burned TOSCO Spent Shale.

Figure III 9 summarizes the optimum moisture added, found or estimated for mixes with 0%, 10%, 20%, and 30% burned TOSCO spent shale in the unburned TOSCO II spent shale. "Ample" moisture contents called for in Section II C, the Experimental Plan, Table II 1 have been arrived at by adding 5% water to that needed for optimum density plus that needed for short term hydrate formation. Short term hydrate formation is mostly the moisture disappearance by hydrate formation involving the burned TOSCO material. The moisture disappearance was derived from Figure III 10 which is based on a comparison of the water found by oven drying at 50°C with the water added to the mix for mixes with 100% and 50% burned TOSCO spent shale and several added water contents. Evidently the higher the water content of the spent shale the more hydrates are formed, at least for the limited times of observation for Figure III 10. Also their appears to be a

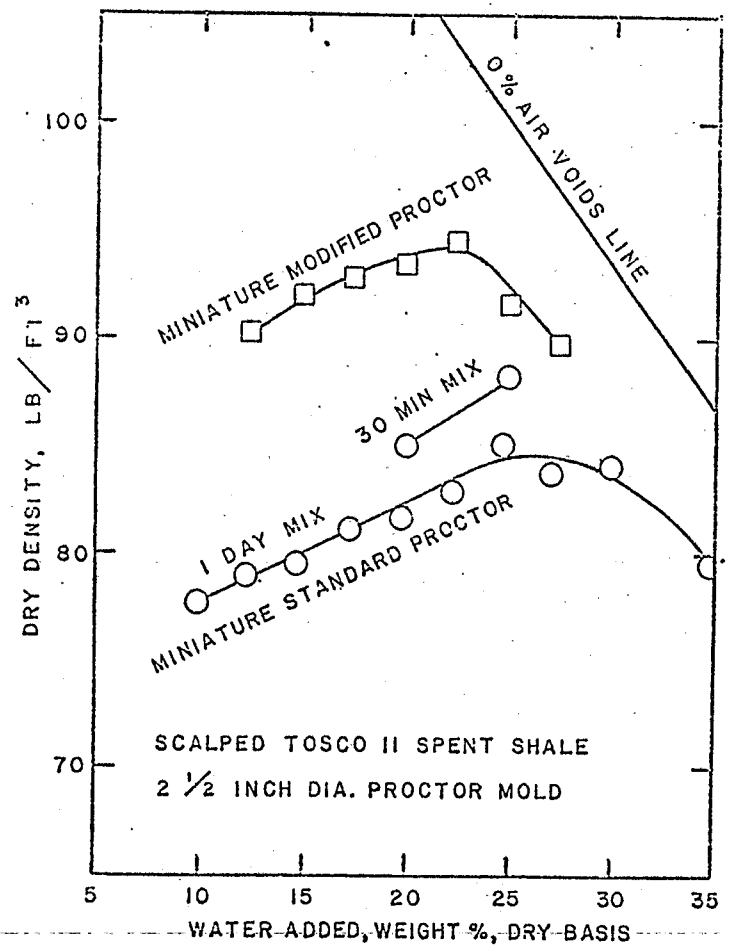

Figure III 7. Miniature Compaction Curves for TOSCO II Spent Shale.

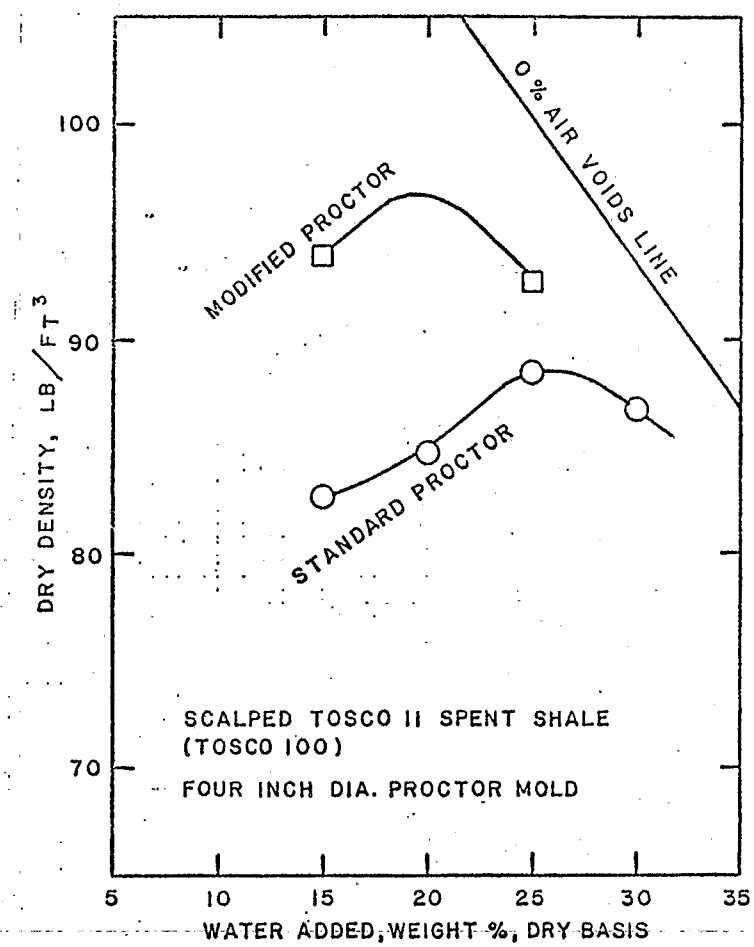

Figure III 8. Four Inch Mold Compaction Data for TOSCO II Spent Shale.

synergistic capture of water by the otherwise rather inert to water TOSCO II spent shale in the presence of burned TOSCO spent shale, perhaps through pozolonic reactions activated by the high pH of the burned spent shale. These have been considered in a way as the water disappearance for 10, 20 and 30% burned TOSCO II mixtures was prorated from the 50% curve of Figure III 10.

In Table II 1 showing the Experimental Plan the water contents needed for the various specimens tabulated is noted as determined by the above methods. Admittedly for some of these specimens containing burned spent shale the water may be underestimated for the long term. By use of EGA scans showing hydrate water evolution to 500°C for specimens after curing adjustments perhaps should be made in the water contents for any future mixes.

3. Lurgi Spent Shale

Figure III 11 shows the miniature proctor compaction curves for the Lurgi spent shale. From these optimum moisture added of 22% for modified and 30% for standard proctor may be read or estimated. The water disappearance curve for very short times is shown in Figure III 12. For "ample' moisture specimens 27% and 30% moisture have been taken.

4. Mellowed Lurgi Spent Shale - Lurgi Spent Shale Mixtures.

Figure III 13 shows miniature modified proctor compaction curves for mixtures of mellowed and unmellowed Lurgi spent shale that were used. From these curves optimum moisture added of 24% for modified proctor may be read for the 50-50 mixture and 15% for the 75-25 mixture. Twenty five percent was used for both cases to produce ample moisture cases but without producing a too plastic beginning material.

5. Mellowed Burned TOSCO Spent Shale - TOSCO II Mixtures

Figure III 14 shows miniature modified proctor compaction curves for mixtures of mellowed burned TOSCO spent shale with TOSCO II spent shale. Optimum moisture added contents of 37% and 49% respectively, were found for a 50-50 mixture and a 75-25 mixture. Percentage moisture added of 40% and 55% have been used to make ample moisture cases.

G. Atterberg Limits of Mixtures

Although the Atterberg limits were not used in compounding the mixtures used in this work they may be of interest as some indication of the nature of mixes for full scale handling and compaction.

1. TOSCO II and Burned TOSCO - TOSCO II Spent Shale Mixtures

Figure III 15 shows the liquid limit and plasticity limit for 0%, 10%, 20% and 30% burned TOSCO spent shale in TOSCO II spent shale along with the plasticity index.

2. 50% Mellowed Burned TOSCO - 50% TOSCO II Mixture

The liquid limit, plastic limit and plasticity index for 50%, mellowed burned TOSCO in TOSCO II spent shale is 64.4%, 52.7%, and 11.7% respectively. Those of 100% mellowed burned TOSCO spent shale are 121.0%, 83.5%, and 37.5 respectively (mellowing autoclave run M15).

3. 75% Mellowed Burned TOSCO - 25% Burned TOSCO (TA) Mixture

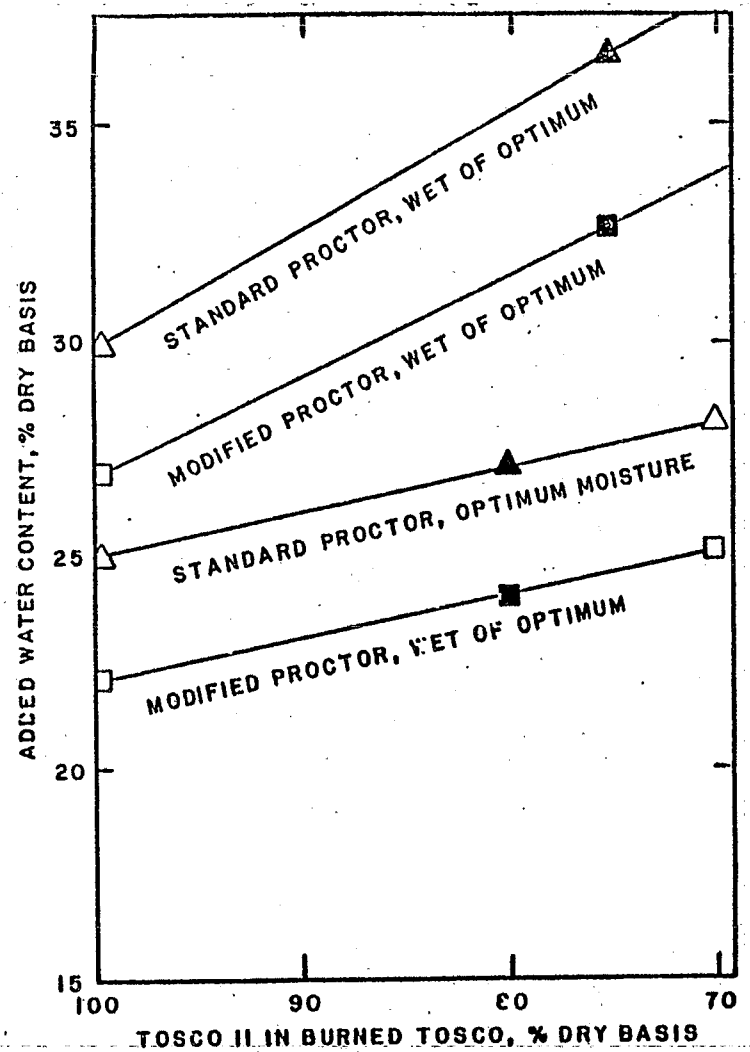

Figure III 9. Summary of Optimum Moisture Needed to be Added and Wet of Optimum Moisture Needed to be Added to Mixtures of TOSCO Spent Shale with 10%,20%, and 30% Contents of Burned TOSCO Spent Shale

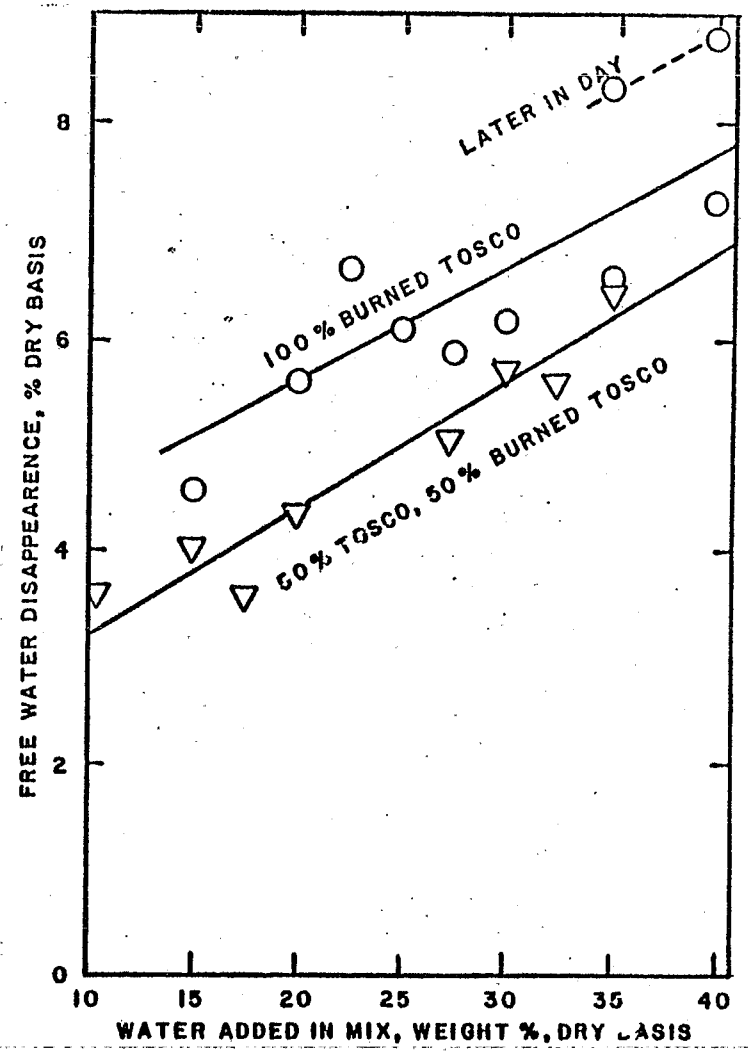

Figure III 10. Disappearance of Water Due to Hydrate Formation for 50% Burned TOSCO Spent Shale with 50% TOSCO II Spent Shale and Estimates of this for Other Ratios

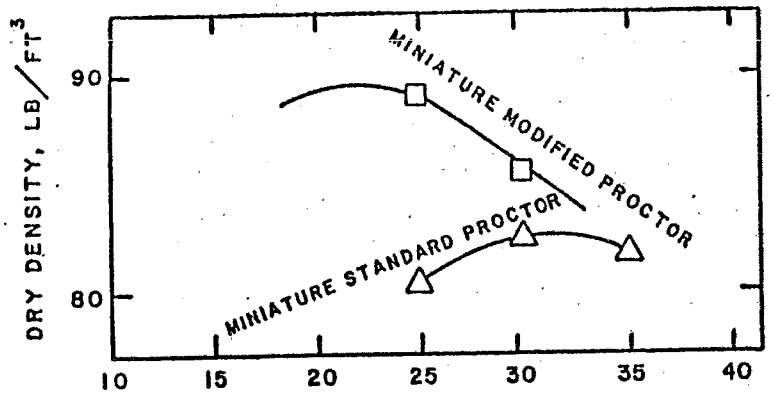

Figure III 11. Compaction Curves For Average Lurgi Spent Shale, 30-60 Minutes after Mixing

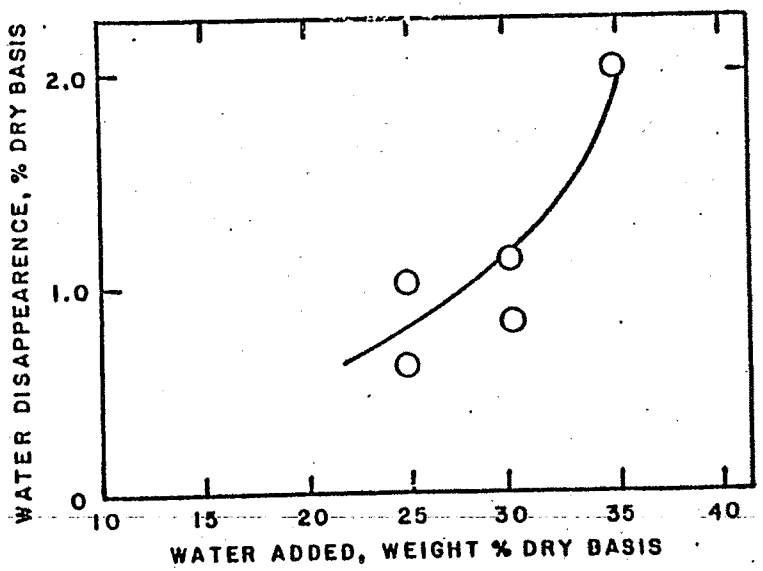

Figure III 12. Water Disappearance in Average Lurgi Spent Shale

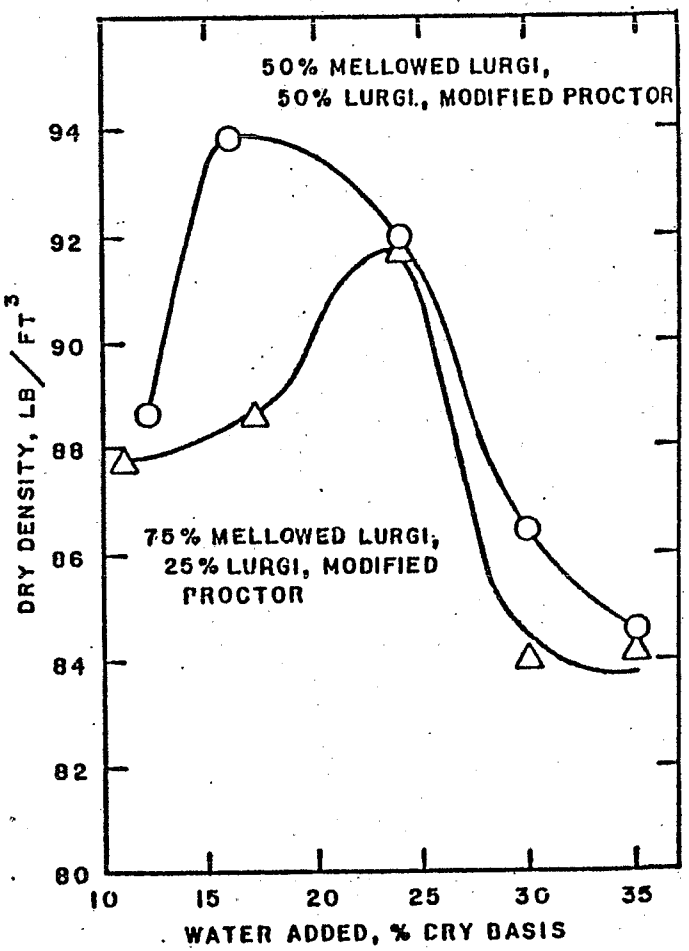

Figure III 13. Compaction Curves for Mixtures of Mellowed and Unmellowed Lurgi Spent Shale

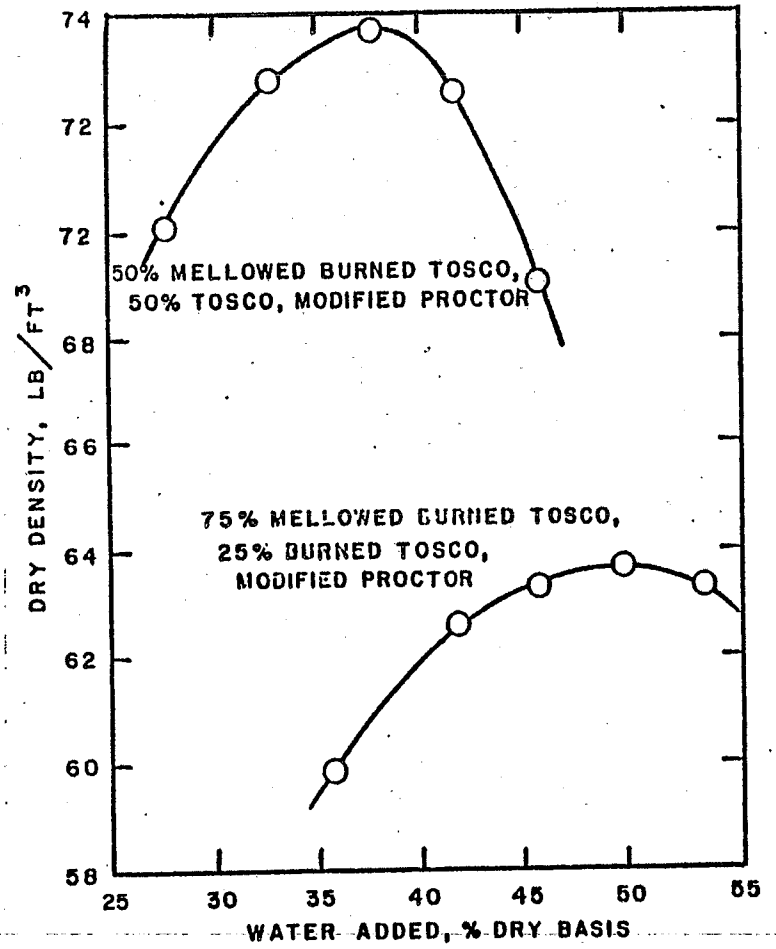

Figure III 14. Compaction Curves for Mixtures of Mellowed Burned TOSCO with Burned TOSCO and Unburned TOSCO II Spent Shale

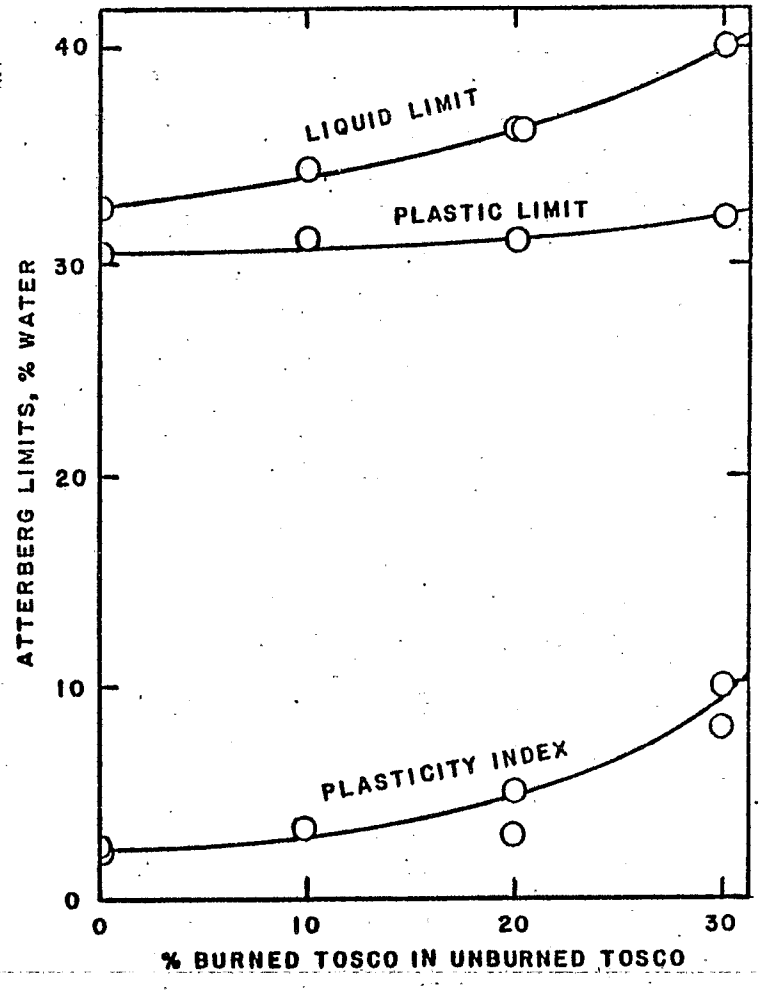

Figure III 15. Atterberg Limits of Burned TOSCO TOSCO II Spent Shale Mixtures

The liquid limit, plastic limit, and plasticity index of this mixture freshly prepared is 90.7%, 64.9%, and 25.8% respectively.

4. 75% Mellowed Lurgi - 25% Lurgi Mixture
   Liquid limit 43.5%, plastic limit 34.5%, plasticity index 8.0%.

5. 50% Mellowed Lurgi - 50% Lurgi Mixture
   Liquid limit 43.1%, plastic limit 36.1%, plasticity index 7.0%.

IV. APPARATUS AND PROCEDURES

A. Compaction of Specimens in Spring Oedometers and Measurement of Apparent Dry Density

Materials to be tested in all phases of this program were compacted with either a modified proctor or a standard proctor level of effort. These tests include samples for the spring oedometer/torsion tester, pneumatic arm oedometers, Brazil tests, permeability tests, and the optimum water content/maximum density tests. All compacted test specimens were 6.35 cm (2.5 in.) in diameter and, with the exception of the Brazil test specimens discussed later, were either 2.54 cm (] in.) in height or in the specific case of the spring oedometers at or near that height.

Due to the somewhat "non standard" diameter of the test specimens a miniature proctor hammer was constructed for sample compaction. The hammer consisted of a standard sleeve type drop weight with a fixed drop height of]2.80 cm (5.04 in.). The diameter of the brass cylindrical head was 3.]8 cm (].25 in) or the radius of the specimens. Two removable weights served as a handle. One weight was attached for standard proctor compaction and the other for modified proctor compaction. Compaction efforts for a 20% or 5 mm over height sample (for trimming) was 656 kv/m^3 (]3676 ft-lbs/ft^3) for the standard proctor effort and 2929 kV/m^3 (548]] ft-lbs/ft^3) for the modified proctor effort. This provided a 4 to] difference in energy/unit volume between the two methods. During standard proctoring, the sample was added to the test mold in three layers, each layer receiving 25 hammer blows. For the modified proctor samples 5 layers each with 25 hammer blows were used.

Apparent Dry Density was obtained for specimens compacted in the spring oedometer by weighing all the damp mixed material added in lifts for proctoring. Care was taken to avoid evaporation of the moisture in this operation as much as possible.

The volume of the specimen resulting was calculated knowing the oedometer sheaths internal diameter and specimen height obtained from measurement of the piston rod protrusion above a selected flat area of the brass lead screw nut flange of the oedometer sheath before and after making the specimen in the sheath. An eight slotted brass spacer of known thickness was inserted when measuring the protrusion of the piston rod with the empty oedometer and its thickness properly subtracted. This was necessary because of the brass vanes protruding from the otherwise flat piston pore stone and pedestal pore stone surfaces which therefore can not be made to meet per se for the empty oedometer measurement. Since each set of oedometer sheaths, pedestals, and pistons and piston rods gives slightly different piston rod protrusions when assembled, empty separate blank protrusion measurements are needed for each set. Moreover, since a variable amount of looseness or slop results from clearance between the pedestal pins and their mating holes in the sheath the blank protrusion of the piston rod must be measured while supporting the sheath with the weight of the piston, piston rod, slotted spacer, and pedestal weights forcing the pins downward.

B. Curing and Consolidation in Spring Oedometers and Consolidation Curves

The specimens were sealed by O-rings to prevent evaporation of water during curing and consolidation. The load was applied by the spring (essentially constant for the small changes in the specimen length as a function of time) and the displacements were measured by the linear variable differential transformer (LVDT). Displacements were recorded by computerized data collections at various times during the curing cycle. These data were used to produce the consolidation curves.

C. Permeability Measurement

The permeability of the spring oedometer specimens was generally determined at a constant head of 20 psi. The water used in the permeability experiments was deaired. The air from the top pore stone and duct and perhaps some from the sample was evacuated by a roughing pump to facilitate the saturation of the specimen. The permeability is calculated from the measurement of the total discharge volume, Q, accumulated in time, t; the specimen dimensions; and the head.

D. Torsion Triaxial Machine and Shear Strength Measurement

The triaxial torsion machine was designed to produce strains under triaxial loads that simulate conditions expected for liners of spent shale piles. Hence the strains are generally beyond that possible in many compressive triaxial machines.

At first it was not known how silty the spent shale materials would generally be. Silty samples in the torsional triaxial machine are advantageous in that rapid draining of any pore pressure occurs and the material can be considered as a "noncohesive" or granular type soil in which the peak shear strength and residual shear strength are proportional to the normal pressure on the failure plane, (in the present specimens nearly equal to the vertical pressure on the specimen.)

With such silty samples where strength is proportional to normal pressure the use of angles of internal friction, ϕ_p and ϕ_R for peak and residual strengths is useful and represents a kind of normalization:

$$\phi_p = \arctan \frac{\tau_P'}{\sigma_N'}$$

$$\phi_R = \arctan \frac{\tau_R'}{\sigma_N'}$$

where τ_P' and τ_R' are effective shear strengths uninfluenced by water pressure (zero, pore pressure) at the failure planes and σ_N' is the effective normal pressure on the failure plane. With zero pore pressure or completely drained conditions these stresses are soil skeleton stresses where mineral grain to grain contact friction and disengagement of grain interlocking forces are very important.

With nongranular or "cohesive" material such as clay the permeability is so low that very long times are needed for drainage to zero pore pressure (or pore pressure equal to ambient hydrostatic pressure). Then the mineral grains can float in a cushioning fluid of pore water (particularly when the soil is saturated or has no air in the voids). This causes lower shear

strengths than with granular material when drainage of pore pressure is inadequate as it is with all but very slow shear testing speeds. In addition the clay mineral grains are usually platy and slippery, especially under defloculated conditions (spent oil shales having high pH and calcium and magnesium ions in solution should tend to be floculated, those having lower pH and sodium ions may tend to be defloculated) which will further lower the shear strength and friction angles if they are compared with drained conditions.

Since cohesive soil or clays have a different character, are more slippery, due to great degree to their very low permeability, and since liners made from spent oil shale should probably have as low a permeability as possible the nature of clays should be considered. Clays are susceptible to "sample disturbance" by rough handling due to overconsolidation. Silty material, which the great majority of specimens tested in this program have been, are not as susceptible to overconsolidation and sample disturbance. This is fortunate in that the torsional triaxial apparatus was still being shaken down and proven as some of the more silty specimens were being tested on it.

1. Neutralizing Sample Disturbance by Testing Sample of Known Overconsolidation Ratio and Use of SHANSEP

Ladd and Foott (1974) in a paper on a new design procedure for stability of soft clays have pointed out that major variations in strength can be caused by sample "disturbance", strength anisotropy, and strain rate effects and that "none of these effects is explicitly included in present design practice". These writers remark that the use of field vane data (from an in-situ technique) avoids some of the difficulties of the use of the unconfined (u) or unconsolidated undrained (UU) shear tests but good correlations for this highly empirical method are limited to a few well known earth failure cases.

They described the "SHANSEP" method of stability design evolved at MIT for soft clays. In this method the problem of sample disturbance is solved by evaluating shear strengths at known overconsolidation ratios (of unity or above). Plotting normalized (by dividing by σ_v) shear strength vs OCR is then done to secure useful shear strength data.

Even in the simple case of soft uncemented clay, however, the securing of a known overconsolidation ratio is not simple if the sample has been allowed to swell when removed from its in-situ vertical compression effective stressed state. Merely compressing it back to the in-situ vertical effective stress σ_v is not adequate to secure an overconsolidation ratio of unity again. Due to strains in other than the vertical direction which are irreversible a more dense compression is actually required so the virgin compression line on a void ratio vs vertical effective stress plot is achieved. One should consult Figure 6 in Ladd and Foott's paper for clarification, if needed, but in brief the specimen is consolidated to a σ_v greater than found in situ to nullify disturbance.

In order to minimize disturbance of the specimen we have designed a special "torsion triaxial" test follow in laboratory spring oedometer K_o consolidation of a specimen. In our present procedure the latter follows proctor compaction. As a goal, during careful transfer of the sample from the oedometer cell to the torsion shear tester, neither swelling nor further

densification of a "soft clay" should occur and the shear strength will still correspond to that of an over consolidation ratio of unity and can be normalized by dividing by σ_v' for use in the SHANSEP method.

Figure IV 1 is a sketch of the apparatus for transference of consolidated specimens to the triaxial torsion shear machine. The system is described in Section IX of the Fifth Progress Report to E.R. Bates of EPA, Cincinnati (Culbertson, Habenicht et al., 1983). One modification has been use of thicker rubber membranes and discarding of the O-rings around the membrane and the O-ring snapper.

2. Handling of Cemented Clay (or Spent Oil Shale) in the Same Torsion Triaxial Apparatus As Designed for Soft Clay (or Spent Oil Shale)

A second reason, other than that of a clayish specimen, for use of the special torsion triaxial test is that the specimen may be somewhat cemented. Of course careful transfer of such a specimen from its consolidated and aged state in the spring oedoemter to the confining pressure of the triaxial bomb is first required as for a soft clay specimen. The same normal pressure on the specimen and same confining pressure as existed in its stay in the spring oedometer cell is desired during removal of the oedometer's confining sheath in the confining pressure can. Otherwise a tendency for longitudinal strain or lateral strain will exist which may cause premature disruption of cementation, an intolerable irreversible process for our purposes. Subsequent torsion testing may then not show full peak strength which is also needed to calculate an accurate brittleness index.

Clearly if the specimen is cemented the exact SHANSEP methodology described above can not be applied well, for during the procedure of greatly compressing the already possibly swelled and disturbed specimen (taken from its compressed in-situ environment) breaking of cementation will tend to occur, even if breaking had not occurred during swelling itself. Even if a means of transferring the specimen from the consolidated or in-situ environment to the test machine without disturbance is used (such as we have developed for the present spring oedometer - torsion triaxial test system) the SHANSEP approach may fail, if the specimen is cemented, because the plot of normalized shear strength vs overconsolidation ratio may fail. The latter because the peak strength due to cementation may not be well distinquishable from strength due to normal or over consolidation, particularly if shear strength is obtained from compressive triaxial tests where brittleness index is not obtainable.

The torsion triaxial test at slow enough strain rate for drainage is seemingly applicable for either a soft clay or a cemented clay. We have here used it for silty clays which are generally more or less cemented and applied friction angle calculations. An attempt at determination of K for a specimen before torsion testing it to destruction might show the first indication of whether it is actually much cemented by its rigidity when normal stress and/or confining stress is changed. If K can not be determined due to too stiff a specimen, the subsequent torsion test should verify cementation by giving a high brittleness index (peak strength/critical or residual strength) derived from the torsion stress vs strain curve and a steep initial stress strain curve accompanied by low pore pressure change until brittle failure. We have not tried to determine K with the present silty specimens but have generally assumed a value of 0.5

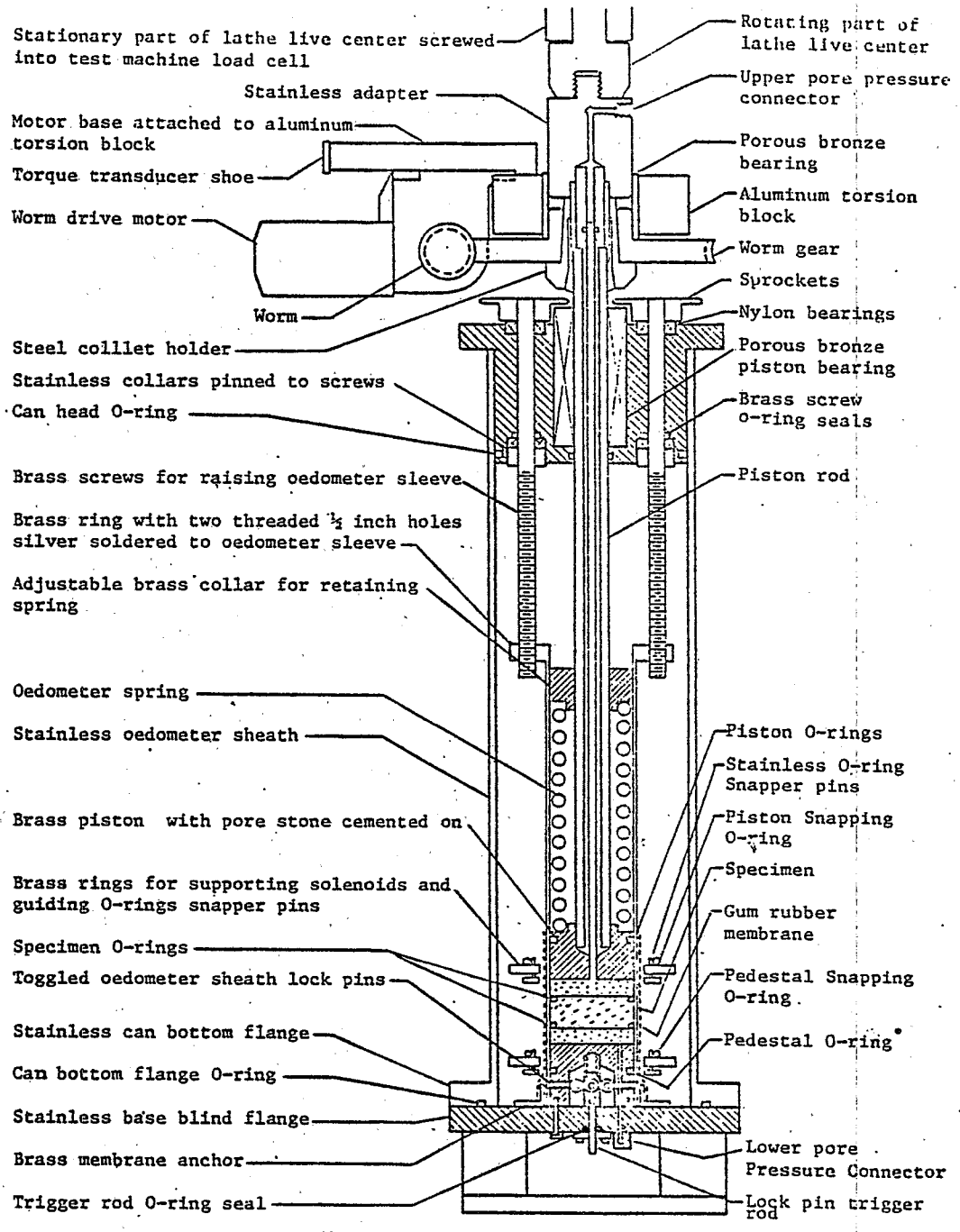

Figure IV 1.
Apparatus for Transference of Spring Oedometer Consolidated Specimens to Triaxial Torsion Shear Machine

to 0.7. The use of proctor compaction rather than static compaction makes K hard to estimate.

To transfer a laboratory consolidated specimen from the spring oedometer to the pressure chamber of a "triaxial" test machine by removing its confining sheath, as herein done, involves some friction between the specimen and sheath. This, in a tall specimen such as needed in the compressive triaxial shear strength test, will create more specimen disturbance (especially at the top end of the specimen) than in a short specimen such as suitable for a torsion shear strength test. If wall friction is high and the specimen relatively soft and tall enough, shortening of the specimen can occur during sheath removal to densify the material enough that, with fixed upper and lower pore stone spacing, the specimen will separate from the lower pore stone. A cemented specimen might not show such an effect but a weakly cemented one may have its cementation irreversibly destroyed. We use a teflon coated sheath and short specimens to reduce such friction. Short specimens are not suitable for compressive triaxial tests.

3. Advantages of Torsion Shear Strength over Compressive Triaxial Shear Strength for Study of Cemented and Uncemented Clay-like Spent Oil Shale

a. The tall specimen in the usual compressive triaxial test is not well suited to stress-strain curve determinations where large strains are needed before final "failure" such as in relatively plastic specimens or specimens showing a measure of plasticity after initial cementation or brittle peak strength. Much strain as the specimen is longitudinally compressed results either in a squashed specimen of increased cross section (which must be at least accounted for in load per unit area calculation) if the specimen is relatively plastic or in a diagonally, conically, or otherwise more brittle fractured specimen which is unsuitable for extended testing to residual strength. Calculation of brittleness index from a too incompletely developed residual strength is not desirable.

b. The accurate measurement or drainage of specimen pore pressure through top and bottom pore stones is greatly speeded for a relatively short specimen.

4. Data from Torsion Stress Strain Curve

In the torsion operation a peak strength followed by a "critical" or residual strength is often observable in the torsion stress-strain plot. (See the curve for loading 42 in Figure V 2). The difference between peak and residual strengths may sometimes include cementation strength. If cementation strength is involved a steep initial stress-strain plot occurs. Also a sharp peak strength pip is observed. These indications of cementation are qualitative only, but they are obtained at the high vertical stress representative of a deeply buried liner and under test procedures designed to minimize the risk of premature fracturing of the specimen.

Data obtained from the stress-strain curve: are peak shear strength and "residual" shear strength calculated from the torsion moments at the peak and later flat part of the curve, initial stiffness from the initial slope, and strain to peak strength as measured by angle of piston twist to peak strength. Other pertinent data for the specimen are initial vertical force on it from the oedometer spring and the sag of this force (due to overconsolidation and/or too low an arbitrarily established lateral

confining pressure) after the sheath has been pulled from the specimen. The vertical pressure was reestablished before torsion (for later runs) and held fixed during torsion by platen movement of the Instron test machine. This in the future could be automated by feed back from the load cell measuring the vertical force.

5. Handling Vertical Pressure in Torsion Test

As mentioned above during unsheathing of the specimen before torsion there is a sagging of vertical force exerted on the specimen even though the piston and pedestal are in fixed positions during this operation. This may amount to a loss of]/3 to]/2 of the original consolidation pressure exerted by the spring in the oedometer phase.

Later torsion tests, those performed further out on the learning curve and more refined, the sagged vertical pressure was increased to reestablish the consolidation pressure before torsioning the specimen and the vertical pressure was then held as fixed as possible to this value during torsioning by manually controlled movement of the platen of the Instron test amchine. The platen movement could in the future be profitably automated using an error signal from the difference between load cell output and a fixed reference voltage. The adjusted vertical pressure (column]3) equals the consolidation pressure (column 8) in Table V 2 for these more refined tests.

In earlier tests, vertical pressure after sheath pulling was not restored after sagging and, moreover, the vertical pressure varied throughout torsioning of the specimen. As generally these early specimens were silty and therefore well drained during torsioning, the simple proportionality between shear strengths and vertical pressure of Coloumbs law and a constancy of peak friction angle O_P and residual friction angle O_R was assumed. For some early tests, then, double data rows are presented in Table V 2 corresponding to different vertical pressures (column]3) occurring at the peak strength and at the residual strength. Moreover, generally for these tests the vertical pressure (column]3) was not adjusted to match the consolidation pressure (column 8) as it was in later tests.

For earlier tests vertical pressure on the specimen was not controlled during torsion but generally rose slightly until peak strength was reached then fell as residual strength was approached. For such tests, a different vertical pressure at residual shear strength than at peak shear strength was had, and accounted for, in calculating the brittleness index or friction angles O_P and O_R. For the brittleness index the O_R was normalized up to that expected for the higher vertical pressure assuming non cohesive material and zero cohesive intercept, as is usual for non cemented permeable material. By the time residual strength is developed any former cementation at the slip plane is irrelevant and this calculation seems good even for cemented specimens.

In summary, for later more refined tests, vertical pressure on the specimen before pulling off its confining sheath was not only initially made equal to original spring consolidation pressure but was reestablished after unsheathing the specimen by upward test machine platen movement. Vertical pressure was then held approximately fixed during torsion in these runs by continual adjustment of the position of the platen. Cemented or stiff specimens at the early stage of twisting needed lowering of the platen but

after peak strength developed the platen needed to be raised slowly in order to hold the vertical pressure on the specimen approximately constant.

The following data reporting form was used during performance of more refined tests. A calculation is required part way through the test to establish the load cell recorder pen position to be maintained during torsioning so vertical pressure on the specimen equals consolidation. The symbols in columns 8, 9, 10, 11, 12 and 13 in Table V 1 have the same meaning as those in this form.

6. Advantages of Membrane Walled Specimen for Torsion Shear Test

A number of advantages derive from enclosure of the torsion test specimen in a gum rubber membrane instead of a rigid metallic container. The rubber membrane is applied to the specimen under the selected confining pressure as the spring oedometer sheath is pulled from the specimen through use of the apparatus sketched in Figure IV 1. Some of the advantages are as follows:

a. There is no wall friction to impede rotation of the specimen. This allows a lower and more true shear strength result. Also the lack of stress gradient at the wall may allow a sharper peak strength pip.

b. There is no wall friction to impede vertical expansion or contraction of the specimen hence the vertical stress is true specimen stress. This seems to allow the possibility of measurement of K in the relatively undisturbed specimen from K_o consolidation as it rests in the confining pressure container before the specimen is destroyed in the torsion shear test. This is accomplished in concert with the expandable or contractable specimen diameter also enabled by the membrane wall. The ratio of change in confining stress with normal stress at low strains is taken to be K. This has not been tried in the present work as the specimens have been so silty and not generally cohesive.

c. A thicker specimen is useable in the torsion shear strength test due to nil wall friction. This should allow an easier performance of K measurement as above but it has also, with application of paint stripes to the specimen, allowed easy viewing of the mode of failure.

d. The mode of shear can be observed through final shape of initially vertical paint stripes on the specimen. Simple diffuse shear vs slip plane shear can be distinquished.

e. As K varies with extent of shear strain, for example as critical state is approached and volume of specimen expands or contracts, the confining pressure can be increased or reduced respectively to maintain a fixed vertical pressure throughout the shear operation. Other control methods also come to mind. For example, a constant diameter specimen might be maintained after caliper sensing of diameter during shear through movement of the piston on specimen. We have used in the present work two other methods handling vertical pressure discussed in 5 above.

f. The low wall friction should allow trial of dynamic shear stress relaxation examination of the specimen for cementation. This was not done in this work.

E. Drying Oven

Drying of test specimens as well as all drying of materials for this project was performed in a forced draft oven with continuous purging of fresh air from the outside. Samples were spread out or broken up as in the case of torsion test specimens, into 9 by 9 cm. disposable plastic petri dishes with sample designations clearly written on their sides prior to being placed into the oven. The drying temperature of this oven is carefully controlled at 48°C (118°F) by a proportional controller. This moderate temperature was carefully chosen in order to prevent the destruction of hydrates and carbonates. Higher temperatures were proven by DSC/EGA analysis to reduce or even eliminate low temperature (80-150°C) hydrated species. Likewise some carbonate materials showed low temperature thermal deterioration with time. Typical sample drying times for achieving a constant weight were on the order of 18 to 24 hours. Even if samples were left in the oven for extended periods, we fee confident that no deterioration would occur. Drying was sufficient, on the other hand, to provide for stable constant weight over time and very low DSC/EGA evolved water in the 30 to 50°C ranges. This test proved that all water in the samples was chemically associated with the sample.

Open air drying of the samples at room temperatures did not produce a constant weight for several days and the weights of many materials were found to vary with changes in humidity. For this reason, oven dried samples that were intended for further analysis, were stored in a constant 30% humidity cabinet maintained by a supersaturated calcium chloride solution prior to analysis or sealed in glass bottles. The capacity of the oven was on the order of 60 samples at a time while the constant humidity chamber could hold 27 samples. Drying is of particular interest to a program of this sort both to obtain water content data and as a means of quenching chemical activity in mellowing or aging materials thus fixing their chemical composition at some given time for later analysis by DSC/EGA or X-ray diffraction.

F. EGA Apparatus for Hydrate Water Determination

Small ground samples, 20-50 milligrams, of cured spent shale specimens retrieved after torsion testing and oven drying at 48°C are encapsulated in the standard Perkin Elmer aluminum foil sample cups. The aluminum lids are fastened by crimping of the top edge of the cup over them in the standard die. One sample at a time is run in the Perkin Elmer DSCI differential scanning calorimeter from 50°C to 500°C. The temperature rate of rise is 10°C per minute. Water vapor and CO_2 evolved into a nitrogen carrier gas are monitored by the gas thermal conductivity cell supplied with the DSCI and by a non dispersive infrared CO_2 analyzer. Under conditions of operation the conductivity cell responds to water vapor and practically not at all to CO_2. The signals are collected by a Hewlett Packard 9825T computer controlling a H.P. 3495 A scanner, 3455 A digital voltmeter and H.P. 9885 M flexible disk drive. Data so collected can be plotted later by a H.P. 9872 A plotter to varied format. The Perkin Elmer DCI gas thermal conductivity cell is of the semi diffusion type. Its ability to discriminate against CO_2 may be due to the 180°C operating temperature used.

Figure IV 2 is an example of the water indication recorded from a series of specimens containing burned TOSCO spent shale and unburned TOSCO spent shale. An advantage of EGA determination of species is that the peak areas may be integrated and are proportional to various species present. X-ray diffraction peaks generally can not be used in this way although x-ray diffraction often gives more positive identification.

G. X-ray Diffractometer

Many x-ray diffraction powder patterns previously were obtained with a Phillips diffractometer scanned with a synchronous motor with peaks plotted on a synchronous motor driven strip chart recorder. These specimens were often of 100% burned TOSCO spent shale with various water contents and curing times and sometimes spiked with gypsum, $Ba(NO_3)_2$, or $BaCl_2$. Autoclave mellowed spent shales were also studied by this equipment. Some of these pertinant previous results are presented later in the present report.

An interesting species formed during autoclaving of the burned TOSCO spent shale appeared to have powder diffraction lines corresponding to the magnesium bearing clay mineral stevensite. The basal spacing and some other lines seemed to confirm this. There was faint evidence of the basal superlattice line also but the low angle scatter and/or interference by the direct beam made this uncertain.

Resumption of x-ray studies on specimens prepared for implementation of the present experimental design was attempted with a revised x-ray diffraction system. This system uses different sensor and amplifier and has been aligned differently. Goniometer scan is by stepper motor and peaks are stored on the hard disk of a Nicolet computer system. The background noise of this system as then aligned was more than with the former uncomputerized system. Also the spectra are obtained on many short segments of ink jet printer paper which must be scotch taped together to give a whole spectrum, moreover with neither 2θ nor intensity rullings on the final chart.

Autoclave mellowed Lurgi (M 14) and burned TOSCO (M 15) samples were run on the Philips diffractometer in standard powder holders at 35 kilovolts and 25 milliamps using the Nicolet computer stepped system at 2 seconds for each .04 2θ step.

Also a series of patterns were made in which a lead knife edge shield was used to cut off various amounts of the grazing direct beam at low angles for 2θ. The specimen was autoclave mellowed burned TOSCO, run M15, which was expected to show a stevensite pattern. So much background was had and/or so little stevensite was present that none could be identified. These negative results and other negative results on concentrated clay sized material on glass slides lead to trial of a Guinier transmission technique with different system hardware.

A raw nearly unretorted TOSCO shale sample obtained by extracting large fragments which had quickly by-passed through the TOSCO II rotary retort was then ground and soaked overnight in distilled water and sonically treated four minutes to further separate the clays. The slurry was filtered through a 62 m mesh to isolate the silt and clay sized particles from the larger aggregates. The clay-silt mixture was centrifuged at 600 RPM for 5 minutes.

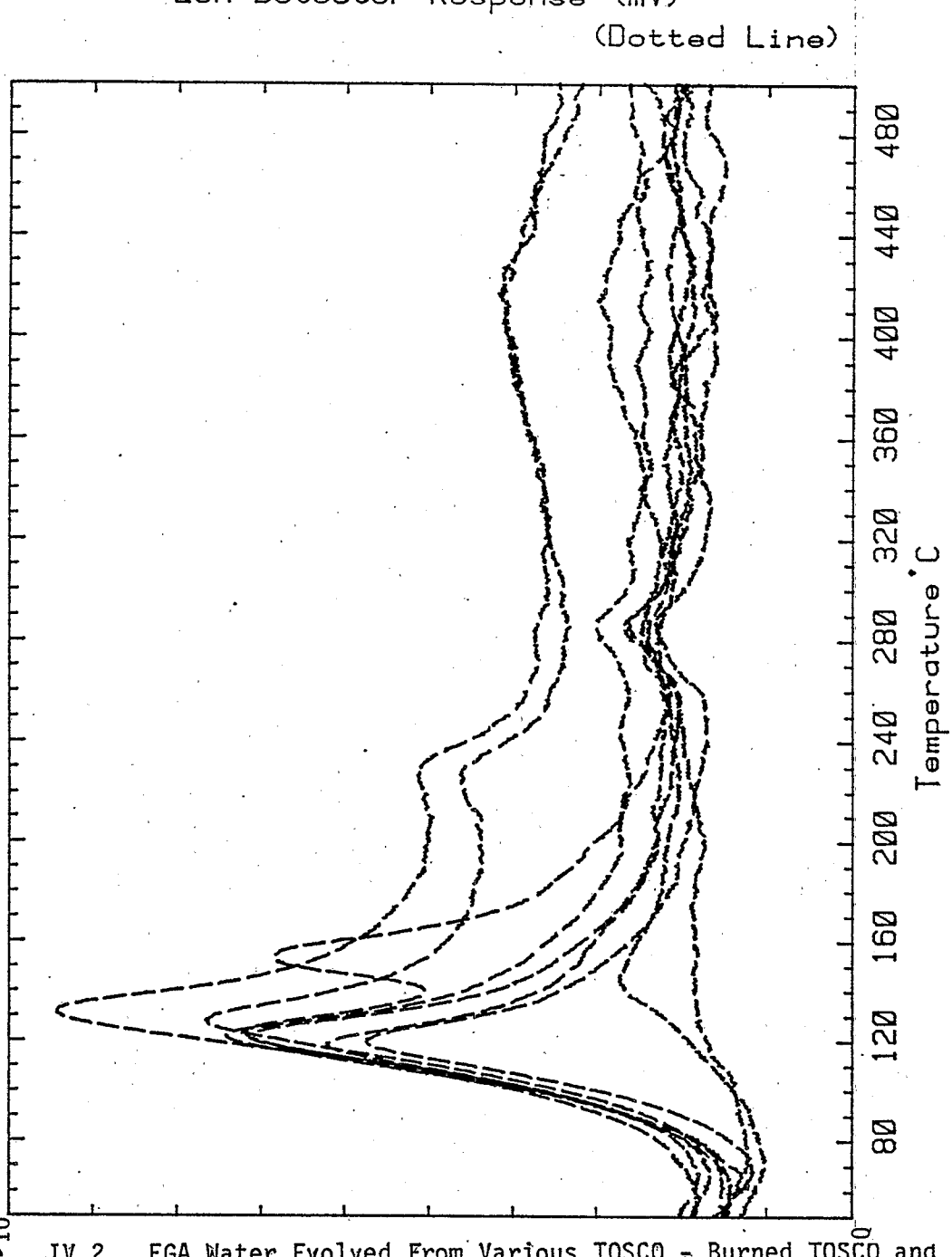

Figure IV 2. EGA Water Evolved From Various TOSCO - Burned TOSCO and Lurgi Spent Shale Samples From Torsion Test

The supernatant liquid was decanted off into a flask and the large volume of water was filtered through a millipore with vacuum. The filter cake contained the clay sized material and was transferred to a glass slide for x-ray diffraction. For each sample 3 patterns were generated: 1) whole untreated sample, 2) clay size, 3) silt size. The expected illite pattern was not seen.

Because the superlattice structure of stevensite was under the threshold 20 of the Philips diffractometer, the Guinier transmission technique was employed. Here, a sample of autoclave mellowed (M 15) burned TOSCO was packed untreated for the first run, and glycolated for the second run.

The sought superlattice lines of stevensite were still not seen and moreover even more background energy was had at low angles of 20 than when M15 was examined with the Philips powder diffractometer system. It might be tentatively concluded that the transmission Guinier technique indicates very finely divided particulates are present in the autoclaved mellowed burned TOSCO sample M 15. Perhaps it might also be concluded that mellowing run M15 was too vigorous for optimum formation of stevensite. Perhaps it formed initially only to be attacked and transformed to some other species of very fine particle size as yet unidientifed. The temperature and pressure of run M15 were slightly higher than for any other autoclaving (see Figure B III 6).

H. Brazil Tensile Strength Test

The behavior of liner material candidates under tension forces may be of some importance in determining their ultimate usefulness. Tensile strength studies are sometimes performed on embankment and dam core materials but no single method has yet been standardized for their direct measurement. Direct uniaxial tension testing and flexure beam approaches were ruled out and the Brazilian method was chosen as having had considerable backing in the literature. Sample preparation was almost identical to the oedometer sample loadings. In addition, aging and sample handling are easier and less subject to detrimental handling.

In this test, cylindrical test specimens are placed under uniaxial compression normal to their diameter. This force creates a diametral tension stress at right angles to the applied force. Failure occurs along the line of compression. Applied load and tensile strain is recorded until failure occurs. The tensile strength of the specimen is then calculated using the formula

$$\sigma_{xc} = \frac{P}{\pi r l}$$

where σ_{xc} = the tensile strength at the specimens center, P = total applied compressive load at failure and r and l the radius and length of the cylinder.

1. Apparatus

A Soil Test U-160 unconfined compression/deformation apparatus was fitted with a motor drive system to provide a constant 0.071 mm/min (0.0028 in/min) rate of crosshead motion. The proving ring assembly was connected

to a linear variable differential transformer (LVDT) which in turn was connected via its power supply and amplifier to one channel of a dual pen strip chart recorder. This channel provided a direct record of the applied load. A second channel was connected via another LVDT to a scissors type caliper assembly that monitored the deformation of the specimen at right angles to the applied compressive load, i.e., tensile strain. The sample end of the calipers were outfitted with pivoting anvils that rested against the sides of the specimen. These anvils allowed an averaging of tensile strain along the entire length of the specimen. Contact with the specimen sides was maintained with a light rubber band located at the LVDT end of the calipers. This provided sufficient springiness to maintain adequate contact between the anvils and specimen while not restricting the strain of the specimen by more than a few ounces of pressure.

In order to insure proper load distribution between the compressive loading plates and the sample under test, narrow rubber strips 16 mm (0.629 in) wide by 3 mm (0.118 in) thick running the length of the test specimen were used. Several different rubber composition were tried, in order to find a reasonable compromise between harder materials which did not conform sufficiently with sample irregularities and softer materials which allowed sample irregularities to come against the loading plates. Many of the samples tested in this project were harder than typically encountered in soil tension testing resulting in a choice of slightly harder than optimum material. The narrow width of the rubber strips prevents the contact area from becoming excessive thus reducing tensile stress through the application of excessive nontangential forces.

2. Calibration

The compression axis of the test apparatus i.e. the proving ring/LVDT assembly was calibrated against an Instron compressive strength machine. The Instron load cell was in turn calibrated with test weights. The proving ring/LVDT assembly proved linear throughout a 300 pound range well in excess of expected tensile test loads. Above 300 pounds, the LVDT was out of range and became nonlinear. This limit was also the upper recommended limit of the proving ring assembly itself.

The tensile strain indicator channel was calibrated by loading the Brazil test apparatus with a 63.5 mm (2.5 in) diameter copper test cylinder. After seating the caliper anvils against the cylinder and zeroing the recorder, the distance between the anvils was widened in successive stages by placing shims between anvil and test cylinder. This action simulated an actual test condition. The increase in width was correlated with the strip chart recorder output for final calibration in Volts/cm (Volts/inch) of strain. Minimum recordable strain is on the order of 0.02%.

3. Sample Preparation

The samples to be tested in accordance to the test plan of Table II 1 were those for which spring oedometer/torsion shear samples were made. Fewer samples were required however since permeation was not a possible variable for the Brazil tensile test. Samples were mixed as for oedometer tests with appropriate water contents, mixed for the recommended 30 minutes and proctor compacted into a 3 piece split brass mold measuring 3.81 cm (1.5 inches) in length and 6.35 cm (2.5 inches) in inside diameter. The polished interior of the mold was greased with a silicone grease as a mold release compound, even so, the removal of the brass sides from several samples proved

disasterous resulting in the removal of large chunks of specimen. Some specimens required the molding of 5 or more samples before a structurally perfect product was produced. Duplicate and triplicate samples were provided for all tests.

Proctoring was done in accordance to Table II 1 with roughly 2/3 of the samples receiving a modified proctor compaction and 1/3 a standard proctor compaction. The number of layers was increased from 5 to 7 for the modified proctoring and from 3 to 5 for the standard proctoring in order to adjust for the 50% increase in compacted thickness. The number of proctor hammer blows per layer was changed to 27 for modified and 23 for standard proctor in order to maintain a consistent energy/volume ratio. Dry densities of test specimen were checked against the dry density of similar samples compacted in the oedometer rings verifying that compaction efforts were indeed about the same in both cases.

Immediately after compaction, the sample retaining ring was stripped away and the sample was briefly dipped into a mixture of 50% parafin, 50% petrolatum in order to provide an impermeable layer inside of which the sample would be aged. These were then placed inside a ziploc bag for further protection and stored until tested. The wax mixture has a very low melting point ($\simeq 50^{\circ}C$) and results in minimal heating and sample water loss. The higher water content Lurgi samples were so mushy at the onset that they were especially difficult to dip and a special spoon had to be used to gently lower them into the wax melt.

4. Testing

The sample to be tested was removed from its ziplock bag and the wax was removed from two diametral sides of the cylinder. The rubber pads were placed on these bare areas and the specimen was inserted into the testing apparatus. The crosshead was manually positioned so as to just contact the test specimen between the proving ring and the crosshead plates as indicated by a slight movement of the recorder pen. The strain anvils were then brought into contact with the sides of the specimen and the strain recording pen was zeroed. The motor drive was then activated and the recorder was turned on. Typical testing times were on the order of one hour/test but ranged from 30 minutes to 3 hours.

All samples failed with a visible vertical tension crack on both faces at the time of failure with the exception of the TOSCO 70/30 mixtures which did not fail below the maximum permissible compression force and the drier samples of a 75/25 mellowed TOSCO series which were weaker along their compaction planes and produced failure in a mode similar to a stack of poker chips. Compressive force at failure ranged from typical soil-clay values of 25 pounds to more cement like 300 pounds. They equate to tensile strengths of from 4 to greater than 50 pounds per square inch. Results of these tests are presented in Table V 3. As seen in this table, tensile strain for the majority of tested specimens was zero just prior to tensile failure indicating a cementatious non plastic behavior.

I. Pneumatic Loaded Arm Oedometers

The spring loaded oedometer cells used in this program are capable of obtaining compressability (consolidation) data only at one loading pressure, i.e. that of the spring force. In addition, due to the fact that

considerable time elapses (2-3 min) between the initial loading of the specimen and the first consolidation data point collection, much and often all of the primary compressibility has already taken place. In order to obtain information regarding the behavior of the test specimens both immediately upon the application of a load (primary consolidation) and under the influences of different loads, a set of pneumatically loaded arm oedometers were employed. Four of these oedometers are available and can be operated simultaneously. A computer controlled interface automatically adjusts load pressures at the required time intervals as well as collecting the consolidation data.

The consolidometers (oedometers) themselves consist of a pivoted lever arm, the long end of which is attached to a pneumatic cylinder. The arm pivot consists of a double row of ball bearings. The short end of the lever arm presses downwards against the top of the sample cell upon application of air pressure to the pneumatic cylinder.

The sample cell consists of a spherical bearing pivot which transfers the force from the arm to the sample loading plate while allowing for pivotal alignment between the arm and loading plate. The sample is confined within a circumferential brass ring and between two porous discs. The loading plate presses downward against the top porous stone whose diameter is less than the confining ring and is therefore free to move in reference to the confining ring. The sample and ring sit upon the lower pore stone which in turn rest on the base of the consolidometer. This arrangement is known as a fixed ring cell in that the ring and lower pore stone are connected with each other and all consolidation occurs with the movement of the upper pore stone. In order to reduce frictional effects between the sample and confining ring, the inner surface of the brass confining ring is highly polished and is lightly greased before use. The pore stones allow for drainage of water pressure from the sample on both faces. For this series of tests, the samples were consolidated at their compacted water content and were not inundated with water as is done in more traditional soil consolidation testing. Ziplock plastic bags maintain a saturated atmosphere around the samples and porestones in order to prevent any drying out of the specimens under test.

Gas pressure is applied to the pneumatic cylinders through a manifold connected to electric solenoid valves which in turn are connected to gas pressure regulators. Gas pressure is supplied to the regulators from high pressure nitrogen bottles with primary pressure regulation at the bottles. The computer then activates the solenoid valves in a timed sequence to provide a series of five different consolidation pressures. The following table lists the pneumatic cylinder pressures and their corresponding consolidation effects as seen by the specimen under test.

Cylinder Gas Pressure	Normal Pressure Applied to Test Specimen			
(PSI)	PSI	Kpa	$\#/ft^2$	$tons/ft^2$
10	19.4	133.6	2791	1.40
20	38.8	267.3	5581	2.79
40	77.5	534.5	11163	5.58
80	155.0	1069.0	22326	11.16
160	310.1	2138.0	44652	22.33

The vertical consolidation of the specimen measured by a linear variable differential transformer (LVDT) which monitors the movement of the oedometer are directly over the sample. Resolution of this measuring device is better than 0.002 mm (7.9×10^{-5} in). The output from the four LVDTs is recorded by a digital printer. Data is recorded under computer control on a logarithmic time base beginning at one second after a load is applied to the specimens under test. After primary consolidation data is collected at one pressure, the next higher pressure is applied to the sample and the log data acquisition timing curve is restarted. A typical consolidation test for all five pressure ranges requires from between 8 and 12 hours. Although secondary consolidation over a long time base could be measured with this apparatus, thermal drift of the pressure regulating system causing long term pressure variations make these measurements impractical. Spring loaded and dead weight oedometers are more suited to these measurements.

1. Sample Preparation

The sample to be tested is first mixed in accordance to the prescribed water content for 30 minutes in a ziplock bag. The sample material is then loaded into a greased retaining ring and compacted to the desired level. Both standard and modified proctor levels of compaction were used on this program in accordance with the mast sample matrix although typically only standard proctor would be considered for consolidation testing purposes. The sample was proctored in the prescribed number of levels and proctor hammer blows. After compaction, the sample is carefully trimmed even with the ends of the sample ring and weighed for initial density determination. The sample is then sandwiched between upper and lower pore stones and the entire assembly is sealed in a ziplock bag. The sample is then placed bag and all in the arm oedometer for testing. After testing, the weight of the sample is again recorded in order to determine any water loss through consolidation and final density. Specimen diameter was 6.35 cm (2.5 in.) with an initial height of 2.54 cm (1.0 in.).

2. Data Reduction

The consolidation reading may be plotted against time on either semilog or square root scales for each incrimental stress applied to a given sample. Higher accuracy is obtained from log time/settlement curves for more clay like materials like the mellowed TOSCO mix materials, while square-root time/settlement curves lend themselves to better analysis of higher permeability more sandy materials such as the Lurgi specimens.

Void ratio, coefficient of consolidation c_v, coefficient of secondary compression c_α, compression index c_c may then be calculated.

V. RESULTS

Data resulting from the main series of experiments previously outlined in the experimental plan, Section II C, are presented in Section V A, Table V 1 and Table V 2. In addition Section V B here presents results of "tensile" strength determination by the Brazil indirect method in a series of experiments paralleling the main experiments except that spring consolidation during curing was omitted. Section V C here contains results from another series of side experiments on the same sort of materials used in compacting specimens for Sections V A, and V B. For Section V C compressiblity of standard proctor and modified proctor compacted materials was determined in 2½ inch diameter by one inch high pneumatic loaded consolidation cells which are here called pneumatic oedometers to distinguish them from the spring oedometers involved in the main series of experiments. These compressibility, coefficients allow further insight on the nature of the materials and changes as curing and consolidation at around 280 psi vertical pressure proceedes.

A. Results from Compacted, Cured, Permeated and Torsion Sheared Specimens of the Spring Oedometers

1. Initial Apparent Dry Density

Precautions and procedure for determination of the apparent dry density of a spring oedometer specimen are in Section IV A. When spent oil shale, particularly burned spent oil shale, is mixed with water hydrates such as brucite, tobermorites, ettringite, gypsum, and possibly some $Ca(OH)_2$ form which cause the true dry density of a specimen to be greater than the apparent dry density determined simply by dividing the weight of dry ingredients forming the specimen by the specimens volume. For the purposes of the present investigation the apparent dry density seems adequate for use in monitoring compaction of the specimens. In determining compaction curves of starting mixes, Section III C, the ASTM method of oven drying a part of the specimen after compacting material to a given volume was not used. Rather, water added was used instead of water found by oven drying.

However, in the oven drying procedure used here on crumbs after the torsion test the oven temperature was set at a relatively low 48°C to preserve as many hydrates as possible. Representative crumbs from each spring oedometer specimen after curing, permeability measurement, (if done), torsion testing, and oven drying at 48°C were then analyzed by a water detecting gas thermal conductivity cell EGA attachment for the Perkin Elmer DSCI differential scanning calorimeter. A temperature ramp limit of 500°C was used for the EGA. By 500°C most of the hydrate water is presumed to be evolved at 10°C per minute rate of temperature rise used.

Table V 1 includes the initial apparent dry densities of the specimens compacted in the spring oedometers after any initial consolidation. These figures should be nearly directly comparable with dry densities presented with compaction curves in Section III F calculated from water added.

2. Mineral Grain Density of Cured Specimens

The mineral grain density of cured material after oven drying at 48°C has been determined by a Beckman air pycnometer for the spring oedometer specimens and entered in Table V 1. Mineral grain density is needed for calculation of void ratio. It also seems to be of value as an indication of

Table V-1 K_o Consolidation in Spring Oedometers

Loading #	Specimen Height cm.	Water Added %	Delta Schaevitz Units/Decade	Secondary Compression Index Co	Modified Secondary Compression Index CoC	Final Mineral Grain Density (Cured and Dried) gm/cc	Initial Unwetted Mineral Grain Density gm/cc	O-ring volume cc	Specimen Loaded Weight gm	Initial Dry Density gm/cc	Cured Void Ratio e_c	Initial Void Ratio e_i	Delta Void Ratios e_c-e_i	EGA Sample Weight mg.	Water Peak Area 50-255C	Water Peak Area 255-500C	Calcd. Total Water Area µV-sec	Measured Total Water Area µV-sec	50-255°C Water % (Dry basis)	255-500°C Water % (dry basis)	50-500°C Water % (dry basis)
30	24.3	27	2.9	4.2-E-4	2.4-E-4	2.65	2.75	.566	145	1.49	.775	.840	-.065	65.6	26119	14597	40716	40898	.24	.41	1.16
31	24.7	27	5.4	4.7-E-4	4.3-E-4	2.61	2.75	"	"	1.47	.734	.871	-.096	65.2	25912	6387	23399	32518	.71	.18	.92
32	22.5	25	11.2	1.6-E-3	9.9-E-4	2.71	2.72	"	"	1.64	.651	.656	-.004	59.6	15391	34651	50042	45896	.48	1.09	1.57
33	25.4	25	23.6	3.3-E-3	1.8-E-3	2.65	2.72	"	"	1.45	.827	.871	-.044	63.1	5969	7661	13630	14903	.17	.22	.40
34	25	22	39.5	5.5-E-3	3.1-E-3	2.65	2.72	.566	145	1.51	.754	.797	-.042	-	-	-	0	-	-	-	-
35	25.3	22	13.4	1.8-E-3	1.0-E-3	2.66	2.72	"	"	1.49	.785	.819	-.034	63.6	11837	17853	29690	31411	.34	.52	.87
36	25.2	24	6.1	8.8-E-4	4.8-E-4	2.68	2.78	"	"	1.47	.219	.886	-.067	-	-	-	-	-	-	-	-
37	25.6	24	1	1.4-E-4	7.8-E-5	2.64	2.78	"	138	1.38	.910	1.01	-.103	-	-	-	-	-	-	-	-
38	25.2	24	2.7	3.9-E-4	2.1-E-4	2.62	2.78	.566	138	1.40	.864	.982	-.118	-	-	-	-	-	-	-	-
39	25.4	23	3.7	5.3-E-4	2.9-E-4	2.69	2.75	"	145	1.47	.826	.864	-.037	62.7	25136	29282	54418	55481	.75	.87	1.63
40	25.4	25	3.6	5.2-E-4	2.8-E-4	2.67	2.81	"	"	1.45	.837	.939	-.102	55.1	67122	52477	119599	120120	2.34	1.83	4.18
41	25.1	28	2.7	3.9-E-4	2.1-E-4	2.65	2.81	"	"	1.43	.845	.962	-.117	-	-	-	-	-	-	-	-
42	25.2	28	1.4	2.0-E-4	1.1-E-4	2.63	2.81	.566	145	1.43	.939	.970	-.130	53.1	54582	55685	110267	111666	1.97	2.01	3.99
43	27.7	22	5.4	7.1-E-4	3.8-E-4	2.60	2.62	"	150	1.41	.844	.857	-.013	57.0	49474	32038	81512	79915	1.65	1.069	2.72
44	27.5	22	2.7	3.6-E-4	2.0-E-4	2.50	2.62	"	150	1.42	.828	.844	-.014	-	-	-	-	-	-	-	-
45	26.9	27	6.5	8.8-E-4	4.8-E-4	2.62	2.52	"	154	1.43	.827	.828	-.001	-	-	-	-	-	-	-	-
46	25.2	22	21.0	2.9-E-3	1.6-E-3	2.70	2.72	.566	150	1.55	.744	.751	-.007	58.0	55290	31265	86555	-	1.81	1.02	2.83
47	25.3	22	22.4	3.1-E-3	1.7-E-3	2.71	2.72	"	"	1.54	.755	.758	-.003	60.5	8355	17359	25714	27686	.25	.54	.79
48	25.1	23	.9	1.2-E-4	7.1-E-5	2.71	2.75	"	"	1.56	.753	.780	-.027	47.8	17718	27695	45412	46404	.69	1.09	1.79
49	25.3	23	1.7	2.3-E-4	1.3-E-4	2.64	2.75	"	"	1.53	.723	.794	-.071	70.4	32052	24017	56069	57375	.65	.65	1.49
50	27.4	22	1.4	1.9-E-4	1.0-E-4	2.61	2.62	.566	150	1.42	.835	.837	-.002	-	-	-	-	-	-	-	-
51	27.4	22	2.3	3.0-E-4	1.5-E-4	2.60	2.62	"	"	1.42	.823	.837	-.014	-	-	-	-	-	-	-	-
52	27.5	27	26.0	3.6-E-3	1.8-E-3	2.61	2.52	"	"	1.36	.915	.919	-.003	-	-	-	-	-	-	-	-
53	24.2	28	1.1	1.5-E-4	9.0-E-5	2.65	2.75	"	"	1.54	.721	.786	-.064	69.6	36096	24715	60811	65658	.97	.66	1.64
54	25.5	22	2.0	2.7-E-4	1.6-E-4	2.65	2.72	.566	150	1.53	.731	.772	-.041	-	-	-	-	-	-	-	-
55	25.7	22	10.2	1.3-E-3	7.9-E-4	2.64	2.72	"	"	1.52	.733	.786	-.048	-	-	-	-	-	-	-	-
56	25.7	23	1.8	2.4-E-4	1.4-E-4	2.61	2.75	"	"	1.50	.733	.823	-.090	50.7	23575	9539	33114	37739	.87	.35	1.22
57	25.7	23	2.1	2.8-E-4	1.6-E-4	2.64	2.75	"	"	1.50	.751	.823	-.071	61.1	25264	11761	37025	36680	.77	.35	1.13
58	23.7	25	.5	6.8-E-4	4.2-E-5	2.7	2.81	.566	155	1.65	.620	.692	-.071	58.2	63409	48603	112012	109139	2.08	1.60	3.69
59	23.4	34	.2	3.6-E-4	2.1-E-5	2.63	2.81	"	150	1.52	.728	.850	-.122	65.6	63420	54965	118385	119466	1.84	1.60	3.45
60	27.9	24	.8	1.0-E-4	5.7-E-5	2.66	2.78	"	160	1.47	.610	.894	-.084	-	-	-	-	-	-	-	-
61	24.5	29	2.7	3.8-E-4	2.2-E-4	2.66	2.78	"	155	1.56	.709	.784	-.075	-	-	-	-	-	-	-	-
62	23.9	28	1.8	2.6-E-4	1.5-E-4	2.71	2.75	.566	150	1.56	.736	.763	-.026	51.8	19683	15461	35144	34745	.71	.55	1.27
63	25.4	24	21.1	2.9-E-3	1.6-E-3	2.66	2.78	"	150	1.51	.755	.838	-.083	-	-	-	-	-	-	-	-
64	23.8	30	2.5	3.8-E-4	2.1-E-4	2.59	2.62	"	140	1.44	.798	.820	-.021	-	-	-	-	-	-	-	-
65	24.2	30	18.3	2.7-E-3	1.5-E-3	2.59	2.62	"	140	1.41	.836	.851	-.016	-	-	-	-	-	-	-	-
66	24.1	29	2.0	2.8-E-4	1.5-E-4	2.67	2.78	.283	150	1.53	.745	.820	-.075	-	-	-	-	-	-	-	-
67	24.1	24	1.5	2.0-E-4	1.2-E-4	2.65	2.78	"	"	1.59	.669	.750	-.081	-	-	-	-	-	-	-	-
68	25.0	25	1.4	2.0-E-4	1.1-E-4	2.67	2.81	"	"	1.52	.760	.852	-.091	63.2	59674	-	59674	74466	1.77	0	1.77
69	24.7	27	10.1	1.4-E-3	8.1-E-4	2.61	2.62	"	"	1.51	.725	.729	-.003	-	-	-	-	-	-	-	-
70	24.7	27	4.0	5.7-E-4	3.2-E-4	2.67	2.72	.283	150	1.51	.762	.793	-.030	-	-	-	-	-	-	-	-
71	24.7	25	16.0	2.2-E-3	1.2-E-3	2.70	2.72	"	"	1.54	.753	.765	-.012	-	-	-	-	-	-	-	-
72	27.0	22	12.4	1.6-E-3	9.1-E-4	2.62	2.62	"	"	1.44	.815	.816	-6.93	-	-	-	-	-	-	-	-
73	26.5	22	3.8	5.1-E-4	2.9-E-4	2.60	2.62	"	"	1.47	.772	.782	-.010	-	-	-	-	-	-	-	-
74	23.9	34	1.4	2.1-E-4	1.1-E-4	2.67	2.81	.283	150	1.48	.801	.897	-.096	-	-	-	-	-	-	-	-
75	25.3	24	1.2	1.7-E-4	9.8-E-5	2.71	2.78	.283	150	1.51	.783	.837	-.049	-	-	-	-	-	-	-	-
76	23.9	25	.9	1.2-E-4	7.5-E-5	2.67	2.81	.566	"	1.59	.674	.763	-.089	-	-	-	-	-	-	-	-
77	24.1	25	3.9	5.4-E-4	3.2-E-4	2.656	2.81	.283	"	1.57	.681	.785	-.103	-	-	-	-	-	-	-	-

Table V-1 K_o Consolidation in Spring Oedometers (Cont'd)

Loading #	Specimen Height mm.	Water Added %	Delta Schaevitz Units/Decade	Secondary Compression Index Ca	Modified Secondary Compression Index CaC	Final Mineral Grain Density (cured and Dried) gm/cc	Initial Unwetted Mineral Grain Density gm/cc	O-ring volume cc	Specimen Loaded Weight gm	Initial Dry Density gm/cc	Cured Void Ratio e_c	Initial Void Ratio e_i	Delta Void Ratios e_c-e_i	EGA Sample Weight mg.	Water Peak Area 50-255C	Water Peak Area 255-500C	Calcd. Total Water Area μV-sec	Measured Total Water Area μV-sec	50-255°C Water % (dry basis)	255-500°C Water % (dry basis)	50-1000°C Water % (dry basis)
78	27.3	30	25	3.5-E-3	1.9-E-3	2.61	2.652	.283	150	1.33	.948	.957	-.008	-	-	-	-	-	-	-	-
79	23.6	30	27.6	3.9-E-3	2.3-E-3	2.59	2.62	"	"	1.55	.674	.840	-.166	-	-	-	-	-	-	-	-
80	28	24	7.1	1.0-E-3	5.0-E-4	2.70	2.78	"	"	1.36	.974	.871	-.103	-	-	-	-	-	-	-	-
81	25.4	24	5.8	8.0-E-4	4.3-E-4	2.67	2.78	"	"	1.45	.840	.656	-.184	-	-	-	-	-	-	-	-
82	25.2	25	23	3.2-E-3	1.8-E-3	2.67	2.66	.283	150	1.55	.674	.871	-.100	-	-	-	-	-	-	-	-
83	25.2	25	28.9	4.0-E-3	2.2-E-3	2.67	2.66	"	"	1.45	.639	.797	-.041	-	-	-	-	-	-	-	-
84	25.8	25	15.9	2.2-E-3	1.2-E-3	2.64	2.65	"	"	1.47	.790	.819	-.028	-	-	-	-	-	-	-	-
85	25.4	25	18.6	2.6-E-3	1.4-E-3	2.66	2.65	"	"	1.49	.779	.886	-.107	-	-	-	-	-	-	-	-
86	26.7	55	25	4.3-E-3	1.8-E-3	2.88	2.80	.283	150	1.14	1.336	1.01	.322	36.4	62200	58651	120841	-	3.36	3.17	6.53
87	25.6	40	18.4	2.9-E-3	1.4-E-3	2.63	2.72	"	"	1.32	1.028	.982	.037	-	-	-	-	-	-	-	-
88	25.5	28	9	1.2-E-3	7.0-E-4	2.65	2.81	"	"	1.45	.820	.864	-.044	68.0	65607	25325	90932	-	1.83	.79	2.53
89	25.4	28	8.5	1.2-E-3	6.7-E-4	2.70	2.78	"	"	1.46	.845	.939	-.093	-	-	-	-	-	-	-	-
90	25.3	27	.7	1.0-E-4	5.7-E-5	2.67	2.75	.283	150	1.48	.805	.962	-.157	73.2	23267	19924	43191	42564	.59	.50	1.10
91	25.6	25	45.5	6.4-E-3	3.5-E-3	2.67	2.72	"	"	1.47	.814	.970	-.156	57.0	8543	9456	17999	18989	.27	.30	.58
92	26.7	55	57	1.0-E-2	4.2-E-3	2.75	2.80	"	"	1.14	1.399	.857	-.541	45.9	67984	57714	125698	-	2.89	2.44	5.33
93	25.6	40	27.1	4.3-E-3	2.1-E-3	2.70	2.72	"	"	1.82	1.038	.844	-.194	-	-	-	-	-	-	-	-
94		22	12.3	1.6-E-3	9.1-E-4	2.66	2.72	.283	150	1.52	.756	.765	-.009	66.9	7154	19888	27042	27450	0.20	0.55	0.75
95		27	16.4	2.3-E-2	1.3-E-3	2.72	"	"	"	1.50	.752	.760	-.008	80.8	9550	9256	18806	19203	0.22	0.21	0.43
96		32	21.0	2.9-E-3	1.6-E-e	2.71	2.72	"	"	1.49	.758	.758	-.010	72.3	12418	18149	39558	31215	0.32	0.46	0.78
97		23	2.6	3.9-E-4	2.1-E-4	2.70	2.75	"	"	1.54	.754	.780	-.026	56.3	12038	7796	19834	20010	0.40	0.26	0.66
98		28	1.5	2.0-E-4	1.1-E-4	2.73	2.75	.283	150	1.53	.719	.772	-.053	67.6	6777	5244	12021	12157	0.19	0.14	0.33
99		33	2.1	2.8-E-4	1.6-E-4	2.71	2.75	"	"	1.50	.700	.729	-.029	43.4	8496	6024	14520	15438	0.36	0.26	0.62
100		22	7.4	1.2-E-3	5.1-E-4	2.59	2.62	"	"	1.44	.823	.838	-.015	62.2	40080	37604	77684	78759	1.20	1.12	2.32
101		27	14.3	2.2-E-3	1.3-E-3	2.58	2.62	"	"	1.37	.907	.915	-.008	58.8	23091	16072	39163	39987	0.73	0.51	1.24
102		32	19.6	3.0-E-3	1.5-E-3	2.57	2.62	.283	150	1.34	.725	.730	-.005	73.8	34307	31878	66185	67143	0.86	0.80	1.66
103		40	24.6	4.2-E-3	1.9-E-3	2.70	2.72	"	"	1.56	1.13	.88	.025	35.8	21361	25810	47171	49187	1.11	1.34	2.45
104		45	31.8	4.6-E-3	2.1-E-3	2.67	2.72	"	"	1.34	1.24	.83	.041	38.4	19857	18454	38311	39942	0.96	0.89	1.85
TOSCO II												-	-	56.9	6367	13019	19386	-	.20	.42	.63
Burned TOS												-	-	42.9	5770	10727	16497	-	.25	.46	.71
Dried M14												-	-	73.0	47553	40850	88403	-	1.23	1.06	2.29
Dried M15												-	-	24.2	29998	37770	67768	66746	2.41	3.03	5.44
Lurgi												-	-	44.01	10946	11382	22328	-	.46	.48	.94

Table V 2 Starting Materials Permeability from "In Situ" Spring Oedometer Specimens, and Results from Torsion Tests

Column # – 1	2	3	4	5	6	7	8	9	10	11
Loading Number	Spent Shale Type	Water Content Percent	Curing Time Before Tor- Days	Proctor Com- paction	Permeability cm/sec	Curing Time Be- fore Perm. Meas. "days"	Time Between Permeation Start and Torsion "days"	Consolidation Pressure PSI	Torsion Confining Pressure PSI	Initial Piston Rod Force Lb	Initial Vertical Pressure PSI
30	TOS90	27	35	Std				257.9	0+++	–	–
31	TOS90	27	35	Std	1.64 E-5	28	7	283.7	125	+40	107.8
32	TOS100	25	39	Std	7.51 E-6	32	7	290.1	126.0	10	102.6
33	TOS100	25	32	Std			–	270.8	117.6	34	100.7
34	TOS100	22	40	Mod	4.45 E-6	34	6	270.1	117.6	47	103.4
35	TOS100	22	37	Mod				288.8	125.4	17	103.5
36	TOS80	24	73	Mod	1.78 E-7	72	1	296.6	207.6	-85	148.2
37	TOS80	24	38	Std	1.84 E-5	32	6	296.6	0	NA	NA
38	TOS80	24	32	Std				257.8	112.0	+3	90.0
39	TOS90	23	39	Mod	1.56 E-6	33	6	296.6	128.8	32	109.9
40	TOS70	25	74	Mod				283.7	198.6	155	190.0
41	TOS70	28	40	Std	3.29 E-8	31	8	283.7	123.2	20	102.3
42	TOS70	28	32	Std			–	283.7	123.2	-20	94.2
43	Lurgi	22	76	Mod	4.62 E-6	69	7	309.5	216.6	-130	146.3
44	Lurgi	22	76	Mod			–	314.6	190.0	-80	135.2
45	Lurgi	27	71	Mod	6.19 E-7	70	1	299.2	209.4	-59	155.0
46	TOS100	22	73	Mod	1.21 E-6	68	5	283.7	198.6	42	166.9
47	TOS100	22	73	Mod				301.7	211.2	-102	147.6
48	TOS90	23	71	Mod	4.19 E-7	68	3	NA	NA	NA	NA
49	TOS90	23	34	Mod			–	255.3	110.9	23	93.1
50	Lurgi	22	14	Mod			–	309.5	173	-53	127.2
51	Lurgi	22	15	Mod	6.40 E-6	14	1	283.7	135	0	107.7
52	Lurgi	27	18	Mod	9.78 E-7	14	4	314.6	140	top 3/32" O-ring dragged	
53	TOS90	28	19	Mod	9.05 E-7	14	5	278.5	200	-100	139.1
54	TOS100	22	21	Mod	2.89 E-6	17	4	299.2	130	70	117.9
55	TOS100	22	21	Mod	2.92 E-6	17	4	299.2	130	-20	99.6
56	TOS90	23	25	Mod	1.20 E-6	17	7	299.2	130	-55	92.5
57	TOS90	23	25	Mod	1.20 E-6	17	7	291.4	130	10	105.7
58	TOS70	25	38	Mod	3.71 E-8	33	3	288.8	125.4	-20	95.9
59	TOS70	34	38	Mod	2.03 E-9	33	3	299.2	129.9	20	107.7

Table V-2 (Cont'd)

Column # - 1 Loading Number	Spent Shale Type	2 Water Content Percent	3 Curing Time Before Tor- Days	4 Proctor Com- paction	5 Permeability cm/sec	6 Curing Time Be- fore Perm. Meas. "days"	7 Time Between Permeation Start and Torsion "days"	8 Consolidation Pressure PSI	9 Torsion Confining Pressure PSI	10 Initial Piston Rod Force Lb	11 Initial Vertical Pressure PSI
60	TOS80	24	38	Mod	4.67 E-7	32	4	309.5	134.3	-5	106.1
61	TOS80	29	39	Mod	4.29 E-8	32	5	294.0	127.7	-25	96.7
62	TOS90	28	48	Mod	1.24 E-6	29	19	283.7	200.4	NA++	NA
63	TOS80	24	28	Mod			-	281.1	122.1	10	99.4
64	Lurgi	30	46	Std	8.82 E-7	32	14	283.7	198.6	-27	152.9
65	Lurgi	30	44	Std			-	265.6	0+++	99.7	20.3
66	TOS80	29	29	Mod	2.10 E-7	23	6	286.3	124.3	-20	95.1
67	TOS80	24	16	Mod			-	288.8	125.4	-20	95.9
68	TOS70	25	43	Mod			-	288.8	202.2	-40	153.1
69	Lurgi	27	43	Mod	2.31 E-7	40	3	283.7	198.6	-20	154.3
70	TOS100	27	23	Std	5.08 E-6	16	7	286.3	124.3	30	105.2
71	TOS100	25	38	Std	3.30 E-6	15	18	283.7	198.6	0	158.4
72	Lurgi	22	38	Mod	2.25 E-6	35	3	296.6	207.6	-110	143.1
73	Lurgi	22	38	Mod			-	299.2	209.4	-130	140.5
74	TOS70	34	34	Mod	3.19 E-9	21	13	260.5	182.3	-55	134.2
75	TOS80	24	65	Mod	4.47 E-7	31	3	283.7	198.6	-195	118.7
76	TOS70	25	37	Mod	1.99 E-9	36	4	281.1	196.8	-60	144.7
77	TOS70	25	32	Mod			-	245.0	171.5	-70	122.5
78	Lurgi	30	25	Std	3.55 E-6	22	3	291.4	204.0	-140	134.2
79	Lurgi	30	22	Std			-	275.9	193.2	-120	129.6
80	TOS80	24	25	Std	1.77 E-6	22	3	299.2	209.4	-162	101.0
81	TOS80	24	22	Std			-	299.2	209.4	-35	159.9
82	MelLurgi75	25	24	Mod	2.44 E-6	24	2	288.8	202.2	-155	129.7
83	MelLurgi75	25	29	Mod	1.75 E-6	22	3	301.7	211.2	-180	131.8
84	MelLurgi50	25	24	Mod	2.67 E-6	22	2	283.7	198.6	-100	138.0
85	MelLurgi50	25	29	Mod	169 E-6	30	3	287.6	201.3	-90	142.2
86	MelTOS75+TA	55	24	Mod	3.84 E-8	24	1	281.1	205.8	-90	145.8
87	MelTOS50	40	24	Mod	4.36 E-7	24	1	294.0	196.8	-20	152.9
88	TOS70	28	11	Std			-	296.6	207.6	-40	157.4
89	TOS80	28	12	Std	1.50 E-6	13	1	285.0	199.5	-80	142.8
90	TOS90	27	11	Std			-	270.8	189.6	-102	130.4
91	TOS100	25	12	Std			-	286.3	200.4	-22	155.3
92	MelTOS75+TA	55	10	Mod	1.78 E-7	10		273.4	191.4	-80	136.3
93	MelTOS50	40	11	Mod	3.64 E-7	11	2	288.8	202.2	30	167.4
94	TOS100	22	295	Mod	2.25 E-6	290	5	309.5	216.0	64	79.6
95	TOS100	27	293	Mod	2.38 E-6	290	3	271.0	190.0	10	78.9
96	TOS100	32	281	Mod	2.73 E-6	276	5	232.1	162.5	93	50.6

Table V-2 (Cont'd)

Column # - 1	2	3	4	5	6	7	8	9	10	11
Loading Number	Spent Shale Type	Water Content Percent	Curing Time Before Tor- Days	Proctor Com- paction	Permeability cm/sec	Curing Time Be- fore Perm. Meas. "days"	Time Between Permeation Start and Torsion "days"	Consolidation Pressure PSI	Torsion Confining Pressure PSI	Initial Piston Rod Force Lb	Initial Vertical Pressure PSI
97	TOS90	23	264	Mod	6.51 E-7	257	7	283.7	198.6	32	85.6
98	TOS90	28	246	Mod	6.22 E-7	243	3	283.7	198.6	20	88.7
99	TOS90	33	247	Mod	6.61 E-7	237	10	257.9	180.5	95	55.9
100	Lurgi	22	264	Mod	3.3 E-6	250	14	296.6	207.6	124	64.0
101	Lurgi	27	231	Mod	4.9 E-7	221	10	296.6	207.6	100	73.9
102	Lurgi	32	230	Mod	4.2 E-7	225	5	258.1	180.5	84	99.7
103	MelTos40	40	260	Mod	8.2 E-7	253	7	263.1	184.5	37	105.1
104	MelTos45	45	288	Mod	9.3 E-7	268	20	232.1	162.5	30	95.5

++Pin Toggles broken before pulling sheath
*Normalized to adjusted vertical pressure of peak shear strength after raising platen
**Normalized to verti. press. at peak str. without raising planten
+ Due to specimen fracture
+++Normalized to vert. press. at peak str. without raising platen

Column number references:
10 - After confining pressure applied and spring removed
11 - After confining pressure applied and spring removed $\frac{Ca}{4.909} + 0.79756$

Table V-2 (Cont'd)

Column	12	13	14	15	16	17	18	19	20	21	22
Loading Number	$C_b = K+C_a$ Adjusted[a] Piston Rod Force Lb	$\frac{K+Ca}{4.909}+.7975b$ Adjusted Vertical Pressure PSI	P LVDT Peak Shear Volts	R LVDT Resid. Shear Volts	52.17P Peak Shear Strength PSI	^{O} P Peak Friction Angle Degrees	52.17R "Residual" Shear Strength PSI	^{O} R "Residual" Friction Angle Degrees	$\frac{P-R}{P}$ Torsion Brittleness Index	Initial Torsion Stiffness Volts/6^{O}	Twist at Peak Strength Degrees
30	-	-	-	-	-	-	-	-	-	-	-
31	+146 peak	129	2.43								
	-40 res	91		2.10	126.8	44.4	155**	50.1	-.222	2.43	10
32	390	180	2.95	2.85	153.9	40.5	148.7	39.6	.0338	5.88	21
33	360	167	2.7	2.7	140.9	40.1	140.9	40.1	0	7.14	25
34	378	170	2.8	2.8	146.1	40.5	146.1	40.5	0	6.45	33
35	390	179	3.1	3.02	161.7	42.0	157.5	41.3	.0260	5.71	24
36	643	296	5.54	NA	289.0	44.3	NA	NA	NA	9.7	NA
37	NA	NA	NA	NA	NA	NA	NA	NA	NA	7.14	NA
38	294	149	3.48	3.2	181.6	50.6	166.9	48.2	.0805	5.55	9
39	399	184	3.45	3.45	178.0	44.05	178.0	44.05	0	6.66	30
40	614	283	6.7	5.76	349.5	50.9	300.5	46.7	.1403	8.6	12
41	382	176	4.37	4.1	228.0	52.3	213.9	50.6	.0608	9.09	6 est
42	385	176	4.20	3.56	219.1	51.1	185.7	46.4	.152	7.41	9
43	671	309	5.45	5.40	284.3	42.6	281.7	42.3	.0092	7.8	20
44	682	290	4.4	4.6	229.5	38.3	230.0	39.6	-.0454	8.1	20
45	648	299	5.69	5.53	296.8	44.8	288.5	44.0	.0280	7.8	21
46	615	166	7.00	5.70	365.2	52.2	297.4	46.3	.186	7.8	8.5
47	654	301	4.66	4.66	243.1	38.9	243.1	38.9	0	6.0	20
48	NA	NA	NA	NA	NA	NA	NA	NA	Brittle	NA	NA
49	345	158	3.5	3.16	182.6	49.0	164.8	46.1	.0975	6.00	21
50	-10peak	135	2.9								
	-148res	107		2.4	151.3	48.1	157.8**	49.3	-.0430	5.77	12
51	-50peak	97	2.4		125.2	52.1					
	-65res	94		2.2			118.6**	50.6	.0527	6.38	19
52	no data	NA	NA	NA	NA	NA	NA	NA	NA	NA	NA
53	-65	146	2.72	2.72	141.9	44.1	141.9	44.1	0	6.06	24
54	-50@peak	93	2.1		109.5	49.5					
	-20@res	99		1.87			100.4**	44.4**	.083	7.5	13
55	130@peak	130	2.5		130.4	45.1					
	-25@res	98		2.26			156.3*	50.2*	-.0199	7.5	15
56	+60@peak	115	2.62		136.7	49.7					
	-70@res	89		2.20est			148.8**	52.1**	-.088	6.52	16
57	-20@peak	99	2.3	NA	120.0	50.3	NA	NA	NA	5.71	16

Table V-2 (Cont'd)

Column	12	13	14	15	16	17	18	19	20	21	22
Loading Number	$C_b = K+C_a$ Adjusted Piston Rod Force Lb	$\frac{K+Ca}{4.909}+.7975b$ Adjusted Vertical Pressure PSI	P LVDT Peak Shear Volts	R LVDT Resid. Shear Volts	52.17P Peak Shear Strength PSI	θ_P Peak Friction Angle Degrees	52.17R "Residual" Shear Strength PSI	θ_R "Residual" Friction Angle Degrees	$\frac{P-R}{P}$ Torsion Brittleness Index	Initial Torsion Stiffness Volts/6°	Twist at Peak Strength Degrees
58	389	179	3.8	3.7	198.2	47.9	193.0	47.1	.0262	8.69	14 est
59	403	185	4.95	4.0	258.2	54.3	208.7	48.3	.192	8.77	10
60	416	191	3.95	3.85	206.1	47.0	200.9	46.3	.0252	4.29	15
61	396	182	4.43	3.76	231.1	51.7	196.2	47.1	.151	7.69	9.0
62	NA	NA	NA	NA+	NA	NA	NA+	NA+	NA	NA	NA
63	358	170	3.56	NA+	185.7	47.5	NA+	NA+	NA	13.0	
64	615	283	5.2	4.8	271.3	43.7	250.4	41.4	.077	7.78	16.8
65	99	20	.64	.40	33.4	58.7	20.9	-	-	-	1.5
66	385	177	3.97	3.50	207.1	49.4	182.6	45.9	.118	8.47	2.4
67	389	179	3.6	3.25	187.8	46.3	169.6	43.4	.097	6.06	10.2
68	626	288	5.87	5.40	306.2	46.7	281.7	44.3	.80	8.3	8.0
69	615	283	5.48	4.78	285.9	45.2	249.4	41.3	.128	7.5	12.5
70	375	175	2.8	2.9	146.1	39.8	151.3	40.8	-.035	5.00	12.0
71	911	343	4.7	4.42	245.2	35.5	230.6	33.8	.059	6.66	21.0
72	643	296	5.37	5.1	280.1	43.4	266.1	41.9	.0500	6.0	12
73	648	299	5.3	5.1	276.5	42.7	266.1	41.7	.0376	8.8	13
74	564	260	6.35	4.75	331.3	51.8	247.8	43.6	.252	8.13	6.6
75	615	283	5.6	5.08	292.1	45.8	265.0	43.0	.093	7.7	13.0
76	609	281	4.5	4.5	234.8	39.9	234.8	39.9	0	4.2	27
77	530	244	6.1	4.7	318.2	52.4	245.2	45.0	.229	7.9	7.5
78	632	291	4.6	4.36	240.0	39.4	227.5	38.0	.0521	7.0	16
79	598	276	4.56	4.4	237.9	40.76	229.5	39.7	.0353	6.67	12.6
80	648	299	4.8	4.8	250.4	39.9	250.4	39.9	0	9.7	11
81	648	299	4.6	4.6	240.0	38.7slip	240.0	38.7	0 slip	12.0	6.0
82	626	288	4.3	4.3	224.3	37.8	224.3	37.8	0	7.8	17
83	654	301	4.6	4.75	240.0	38.5	247.8	39.4	-.0326	7.1	18
84	615	283	4.67	4.53	243.6	40.6	236.3	39.8	.0300	8.8	18
85	623	287	4.58	4.35	238.9	39.7	226.9	38.3	.050	6.5	15
86	637	294	4.4	5.1	229.5	38.0	266.1	42.1	-.159	8.0	8
87	609	281	4.1	4.3	213.9	37.3	224.3	38.6	-.048	6.7	21
88	643	295	6.5	5.2	313.0	48.8	271.3	42.5	.200	7.6	9.5
89	618	285	4.8	4.65	250.4	41.3	242.5	40.4	.0312	6.0	7.5
90	587	270	4.24	4.24	221.2	39.2	221.2	39.2	0	6.4	18

Table V-2 (Cont'd)

Column	12	13	14	15	16	17	18	19	20	21	22
Loading Number	$C_b = K+C_a$ Adjusted Piston Rod Force Lb	$\frac{K+Ca}{4.909}+.7975b$ Adjusted Vertical Pressure PSI	P LVDT Peak Shear Volts	R LVDT Resid. Shear Volts	52.17P Peak Shear Strength PSI	ϕ_P Peak Friction Angle Degrees	52.17R "Residual" Shear Strength PSI	ϕ_R "Residual" Friction Angle Degrees	$\frac{P-R}{P}$ Torsion Brittleness Index	Initial Torsion Stiffness Volts/6°	Twist at Peak Strength Degrees
91	620	286	4.2	4.4	219.1	37.4	229.5	38.7	-.0476	7.9	26
92	592	273	4.3	4.6	224.3	39.4	240.0	41.3	-.0698	7.3	36
93	626	288	4.28	4.5	223.3	37.7	234.8	39.1	-.0514	NA	NA
94	691	307	4.25	4.35	221.7	35.8	227.0	-0.024	-.024	3.8	25.2
95	687	271	4.51	4.46	235.3	41.0	232.7	0.011	0.011	8.7	18.0
96	503	287	3.65	3.67	190.4	33.6	191.5	-0.005	-0.005	5.6	33.0
97	720	282	4.30	4.52	224.3	38.5	235.8	-0.051	-0.051	7.9	19.8
98	622	259	4.01	4.10	208.7	38.9	213.9	-.026	-.025	9.9	25.3
99	598	296	4.82	2.80	251.5	40.4	146.1	0.419	0.419	9.3	13.2
100	614	301	4.58	4.32	238.9	38.4	225.4	0.057	0.057	8.9	12.0
101	663	372	4.55	2.85	237.4	32.5	201.0	0.154	0.154	8.3	15.1
102	789	256	4.60	4.52	240.0	43.2	235.8	0.017	0.017	11.3	13.8
103	571	261	4.00	4.00	208.7	38.6	208.7	0.000	0.000	6.6	6.0
104	509	235	3.82	3.65	199.3	40.3	190.4	0.045	0.045	4.3	6.6

++Pin Toggles broken before pulling sheath
*Normalized to adjusted vertical pressure of peak shear strength after raising platen
**Normalized to verti. press. at peak str. without raising planten
+ Due to specimen fracture
+++Normalized to vert. press. at peak str. without raising platen

Column number references:
12. $C_b = K+C_a$, Before Torsion
13. $\frac{K+C_a}{4.909}+ 0.7975b$

extent of hydrate formation. Also included in the initial mineral grain density.

3. Cured Specimen Void Ratio

The void ratio for natural soils is often used for correlating with permeability for a given type of soil. A cured specimen void ratio computed from the apparent initial dry density of a loaded oedometer specimen and its mineral grain density after curing is presented in Table V 1. The angle of internal friction at peak strength has also been correlated with void ratio for some materials later.

4. Secondary Compression Index

The secondary compression coefficient C_α is determined from the semilog slope of the secondary compression part of the consolidation curves of the spring oedometer specimens. In general the secondary compression rate is lower for cemented specimens. Many specimens showed increasing slopes at longer times on the semilog plot. Some secondary compression curves are shown in Figure V 1. Final $C\alpha$ values are tabulated in Table V 1.

5. Permeability Coefficient

The permeability of the spring oedometer specimens has generally been determined at a hydraulic differential of 20 psi across the nominal one inch thick specimen. Too low a pressure sometimes allowed no flow at all, perhaps due to hydrophobicity of some specimens. Some specimens at intermediate pressure would balk sometimes and flow again at other times. This also is believed due to hydrophobicity. Obviously an emplaced liner can not rely on hydrophobicity which can reject only, say, 5 psi water head, or whose hydrophobicity is perhaps fleeting. The permeability coefficients are presented in Table V 2, column 5.

6. Shear Modulus During Torsion

Initial stiffness is measured by the initial stress/strain slope during torsion. Cemented, highly compacted, or over consolidated specimens show steeper slopes than soft, normally consolidated, or low brittleness index specimens. The initial slope of the torsioned spring oedometer specimens is given in Table V 2 may be an auxillary measure of specimen softness. The shear modulus G (column 23) has been calculated from this data.

7. Peak Shear Strength

Beyond the initial steep part of the torsion stress/strain curve the curve droops and often a maximum stress develops from which the peak shear strength used here is calculated by the empirical formula having the same form as the derived formula for τ_R discussed later:

$$\tau_p = \frac{3\ (\text{moment})}{2\pi r^3} = \frac{\text{moment}}{\frac{2}{3}\pi(1.25)^3}$$

$$= \frac{\text{inch lbs moment}}{4.091}$$

$$= (52.17)\ (\text{LVDT volts}),\ {}_p\tau \text{ in lb/in}^2$$

The volts EMF output of the LVDT system of the torsion proving ring is read from the stress/strain curves recorded by an X-Y recorder. The X axis of

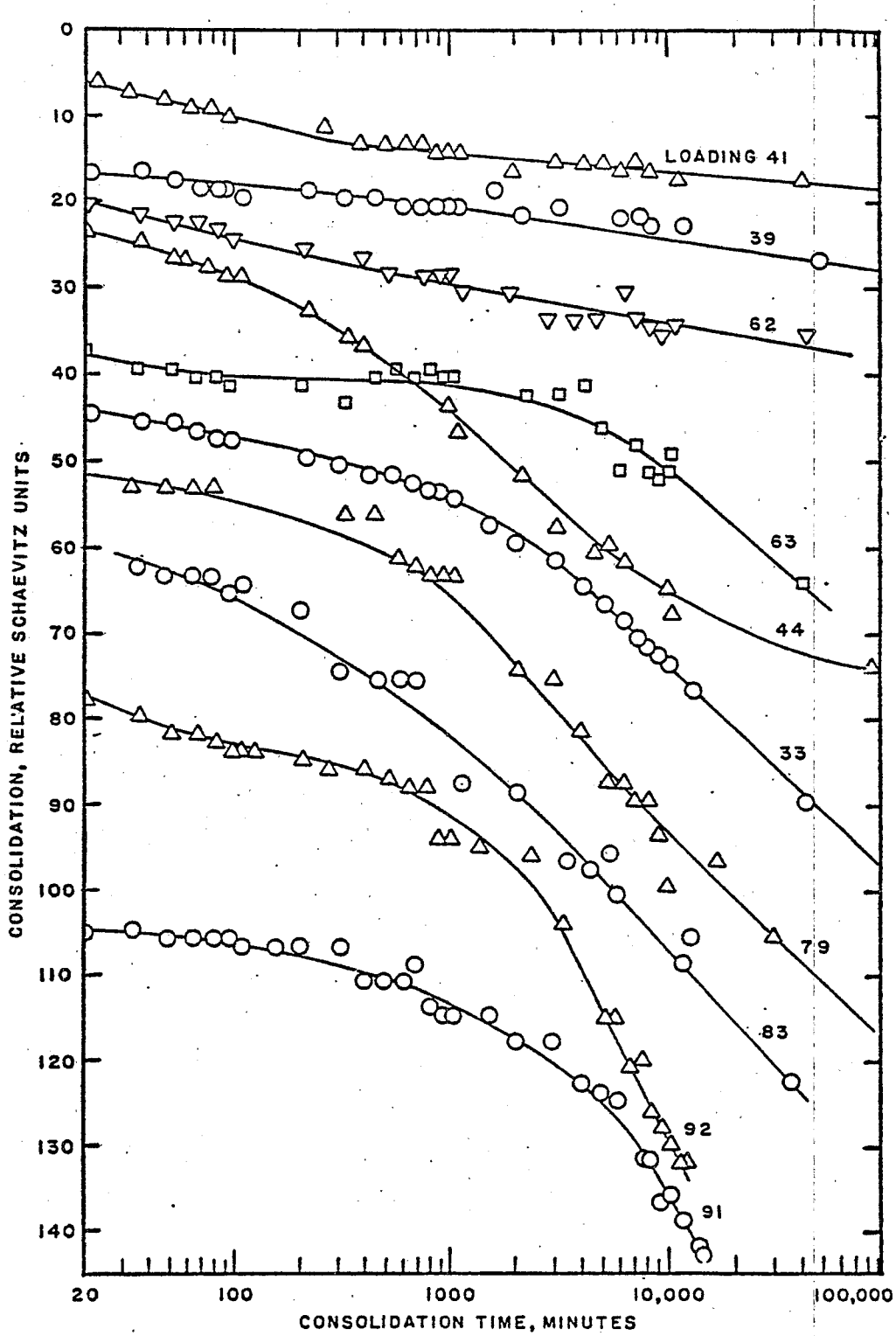

Figure V 1. Some Secondary Compression Curves of Spring Oedometer Specimens.

the pen is synchronized to the extent of rotation of the worm driving the worm gear and a potentiometer while the Y axis of the pen is driven by the LVDT amplifier output.

The peak shear strengths are tabulated in Table V 2.

8. Residual Shear Strength

After a certain amount of shear occurs in the torsion specimen following peak shear strength development the stress subsides and generally asymptotes to a lower value than the peak stress. This is called for these tests the residual shear strength, $_R$, which is usually characteristic of a certain degree of slipperyness of shear "planes" developed in the specimen as shear procedes although sometimes simple shear with no planes develops instead. The "planes" can have a higher pore pressure than the specimen as a whole due to compaction and squeezing out of water from material in the planes or dryer than the whole because of expansion of the material there during shear. In any case, however, any platy clay - like minerals will generally become oriented parallel to the shear plane and eventually increased slipperyness results. Much of the fabric structure causing peak shear strength is worked out during the shearing process producing the residual shear planes. Residual shear strengths are more predictible and characteristic of mineral grain composition of the specimen than are peak strengths which are dependent on distribution of cement, void ratio, water content, soil fabric structure, and age. Table V 2 presents residual strengths of the spring oedometer specimens after torsion. Another concept might call these strengths the "critical" strengths and say these specimens had not yet reached the true residual strength stage of strain which requires a ring shear apparatus which can produce even greater displacement at the shear plane.

A formula for computing residual strength from the torque at that time is

$$\tau_R = \frac{3(\text{moment})}{2\pi r^3} = \frac{\text{moment}}{\frac{2}{3}\pi (1.25)^3}$$

$$= \frac{\text{inch lbs moment}}{4.091}$$

$$= (52.17)\ (\text{LVDT Volts}) \text{ for the present apparatus, } {}_{p}\tau \text{ in } lb/in^2$$

τ_R calculated this way assumes resistance constant with radius due to plasticity of the specimen when residual shear strength has been attained (where residual strength equals critical strength) or constant with radius when sliding friction operates in the slip plane form of residual strength.

9. Brittleness Index

The brittleness index is usually given by

$$BI = \frac{\tau_P - \tau_R}{\tau_P}$$

Non cemented, non overconsolidated, loose structured silty or boulder clay like material may have nil brittleness index. This seems desirable in a liner in that in such material shear planes are less likely to develop and a

TRIAXIAL TORSION SHEAR TEST WORKSHEET

Date of torsion test		Sept. 25, 1985	
Loading No.		36	
Sheath No.		21	
Shale mix and water, %		Tosco 80/20 24	
Compaction, std. or mod. proctor?		C, T_3 Mod. Proc	
Was Specimen permeated?		Yes	
Spring loading hydraulic pressure, a	a	1150	
Consolidation pressure from spring 0.2579 a=A	A	296.6	PSI
Containing can pressure = 0.7 A = b	b	207.6	PSI
Instron pen above balance baseline after pulling sheath observed, c	c	-85	LB
Initial mismatch in soil skeleton pressure after pulling sheath $D = \frac{C}{\quad} - 0.11393a$	D	-148.3	PSI
Increase instron pen reading before torsioning by 4.909 D = X by raising lower platen on slow speed with manual knob	X	728.2	LB
This results in pen position above balance baseline of X + C to hold during torsioning by manual platen position knob adjustment	X+C	643.2	Lb

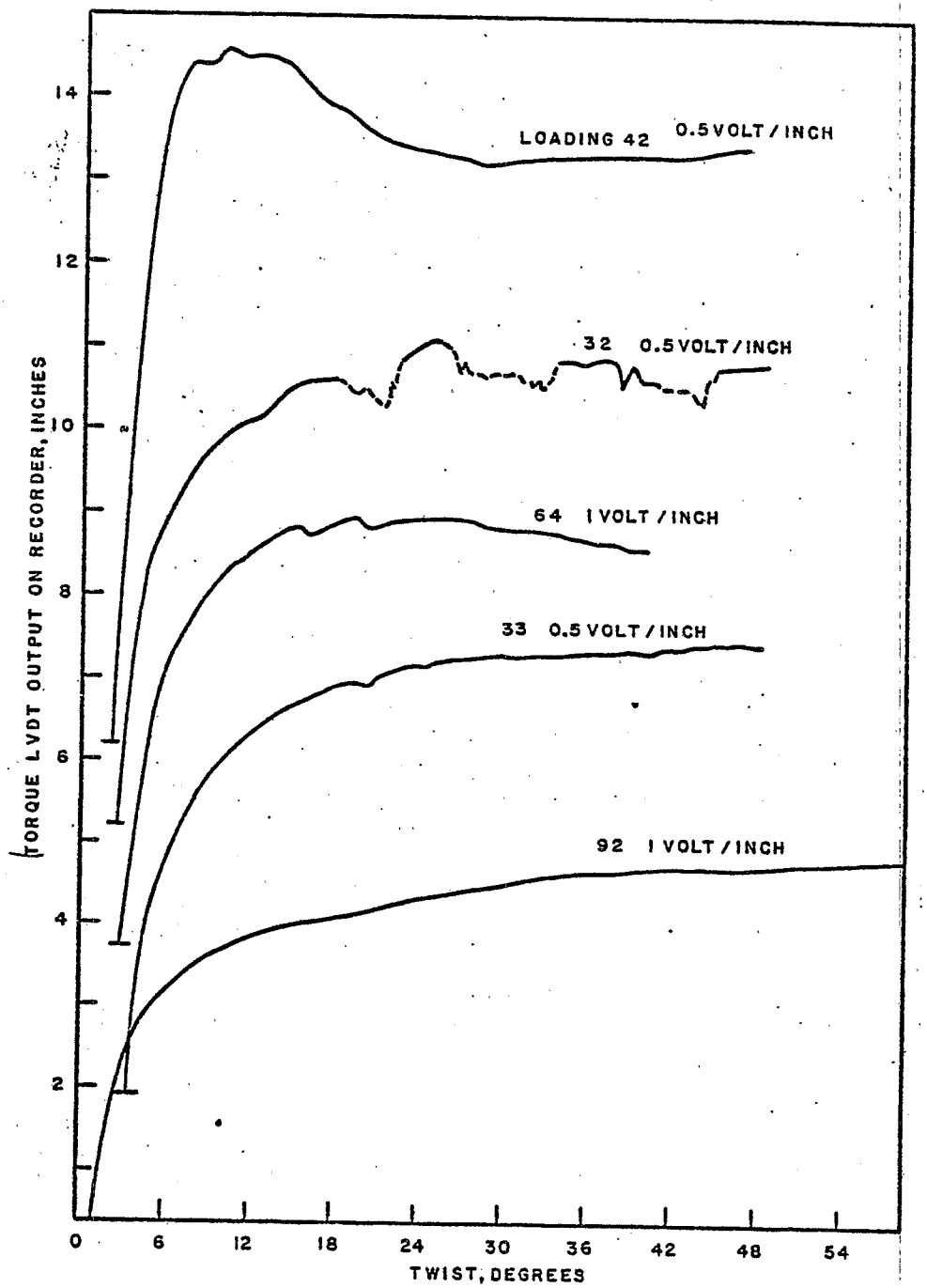

Figure V 2. Some Torsion Stress-Strain Curves, Loadings 32, 33, 42, 64, 92

simple shear or zone shear action may occur. Even low amounts of cementation seem to prevent simple shear but promote shear planes and development of a counter system of jointing during strain in these materials. Table V 2, (column 20) presents the brittleness indices determined.

Figure V 2 shows some torsion stress-strain curves for some oedometer specimens in the triaxial torsion apparatus. Several types of curve are presented. Curve A is for a soft uncemented silty specimen, B for a mildly cemented specimen, C for a more strongly cemented specimen, and D for the special mix of mellowed burned TOSCO with some burned TOSCO. The brittleness index of curve A is zero, of curve B is low, of curve C is high, and of curve D is negative. The negative brittleness index occurs with low permeability clayish specimens which drain more slowly than the usual silty specimen. This is believed to cause some pore pressure development during deformation at the rapid twisting rates of around 9 degrees per minute standardized here when contraction of the specimen soil skeleton during shear occurs.

10. Photographs of Sheared Specimens

Before "loading" or compacting the material into the spring oedometer sheath four yellow acrylic paint stripes were brushed longitudinally on the inside of the sheath at a position including the future location of the specimen in the sheath. These stripes easily transferred from the Teflon-coated inner sheath surface to the specimen when it was extruded from the sheath by sheath raising before torsioning. The greased gum rubber membrane did not attract the paint stripe either after the rubber was laid on the specimen during the sheath raising operation nor during torsioning itself. As a result, if the yellow stripes were not disturbed during compacting by the proctor hammer, the yellow stripes served as a marker of movement of the specimen's outer surface during torsion shear. Shear planes are often clearly distinguished that would be indistinct without the marker lines. Simple shear or zone shear of soft specimens of low brittleness index is indicated by development of diagonal marker stripes without discontinuities. By this means it became apparent that only a little cementation or brittleness index served to inhibit simple shear and produced a few shallow angle shear planes in spiral configuration oriented such that the lowered normal stress on the planes due to rotation of principal stresses was contributing to the development of the spiral fracture.

Figures V 3, 4, 5, 6, and 7 are photographs of marker stripes of the typical torsioned specimens corresponding to the stress-strain curves of Figure V 2.. When the piston was removed by pulling as nearly vertically as possible some tension developed in the specimen which sometimes caused cracking along the weakened slip planes and their easier observation. Joints also were opened up which may not have been very obvious otherwise. These tend to cut across the slip planes at 45°.

11. EGA Determined Hydrate Water

Hydrate species water evolution and carbon dioxide evolution curves of some of the spring oedometer specimens after torsion testing are presented in Figures V 8-32. By integrating the area under peaks along the curves the hydrate water in a particular species formed during mixing with water and curing may sometimes be approximated. Figures V 33-36 show the raw materials autoclave mellowed Lurgi M 14, autoclave mellowed burned TOSCO M 15, unwetted Lurgi, and unwetted burned TOSCO, respectively.

Thus the peaks of water evolution contained in an EGA curve are an aid in identification of hydrate species such as ettringite, gypsum, brucite, etc. and their assay. This work has been done in conjunction with X-ray diffraction as often EGA peaks of two species will overlap. To further aid in identification of species evolved CO_2 has also been recorded with the evolved water on the same chart. Table V 1 summarizes the hydrate water determined by EGA up to 500°C. One entry is for total evolved water, another is for water to 255°C, and another for 255 to 500°C.

B. Brazil Test Results

Table V 3 is a summary of Brazil tensile test results with sample designation numbers paralleling the loading number of Tables B-V I and B-V 2. Suffix B indicates Brazil test, small letters distinguish duplicate specimens.

C. Pneumatic Oedometer Compressibility Coefficients

Table V 4 summarizes results of pneumatic arm oedometer study of standard proctor and modified proctor specimens of freshly mixed material.

TABLE V 3 Summary of Brazil Tensile Strength Tests

Sample Designation	Sample Type	Water Content% (Initial)	Compaction Effort*	Curing Time (Days)	Normal Force at Failure (Lbs)	xc Tensile Strength (PSI)	Lateral or Tensile Strain at Failure	Final Stiffness to Vertical Load Volts
71B a	TOSCO II	25	s	22	24.2	4.1	10	2.3
71B b	"	25	s	22	25.1	4.3	11	2.1
54B a	"	22	m	22	47.5	8.1	NA	3.1
54B b	"	22	m	22	47.5	8.1	4	3.1
54B c	"	22	m	22	45.5	7.7	7	3.2
32B a	"	25	s	45	27.9	4.7	16	2.2
32B b	"	25	s	45	26.7	4.5	18	2.1
34B a	"	22	m	45	43.9	7.5	2	3.5
34B b	"	22	m	44	41.5	7.1	10	3.1
47B a	"	22	m	57	39.1	6.6	5	2.8
47B b	"	22	m	57	39.1	6.6	5	3.5
94B a	"	22	m	255	55.9	9.4	0	3.1
94B b	"	22	m	255	52.6	8.9	0	3.5
95B a	"	27	m	260	37.9	6.4	0	2.2
95B b	"	27	m	260	38.6	6.6	0	2.4
96B a	"	32	m	255	30.9	5.2	0	1.6
96B b	"	32	m	255	27.9	4.7	0	1.6
70B a	TOSCO 90/10	27	m	21	63.9	10.9	0	3.8
70B b	"	27	m	21	66.3	11.3	0	3.9
70B c	"	27	m	21	55.9	9.5	0	3.8
62B a	"	28	m	17	55.9	9.5	0	4.1
62B b	"	28	m	17	62.9	10.7	0	3.7
62B c	"	28	m	17	67.9	11.5	0	3.2
56B	"	23	m	36	93.8	15.9	2	
53B a	"	28	m	42	61.9	10.6	3	3.8
53B b	"	28	m	42	62.9	10.6	4	4.2
39B	"	23	m	45	104.8	17.8	0	5.3
30B a	"	27	s	45	68.9	11.7	6	4.0
30B b	"	27	s	45	69.7	11.8	2	4.0
48B	"	23	m	55	147.3	25.0	4	5.6
97B a	"	23	m	263	123.7	21.0	0	3.8
97B b	"	23	m	263	104.3	17.7	0	3.6
98B a	"	28	m	263	75.8	12.9	0	3.2
98B b	"	28	m	263	62.2	10.6	0	3.0

TABLE V 3 (Cont'd)

Sample Designation	Sample Type	Water Content% (Initial)	Compaction Effort*	Curing Time (Days)	Normal Force at Failure (Lbs)	xc Tensile Strength (PSI)	Lateral or Tensile Strain at Failure	Final Stiffness to Vertical Load Volts
99B a	"	33	m	263	53.9	9.2	3	2.4
99B b	"	33	m	263	49.9	8.5		
66B	TOSCO 80/20	29	m	21	224.6	38.1	0	5.7
80B	"	24	s	31	187.6	31.9	0	5.2
75B a	"	24	m	32	223.6	38.0	0	6.6
75B b	"	24	m	32	259.5	44.1	0	6.6
61B	"	29	m	39	241.5	41.0	0	6.6
60B	"	24	m	40	244.5	41.5	0	6.2
36B	"	29	m	55	73.9	12.6	0	6.5
37B	"	24	s	45	225.5	38.3	0	6.1
59B	TOSCO 70/30	34	m	55	300+	51+	0	6.2
74B	"	34	m	21	300+	51+	0	
58B	"	25	m	55	300+	51+	0	6.4
76B	"	25	m	21	300+	51+	0	
89B	"	28	s	21	300+	51+	0	6.4
41B	"	28	s	55	300+	51+	0	7.7
50B	Lurgi	22	m		300+	51+	0	6.3
51B	"	22	m	23	265.5	45.1	0	6.7
72B	"	22	m	44	279.4	47.4	0	5.6
43B	"	22	m	59	247.5	42.4	0	5.5
78B	"	30	s	21	161.7	27.5	0	5.4
64B	"	30	s	45	179.2	30.4	0	6.1
52B	"	27	m	21	174.1	29.6	0	5.7
69B	"	27	m	46	187.6	31.9	0	5.8
45B	"	27	m	59	195.5	33.2	0	6.8
100B a	"	22	m	250	300+	51+	0	6.3
100B b	"	22	m	250	300+	51+	0	6.5
101B a	"	27	m	245	147.7	25.1	0	5.4
101B b	"	27	m	245	123.4	30.0	0	4.9
102B a	"	32	m	245	31.9	5.4	2	2.8
102B a	"	32	m	250	46.4	7.8	1	3.7
86B	75MelTos/25Burn	55	m	26	182.6	31.0	0	5.3
86B b	"	45	m	26	225.5	38.3	0	4.2

TABLE V 3 (Cont'd)

Sample Designation	Sample Type	Water Content% (Initial)	Compaction Effort*	Curing Time (Days)	Normal Force at Failure (Lbs)	xc Tensile Strength (PSI)	Lateral or Tensile Strain at Failure	Final Stiffness to Vertical Load Volts
86B c	"	40	m	26	182.6	31.0	0	4.2
86B d	"	35	m	26	169.6	28.8	0	4.5
87B a	50MelTos50/TOSII	25	m	27	81.8	13.9	8	3.3
87B b	"	30	m	27	85.8	14.6	17	3.3
87B c	"	40	m	27	61.8	10.5	6	3.1
87B d	"	45	m	27	22.0	3.7	5	1.7
103B a	"	40	m	204	93.1	15.8	3	5.3
103B b	"	40	m	204	107.2	18.2	3	5.5
104B a	"	45	m	204	74.2	12.6	2	5.5
104Bb	"	45	m	204	67.1	11.4	4	3.2
85B a	50MelLurgi/50Lurgi	35	m	27	2.4	0.4	111	0.2
85B b	"	35	s	30	33.9	5.8	110	1.2
85B c	"	30	m	30	119.7	20.3	12	4.9
85B	"	25	m	33	81.8	13.9	0	2.0
93B a	50MelLurgi/50Lurgi	15	m	32	63.8	10.8	0	4.8
93B b	"	30	s	33	50.9	8.6	0	3.9
93B c	"	25	s	33	54.9	9.3	0	4.4
93B d	"	20	m	32	81.0	13.9	0	4.9
83B a	75MelLurgi/25Lurgi	15	m	27	43.9	7.5	0	3.7
83B b	"	20	m	27	43.9	7.5	0	2.6
83B c	"	25	m	27	45.9	7.9	10	3.9
83B d	"	30	m	27	15.0	2.5	12	0.7

*S = Standard proctor
m = Modified proctor
** = Slop of final vertical strain/time curve

TABLE V 4. Pneumatic Arm Oedometer Results from Fresh Specimens: Void Ratios e and Compression Indices C_c

Shale Compaction	Initial Water Added,%	Oedometer Deflect Correctn. mm	Initial Schaevitz Units	Steady State Shaevitz Units	Deflect Corrcd Compress. Total mm	Mineral Grain Density gm/cc	Specimen Loaded Weight gm	Dry Density gm/cc	Void Ratio e	Delta Void ratio	Compress Index Cc
t80 s	24	.008	1908	1901	.006	2.786	135.1	1.345	1.056	-.0581	
	24	.030	1908	1879	.028	2.786	135.1	1.355	1.055	.0018	.0059
	24	.050	1908	1854	.058	2.786	135.1	1.357	1.052	.0024	.0080
	24	.065	1908	1821	.109	2.786	135.1	1.360	1.048	.0041	.0137
	24	.075	1908	1758	.225	2.786	135.1	1.366	1.039	.0094	.0312
t70 m	25	.008	1902	1878	.040	2.819	146.7	1.461	0.929	.1096	-
	25	.030	1902	1807	.160	2.819	146.7	1.467	0.920	.0091	.0303
	25	.050	1902	1740	.274	2.819	146.7	1.474	0.911	.0087	.0288
	25	.065	1902	1649	.441	2.819	146.7	1.484	0.898	.0127	.0422
	25	.075	1902	1501	.727	2.819	146.7	1.501	0.877	.0217	.0722
t70 s	28	.008	1914	1906	.008	2.819	139.3	1.353	1.083	-.2061	-
	28	.030	1914	1856	.086	2.819	139.3	1.357	1.076	.0064	.0212
	28	.050	1914	1793	.192	2.819	139.3	1.362	1.068	.0087	.0289
	28	.065	1914	1692	.379	2.819	139.3	1.373	1.052	.0153	.0509
	28	.075	1914	1504	.745	2.819	139.3	1.393	1.022	.0300	.0993
t70 m	34	.008	1868	1809	.110	2.819	144.5	1.346	1.094	-.0711	-
	34	.030	1868	1700	.306	2.819	144.5	1.356	1.077	.0162	.0539
	34	.050	1868	1602	.482	2.819	144.5	1.366	1.063	.0146	.0484
	34	.065	1868	1439	.793	2.819	144.5	1.383	1.037	.0257	.0855
	34	.075	1868	1174	1.313	2.819	144.5	1.413	0.994	.0430	.1429
lurgi m	22	.008	1925	1917	.008	2.622	137.1	1.397	0.876	.1179	-
	22	.030	1925	1894	.032	2.622	137.1	1.398	0.874	.0017	.0059
	22	.050	1925	1868	.064	2.622	137.1	1.400	0.872	.0023	.0079
	22	.065	1925	1841	.103	2.622	137.1	1.402	0.869	.0029	.0096
	22	.075	1925	1786	.203	2.622	137.1	1.408	0.862	.0074	.0245

Table V 4. (CONT'D)

Shale Compaction	Initial Water Added,%	Oedometer Deflect Correctn. mm	Initial Schaevitz Units	Steady State Shaevitz Units	Deflect Corrcd Compress. Total mm	Mineral Grain Density gm/cc	Specimen Loaded Weight gm	Dry Density gm/cc	Void Ratio e	Delta Void ratio	Compress Index Cc
lurg s	30	.008	1883	1849	.060	2.622	143.2	1.372	0.910	-.0484	-
	30	.030	1883	1768	.200	2.622	143.2	1.380	0.899	.0105	.0350
	30	.050	1883	1701	.314	2.622	143.2	1.386	0.891	.0086	.0285
	30	.065	1883	1617	.467	2.622	143.2	1.394	0.879	.0115	.0383
	30	.075	1883	1458	.775	2.622	143.2	1.412	0.856	.0232	.0771
lurg m	27	.008	1966	1952	.020	2.622	145.3	1.423	0.842	.0143	
	27	.030	1966	1910	.082	2.622	145.3	1.426	0.837	.0045	.0149
	27	.050	1966	1858	.166	2.622	145.3	1.431	0.831	.0061	.0202
	27	.065	1966	1790	.287	2.622	145.3	1.438	0.823	.0088	.0292
	27	.075	1966	1683	.491	2.622	145.3	1.450	0.808	.0148	.0492
t50/50 m	40	.008	1920	1889	.054	2.724	131.4	1.169	1.330	-.5218	-
	40	.030	1920	1809	.192	2.724	131.4	1.175	1.317	.0127	.0421
	40	.050	1920	1648	.494	2.724	131.4	1.189	1.289	.0277	.0922
	40	.065	1920	1413	.949	2.724	131.4	1.211	1.247	.0418	.1388
	40	.075	1920	1053	1.659	2.724	131.4	1.248	1.182	.0652	.2166
t100 m	22	.008	1940	1927	.018	2.72	147.1	1.49 !	0.813	.0000	-
	22	.030	1940	1891	.068	2.72	147.1	1.502	0.810	.0036	.0119
	22	.050	1940	1842	.146	2.72	147.1	1.507	0.804	.0056	.0185
	22	.065	1940	1778	.259	2.72	147.1	1.514	0.796	.0081	.0268
	22	.075	1940	1680	.445	2.72	147.1	1.525	0.783	.0132	.0441
t100 s	25	.008	1822	1784	.068	2.72	136.4	1.360	0.9 8	-.2154	-
	25	.030	1822	1655	.304	2.72	136.5	1.373	0.980	.0186	.0618
	25	.050	1822	1502	.590	2.72	136.5	1.389	0.957	.0225	.0749
	25	.065	1822	1308	.963	2.72	136.5	1.410	0.928	.0294	.0977
	25	.075	1822	1051	1.467	2.72	136.5	1.440	0.888	.0397	.1319

Table V 4.; (CONT'D)

Shale Compaction	Initial Water Added,%	Oedometer Deflect Correctn. mm	Initial Schaevitz Units	Steady State Shaevitz Units	Deflect Corrcd Compress. Total mm	Mineral Grain Density gm/cc	Specimen Loaded Weight gm	Dry Density gm/cc	Void Ratio e	Delta Void ratio	Compress Index Cc
t90 m	23	.008	1885	1867	.028	2.753	149.2	1.509	0.823	.0644	-
	23	.030	1885	1820	.100	2.753	149.2	1.513	0.818	.0052	.0172
	23	.050	1885	1748	.224	2.753	149.2	1.521	0.809	.0089	.0296
	23	.065	1885	1651	.403	2.753	149.2	1.531	0.797	.0129	.0421
	23	.075	1885	1509	.677	2.753	149.2	1.548	0.777	.0197	.0654
t90 s	27	.008	1930	1919	.014	2.753	138.7	1.358	1.026	-.2496	-
	27	.030	1930	1866	.058	2.753	138.7	1.360	1.023	.0035	.0117
	27	.050	1930	1819	.172	2.753	138.7	1.366	1.014	.0091	.0302
	27	.065	1930	1706	.383	2.753	138.7	1.378	0.997	.0168	.0559
	27	.075	1930	1512	.761	2.753	138.7	1.399	0.967	.0302	.1002
t90 m	28	.008	1750	1726	.040	2.753	146.2	1.421	0.936	.0312	-
	28	.030	1750	1688	.094	2.753	146.2	1.424	0.932	.0041	.0137
	28	.050	1750	1638	.174	2.753	146.2	1.429	0.925	.0061	.0202
	28	.065	1750	1568	.299	2.753	146.2	1.436	0.916	.0095	.0317
	28	.075	1750	1478	.469	2.753	146.2	1.446	0.903	.0129	.0431
t80 s	24	.008	1878	1859	.030	2.786	135.0	1.354	1.056	-.1529	-
	24	.030	1878	1815	.096	2.786	135.0	1.358	1.051	.0053	.0178
	24	.050	1878	1761	.184	2.786	135.0	1.363	1.043	.0071	.0237
	24	.065	1878	1672	.347	2.786	135.0	1.371	1.030	.0132	.0439
	24	.075	1878	1514	.653	2.786	135.0	1.388	1.005	.0248	.0823
t100 s	20	.008	1849	1838	.014	2.720	131.0	1.347	1.003	.0675	-
	20	.030	1849	1820	.028	2.720	131.0	1.348	1.002	.0011	.0037
	20	.050	1849	1786	.076	2.720	131.0	1.360	0.9 8	.0038	.0126
	20	.065	1849	1738	.157	2.720	131.0	1.365	0.992	.0064	.0212
	20	.075	1849	1632	.359	2.720	131.0	1.376	0.976	.0159	.0529

TABLE V 4. (Cont'd)

Shale Compaction	Initial Water Added,%	Oedometer Deflect Correctn. mm	Initial Schaevitz Units	Steady State Shaevitz Units	Deflect Corrcd Compress. Total mm	Mineral Grain Density gm/cc	Specimen Loaded Weight gm	Dry Density gm/cc	Void Ratio e	Delta Void ratio	Compress Index Cc
t90 s	22	.008	1821	1797	.040	2.753	136.0	1.387	0.983	-.0075	-
	22	.030	1821	1767	.078	2.753	136.0	1.389	0.980	.0029	.009 !
	22	.050	1821	1714	.164	2.753	136.0	1.394	0.974	.0067	.0223
	22	.065	1821	1634	.309	2.753	136.0	1.402	0.962	.0113	.0376
	22	.075	1821	1465	.637	2.753	136.0	1.421	0.937	.0256	.0852
t 80 s	29	.008	1885	1815	.132	2.786	143.0	1.385	1.011	-.0744	-
	29	.030	1885	1748	.244	2.786	143.0	1.391	1.022	.0089	.0296
	29	.050	1885	1629	.462	2.786	143.0	1.403	0.985	.0173	.0576
	29	.065	1885	1471	.763	2.786	143.0	1.420	0.961	.0239	.0795
	29	.075	1885	1246	1.203	2.786	143.0	1.446	0.926	.0349	.1163
t 70 s	33	.008	1891	1823	.128	2.819	140.4	1.318	1.137	-.2113	-
	33	.030	1891	1753	.246	2.819	140.4	1.324	1.127	.0099	.0331
	33	.050	1891	1615	.502	2.819	140.4	1.338	1.106	.0216	.0719
	33	.065	1891	1415	.887	2.819	140.4	1.359	1.073	.0325	.1081
	33	.075	1891	1123	1.461	2.819	140.4	1.392	1.024	.0485	.1612
lurgi s	40	.008	1909	1886	.038	2.622	137.7	1.224	1.141	-.1166	-
	40	.030	1909	1851	.086	2.622	137.7	1.226	1.137	.0040	.0135
	40	.050	1909	1785	.198	2.622	137.7	1.232	1.128	.0094	.3134
	40	.065	1909	1700	.353	2.622	137.7	1.239	1.114	.0131	.0434
	40	.075	1909	1579	.585	2.622	137.7	1.251	1.095	.0196	.0650
l 75/25s	25	.008	1957	1927	.052	2.665	142.2	1.416	0.880	.2145	-
	25	.030	1957	1871	.142	2.665	142.2	1.421	0.874	.0067	.0222
	25	.050	1957	1795	.274	2.665	142.2	1.429	0.864	.0098	.0325
	25	.065	1957	1695	.459	2.665	142.2	1.439	0.850	.0137	.0456
	25	.075	1957	1531	.777	2.665	142.2	1.458	0.827	.0236	.0783

Figure V 3. Torsioned Specimen of Oedometer Loading 33, A non Brittle Material

Figure V 4. Torsioned Specimen of Loading 64, A Mildly Cemented Specimen.

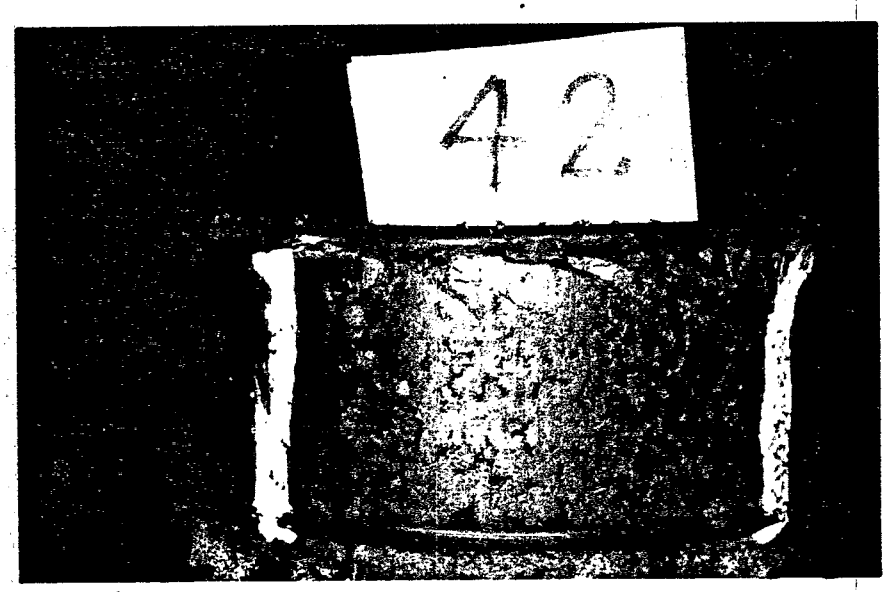

Figure V 5. Torsioned Specimen of Loading 42, A More Strongly Cemented Specimen

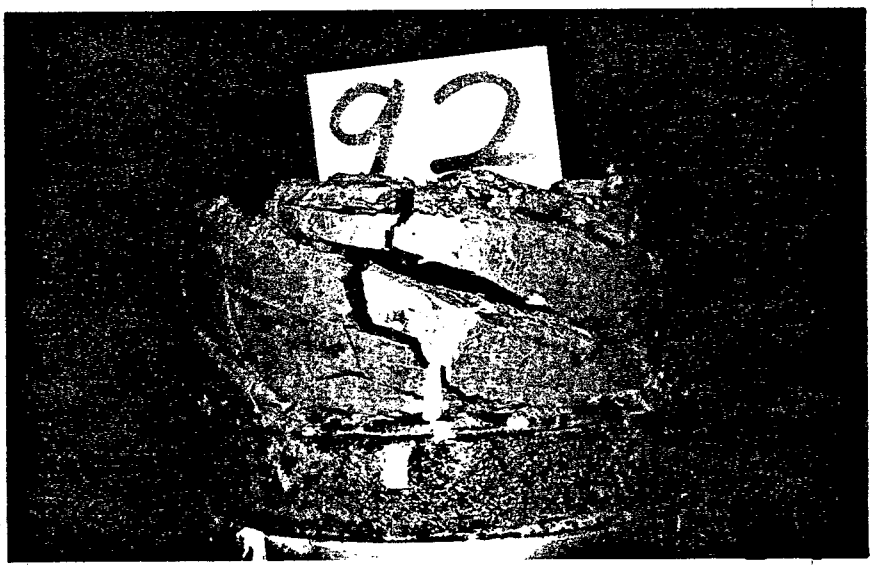

Figure V 6. Torsioned Specimen of Loading 92, A Rather Impermeable Little Cemented Specimen

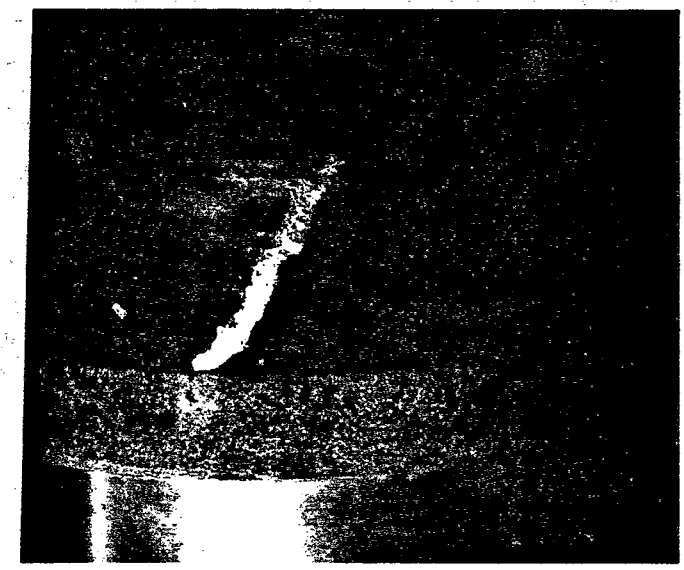

Figure V 7. Torsioned Specimen of Loading 32, A Low Brittleness Material Showing Shear Plane.

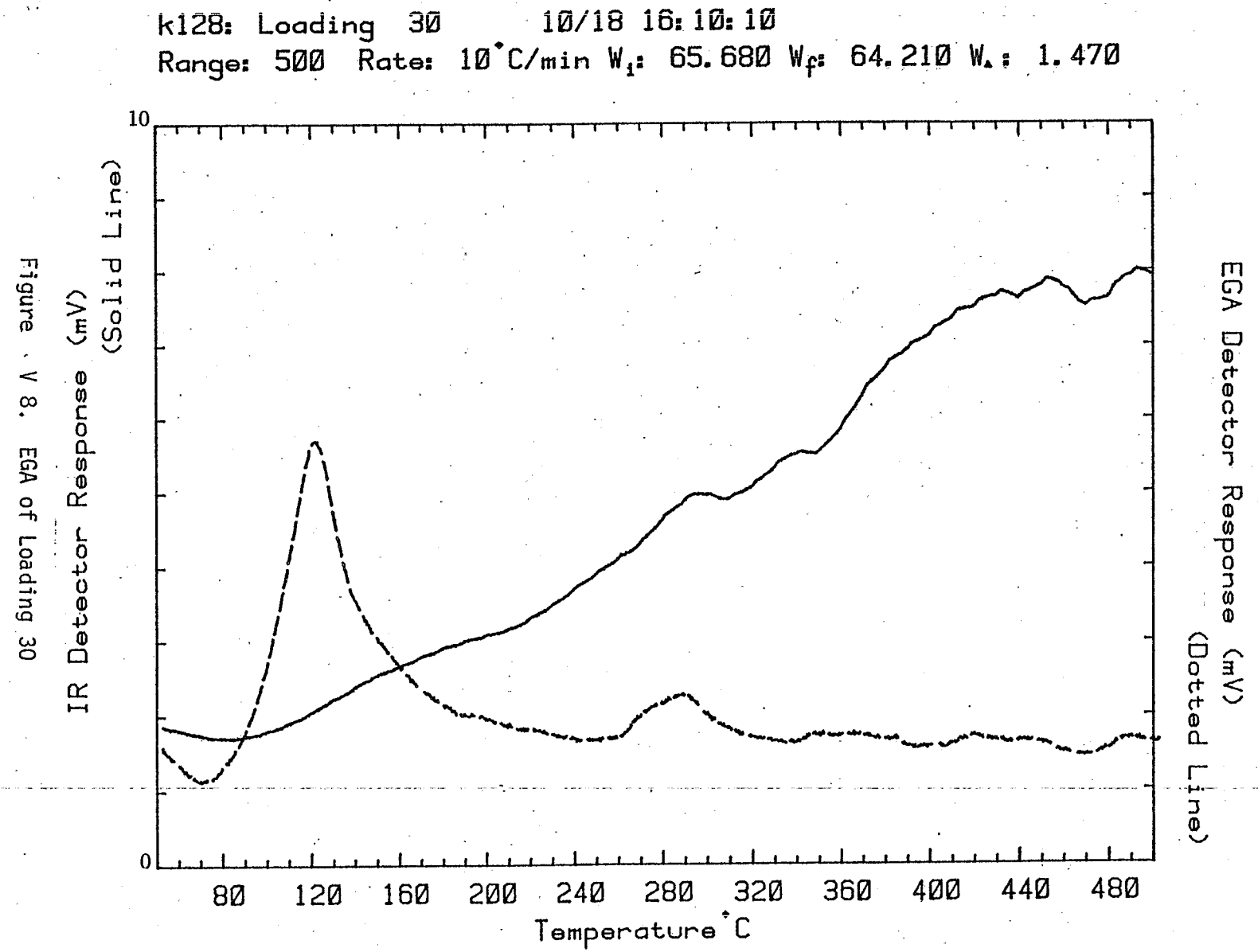

Figure V 8. EGA of Loading 30

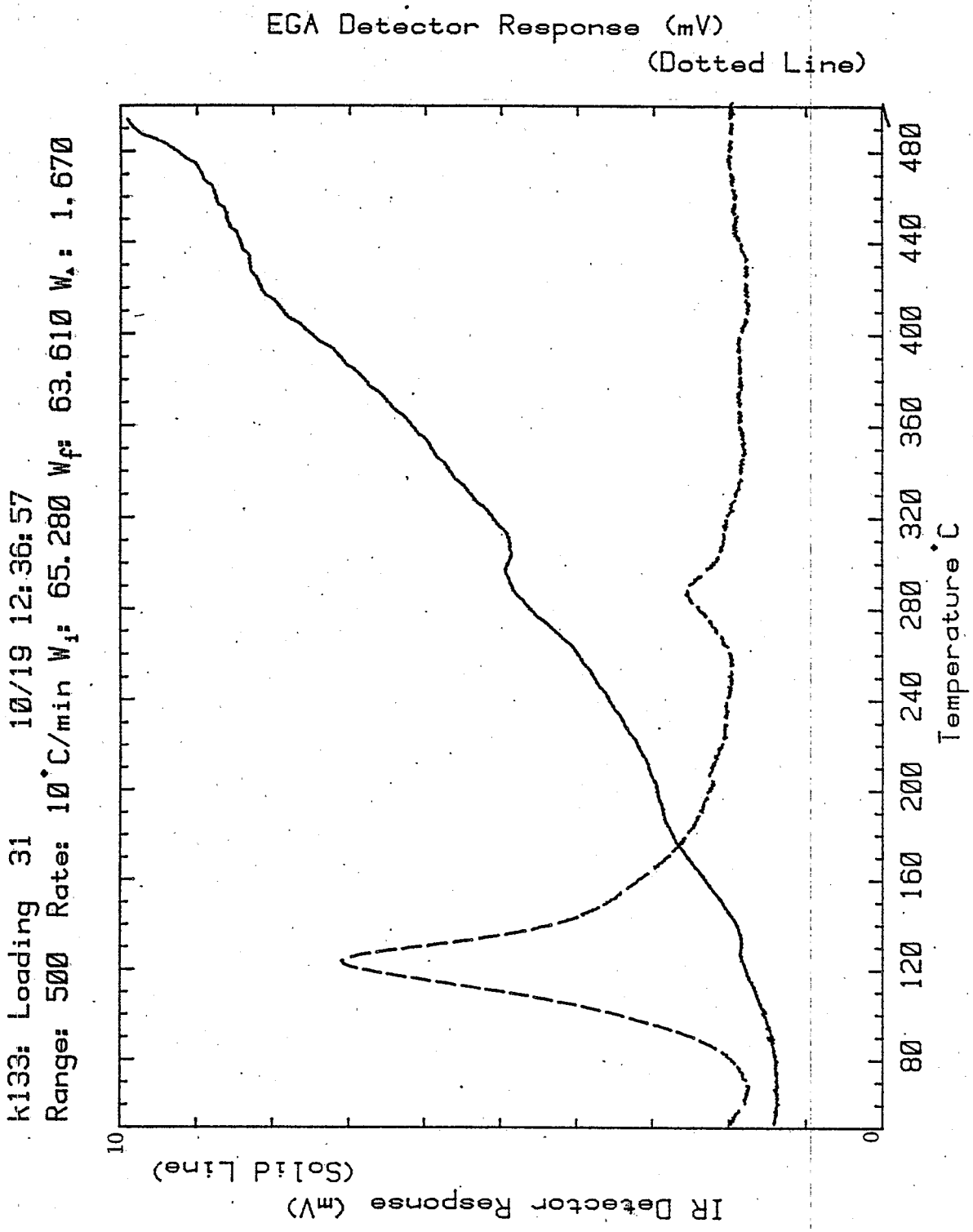

Figure V 9. EGA of Loading 31

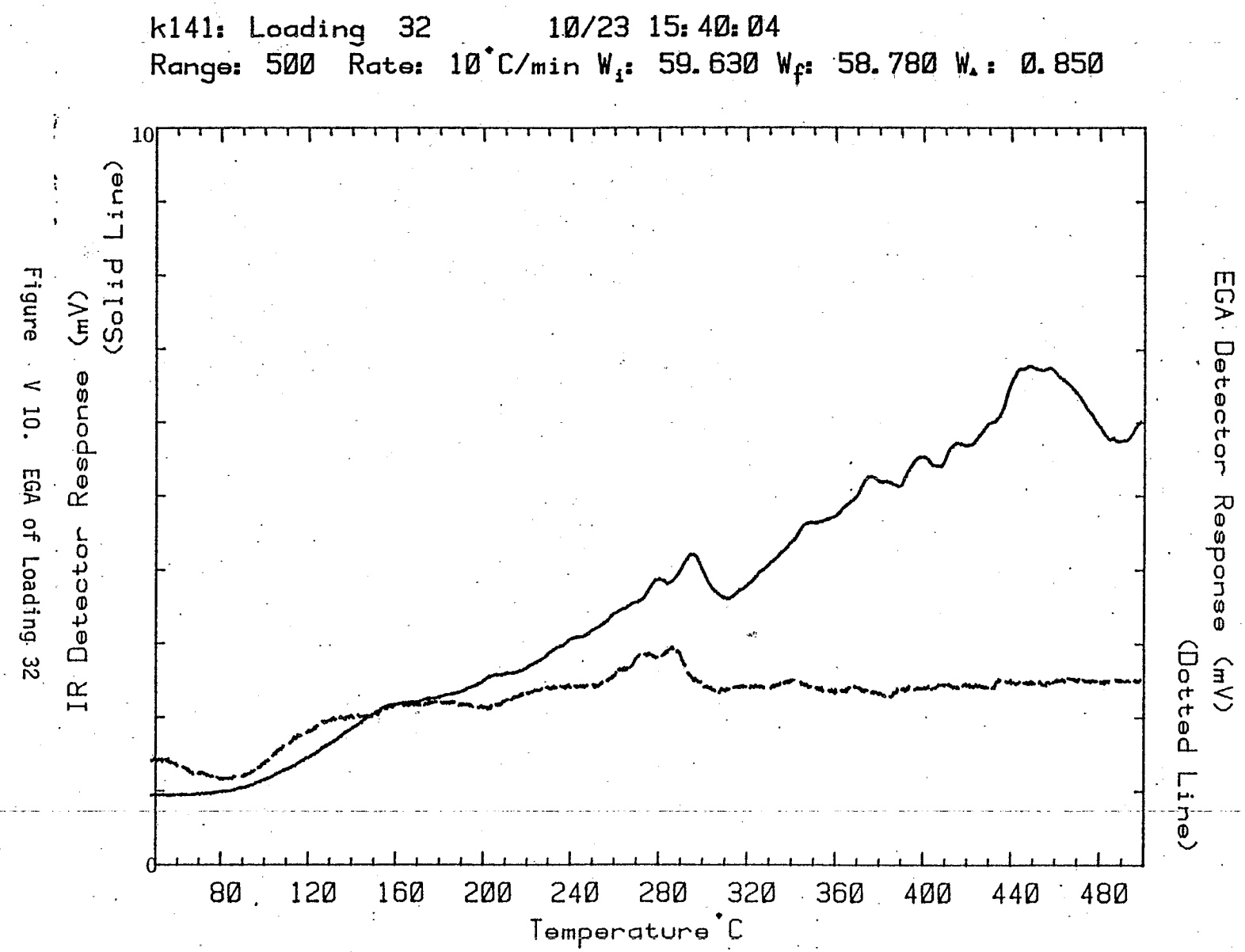

Figure V 10. EGA of Loading 32

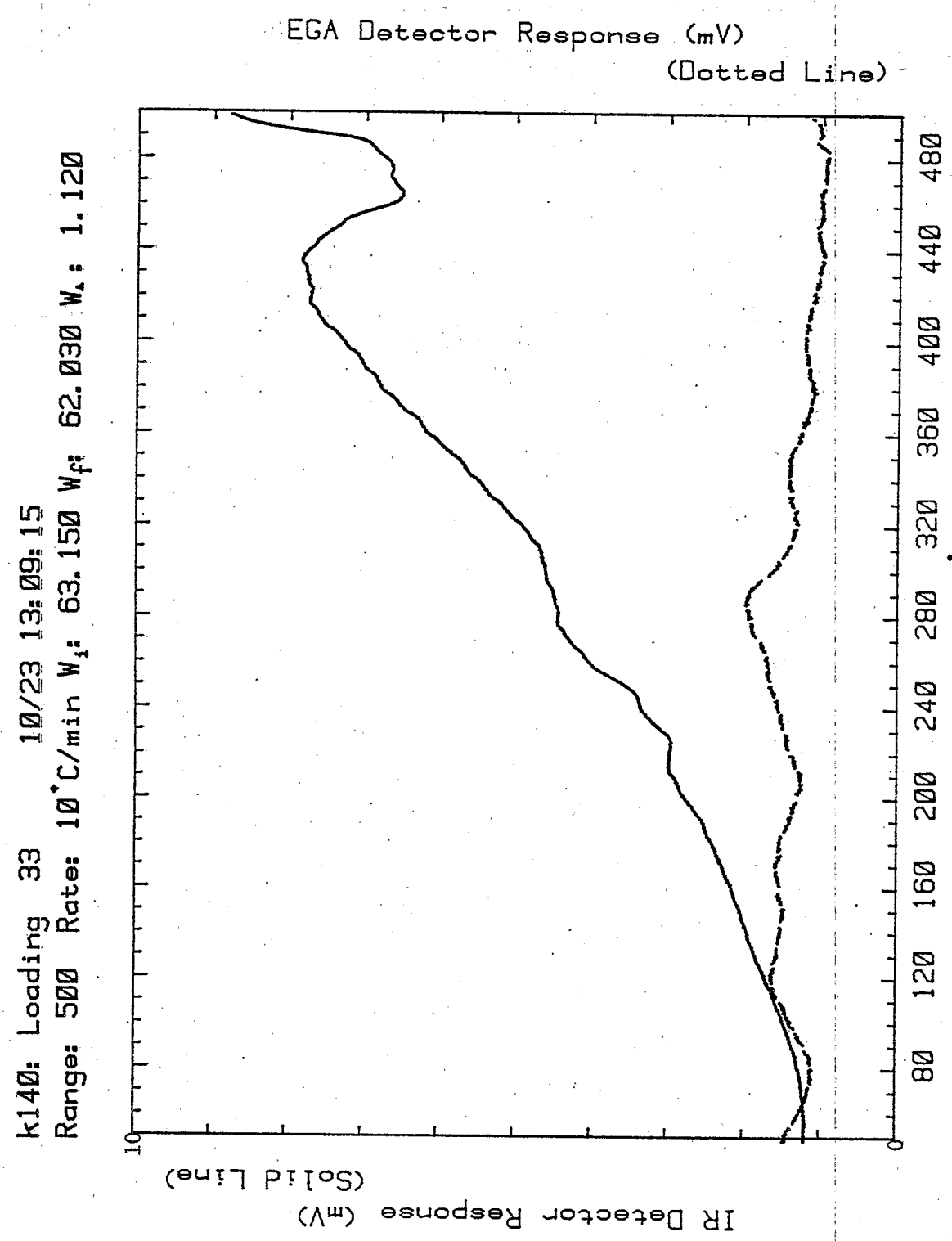

Figure V 11. EGA of Loading 33

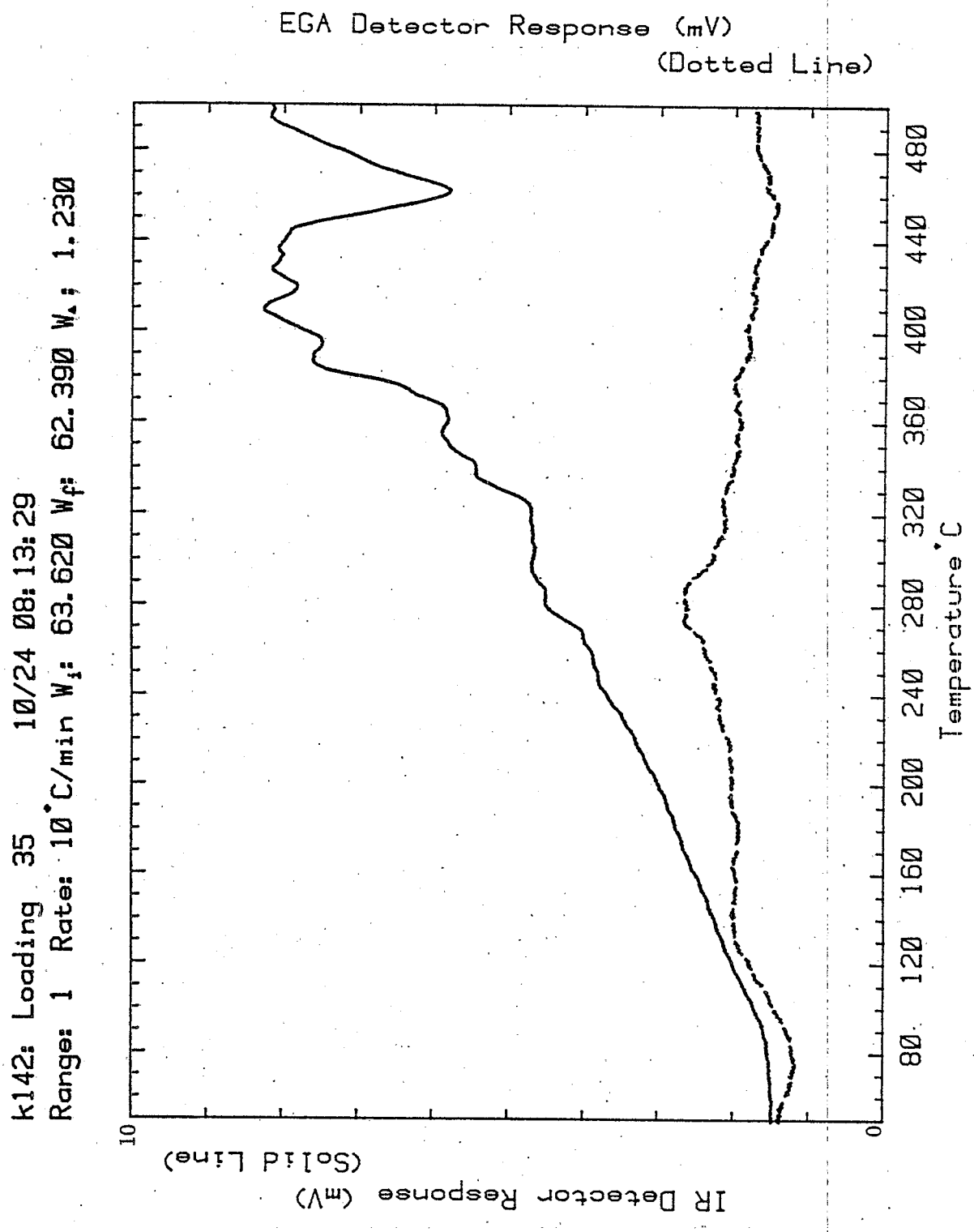

Figure V 12. EGA of Loading 35

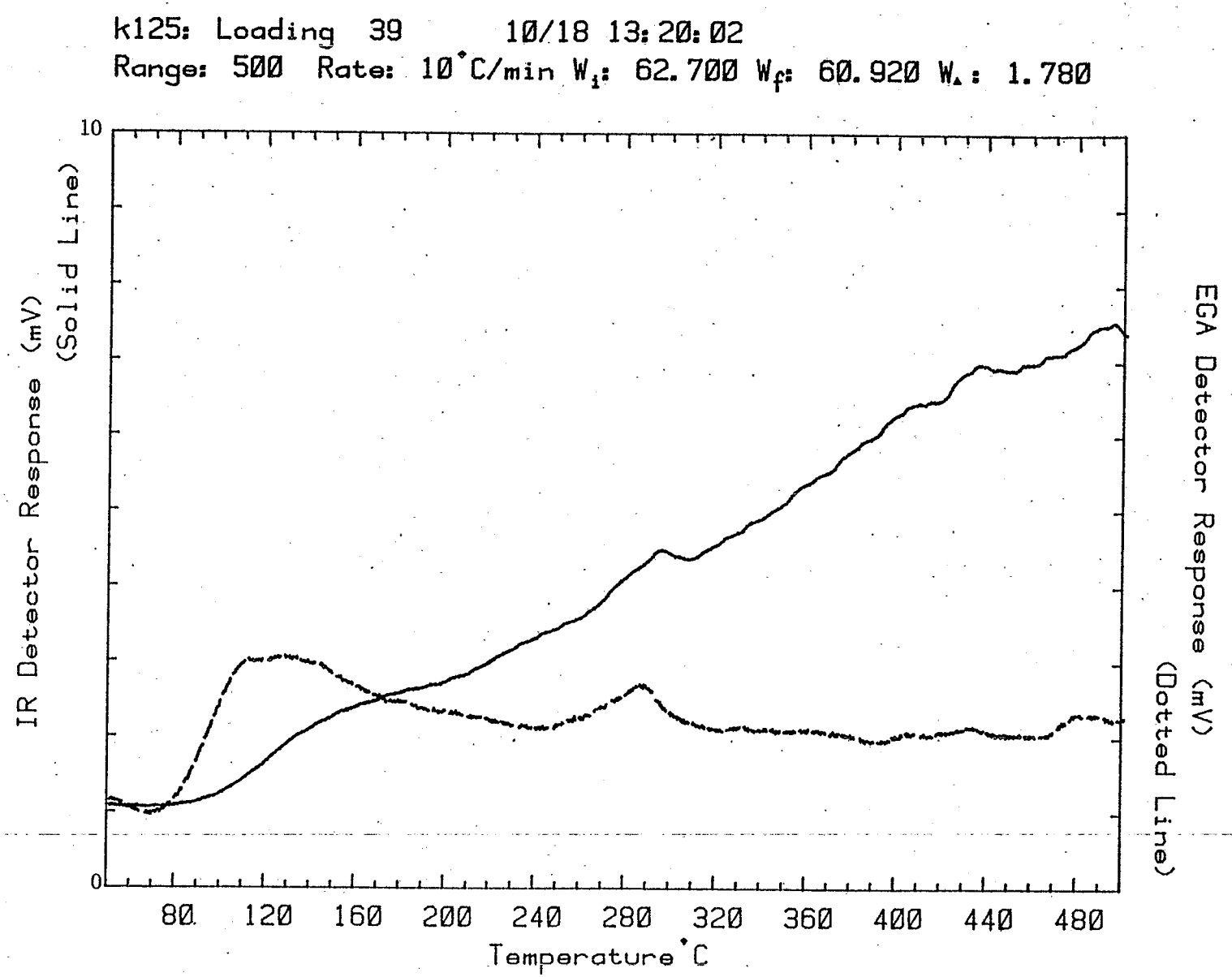

Figure 13. EGA of Loading 39

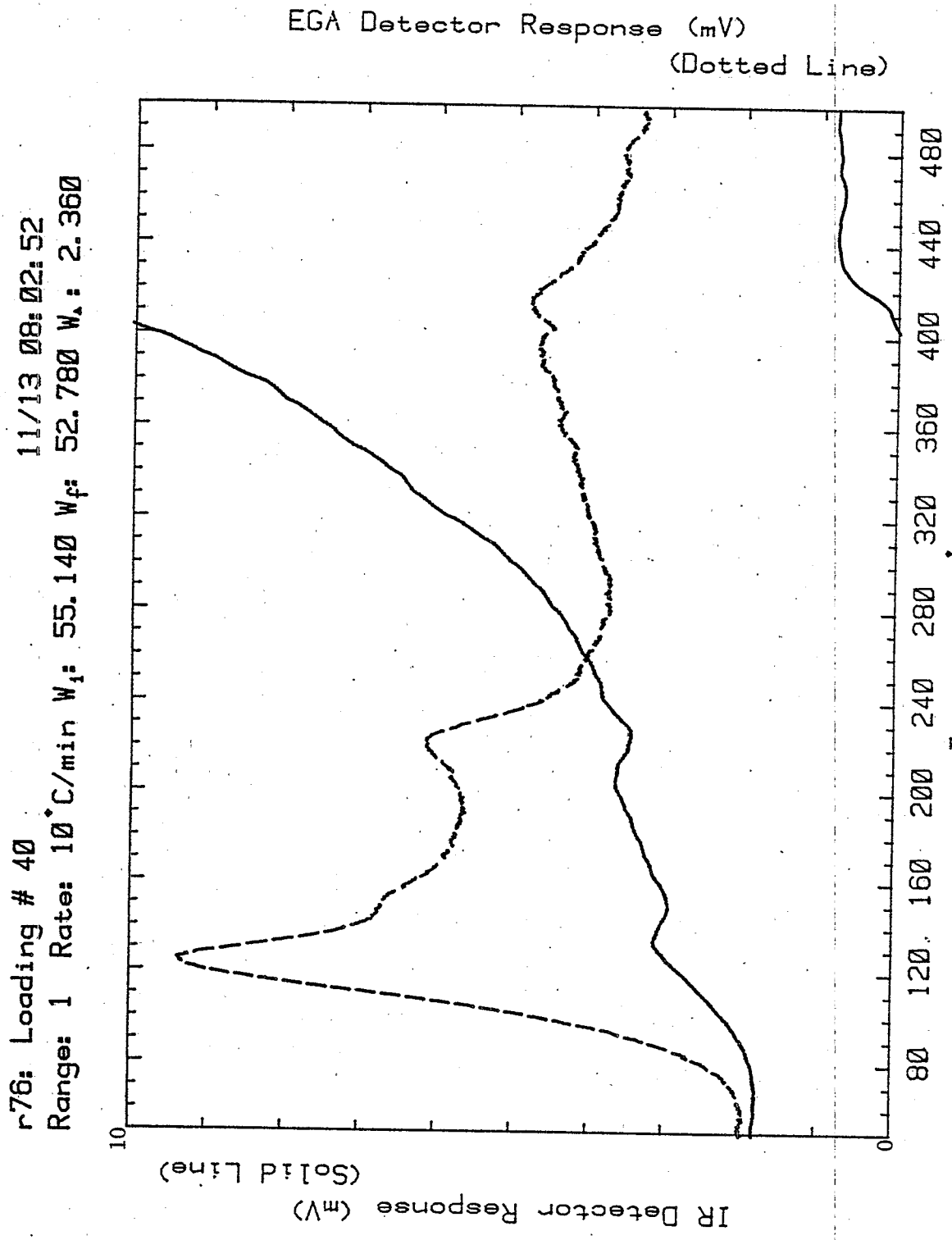

Figure V 14. EGA of Loading 40

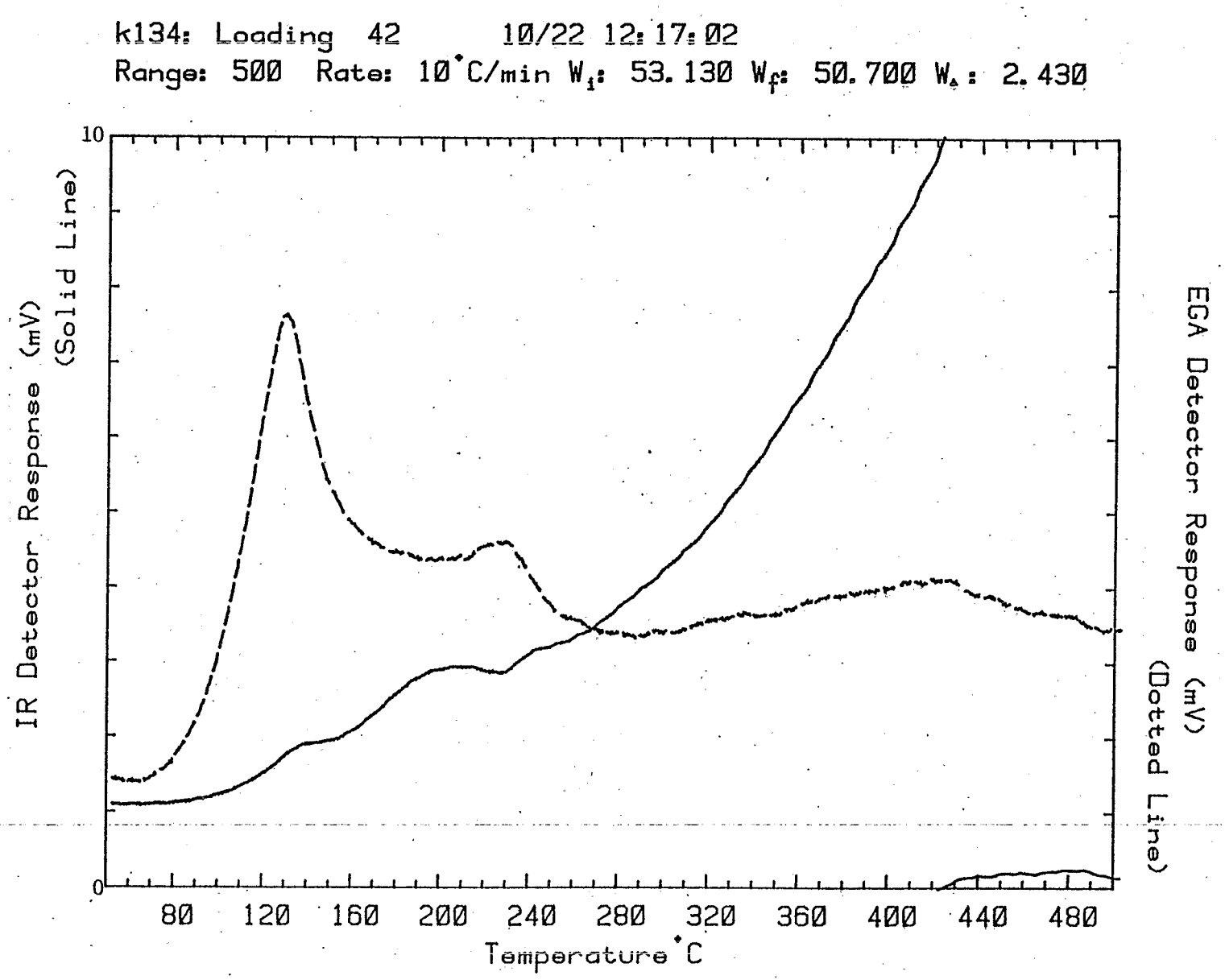

Figure V 15. EGA of Loading 42

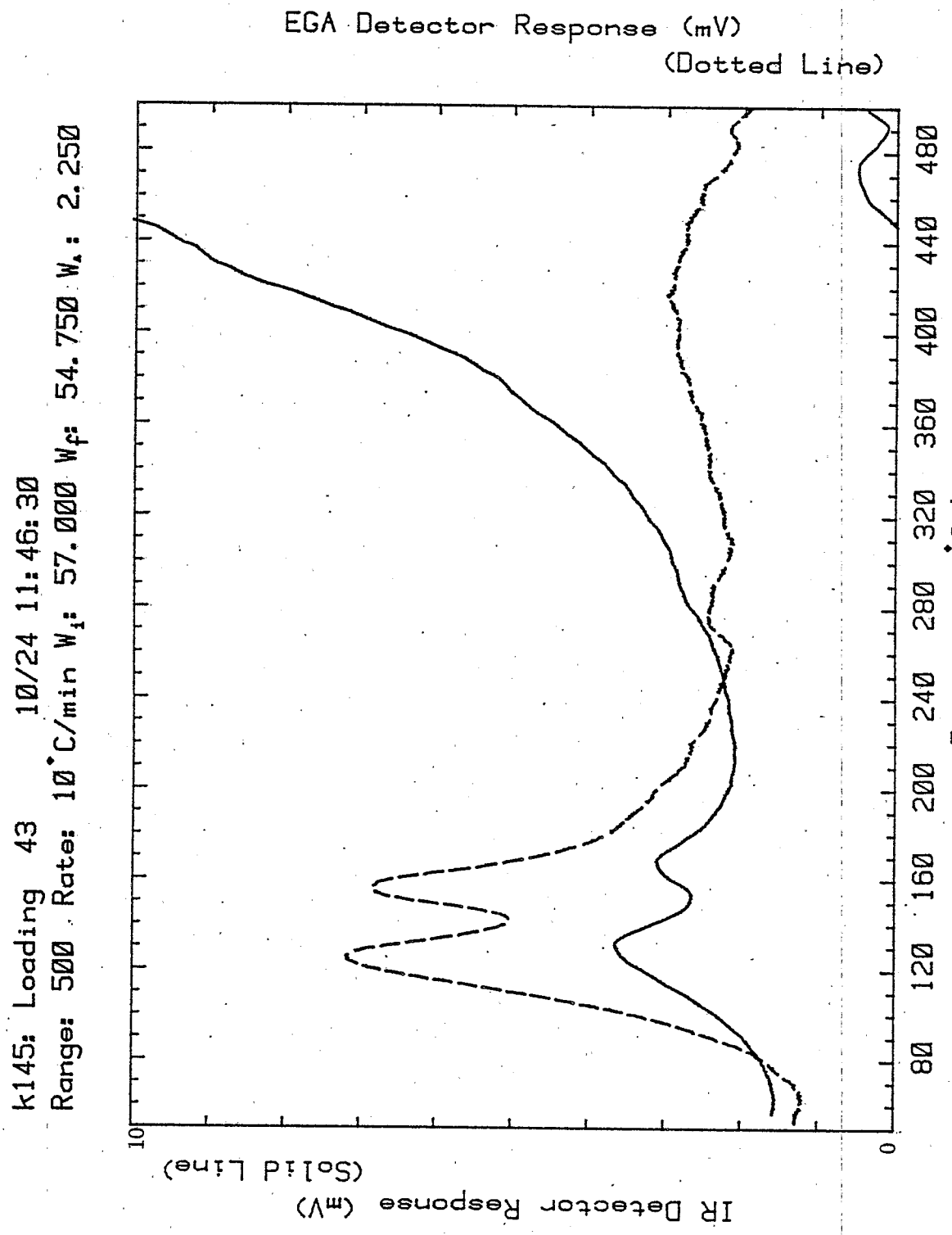

Figure V 16. EGA of Loading 43

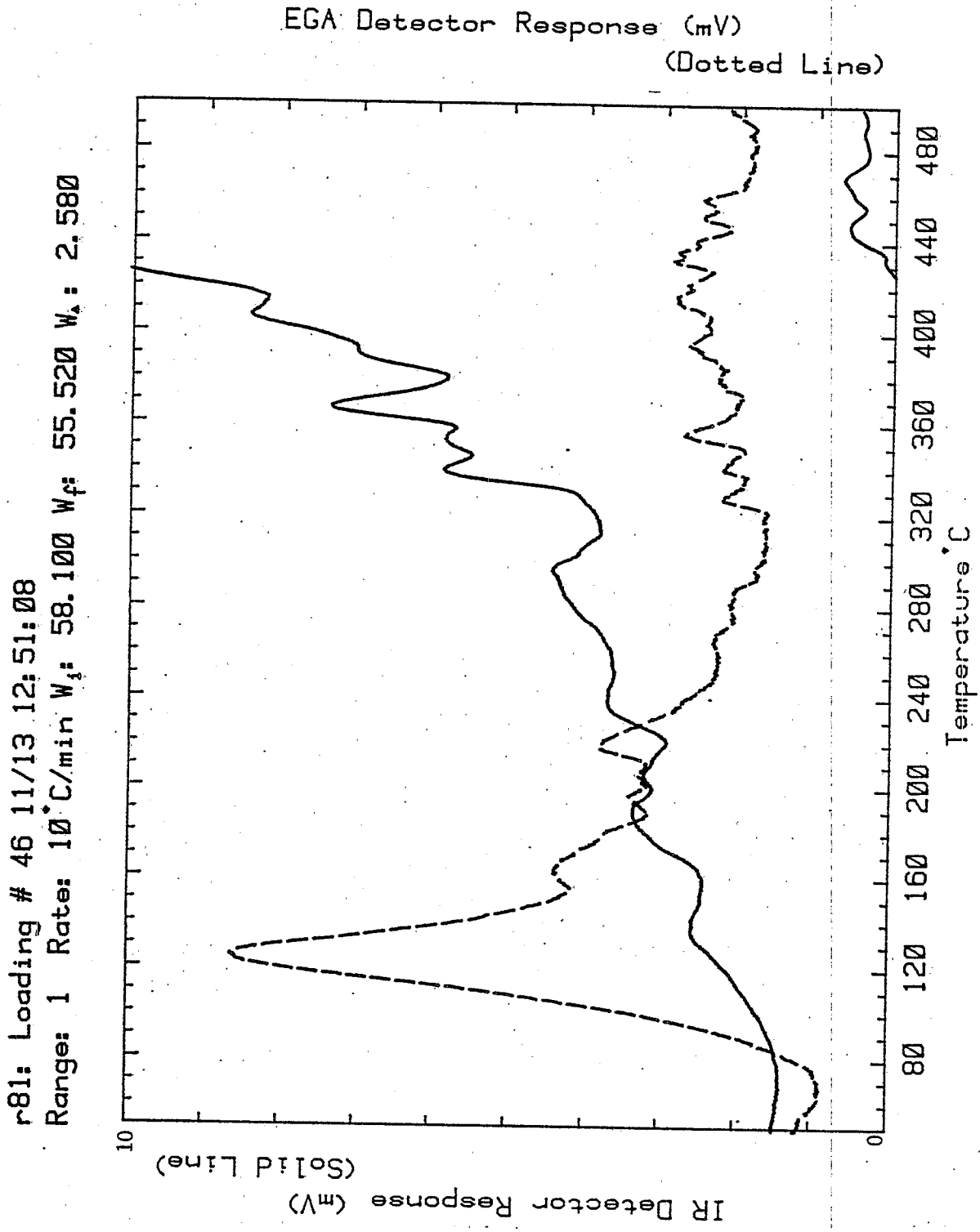

Figure V 17. EGA of Loading 46

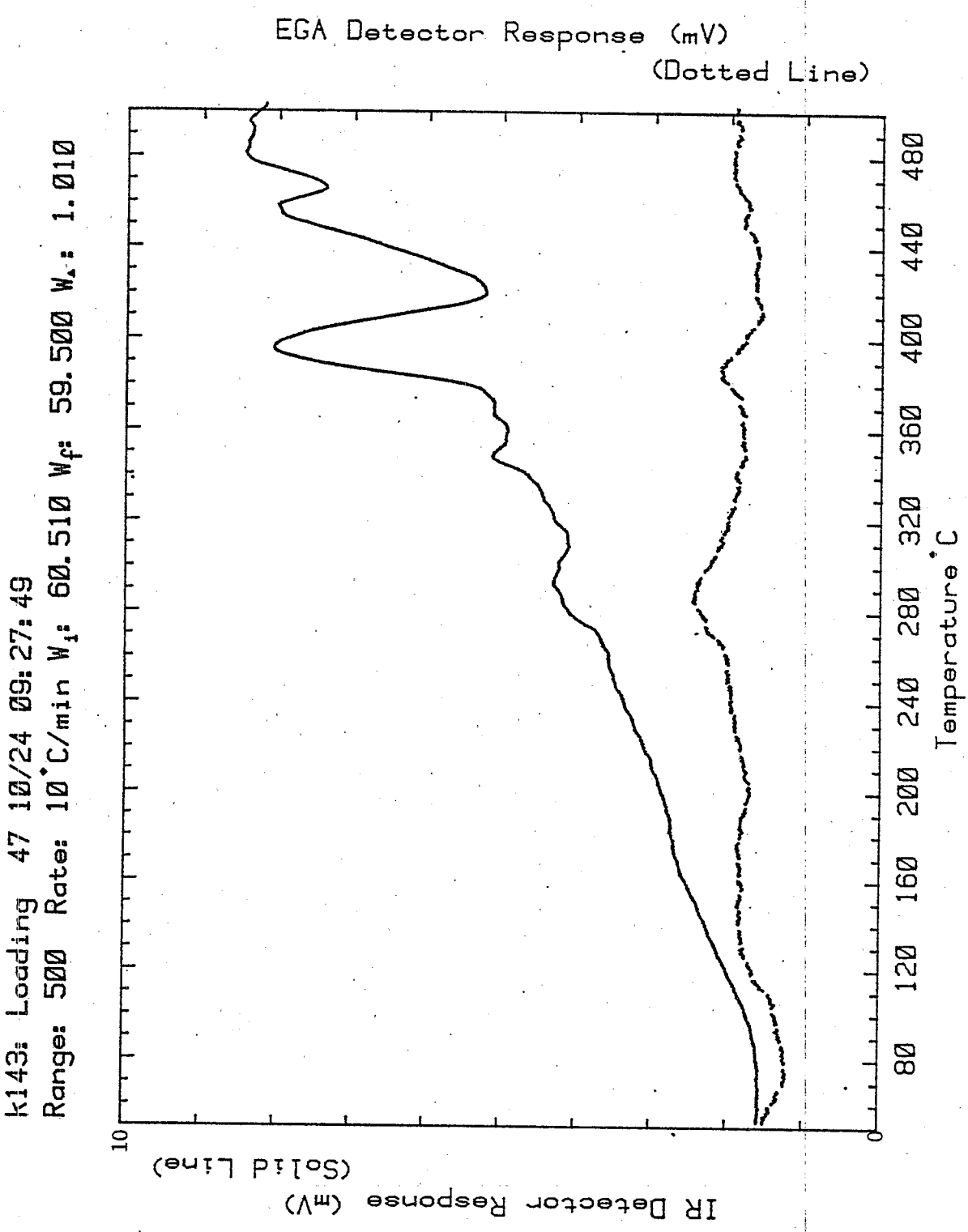

Figure V 18. EGA of Loading 47

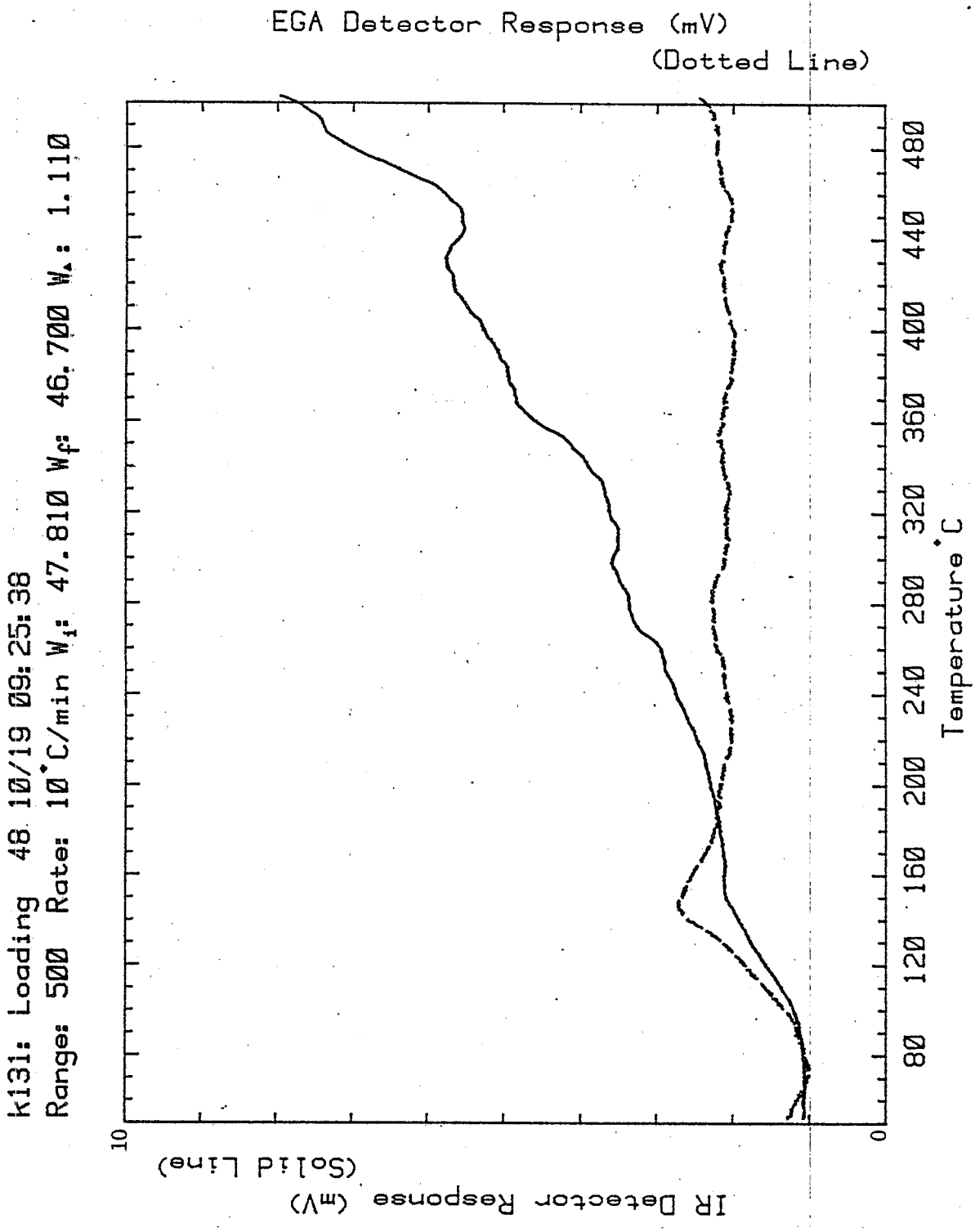

Figure V 19. EGA of Loading 48

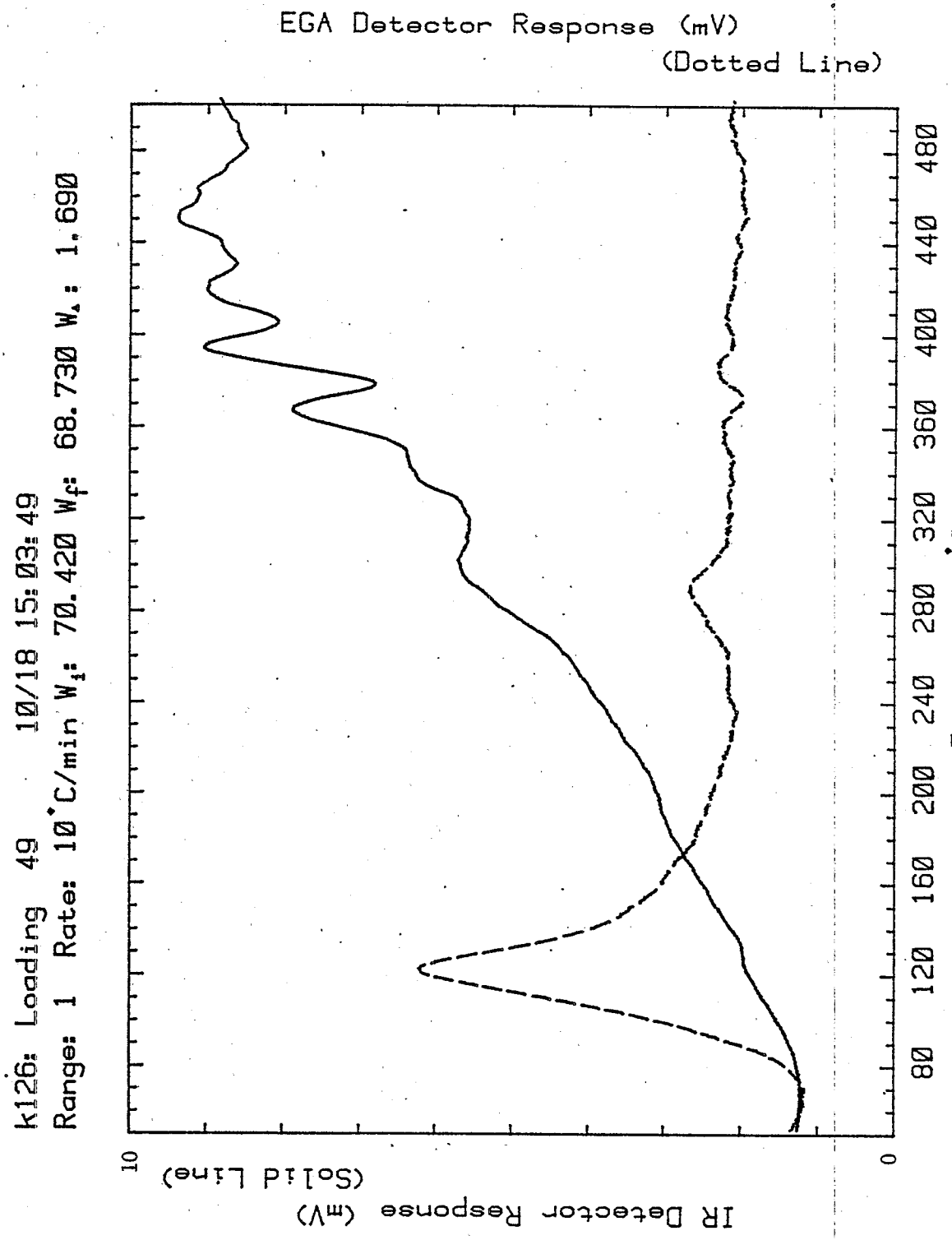

Figure V 20. EGA of Loading 49

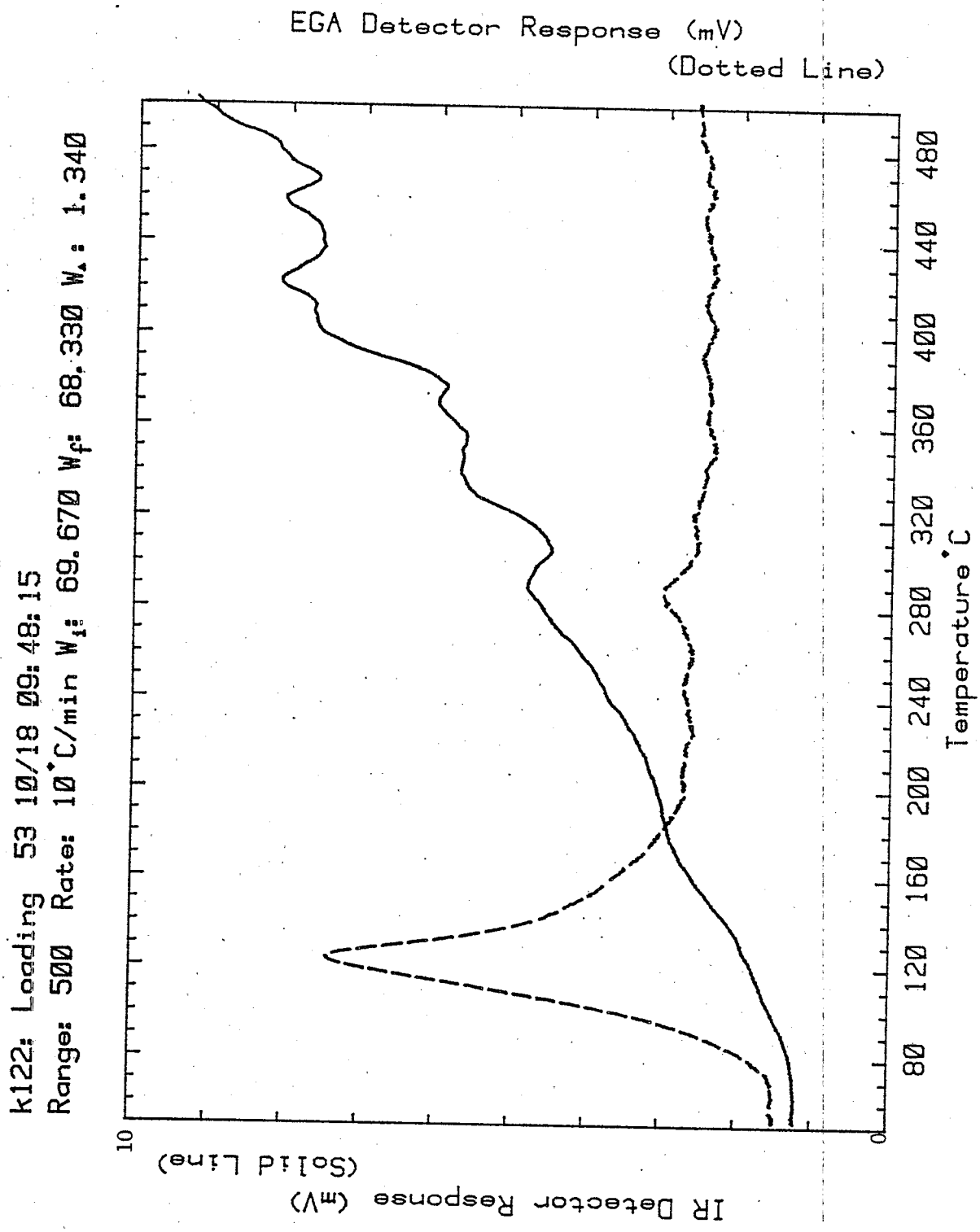

Figure -V 21. EGA of Loading 53

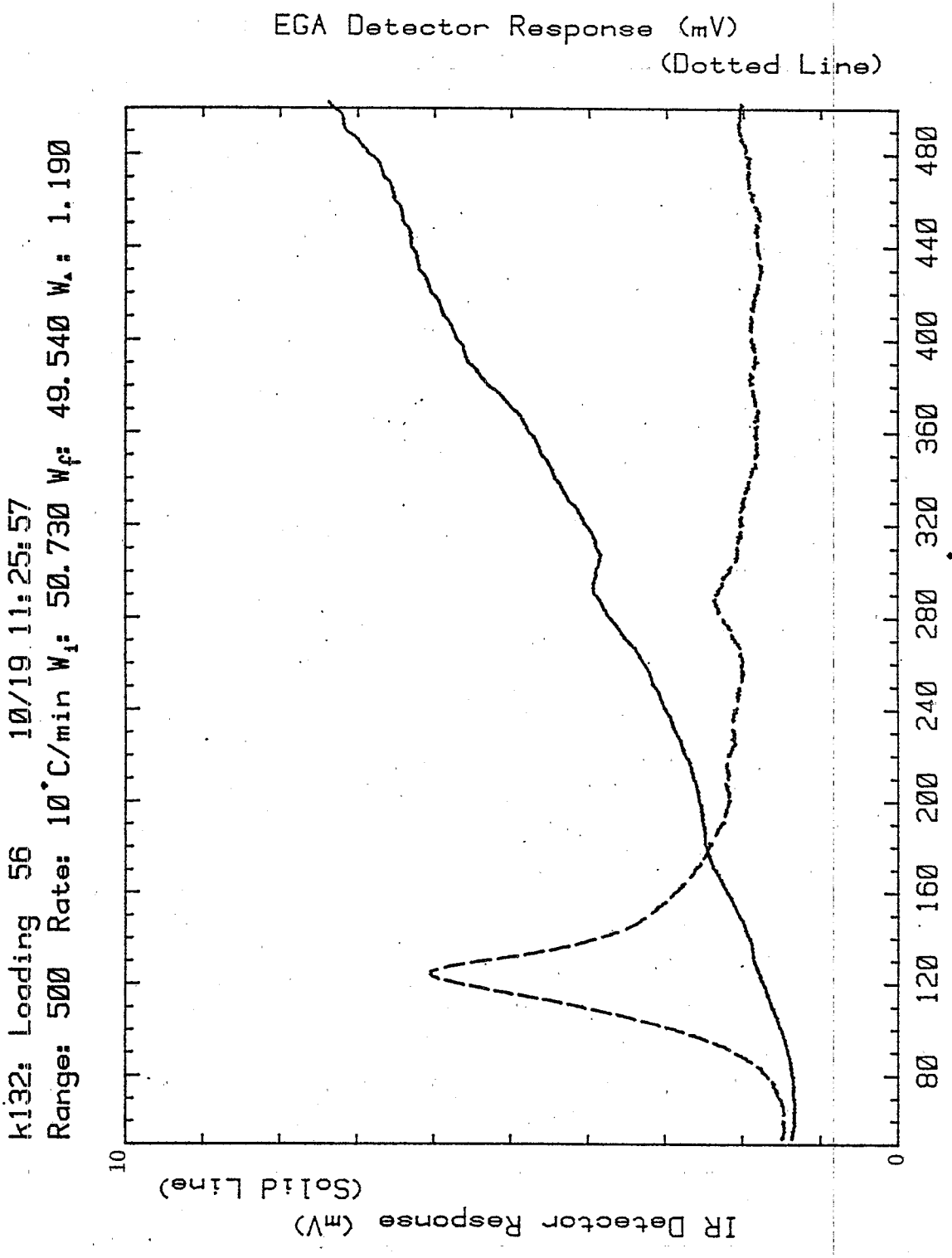

Figure : V 22. EGA of Loading 56

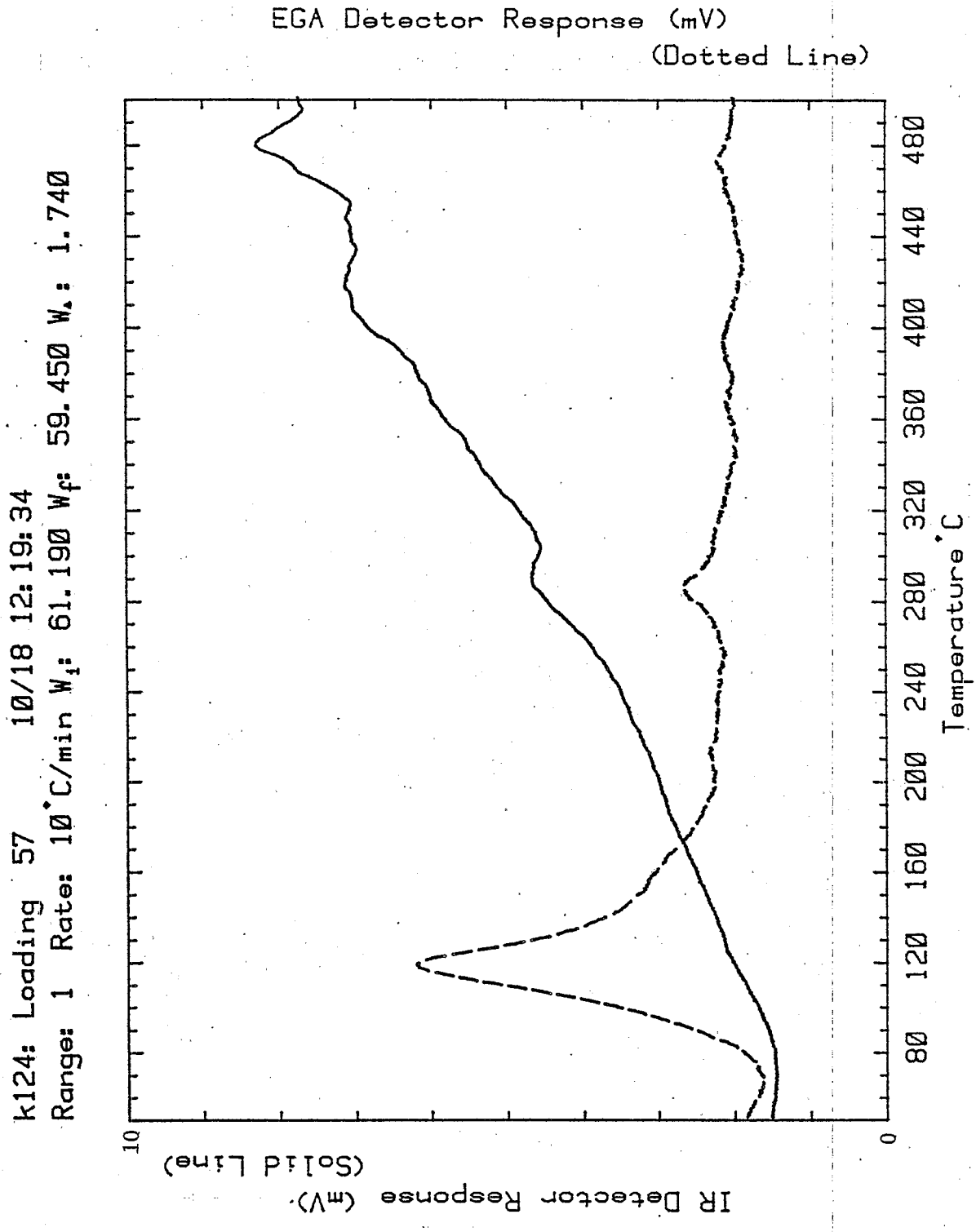

Figure V 23. EGA of Loading 57

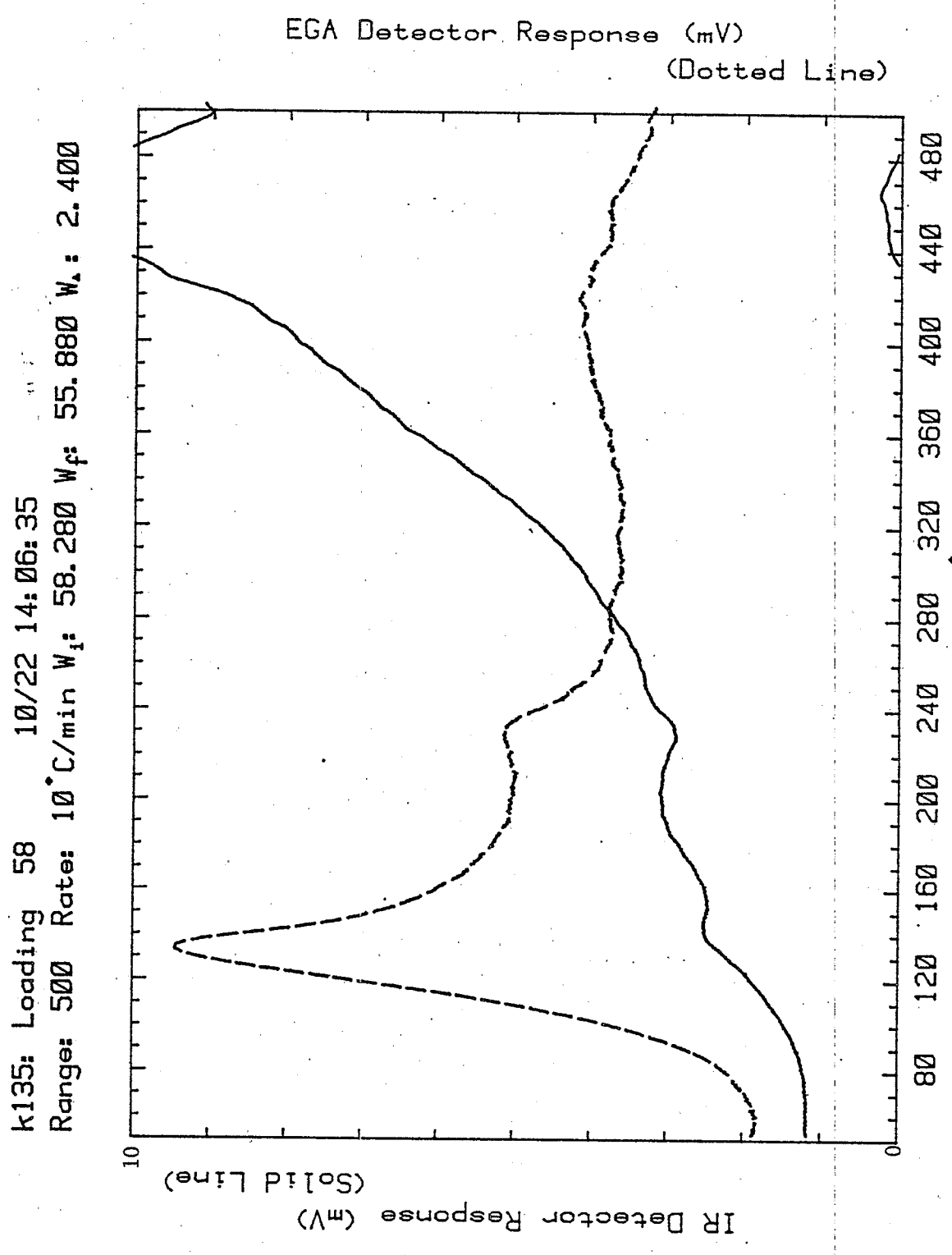

Figure V 24. EGA of Loading 58

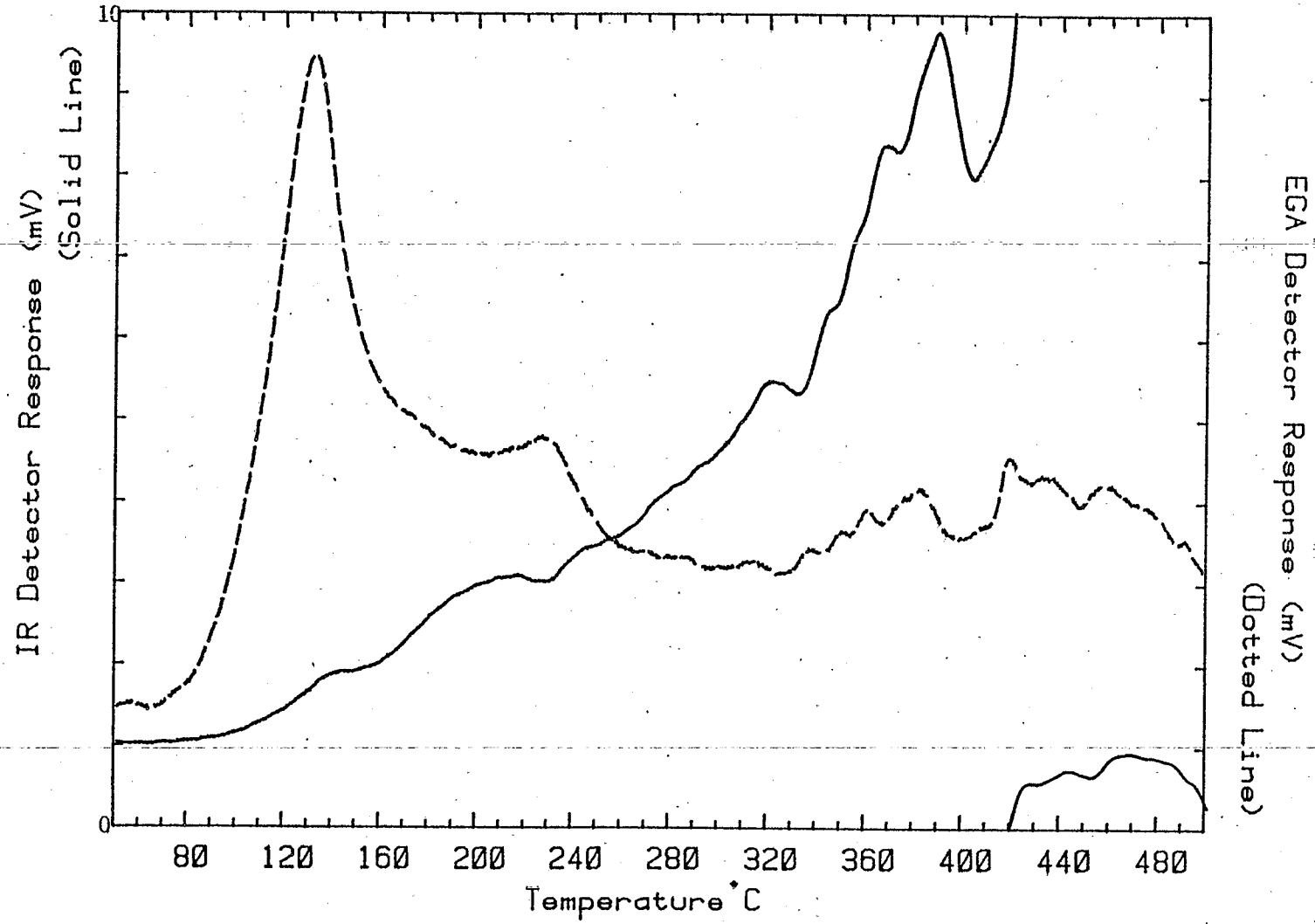

Figure V 25. EGA of Loading 59

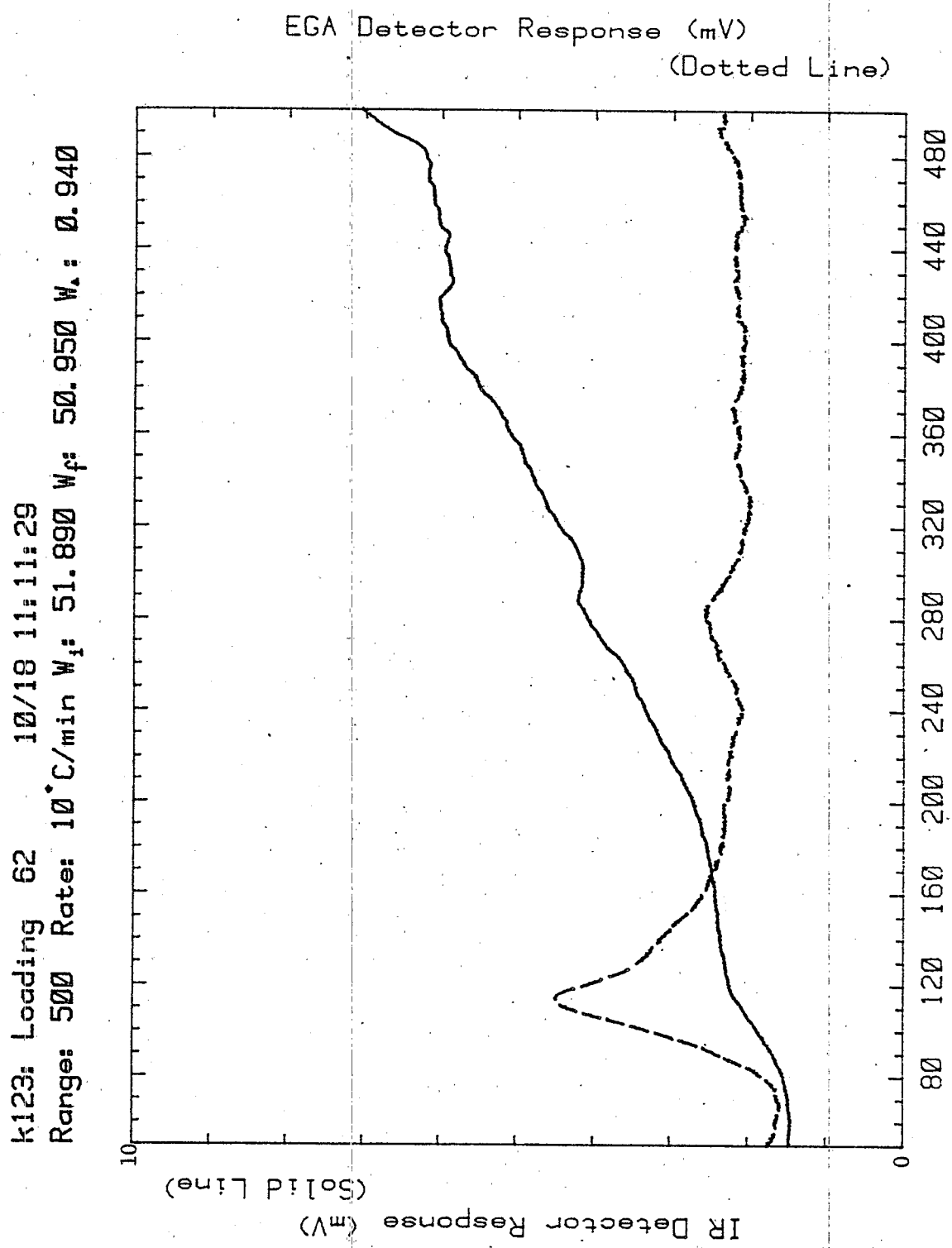

Figure 26. EGA of Loading 59

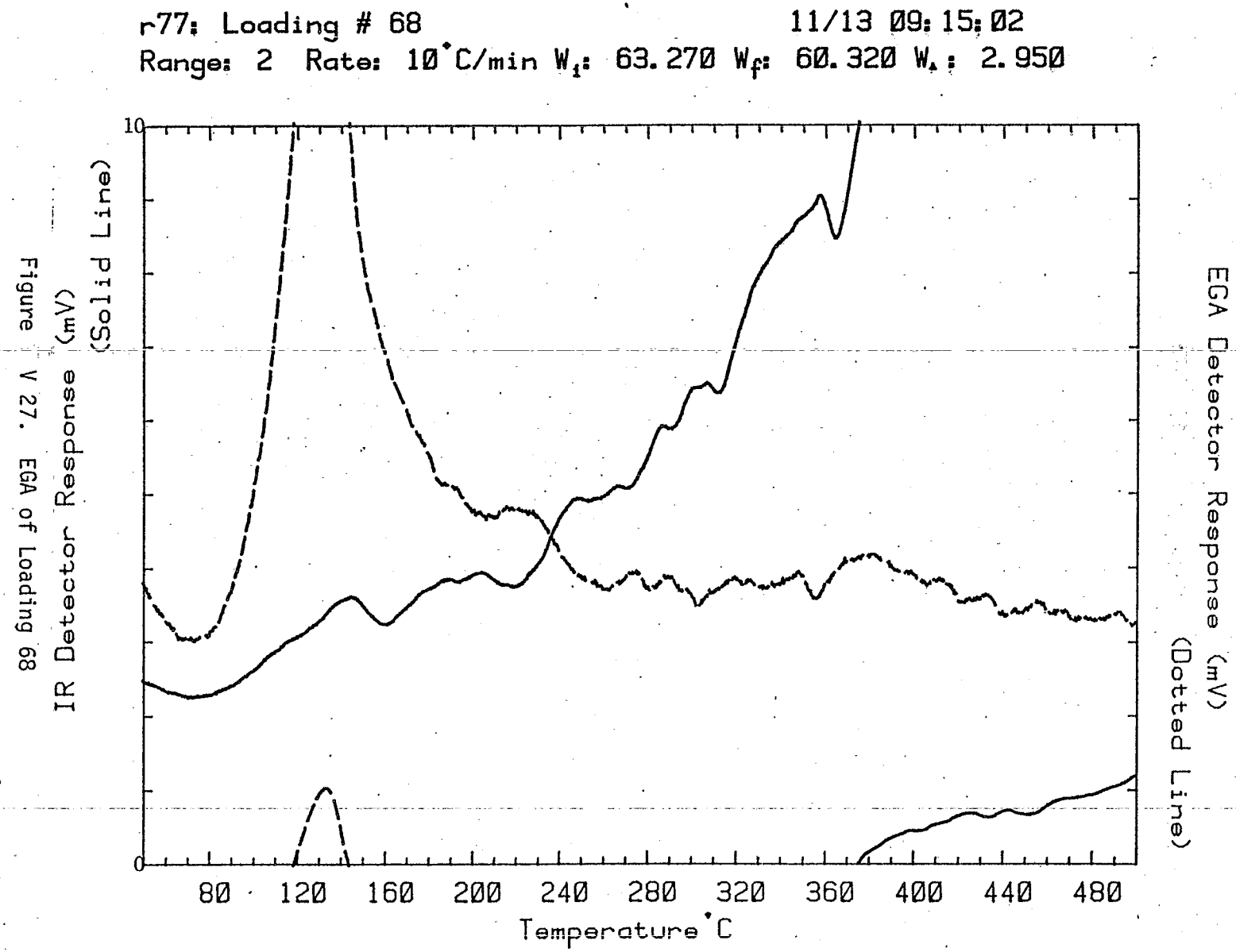

Figure V 27. EGA of Loading 68

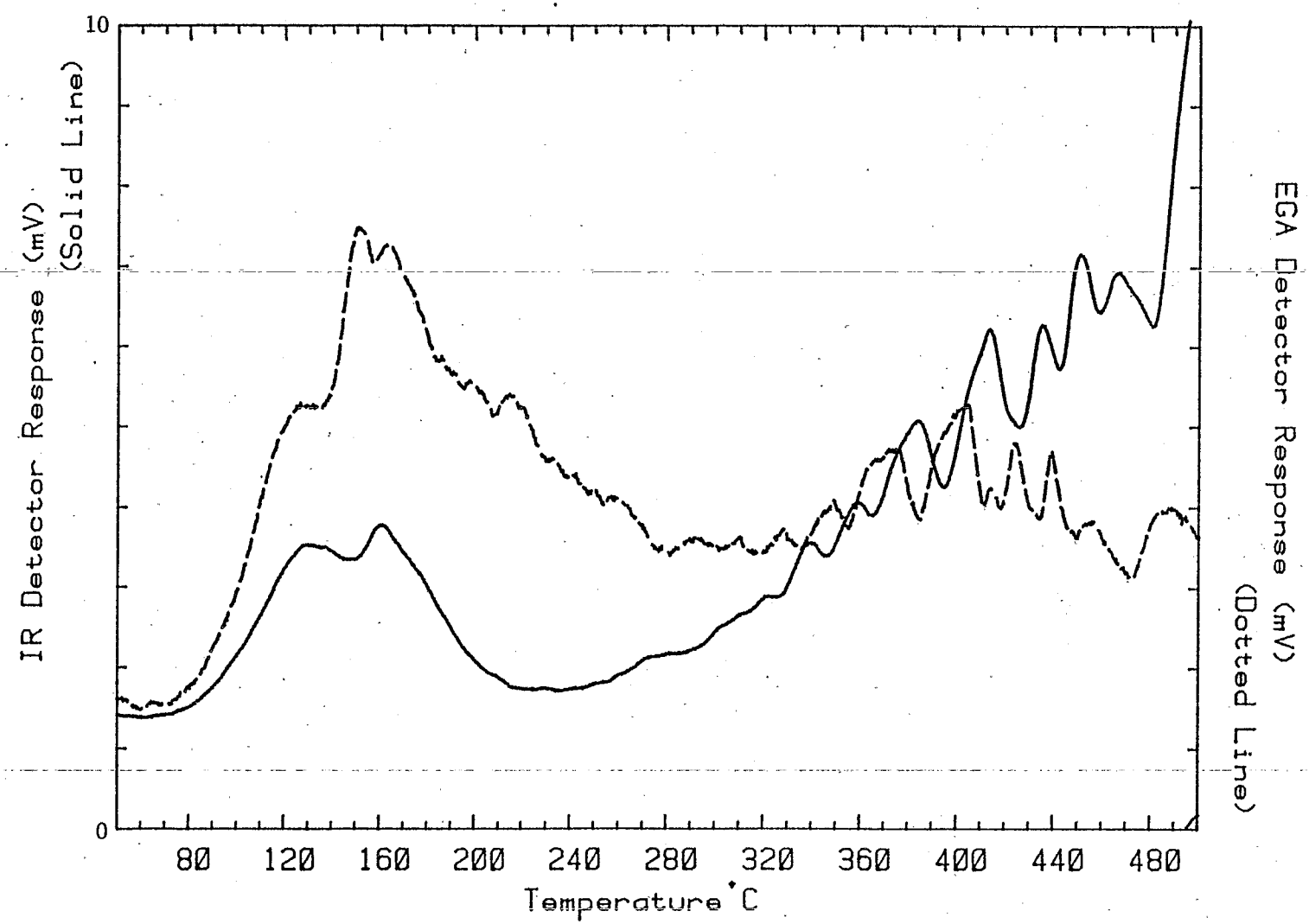

Figure V 28. EGA of Loading 86

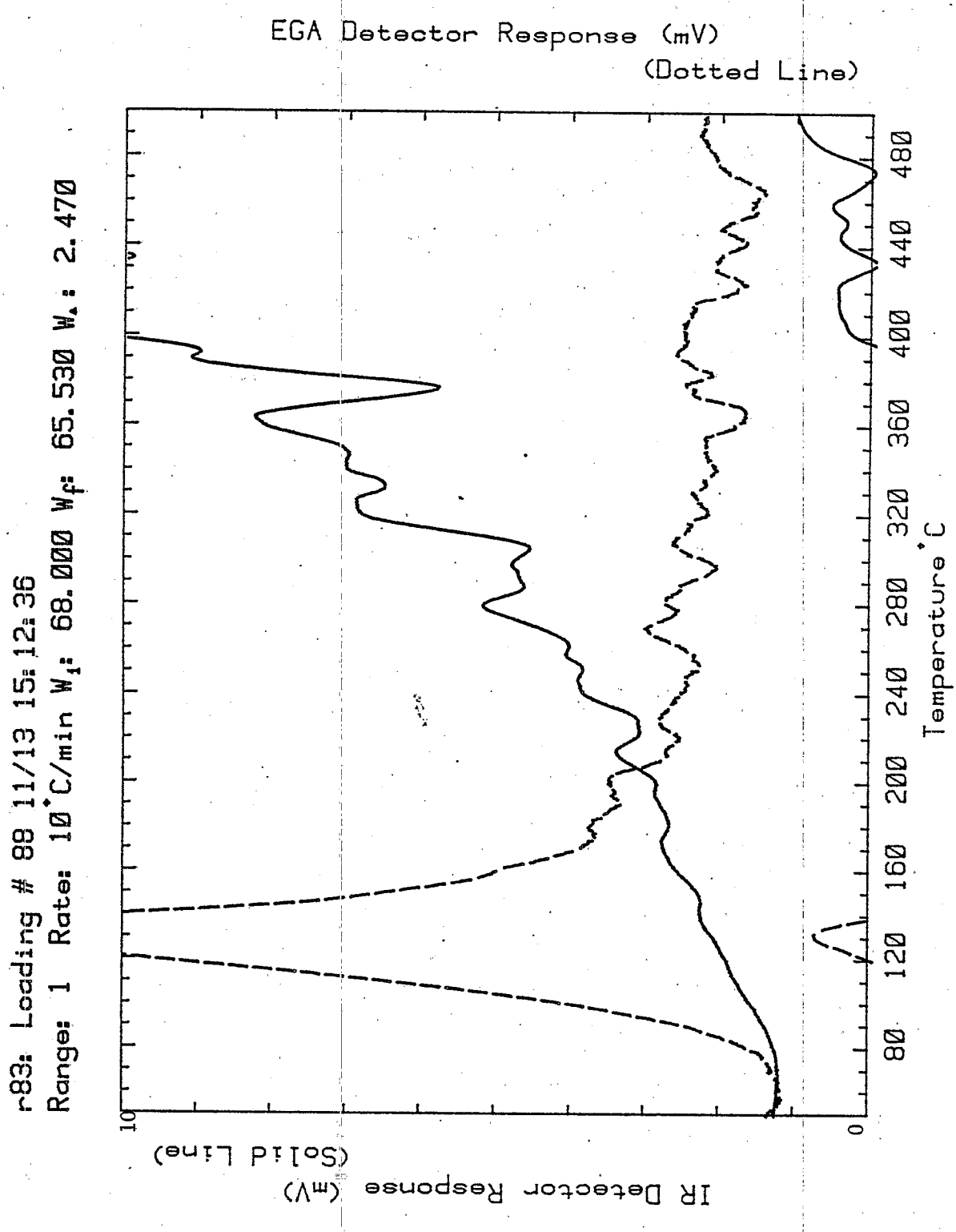

Figure V 29. EGA of Loading 88

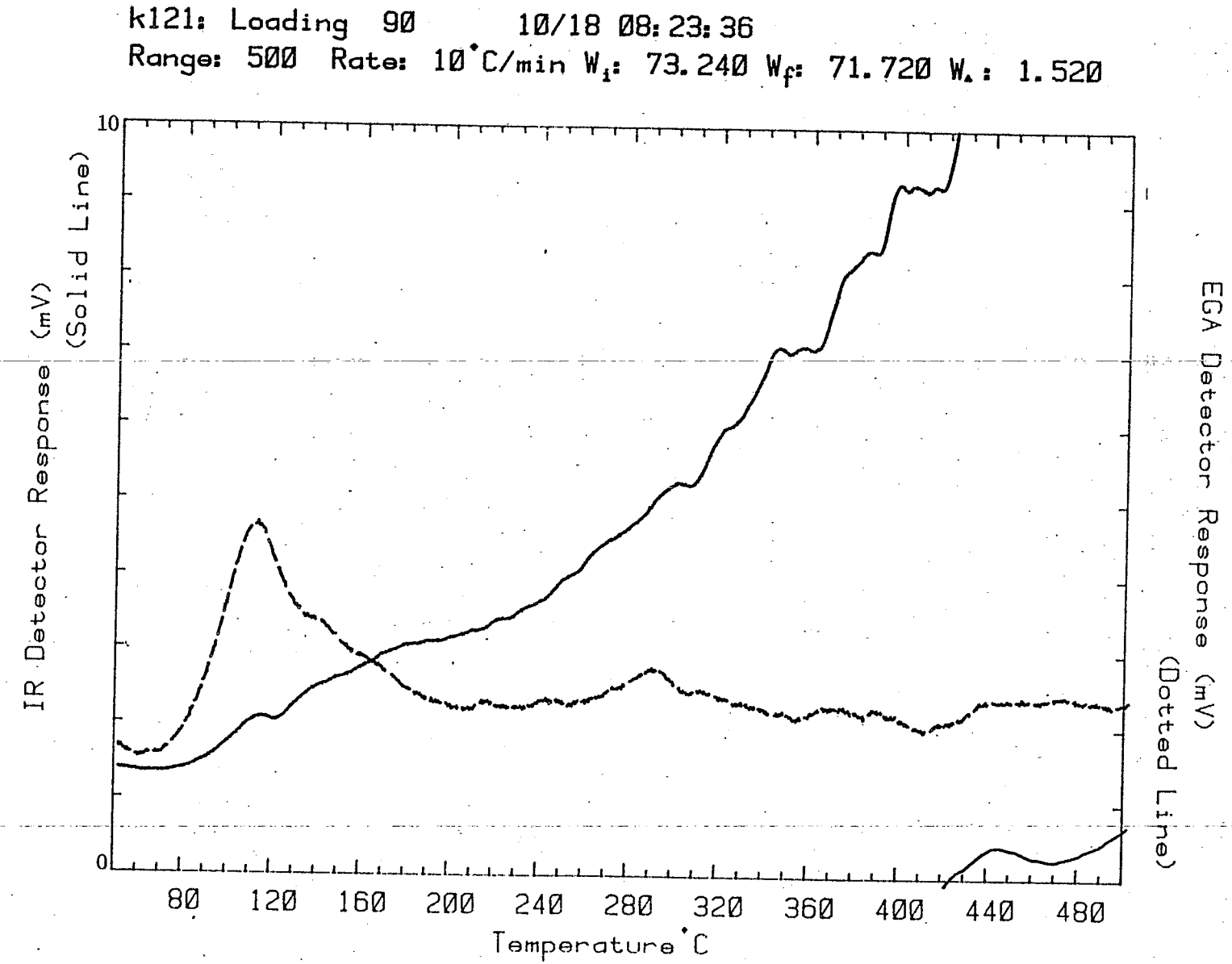

Figure V 30. EGA of Loading 90

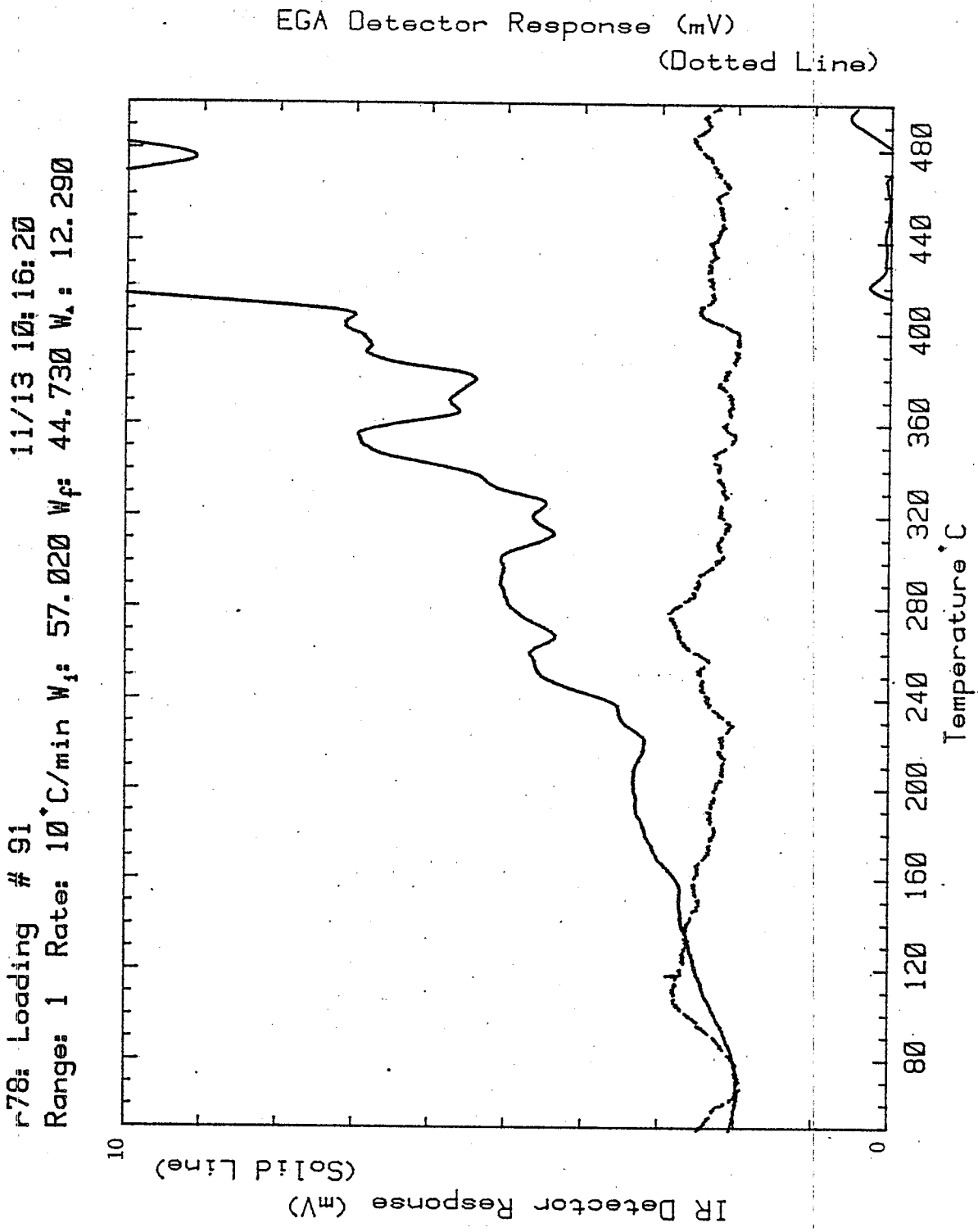

Figure V 31. EGA of Loading 91

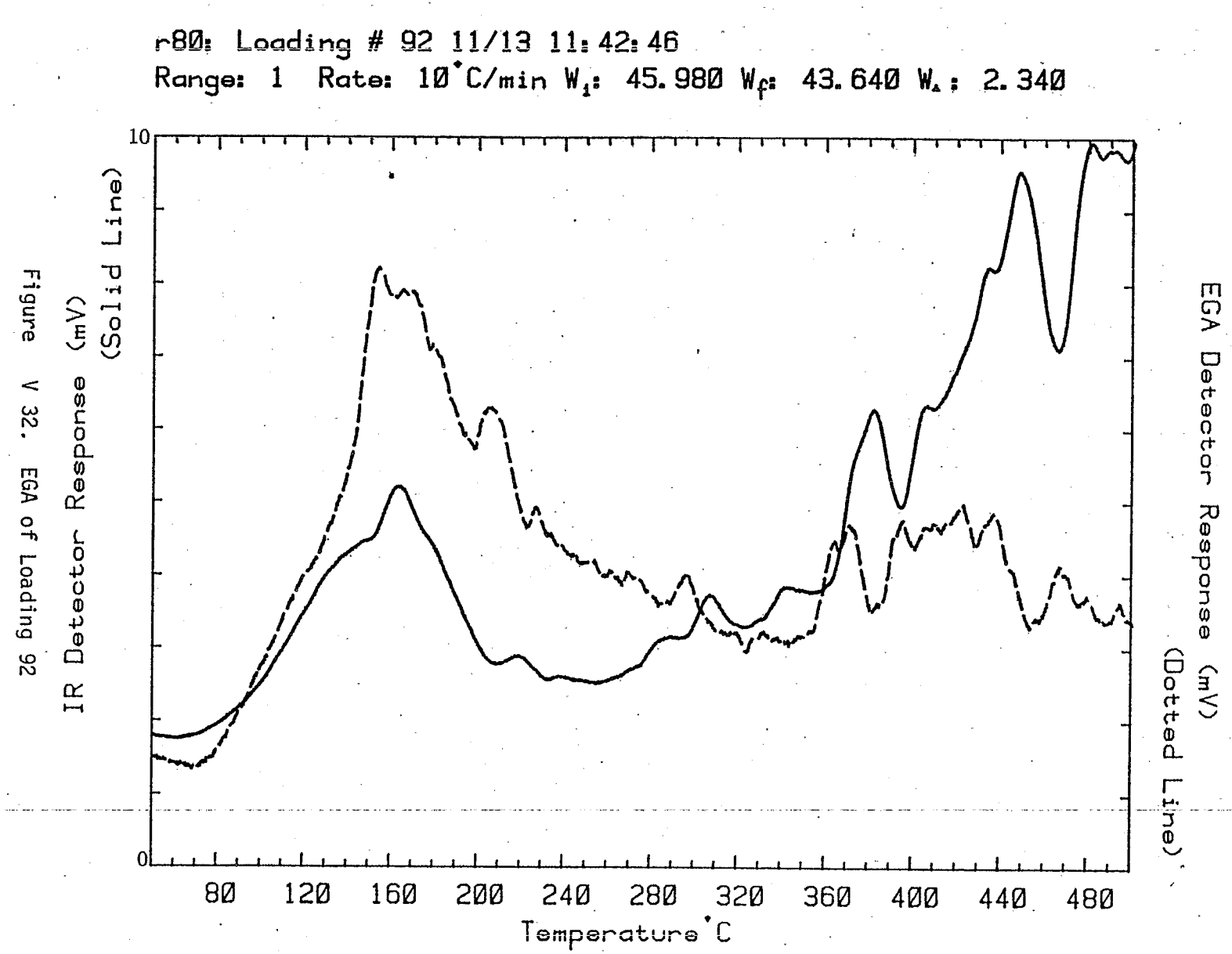

Figure V 32. EGA of Loading 92

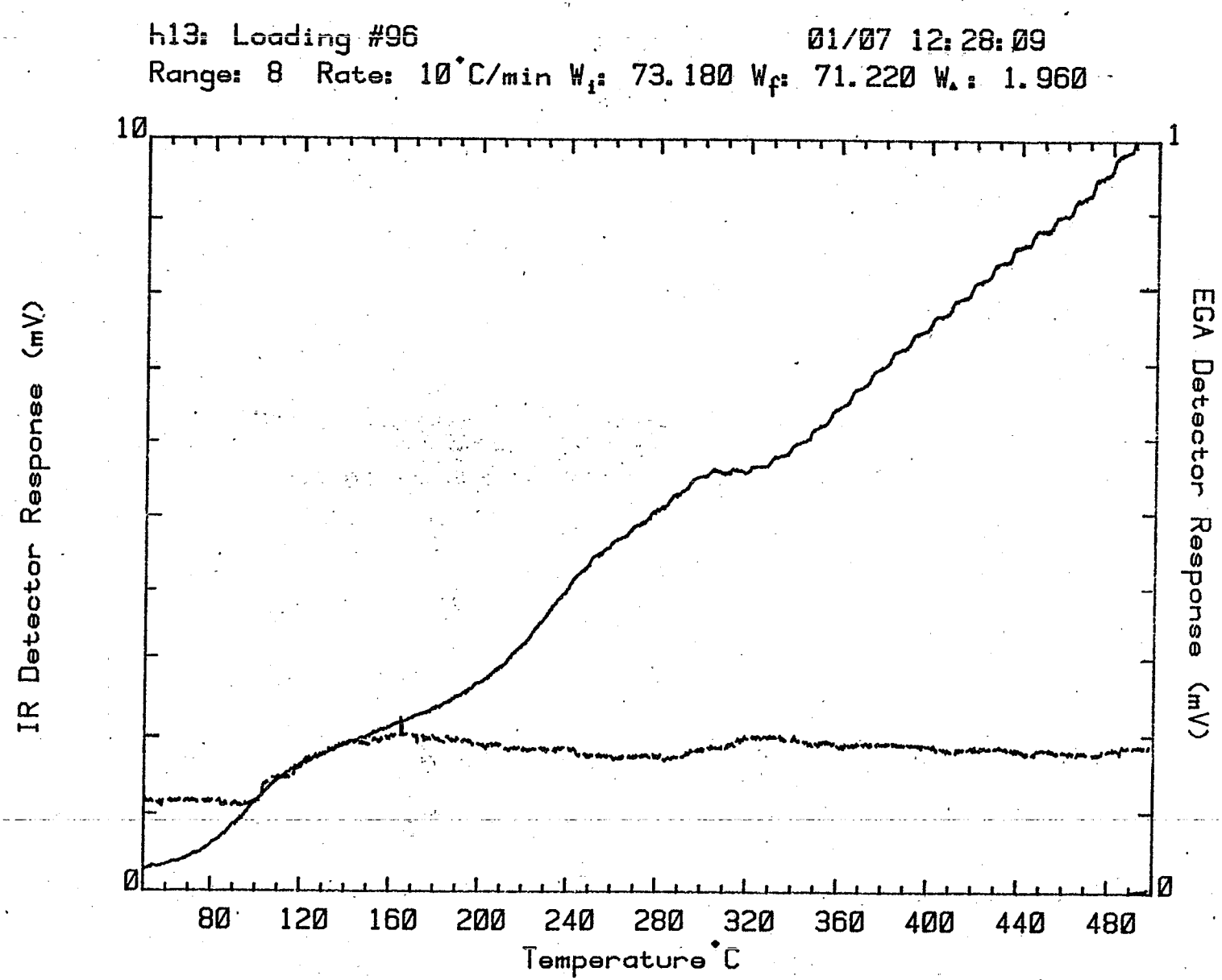

Figure V 33 EGA of Loading 96.

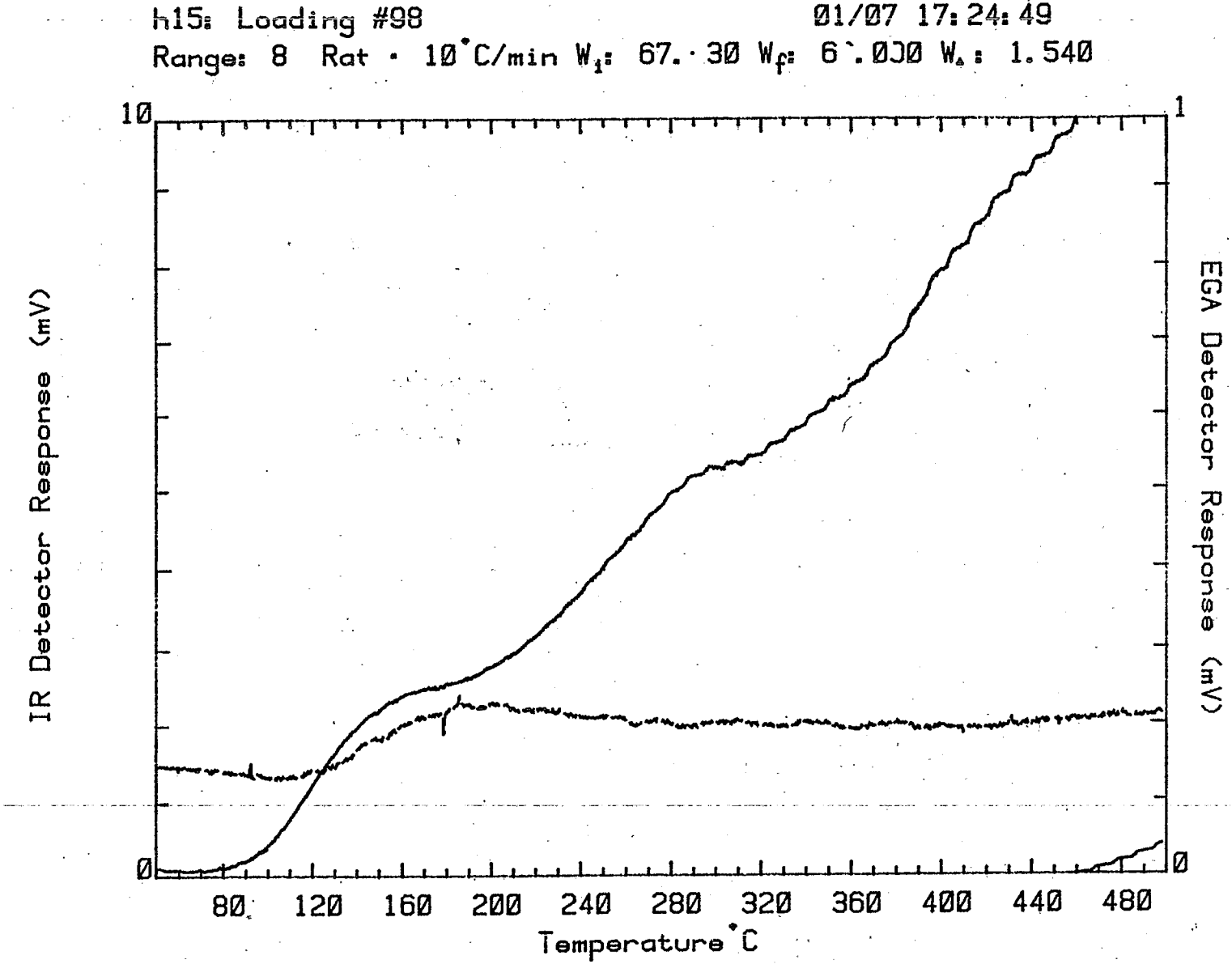

Figure V 34. EGA of Loading 98

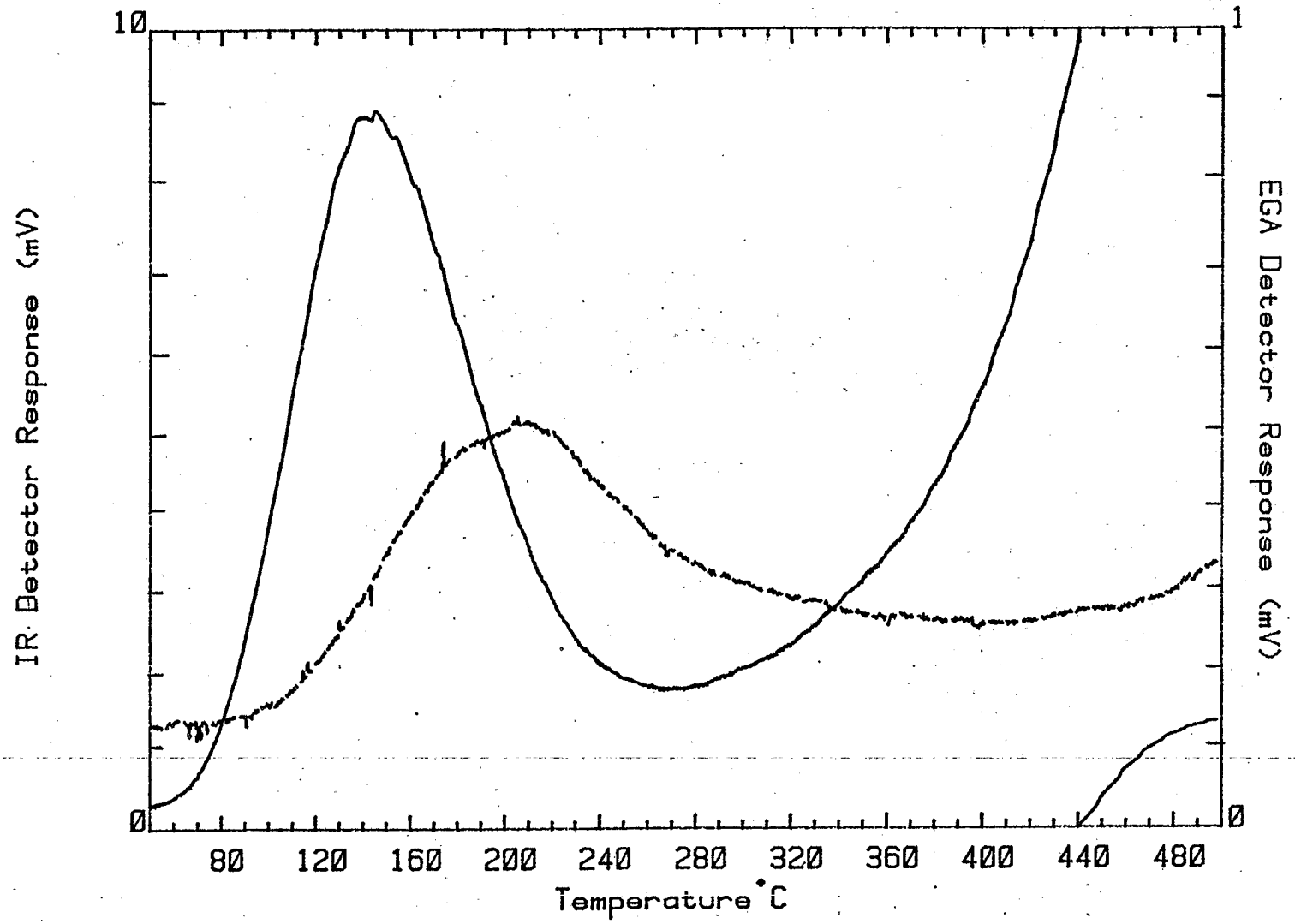

Figure V 35. EGA Of Loading 100

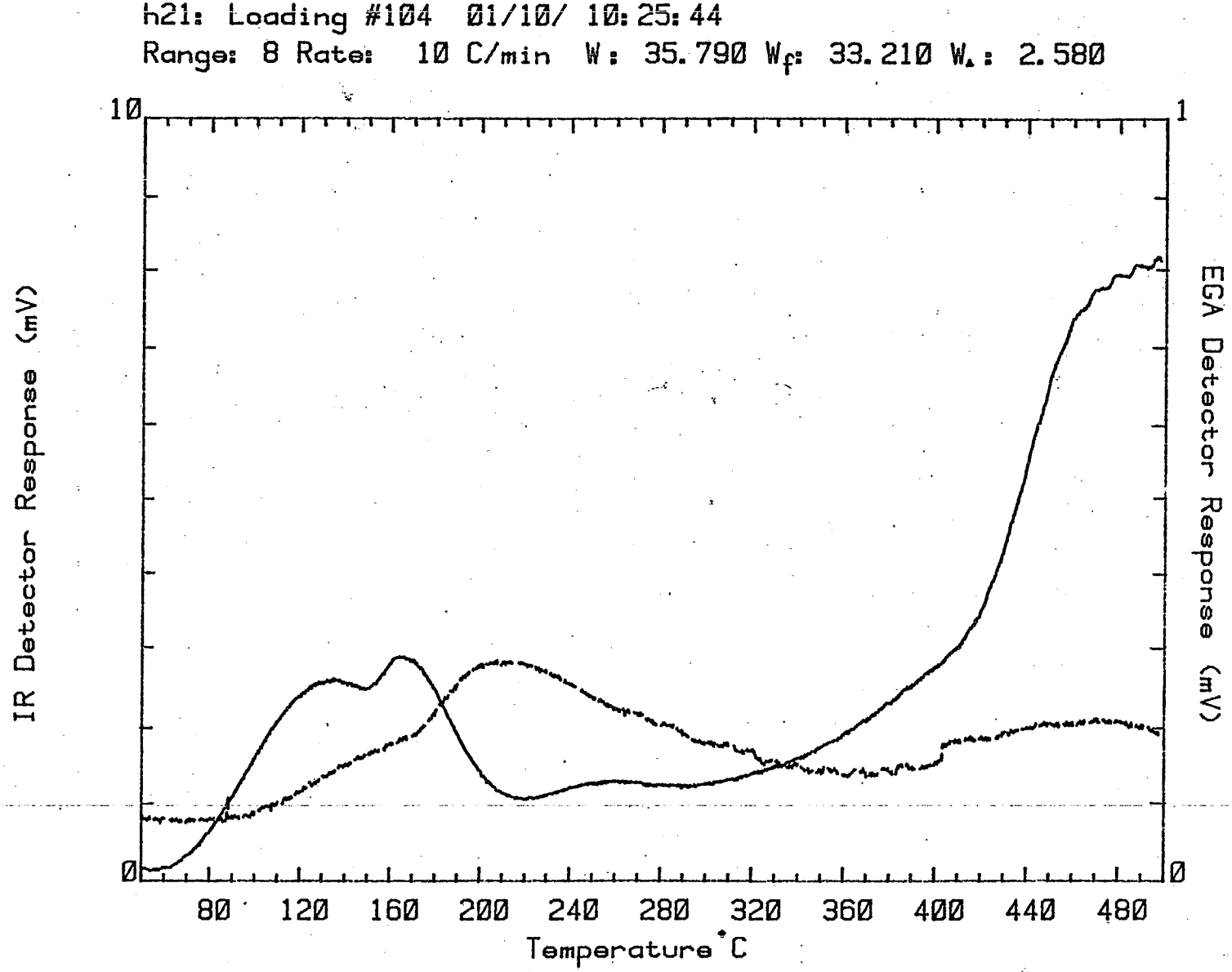

Figure V 36. EGA of Loading 104

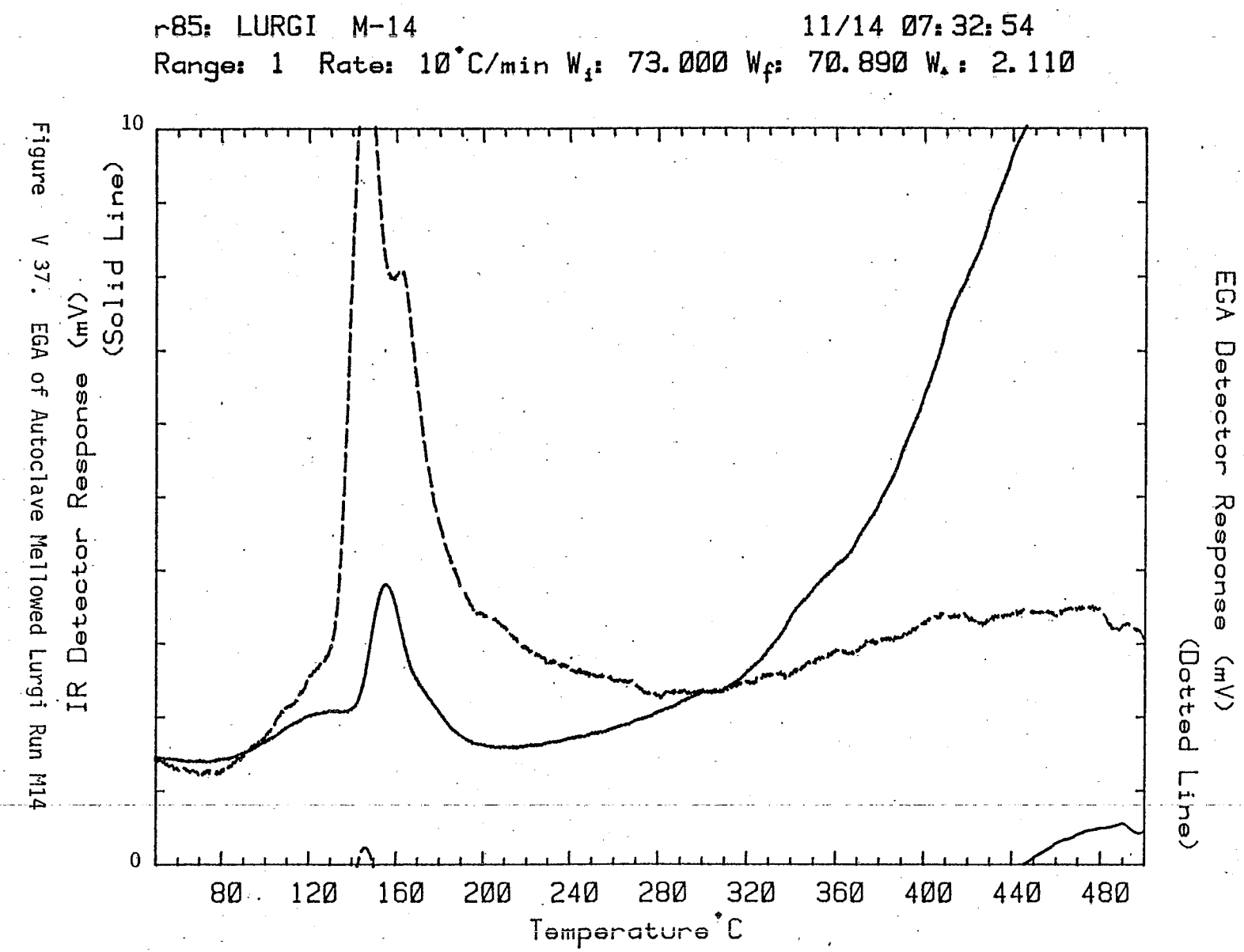

Figure V 37. EGA of Autoclave Mellowed Lurgi Run M14

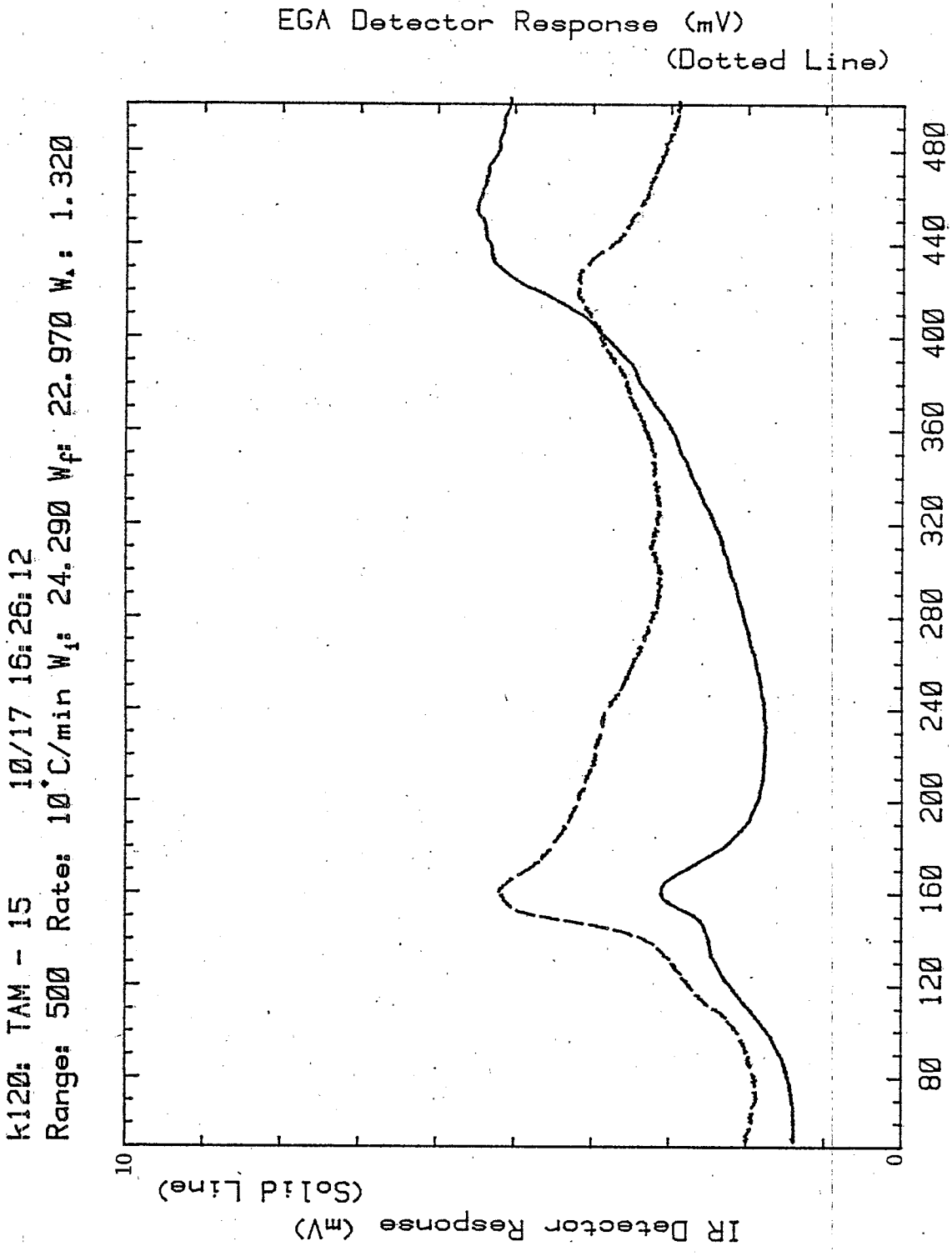

Figure 38 EGA of Autoclave Mellowed Burned TOSCO Run M15

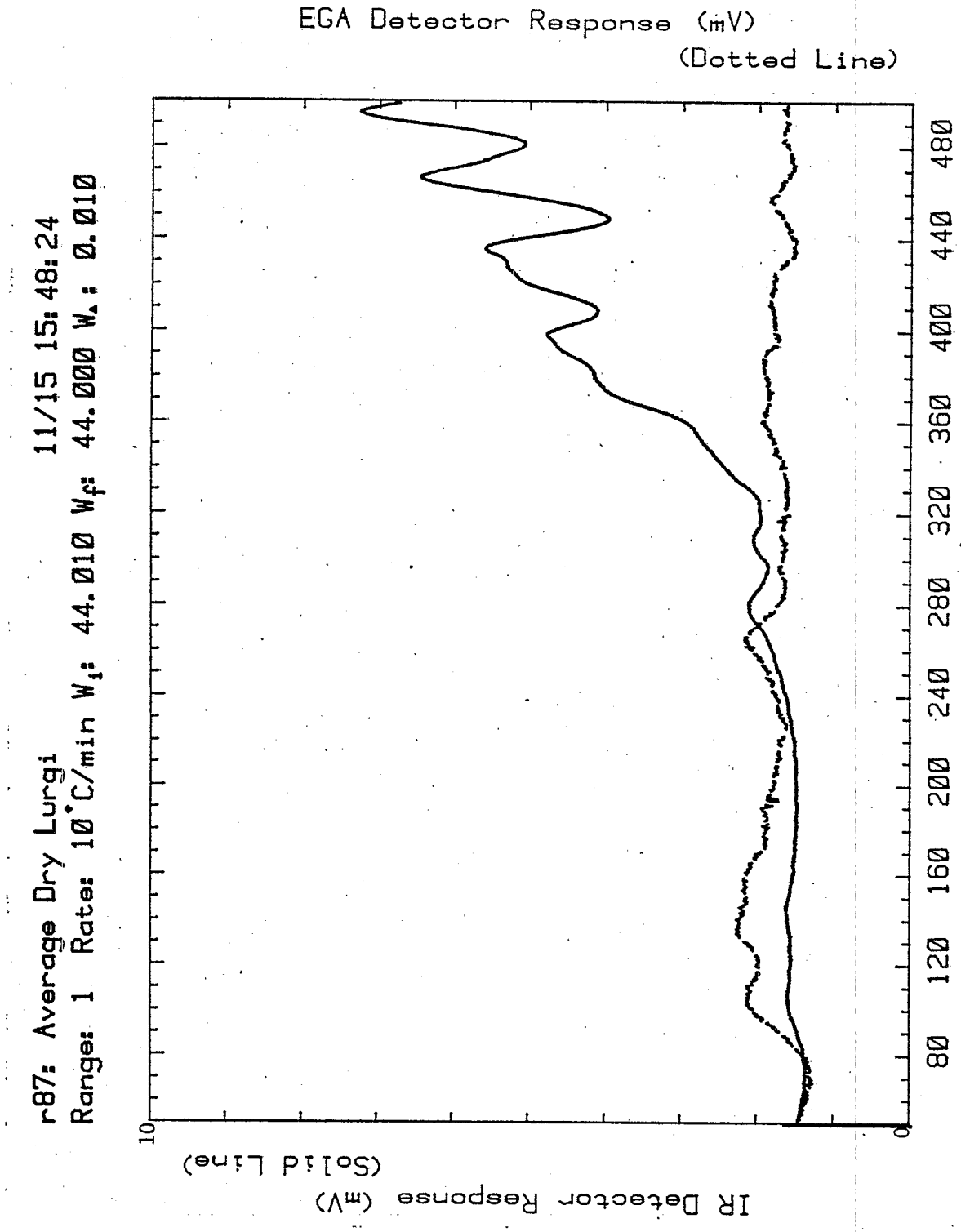

Figure V 39 EGA of Average Uniwetted Lurgi

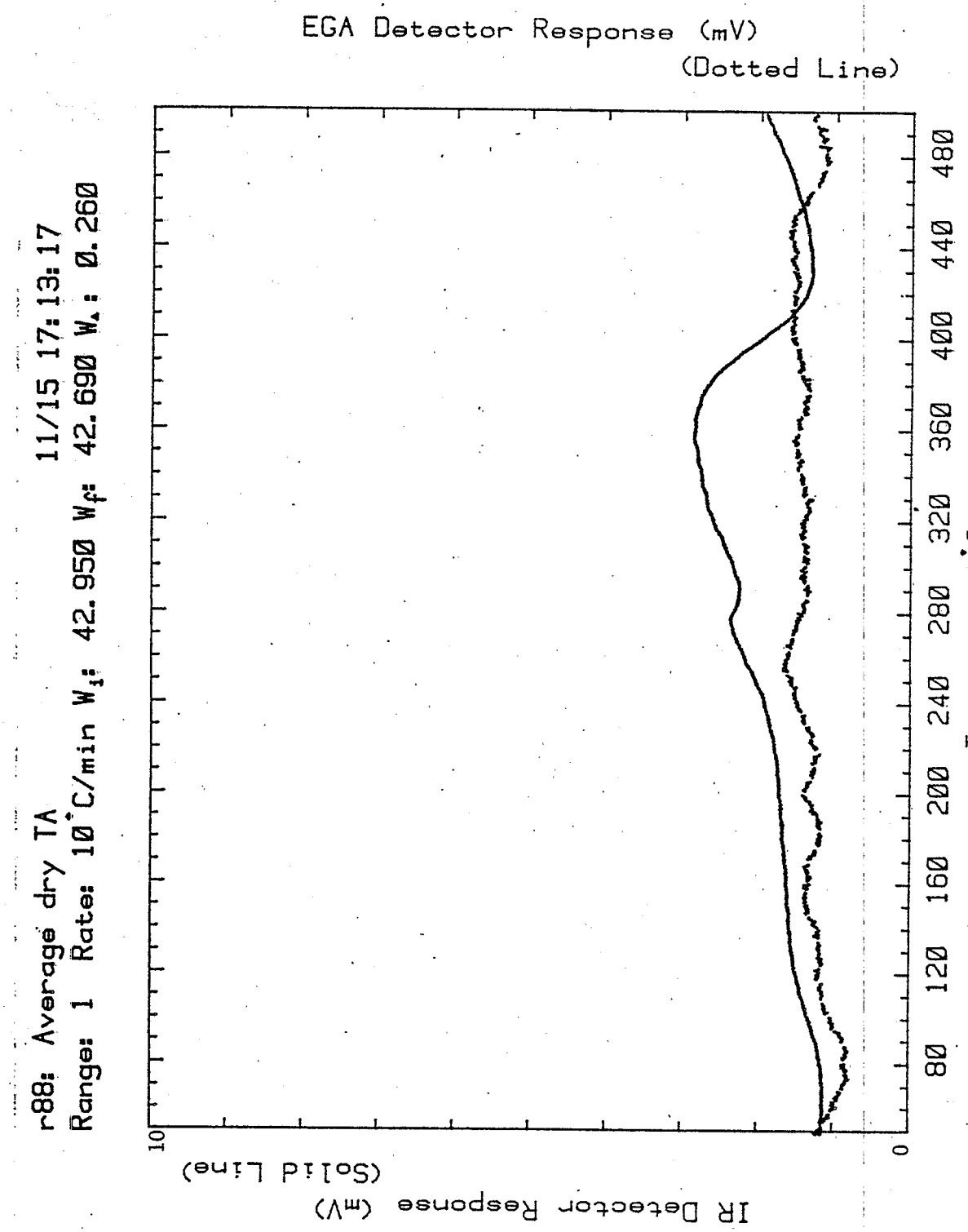

Figure V 40 EGA of Unwetted Burned TOSCO II

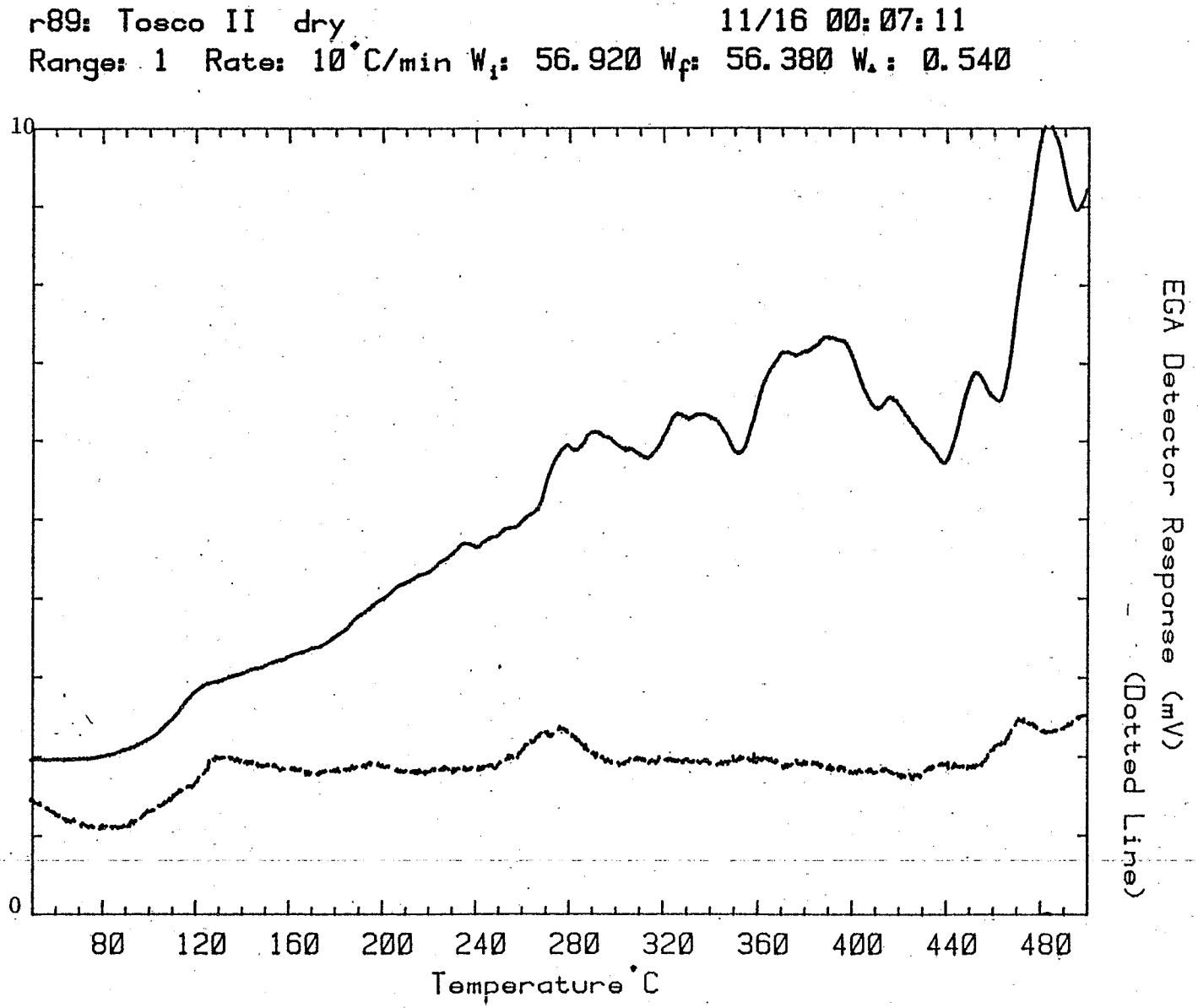

Figure V 41 EGA of Unwetted Unburned TOSCO II

VI. DISCUSSION OF RESULTS

A. Permeability

Permeability coefficients were more reproducible and self consistent than expected. Perhaps the high pores (280 psi) consolidation pressure contributed to minimum channeling along the wall of the oedometer sheath as well as to minimizing flow between peds of soil fabric which may produce variable permeabilities at lower vertical pressures. Also bimodal permeation channel development may be minimized by the compaction at optimum water content often used in producing these specimens.

During mixing of material wetter than optimum, granulation occurred in which pellets of material formed which seemed to be wetter on their surface than inside. This seeming tendency toward synergesis probably disappears as mineral hydrates form during curing but during compaction and initial consolidation the wet surface of the granules may allow smearing of their surfaces with development of parallel alignment of any clay-like mineral platelets present during compaction by proctor hammer. This may account for some of the observed lower permeability at wetter than optimum moisture content compared to a dryer moisture content.

Reduced permeability for compacted specimens of most spent shales at wetter than optimum moisture content was observed. Figure VI 1 shows this effect for both standard and modified proctored specimens made from mixtures of burned TOSCO and unburned TOSCO II spent shale. However, the effect is weak or nil for 100% unburned TOSCO II material, at four weeks curing time. Of course some other factor may be influential with these cementing materials such as increased hydrate formation at higher water contents.

Figures VI 2, 3, 4, 5, 6, and 7 show a general but not universal mild downward trend of permeability at increasing curing times, especially beyond 30 days with the exception of the more cementaceous 70% TOSCO II with 30% burned TOSCO blend and the Lurgi spent shale which showed increased permeabilities beyond 30 days even though the latter had shown a decrease up to 30 days. The lower permeability at wetter than optimum water content is evident again with the Lurgi material in Figure VI 6 when the 22% water added is compared with the 27% water added curves within the modified proctor constraint (square data points).

It is difficult to make sense of the sketchy permeability vs curing time curves of Figures VI 2, 3, 4, 5 and 6. This is perhaps caused by the irregular course of mineral hydrate formation and disappearance as curing time increases. Reduction of the mineral grain density (determined by the Beckman air pycnometer) of pulverized 48°C oven dried material from the torsion test is assumed to be an indication of the extent of hydrate water incorporated in cementaceous and/or bulk producing species in the specimen. Figures VI 8, 9, 10, 11, and 12 plot the remarkable course of the extent of hydrate water present in the specimens after torsion testing as indicated by mineral grain density. If a lower mineral grain density indicates more mineral hydrate water then there is an appreciable maximum in mineral hydrate water at around 20-30 days as curing progresses with time for all unmellowed TOSCO spent shale materials studied including unburned TOSCO II spent shale.

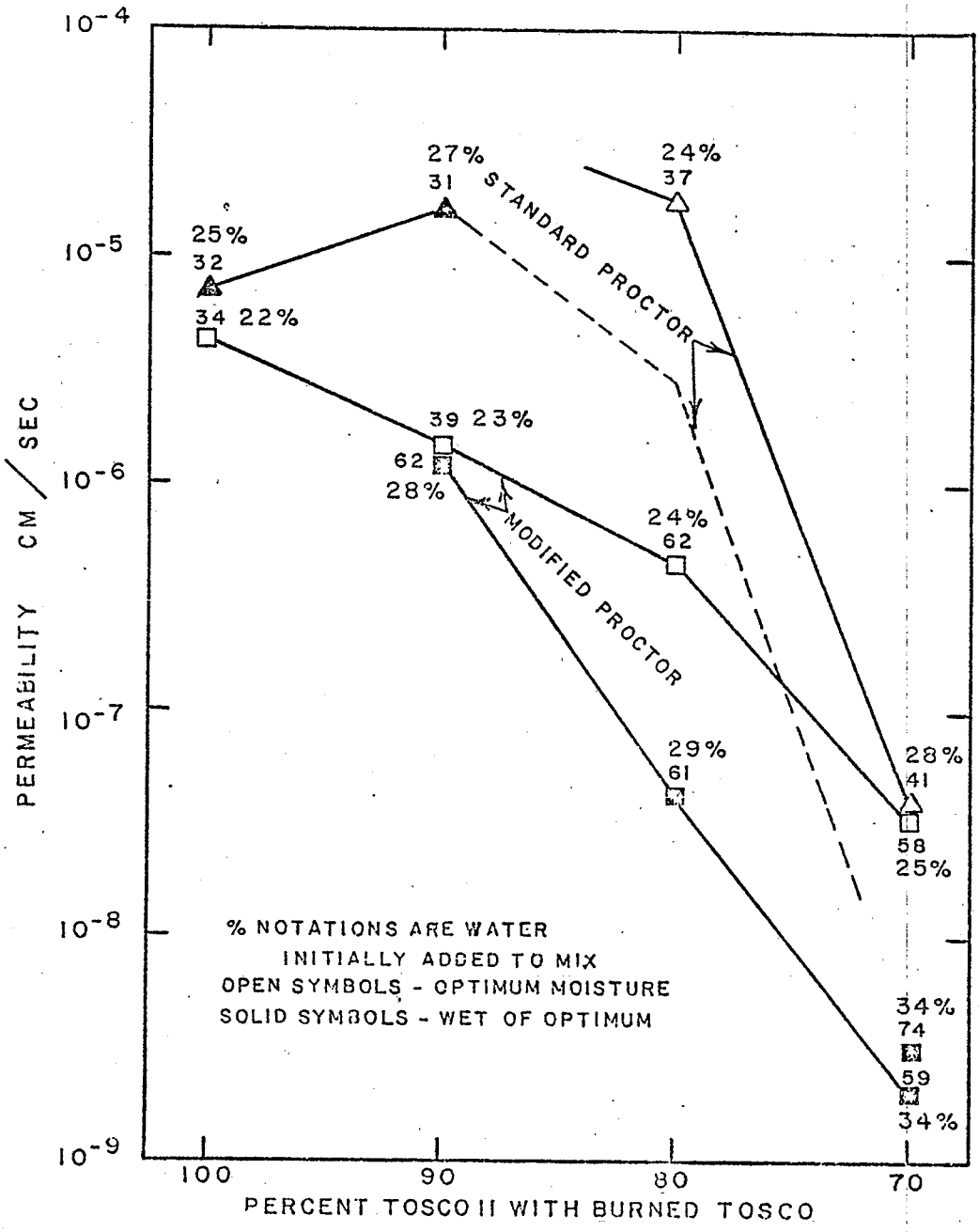

Figure VI 1. Permeability of Mixtures of Burned TOSCO and Unburned TOSCO Spent Shale after Approximately Four Weeks Curing in Spring Oedometers.

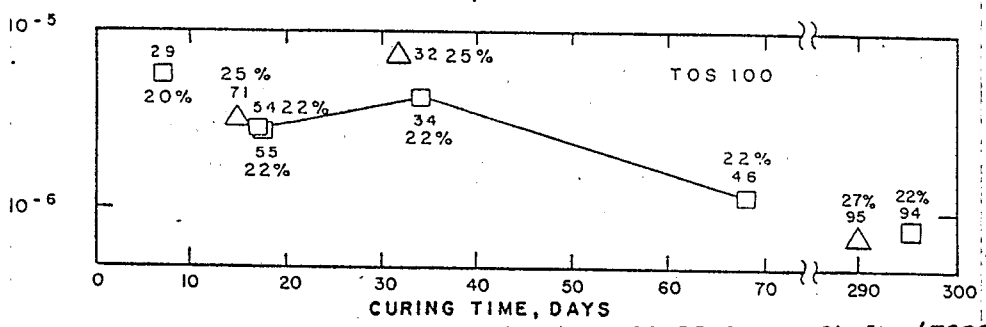

Figure VI 2. Permeability of 100% TOSCO II Spent Shale (TOSCO 100)

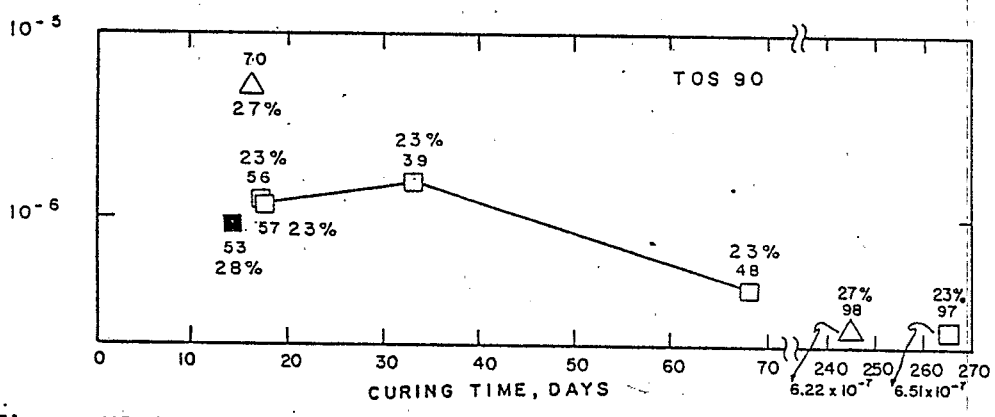

Figure VI 3. Permeability of 90% TOSCO II - 10% Burned TOSCO Spent Shale (TOSCO 90)

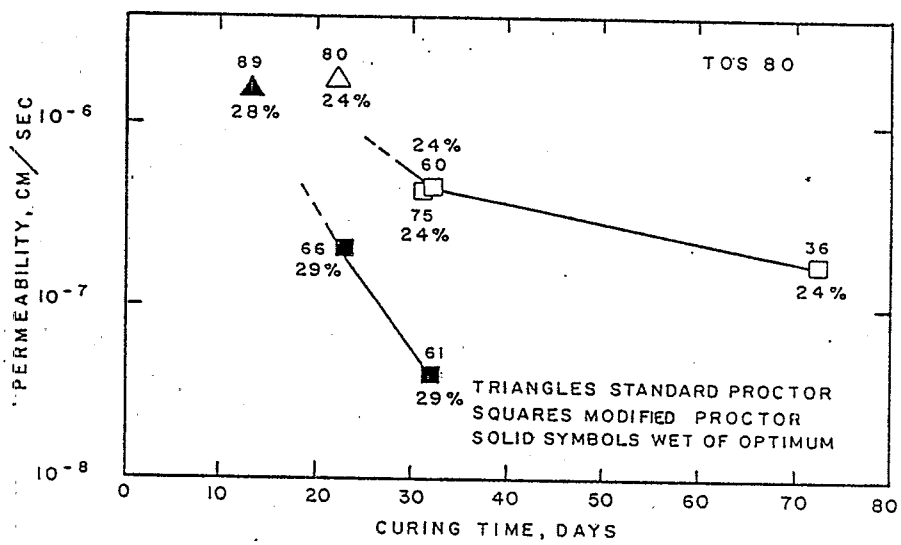

Figure VI 4. Permeability of 80% TOSCO II - 20% Burned TOSCO Spent Shale (TOSCO 80)

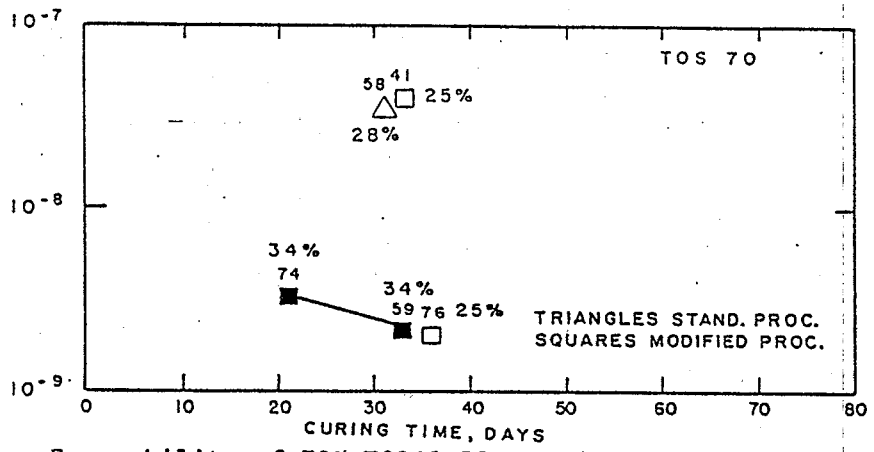

Figure VI 5. Permeability of 70% TOSCO II - 30% Burned TOSCO Spent Shale (TOSCO 70)

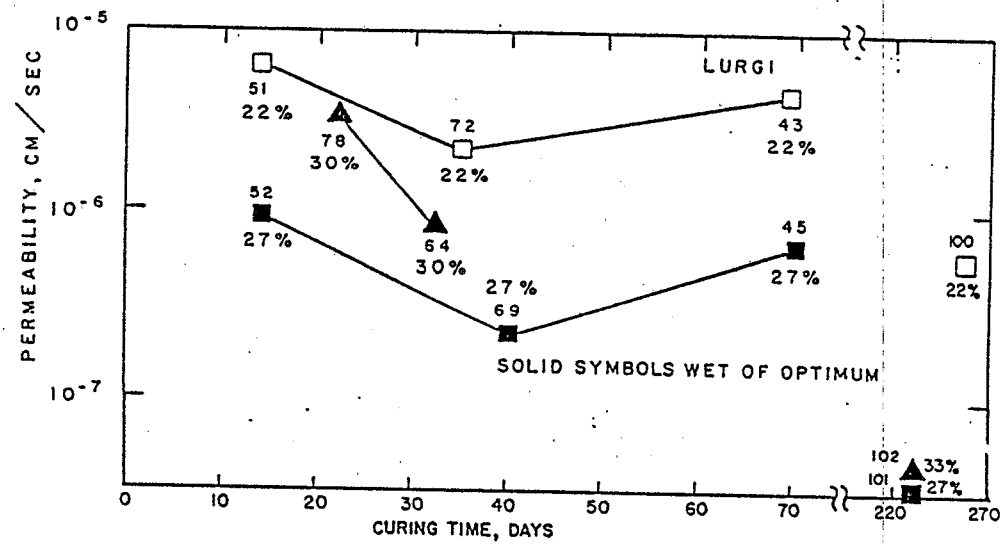

Figure VI 6. Permeability of Lurgi Spent Shale.

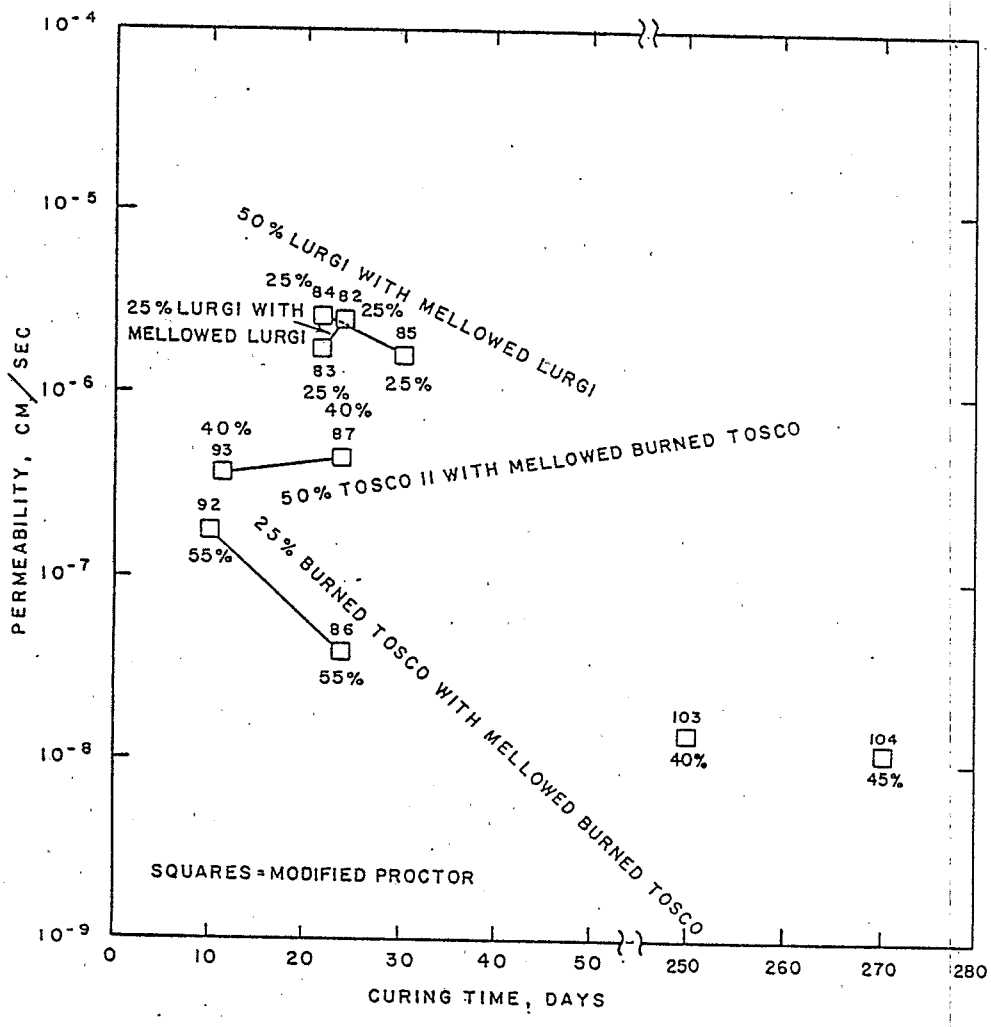

Figure VI 7. Permeability of Mellowed Lurgi (M14) Mixed into Lurgi and Mellowed Burned TOSCO (M-15) Mixed into TOSCO II and into Burned TOSCO Spent Shale.

The Lurgi spent shale, however, showed not only less reduction in mineral grain density after curing compared to the grain density of the uncured dry raw material but no clear cut minimum and some scatter of the data points. Apparently a different cementation mechanism is involved with the Lurgi material than with the TOSCO materials or else the Lurgi pilot plant pre-hydrated the material to considerable extent during post pyrolysis operations.

The interpretation of the minimum in the mineral grain density plots of the TOSCO spent shales (Figures VI 8, 9, 10, and 11) as due to mineral hydrate maxima is substantiated by Figure VI 5, introduced later, which shows maxima in a low temperature evolved gas analysis water peak (at approximately 150°C) at curing times corresponding to the minima in mineral grain density. This peak appears to be due to a tobermorite-like species, CSH I ($CaO\ S_iO_2 \cdot nH_2O$) and ettringite.

Figure VI 13, shows the permeabilities found for autoclave mellowed Lurgi (autoclave run M 14) mixtures with Lurgi, an autoclaved burned TOSCO (M15) mixture with unburned TOSCO II and an autoclaved burned TOSCO (M15) mixture with burned TOSCO spent shale plotted vs void ratio e for certain of the spring oedometer specimens. These were all modified proctor specimens and the water added and curing times are noted by the data points plotted. The low permeability of the 75% autoclave mellowed burned TOSCO spent shale mixed with 25% of burned TOSCO spent shale is to be particularly noted in view of its low cementation to the time curing was stopped. Before concluding that the mixtures containing burned TOSCO spent shale giving the lowest permeability are most desirable in a liner the brittleness of the liner must be considered and also its ability to self heal after fracture or during tension movement.

The permeabilities were determined just before torsion testing, the void ratios were based on mineral grain densities determined on 48°C oven dried material after torsion testing and bulk dry density of the specimens just after loading in the spring oedometers. The bulk dry density was calculated based on water added to the wet mixture loaded into the oedometer.

Figure VI 13 shows that in general the greater the fraction of burned TOSCO spent shale that is blended into the unburned TOSCO II spent shale the less the permeability at a given void ratio. Lower void ratios give lower permeabilities also, however, as is the well known trend for ordinary soils. Fairly clearly the hydrate forming cementation reactions of burned TOSCO containing spent shale reduce permeability beyond that to be expected by simple reduction of void ratio determined using mineral grain density. This may be due to deposition of fine precipitate or gel within the spent shale particles interstitial spaces or it may be due to deposition at spent shale particle contacts that grows to invade the interstitial spaces. Growth of cementaceous hydrates within a given porous spent shale particle should not influence permeability of the specimen much.

B. Peak Angle of Internal Friction ^{O}P Related to Self Healing and Its Trade off with Permeability

Figure VI 14 shows a dilemma in trying to compound a liner material made from any mixture made from burned TOSCO and unburned TOSCO II spent oil

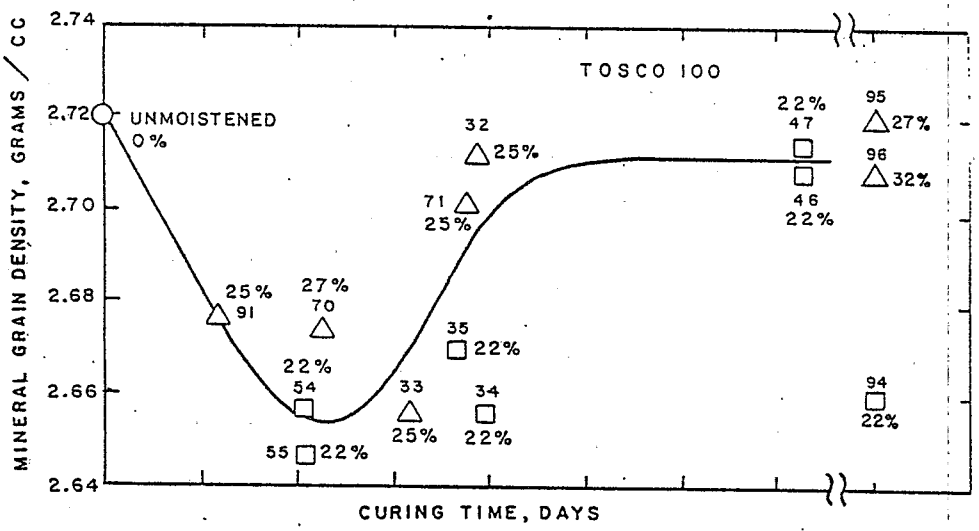

Figure VI 8. Mineral Grain density vs Time for TOSCO 100 Spent Shale

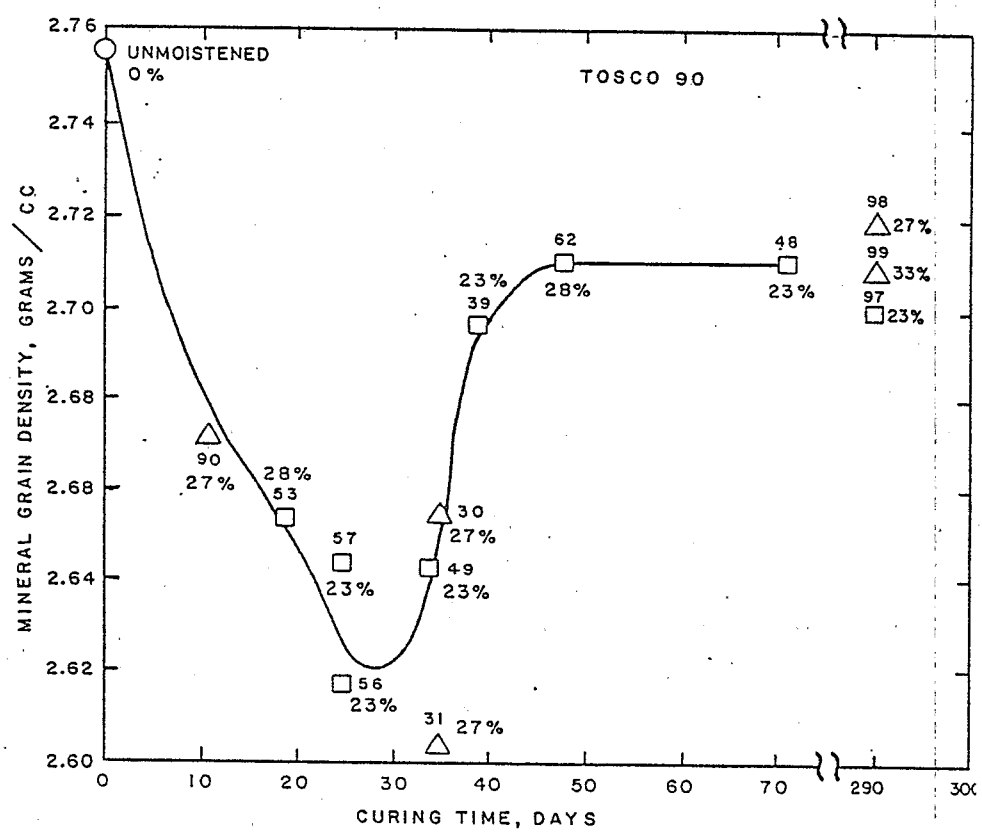

Figure VI 9. Mineral Grain Density vs Time for TOSCO 90 Spent Shale

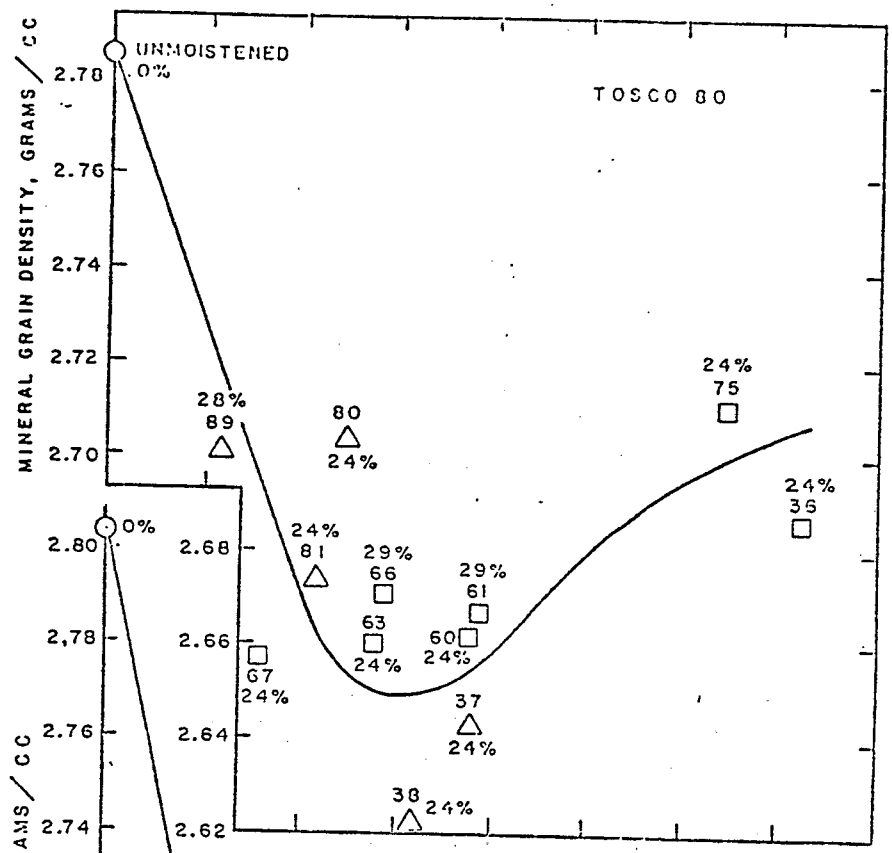

Figure VI 10 Mineral Grain Density vs Time for TOSCO 80 Spent Shale

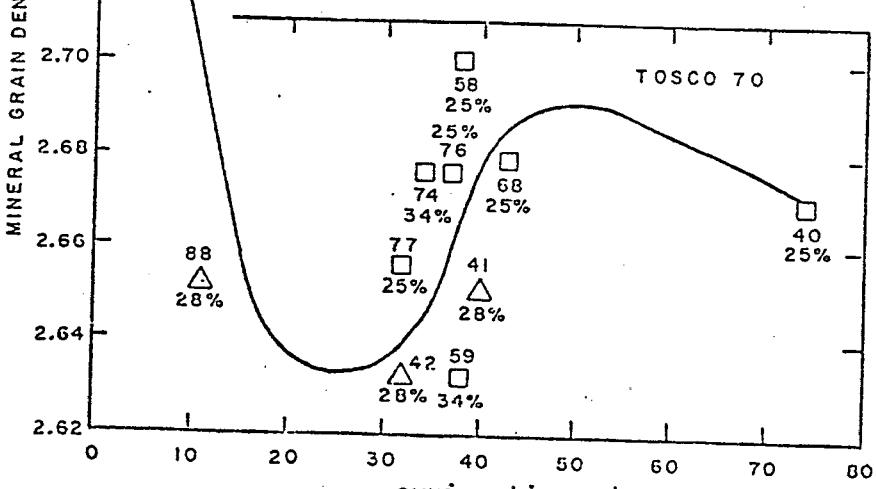

Figure VI II. Mineral Grain Density vs Time for TOSCO 70 Spent Shale.

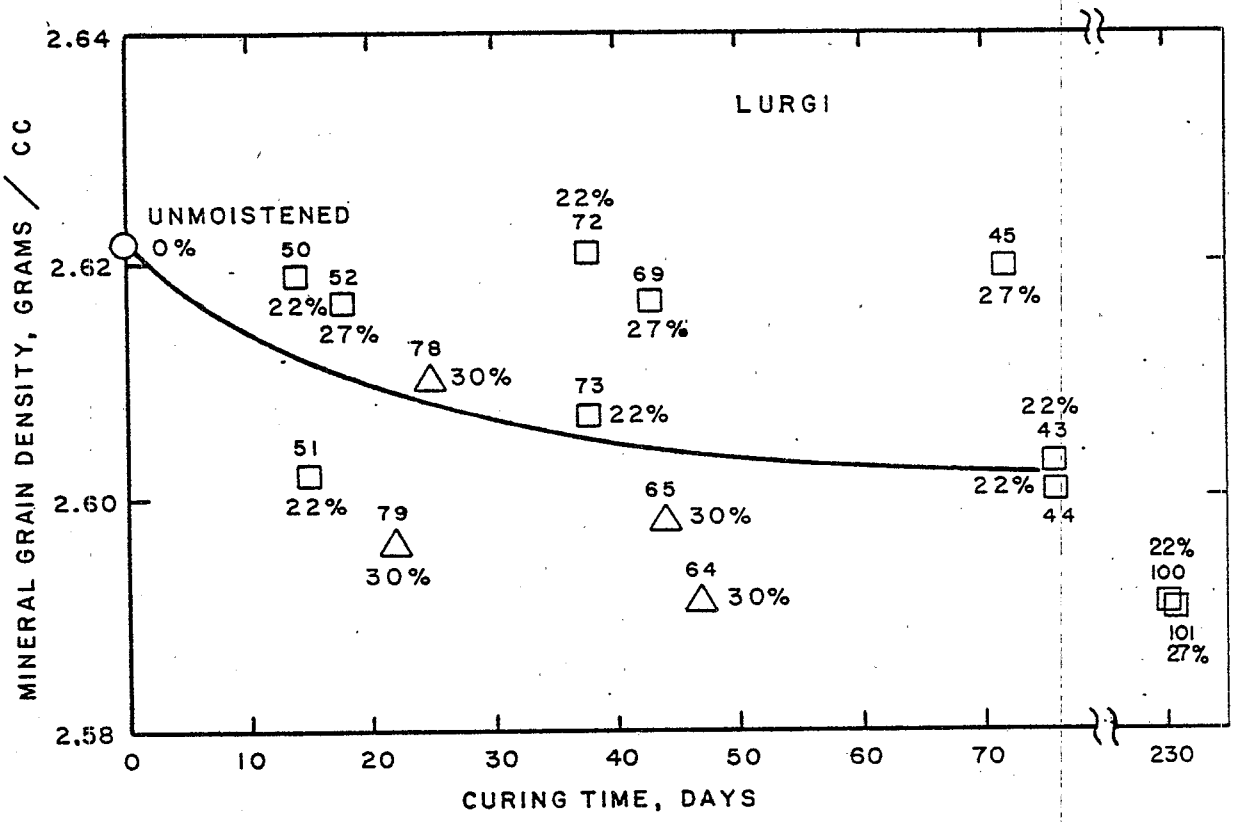

Figure VI 12. Mineral Grain Density vs Time for Lurgi Spent Shale

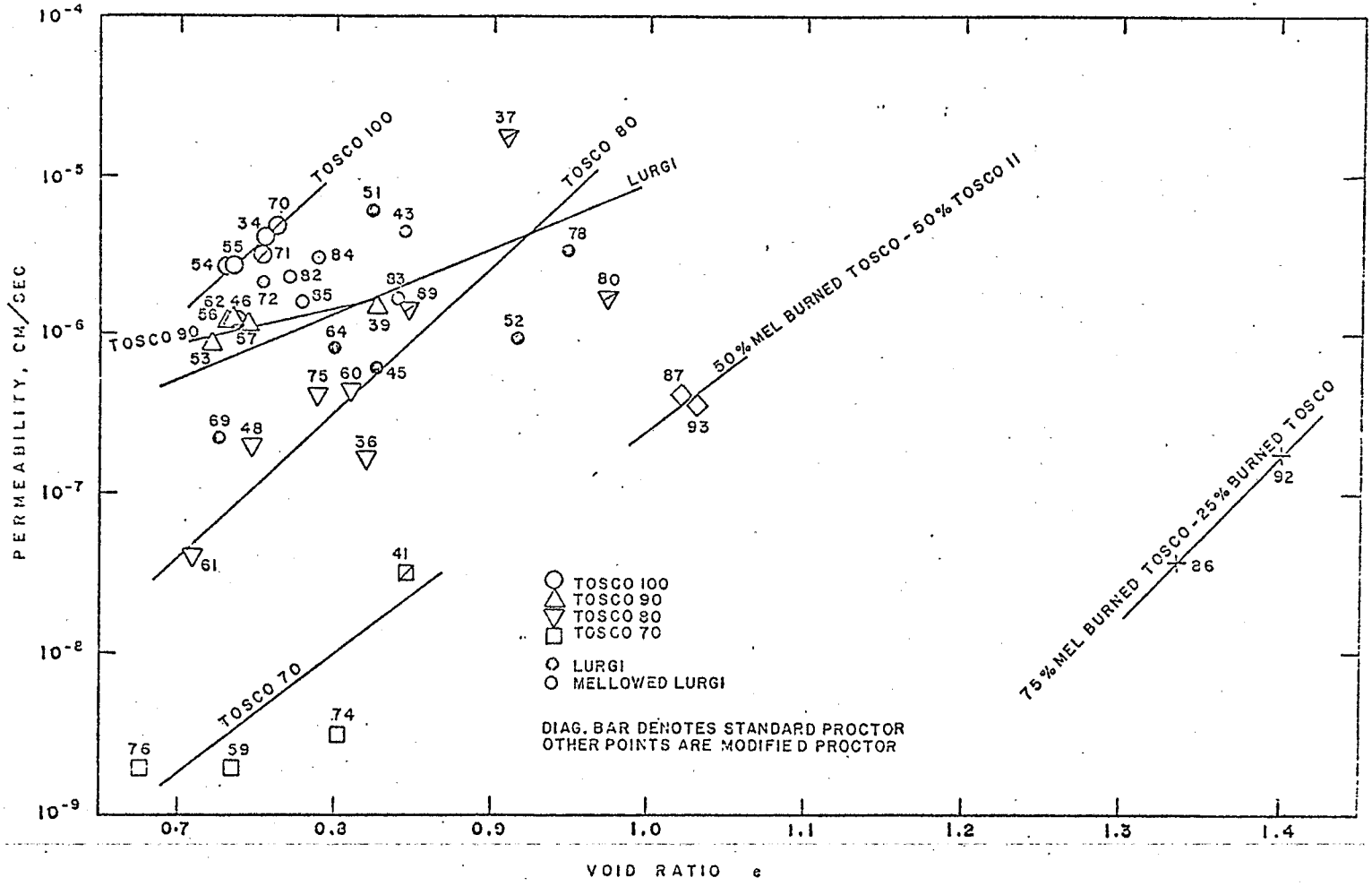

Figure VI 13. Permeability of Spent Shales Correlated with Void Ratio.

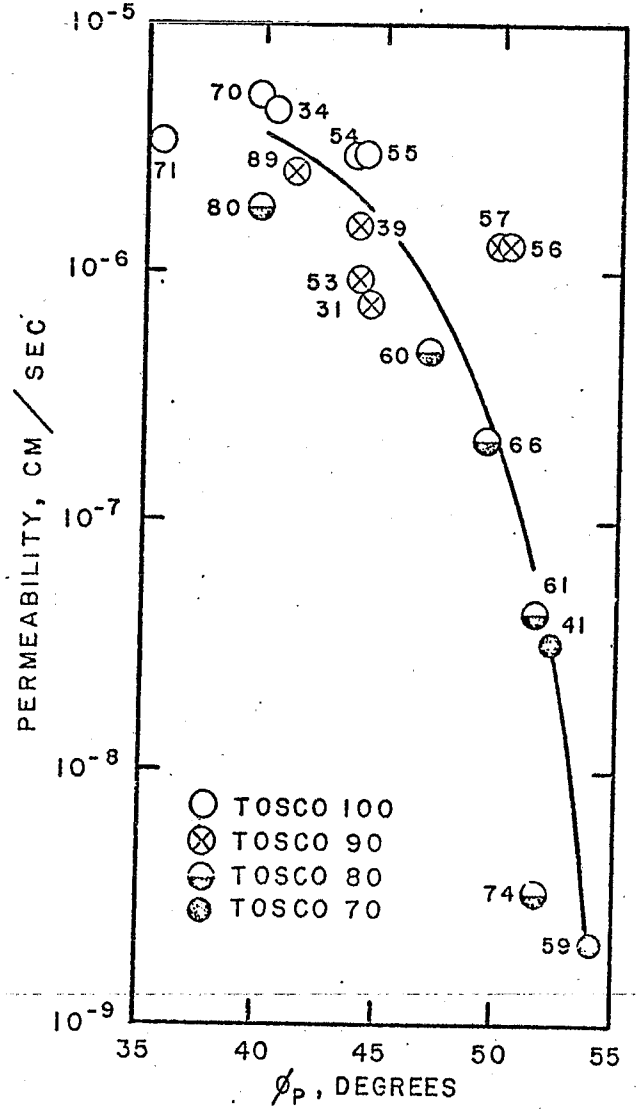

Figure VI 14. Permeability of TOSCO Spent Shale Mixtures Correlated with Peak Friction Angle.

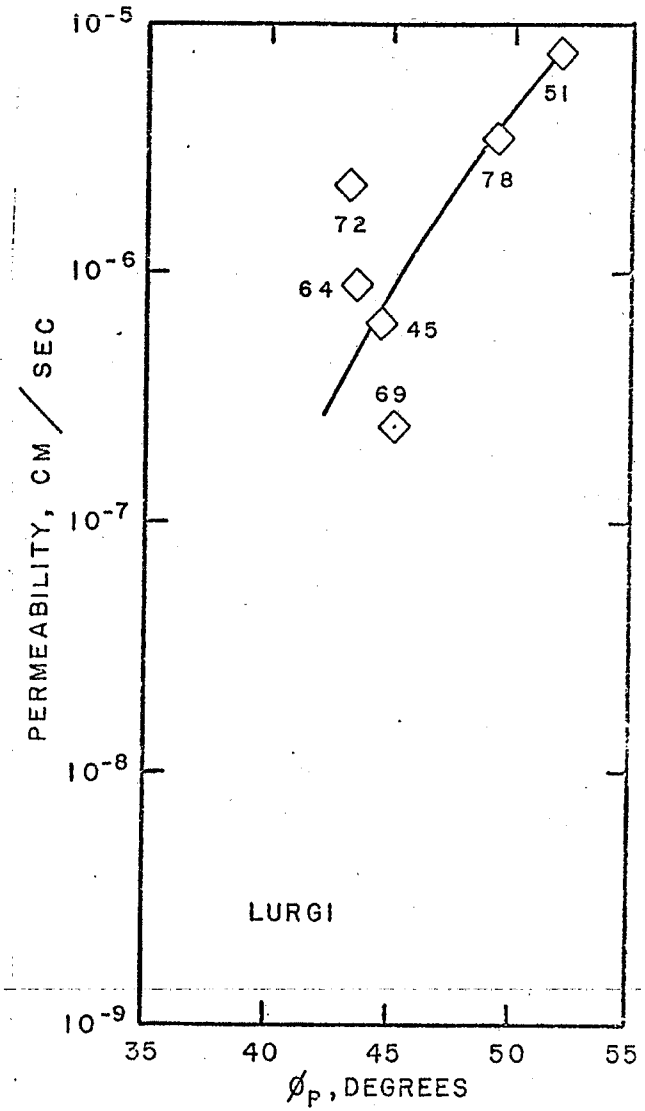

Figure VI 15. Permeability of Lurgi Spent Shale Correlated with Peak Friction Angle.

shale. Both low permeabilities and low peak friction angles are desirable but they seem to be nearly mutually exclusive. A low friction angle allows easier or more extensive rapid self healing. A high peak friction angle is shown by the more cemented specimens.

The peak angle of internal friction plotted in Figure VI 14 is more easily reduced from the torsion data than a normalized peak shear strength. Also ϕ_P may be directly used in one model of the rapid self healing process.

For a silty material (as many of the specimens here studied are) the torsion shear strength measurements give shear strengths proportional to the normal pressure on the failure plane (which is practically the same as the vertical pressure on the specimen). This is because the specimens are small enough so relief of pore pressure of a silty material is rapid and also because cementation in these specimens is nil. For such specimens in such a test that is not too quickly performed, the peak shear strength and residual shear strength data obtained at known vertical pressure can be reduced to ϕ_P and ϕ_R respectively.

Many of the peak friction angles of the more cemented specimens measured are not as high as they should be because the looser, less compacted, specimen material near the top pore stone tends to fail before the more representative center of the specimen. Thus the dilemma in trying to attain low cementation as well as low permeability is probably more serious than even indicated by Figure VI 14. Also probably few if any of the peak friction angles determined by the present torsion apparatus are as high as they should be for the more cemented specimens due to eccentricity of the rotating piston and top pore stone and vanes due to any non trueness or bowing of the piston rods which can cause development of much side thrust without registering of much torque. This would be an insignificant factor, however, with a soft specimen which can deflect to accommodate a little side thrust with no rupture.

The curve of Figure VI 15, permeability vs peak friction angle, for the Lurgi spent shale seems to run counter to the curve of Figure VI 14 for TOSCO spent shales. There appears to be a difference in the materials causing, for the Lurgi, a reduced permeability with reduced angle, but for TOSCO materials an increased permeability with reduced angle. For TOSCO spent shale of Figure VI 14 less cementaceous species seem to be the cause of low friction angles but for Lurgi spent shale of Figure VI 15 greater water content may be operative, at least at the short curing times involved. With the fast setting TOSCO mixtures perhaps the water contents role in softening a material is overshadowed by rapid cementation. With longer curing times perhaps the slow setting Lurgi material would more resemble the TOSCO mixtures in its permeability vs friction angle plot.

C. Residual Shear Strength and Critical Void Ratio Related to Slope Stability

Data obtained as ϕ_P and ϕ_R can be used in a soil mechanics model where drainage of pore pressure is rapid. Drainage of pore pressure in the field is relatively rapid, even for a thick liner layer, if rate of shear is relatively slow. However if pore pressure drainage is not rapid a more complicated and hazardous case must be considered.

Before the liner shears, and therefore before the soil skeleton in the shear zone might be compressed (if its void ratio is above the "critical void ratio" for the material), the peak shear strength may be used to estimate the maximum angle of inclination of a liner below a spent shale pile before the pile will slide through shear failure in the liner parallel to the liner. But if the liner does begin to shear at some place due to the peak strength being locally exceeded, and if the liner material does contract during shear (the "critical void ratio" of the shearing liner being lower than the emplaced liner void ratio), and if pore water pressure can build up in the plane or zone of failure, trouble is probable. Pore pressure will reduce the effective vertical pressure σ_v' and reduce the effective peak shear strength τ_p' of the section of liner beginning to shear. The reduced strength of the initially shearing section and the strain occurring shifts the stress toward the remaining intact section of liner and its strength may also be exceeded. Thus a "progressive failure" occurs which results in a slide.

The most conservative design strengthwise (and possibly the most expensive) is (1) to design using the weak strength developed after shearing occurs with no drainage where the effective normal stress σ is reduced and τ is also reduced (since $\tau = \sigma \cos 0$) or (2) to design with the low residual shear strength τ_R which is developed as the thrust of the failure shear plane increases (and any cementation or particle to particle interlocking is broken and any clayish mineral species platelets are aligned parallel to the plane thus producing a more slippery shear plane), whichever is lowest. It was beyond the scope of this present work to test the true residual shear strength of the many materials and conditions of emplacement here surveyed by the ring shear apparatus

The change in void ratio from emplaced void ratio to the critical void ratio at failure has not been measured in the torsion apparatus used in this study. Probably it is best measured (for plastic specimens) in a conventional "triaxial" soil testing apparatus in which the volume of the specimen can be measured throughout a test. Attempts to make this measurement on cemented specimens will probably be futile, however. It should be done on good candidate (non cementing) liner materials. The change in void ratio at critical conditions (where shearing, particularly simple shearing, has caused the specimen to reach a steady state) helps determine the pore pressure during failure and its degree of influence on the shear strength during failure.

D. Brittleness Index Related to Cementation and Permeability

In calculating the brittleness index two shear strength values τ_p and τ_R must not only be normalized to the same vertical pressure, but good ϕ_p and ϕ_R data is needed as a working number is derived from the difference between two large numbers. This decreases the chances for a good brittleness index, BI, result compared to those for a good ϕ_p. This is believed to be one reason correlations using ϕ_p show less scatter than those using the brittleness index. On the other hand this is not a substitute for BI which is retained in spite of its imprecision for certain illuminating correlations.

Figure VI 16 is a comparison of BI and ϕ_p for Lurgi, TOSCO, and the mixtures involving mellowed material.

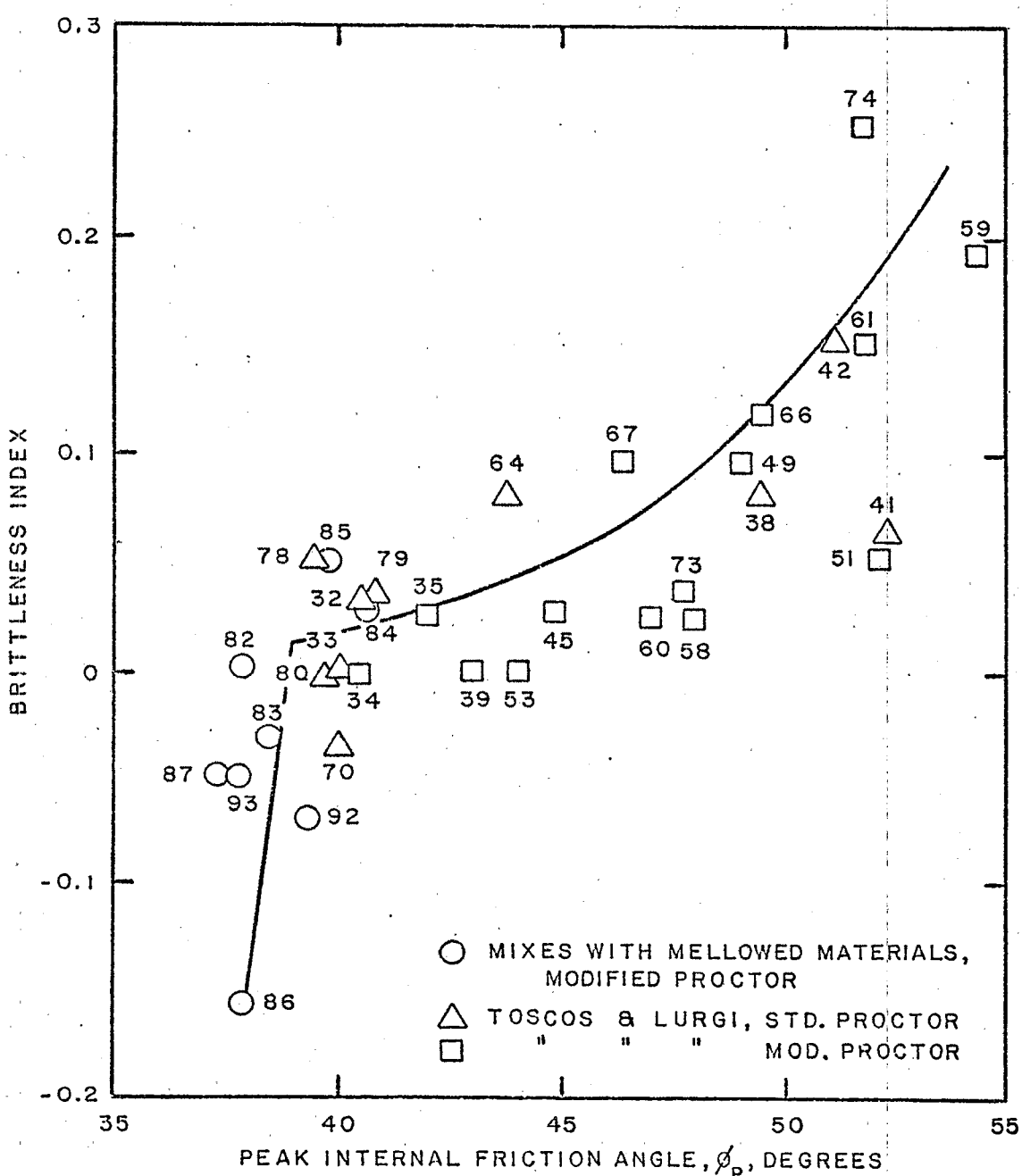

Figure VI 16. Brittleness Index Correlated with Peak Friction Angle.

Figure VI 17 is a plot of permeability vs brittleness index of specimens made from TOSCO 70, TOSCO 80, TOSCO 90, TOSCO 100 mixtures containing mellowed materials, and Lurgi spent shale raw materials. Difficulty in selecting materials giving both low permeability and low brittleness index from materials giving curves on the right of the plot is evident. Some materials of the curve on the left of the plot are, on this basis, perhaps acceptable for a liner, however. These materials give a negative brittleness index calculated from the quick torsion shear strengths ϕ_P and ϕ_R.

The cause of a negative brittleness index seems to lie in low permeability along with neglegible cementation. Low permeability of a specimen in the torsion test is believed to prevent rapid drainage at the beginning of torsion with development of appreciable positive pore pressure as specimen distortion and contraction occurs, which reduces the effective vertical stress σ_v. As twist procedes, the excess pore pressure drains and σ_v increases causing τ to rise. The result is an increasing torque vs time plot on the x-y recorder of the torsion test machine.

For screening candidate liner materials the ability of the torsion test to indicate low permeability, non-cemented, simple shearing materials seems useful. Whether the added ability of the torsion tester to transfer consolidating curing specimens from oedometer to torsion tester without much sample disturbance is essential is perhaps debatable. It seems, however, that every opportunity should be given the specimen to demonstrate any small extent of cementation it has achieved during aging. Disturbance would tend to break the cementation before testing thus reducing the peak of the torsion stress strain curve.

E. Relation of Peak Friction Angle ϕ_p and Brittleness Index BI with Initial Torsional Stiffness and Shear Modulus G

Figure VI 18 is a correlation of peak friction angle ϕ_p with simple shear modulus G obtained from the initial torsional stiffness, derived from volts/degree twist on the stress strain plot. There seems to be a higher curve for brittle material and a lower curve for soft material.

In comparing these G's with others, the increase of G with confining stress (some 280 psi σ_v usually existed here) must be remembered. Some of the points plotted in Figure VI 18 no doubt correspond to specimens with soft tops which too easily sheared and cause displacement of the points downward. Soft tops are caused by poor emplacement of the top pore stone and vanes into the proctor compacted specimen during loading of the spring oedometer.

Apparent higher values of these slow shear moduli for more cemented specimens, suggests that perhaps rapid shear moduli from resonant dynamic tests might be used to nondestructively periodically assay a given curing specimen for cementation. The very small samples needed for an EGA assay suggest this might be periodically done on the specimen also without much altering its integrity for the dynamic test. Perhaps the specimen should be kept under high vertical or high confining pressure to simulate burial even during dynamic G testing. Perhaps it can be shown that proctor compaction is adequate to simulate this and such pressures are unnecessary. With proctor compaction the persistant problem of weak specimen tops would occur.

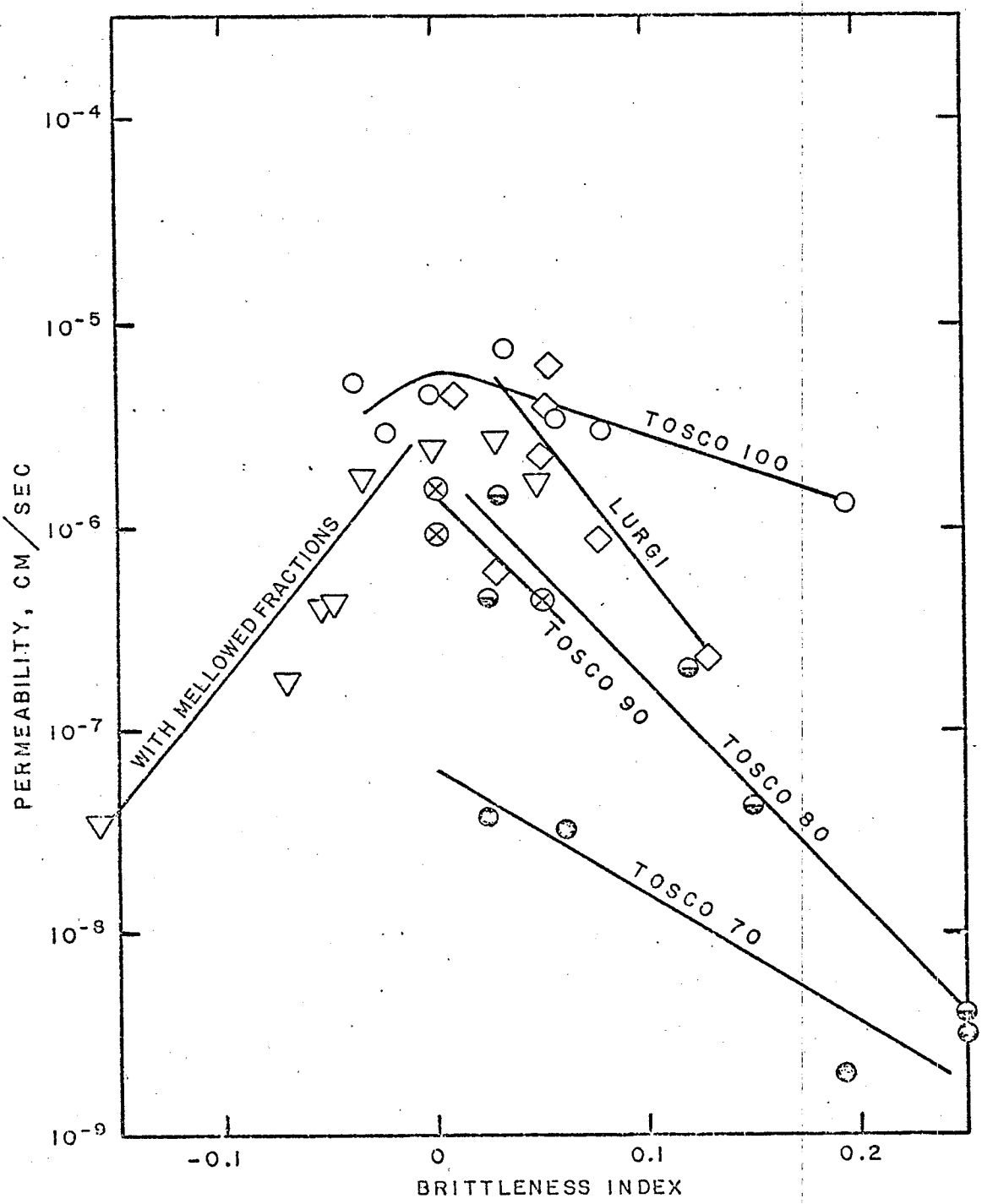

Figure VI 17. Permeability Compared with Brittleness Index

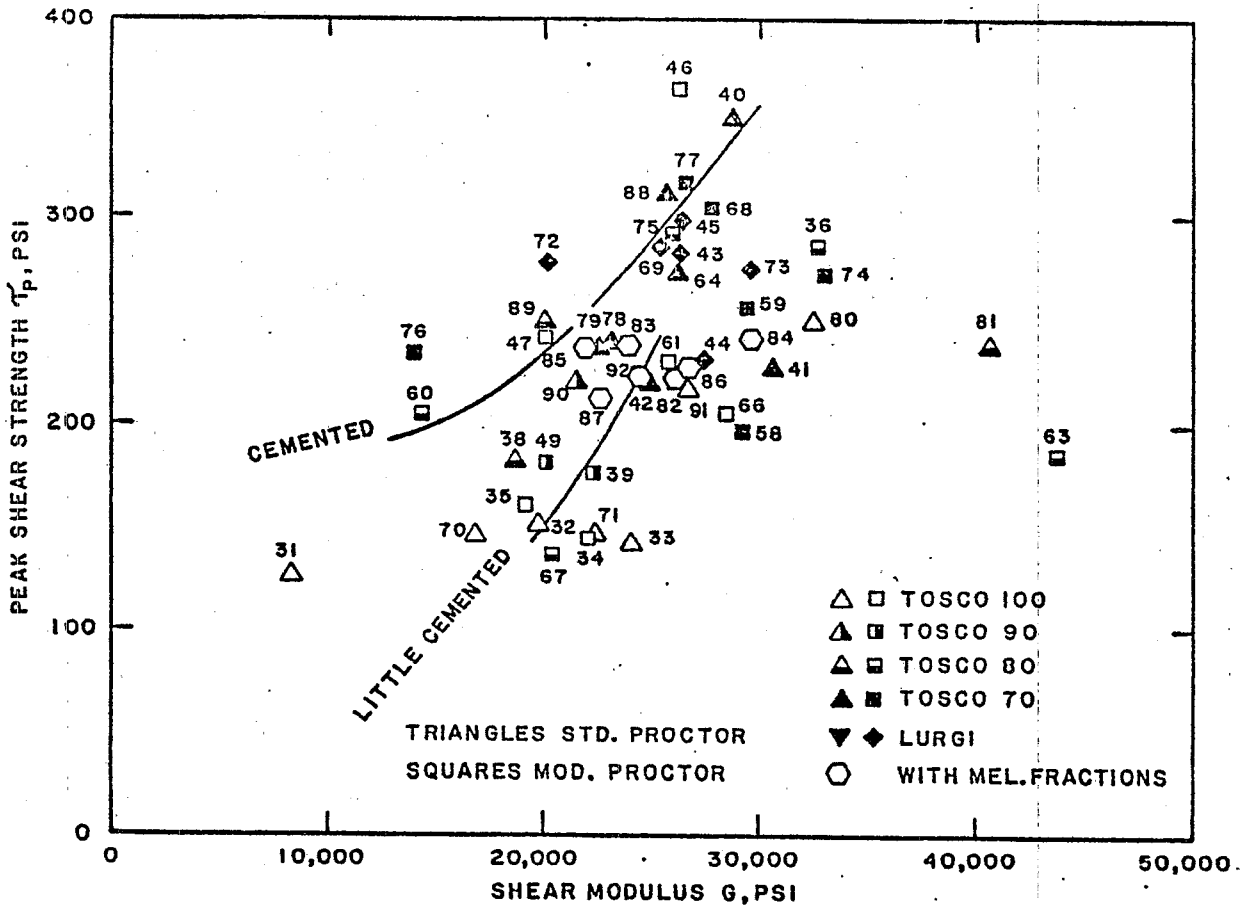

Figure VI.18. Peak Friction Angle Compared with Initial Shear Modulus G

Probably static compaction at the high vertical pressures of interest would simulate a real liner adequately.

Figure VI 19 plotting BI vs shear modulus G also suggests a distinction between brittle and soft material. Here also some points are no doubt too low.

F. Relation of Peak Friction Angle with Twist at Peak Strength

Figure VI 20 shows the peak friction angles of the TOSCO 100, 90, 80 and 70 series and the Lurgi material as a function of twist produced during torsion testing at peak strength. There seems to be a trend for greater twist (or strain) before failure for the less compacted standard proctored material than for the more compacted modified proctored material, especially for material giving lower peak friction angles. Greater strain before failure is advantageous in a liner. This does not necessarily correlate positively with tensile strength, however, which has little relation to strain before failure. Tensile strength is more related to shear strength where a rule of thumb says that it is about 1/20 of the shear strength of a cohesive clay soil.

Also plotted in Figure VI 20 are points for loadings 86 and 92 for a 75% mellowed burned TOSCO - 25% burned TOSCO mix and the point for loading 87 which is of a 50% mellowed burned TOSCO - 50% unburned TOSCO II mix. A large extent of strain before peak strength at low peak friction angles is possible with these mixtures involving mellowed material. In fact this sort of material with low (in these cases negative) brittleness index tends to exhibit simple shear or zone shear and larger twists than those plotted may be more appropriate for this plot since for these materials peak strength does not necessarily imply failure.

G. Relation of Peak Friction Angle and Squashiness With Cured Void Ratio

Figures VI 21, 22, 23 and 24 show a regularity in peak angle of internal friction plotted vs void ratio for cured TOSCO spent shales, TOSCO 100, 90, 80, and 70, as the fraction of cementaceous burned spent shale increases. Greater void ratios (determined after curing) are associated with lower peak internal friction angles for the TOSCO spent shales. This suggests that a liner made from spent shale should be as little compacted as possible so a lower friction angle and resulting greater squashiness is had which allows better self healing of the rapid type, other factors such as not too much shrinkage at a shear zone being acceptable. The squashiness is inversely proportional to the shear strength which for a silty draining material is $\sigma_v \tan \phi_p$.

H. Hydrate Species Determined by EGA

In the early stages of curing of the series of mixtures, TOSCO 100, 90, 80 and 70, rise and fall of an EGA water peak at 115 to 135°C was found. Since both tobernite and ettringite may manifest themselves in this peak some ambiguity exists without x-ray diffraction or other means of distinquishing between them. Figure VI 25 is a plot of this peak curing time for crumbs of spring oedometer specimens after torsion testing. Timing of this peak is similar to that in development of strength of ϕ_p in Figure VI 26.

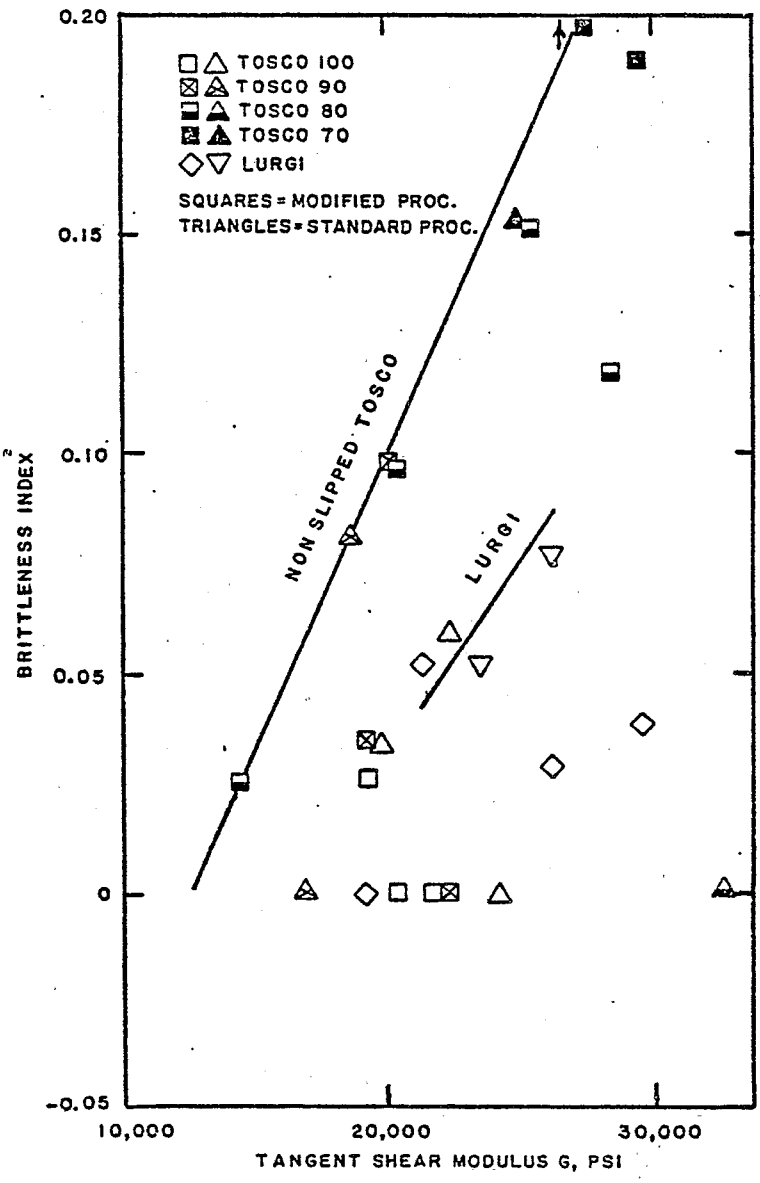

Figure B-VI 19. Brittleness Index Compared with Initial Shear Modulus G

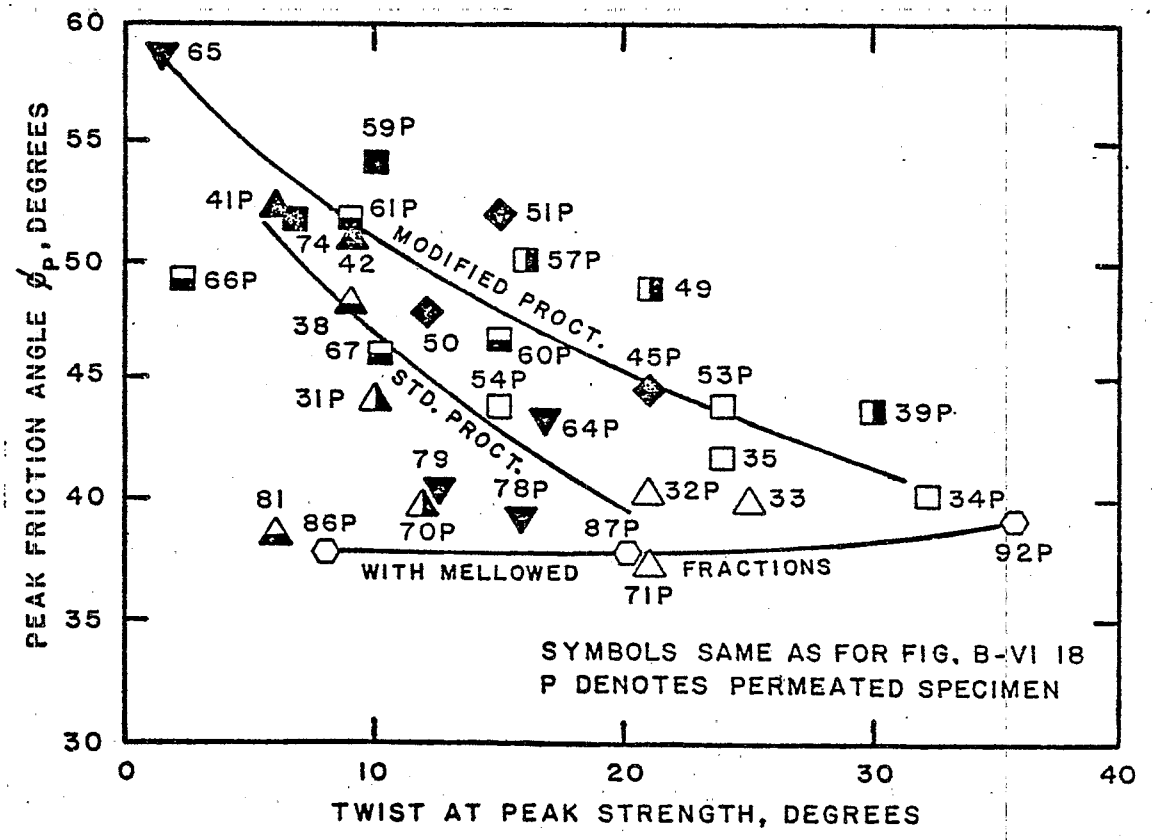

Figure B-VI 20. Extent of Twist at Peak Strength Correlated with Peak Friction Angle

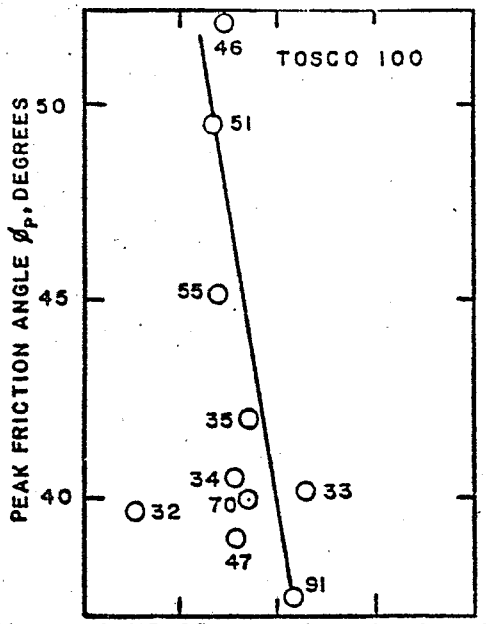

Figure B-VI 21. Peak Friction Angle of TOSCO 100 vs Void Ratio

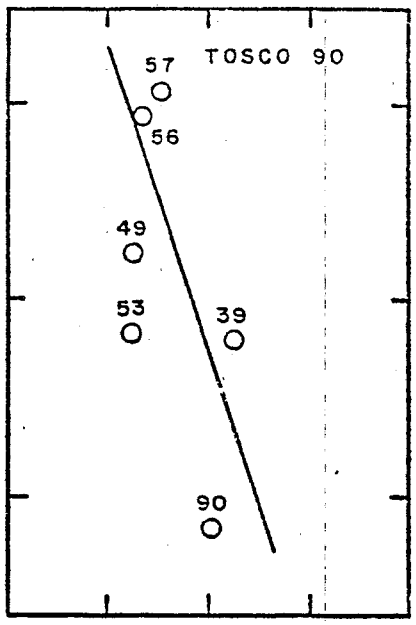

Figure B-VI 22. Peak Friction Angle of TOSCO 90 vs Void Ratio

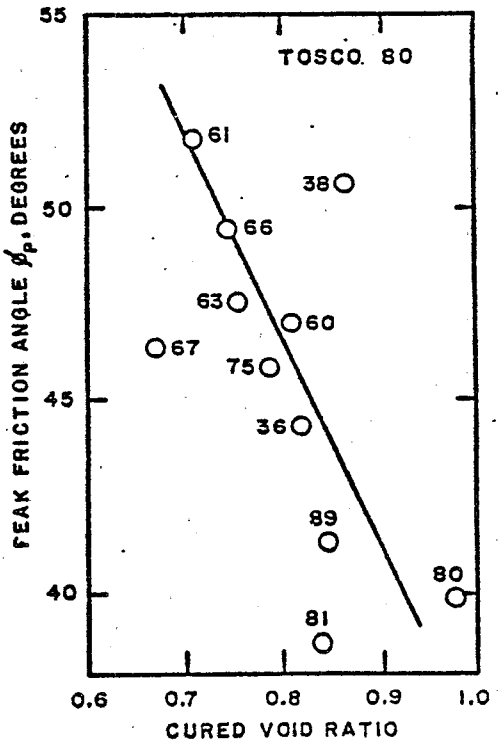

Figure B-VI 23. Peak Friction Angle of TOSCO 80 vs Void Ratio

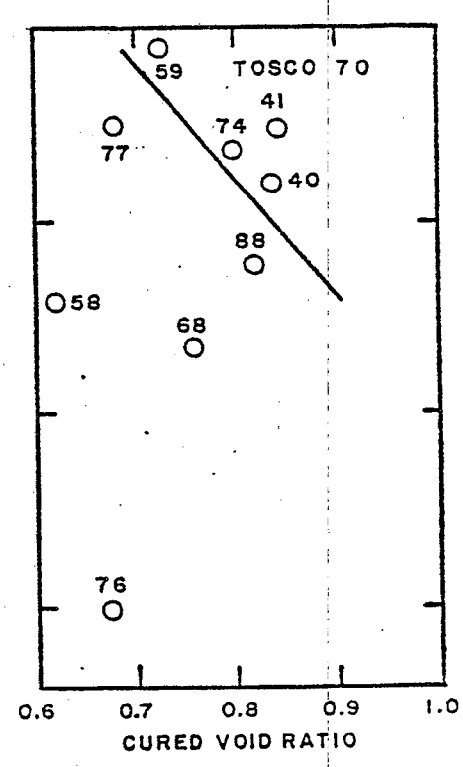

Figure B-VI 24. Peak Friction Angle of TOSCO 70 vs Void Ratio

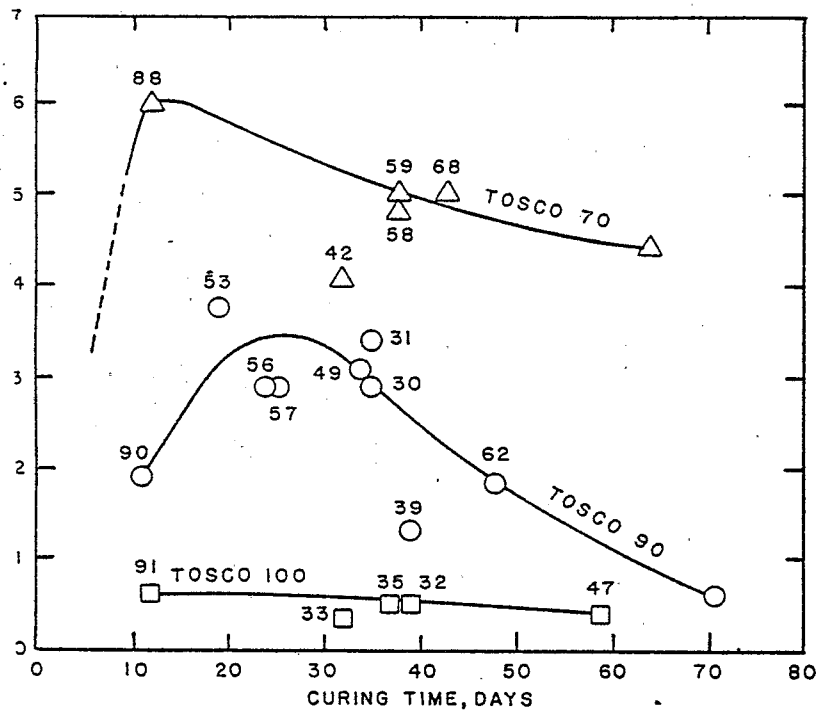

Figure VI 25. EGA Hydrate Water Peak of Tobermorite and Ettringite vs Time for TOSCO 100, 90, and 70 Specimens

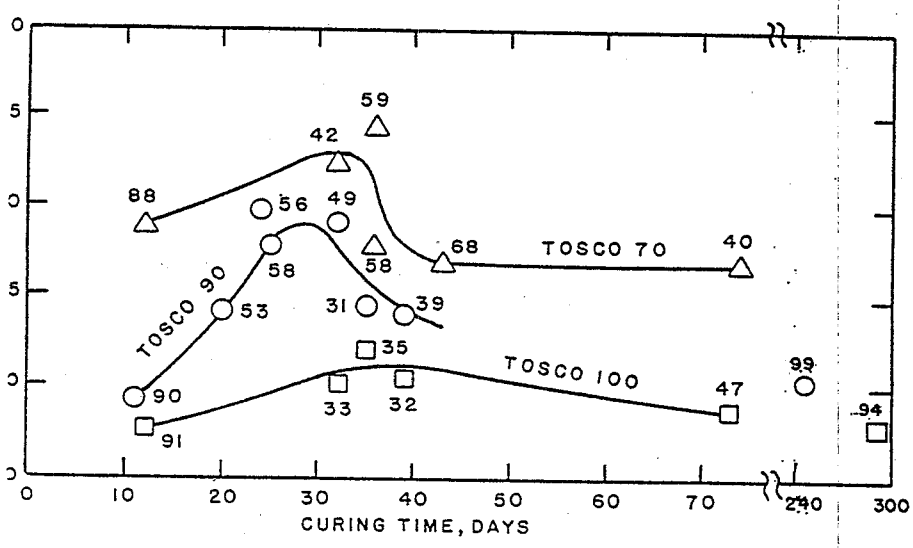

Figure VI 26. Peak Friction Angle vs Time for TOSCO 100, 90, and 70 Specimens.

Another EGA water peak at around 225°C becomes prominent with TOSCO 70 material. This is believed to be where the "carbonate ettringite" (ettringite with sulfate replaced by carbonate) manefests itself as an additional part of its EGA curve. The main part, however, still is at the 115 to 135°C peak as for ettringite itself. There is a sudden appearence of the 225°C peak at a sharp threshold with a burned spent shale content below 70%. This suggests that the pH of the water remaining in the mix and/or the carbonate ion concentration level left after some of the alkalinity and carbonate has attacked the unburned TOSCO II spent shale component of the mixture may determine whether ordinary sulfate ettringite or carbonate ettringite is formed. The identification of this peak is substantiated by its reduction in side experiment curings where some gypsum as a source of sulfate is added, its accentuation when Na_2CO_3 is added, and its elimination when $BaCl_2$ or $Ba(NO_3)_2$ as a sulfate scavenger is added.

Figure VI 27 is a plot of the initial shear modulus G vs the 115 to 135°C EGA peak height for several of the spent shale mixes after curing. Although there is some rise in stiffness at the highest quantities of tobermorite and ettringite found, the effect is not very strong and moreover for low peak heights which are in the low cementation region of most interest the effect is nil. Thus study of cementation of this sort by dynamic G testing does not seem straight forward. It must be recalled that ettringite is not very cementaceous compared to tobermorite and we have not yet analyzed the 115-135°C EGA peak for these.

Figure VI 28 shows strong inverse correlation of twist at peak strength vs the 115 to 135°C EGA peak height. Several high data points are probably the result of slippage between specimen and upper pore stone. Any cementation produced by these hydrates seems to operate against extensive deformation, the action of interest in self healing, rather than against small deformation involved in initial stiffness.

The peak strength friction angle is quite dependent on the extent of formation of cementaceous hydrates under conditions of the torsion test. Peak strength also correlates fairly well with the void ratio within types of spent shale mixtures such as TOSCO 100, 90, 80, 70 or Lurgi. A better correlation with strength than either of the above should be obtained by plotting the family of void ratio vs peak shear strength curves with the amount of tobermorite water present as a parameter (ignoring any ettringite and hydromagnesite cementing action). The tobermorite might be determined assuming all ettringite is the kind with also a peak at 225°C as well as at 120 to 135°C (carbonate ettringite or hydroxy ettringite but not sulfate ettringite). The early peak at 120 to 135°C or so (depending on its height) results from both tobermorite and ettringite largely superimposed. The tobermorite peak area alone might be obtained by subtracting out a calculated carbonate ettringite area for the 115 to 135°C part of its water evolution calculated from a ratio of the 225°C part of its water evolution.

I. Secondary Compression Index $C\alpha$ related to Cementation and Mellowing

Figure VI 29 summarizes $C\alpha$, the secondary compression index of the spring oedometer specimens just before the specimens removal from its LVDT

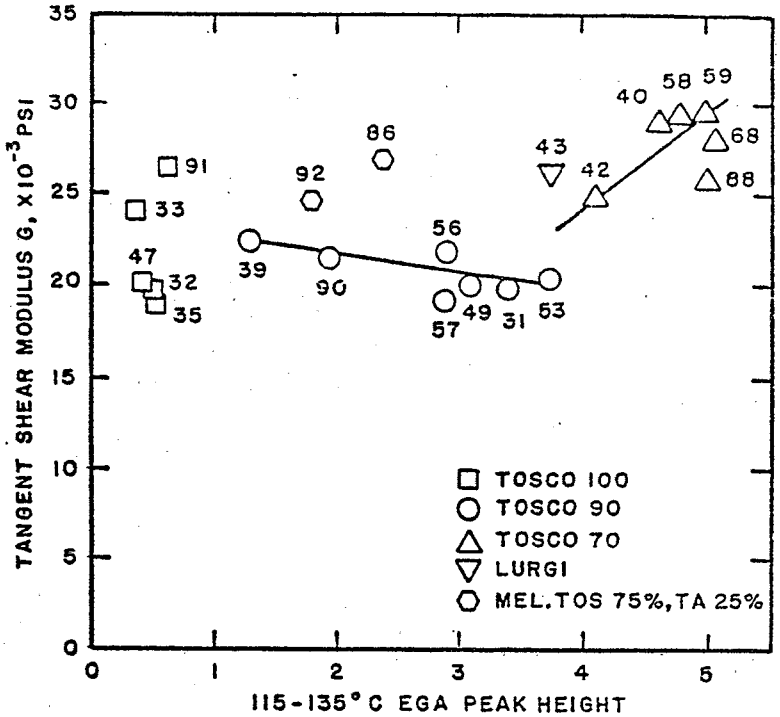

Figure VI 27. Initial Torsional Stiffness vs 115 to 135°C EGA Peak Height

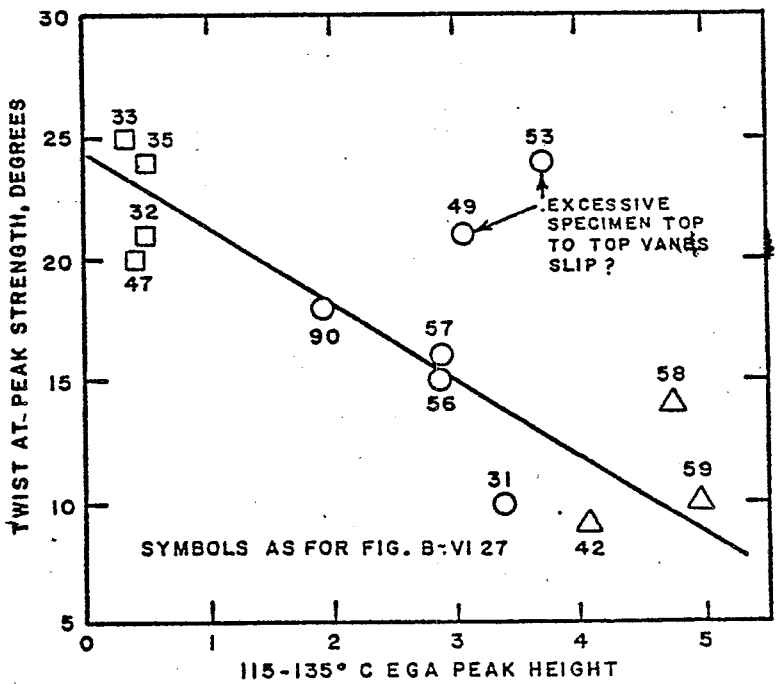

Figure VI 28. Twist at Peak Strength vs 115 to 135°EGA Peak Height

height measurement system prior to permeability determination (if made) and torsion testing. In general some specimens showed a uniform height vs log time plot while others showed a fairly sharp downbend in this plot at around of 1 to 5 days as though some kind of friction of cementation were broken loose then in response to a particular environmental change. The nature of these possible clock reactions has not been considered here but should be at some time for whatever type of material might be considered a further possible candidate liner.

Figure VI 29 shows that at a burned TOSCO spent shale content of about 10% in TOSCO II spent shale shale a minimum C_α occurred for specimens showing a given peak friction angle. Figure VI 29 is a cross plot of the data shown in Figure VI 30, 31, 32, 33, 34 and 35 for the last C_α from the LVDT measurements and the peak friction angle later determined by the torsion tester. The scatter of the data in these latter figures is believed to often be due to premature slippage of the specimen at its weaker top rather than failing in a more representative portion in the middle of the specimen. The "best" curves have been drawn through reasonable higher ϕ_p values of presumed better failed specimens.

It should be commented that none of the C_α values seen to date seem too high for use of a liner for a period of 10,000 years. There is some possibility, however, that the same secondary compression vs log time curves may turn downward even further were specimens studied for longer periods.

The secondary compression index C_α, that can be calcualted from Townsend and Peterson (1979) data for their unscalped TOSCO II spent shale for modified and standard proctor material at 10^4 minutes consolidation and interpolated to a σ_v of 280 psi are about two or three times the values we have found (Figure VI 30). These higher C_α values would be explained if much of the larger chunks of spent shale in their unscalped sample soften when water soaked so the bridging between them is weakened at their point to point contacts. The ϕ values reported by these authors for standard and modified proctor are roughly comparable with ϕ_p measured with our torsion apparatus although a number of variables are important to the exact values which are found.

J. Indirect Tensile Strength (Brazilian) Tests

In Figure VI 35 Brazil indirect tensile strengths of specimens compacted and cured with no confining pressure are compared with the twist at peak strength from the torsion test of counterpart specimens cured in the spring oedometers at around 280 psi vertical pressure and tested near that pressure.

There is a trend in Figure VI 35 for more cementaceous TOSCO 80 material to give greater tensile strength than less cementaceous TOSCO 90 material and for it to give greater tensile strength than the TOSCO 100 material. Lurgi spent shale gives relatively high tensile strengths while mixtures including mellowed material as noted give low to medium tensile strengths. The negative slope of the trend lines drawn for the different materials suggests that the kind of tensile strength measured by the Brazilian tests is a brittle cementaceous type strength associated with rapid attainment of peak cementaceous shear strength as strain progresses.

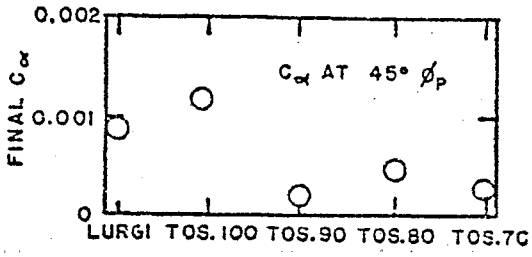

Figure VI 29. Final Cα at 45° Peak Friction Angle for Oedometer Specimens of Various Spent Shale

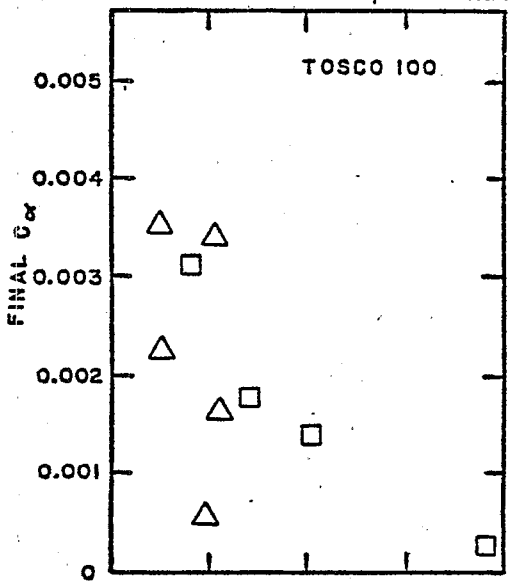

VI 30. Final Cα vs Peak Friction Angle for TOSCO 100 Specimens

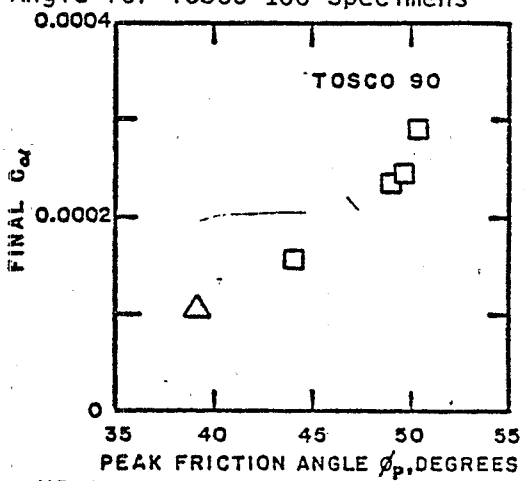

VI 31. Final Cα vs Peak Friction Angle for TOSCO 90 Specimens

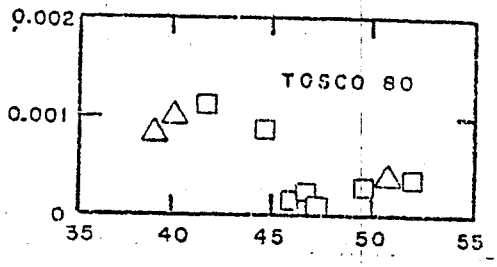

VI 32. Final Cα vs Peak Friction Angle for TOSCO 80 Specimens

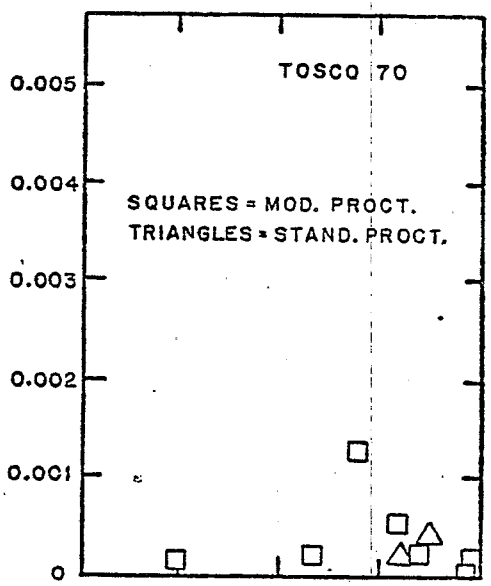

VI 33. Final Cα vs Peak Friction Angle for TOSCO 70 Specimens

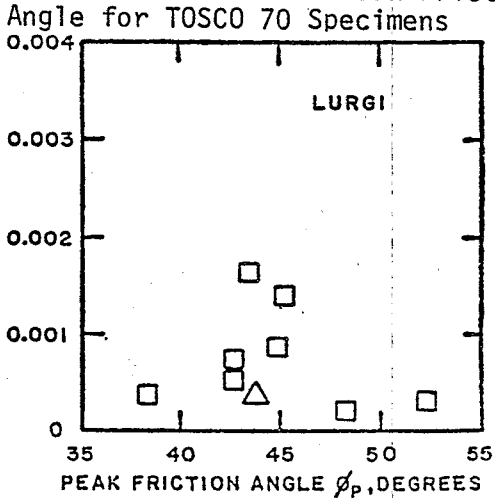

VI 34. Final Cα vs Peak Friction Angle for Lurgi Specimens

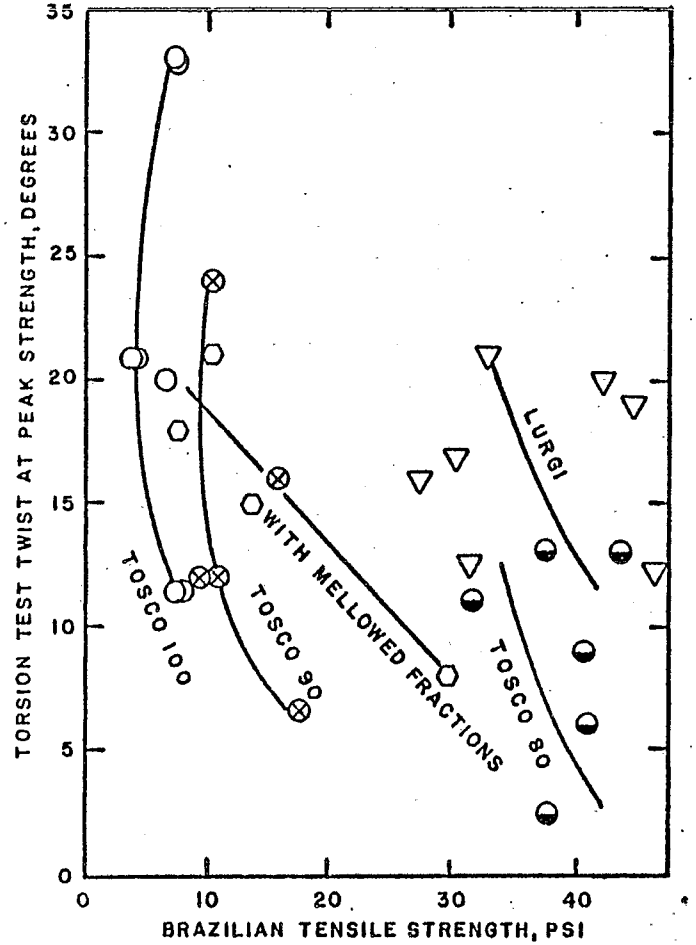

Figure VI 35. Torsion Test Twist at Peak Strength vs Brazil Tensile Strength

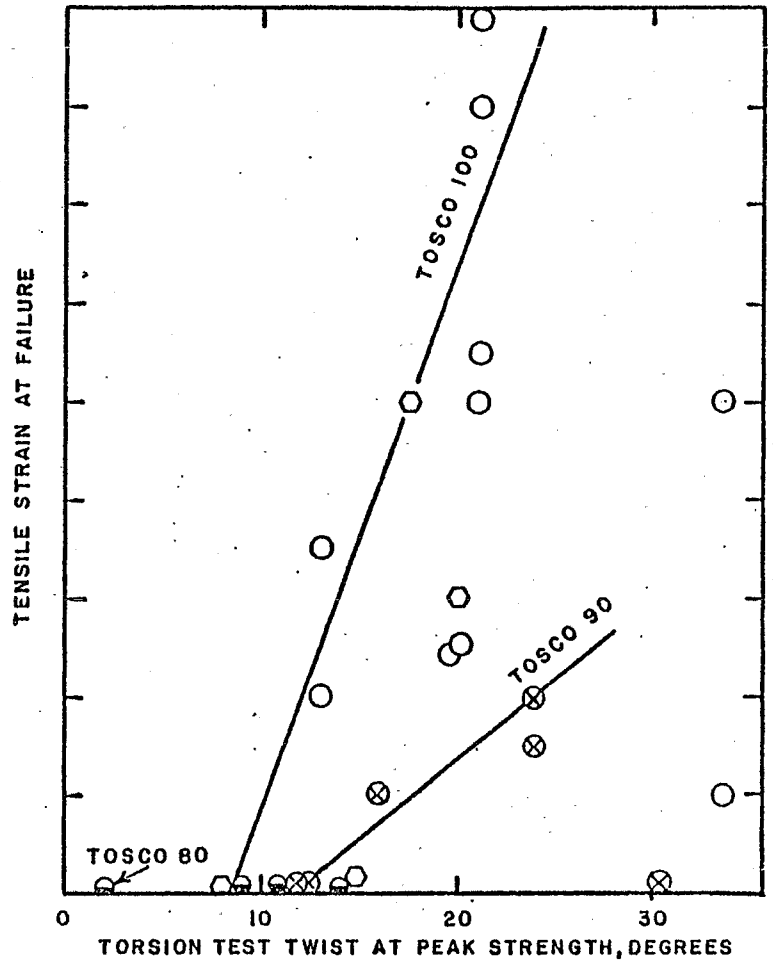

Figure VI 36. Brazil Tensile Strain at Failure vs Torsion Test Twist at Peak Strength

This slope is opposite to that expected for a correlation of the shear test twist and tensile strength for a cohesive plastic material.

For the silty and sometimes cemented materials of most of the specimens studied here high tensile strength primarily indicates cementation. A more clayish material might show both high twist before peak shear strength and relatively high tensile strength. Tensile strength, as weak as it is, in a material at the overburden depths involved for the liner being considered does not seem to be an important consideration in the face of the high vertical stress involved at depth which greatly increases shear strength.

Figure VI 36 is a plot of the tensile strain at failure with the Brazil tests vs the twist at peak strength for the torsion tests. It is concluded that only a little cementation reduces the tensile strain at failure considerably. The largest torsion twists (strains) of cemented specimens and less cemented specimens at peak torsion shear strength seen are about the same but the Brazil test tensile strains at tensile failure are much greater for less cementaceous material.

Figure VI 37 shows some classical shaped tensile strength vs water content curves for specimens made from mixtures involving mellowed materials. Even for the 75% mellowed TOSCO - 25% burned TOSCO specimens which are undergoing some cementation, a peak tensile strength vs water content is observed. The points corresponding to specimen water additions used in the main series of oedometer - torsion tests are indicated by the oedometer loading number of this main series. According to data for these little aged specimens, optimum tensile strength was not usually attained. But as observed above, the tendency of the liner to shear at higher vertical pressure which will far over-shadow the weak tensile strengths.

K. Compressibility Coefficients

Pneumatic arm oedometer tests were made on standard proctored or modified proctored specimens one inch high and 2½ inch diameter. Table II 1 lists the types of mixes studied by arm oedometer. Table V 4 is a summary of some results and some calculations. In the first column t signifie s TOSCO, m modified proctor, s standard proctor, etc.

Primary consolidation was finished after 80 minutes for the one inch thick double pore stone specimens used. For this time the total compression of the specimen from the data collecting computer print out for each loading increment was read and entered in a computer spread sheet program, Table VI 1 column D, as steady state Schaevitz units. After converting these to mm compression and correcting for arm oedometer apparatus deflection at the particular load (column C) the net compression was calculated (column F) for that loading increment. Load increments producing vertical pressures on the specimens of 19.4, 38.8, 77.5, 155.0, and 310 psi were used. From the initial water added, mineral grain density of the initial dry mixture before wetting, specimen loaded weight, cell volume of 80.44 cm^3 and specimen top surface area of 31.67 cm^2 the dry densities and void ratio for each loading were calculated and for each change in load the delta void ratio and compression index C_c were calculated (columns K and L).

From the data calculated in Table V-4 a variety of correlations may be made. Void ratio e plotted against consolidation stress (load) gives

curves typical of silt. Figure VI 38 shows the compression index for the last loading increment (155 to 310 psi) for each specimen, plotted against the initial water added to the specimen in mixing it. There is much similarity in the position of the curves for the various types of spent shale.

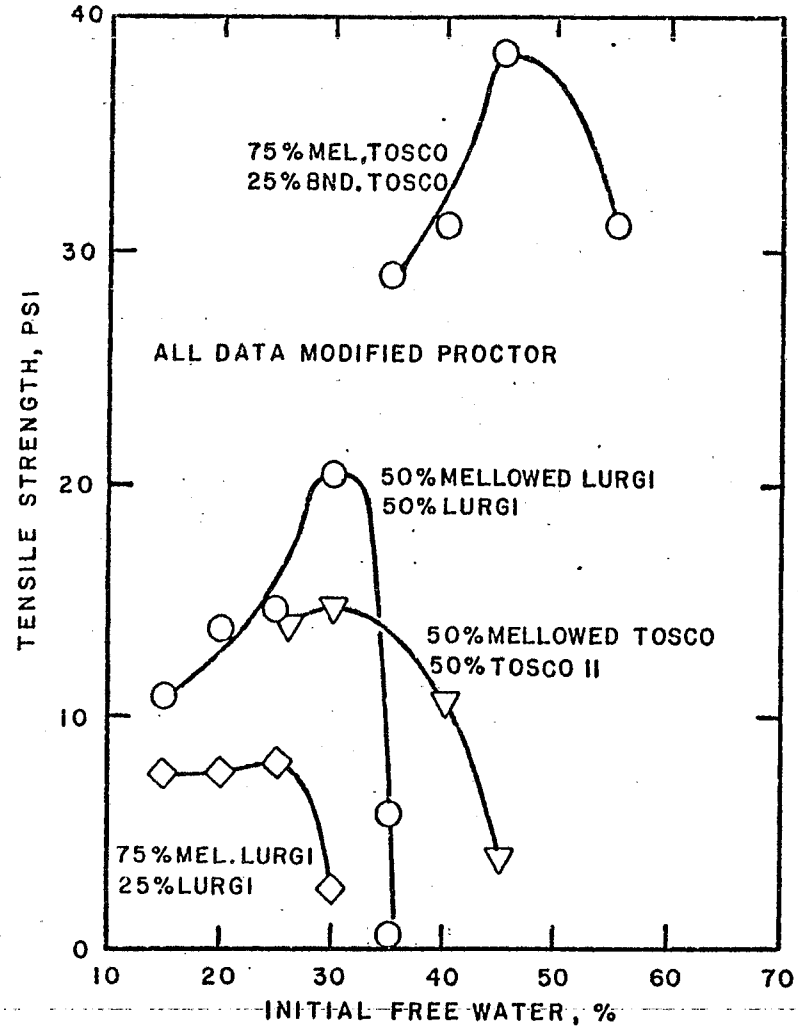

Eigure VI 37. Brazil Tensile Strength vs Initial Water Content

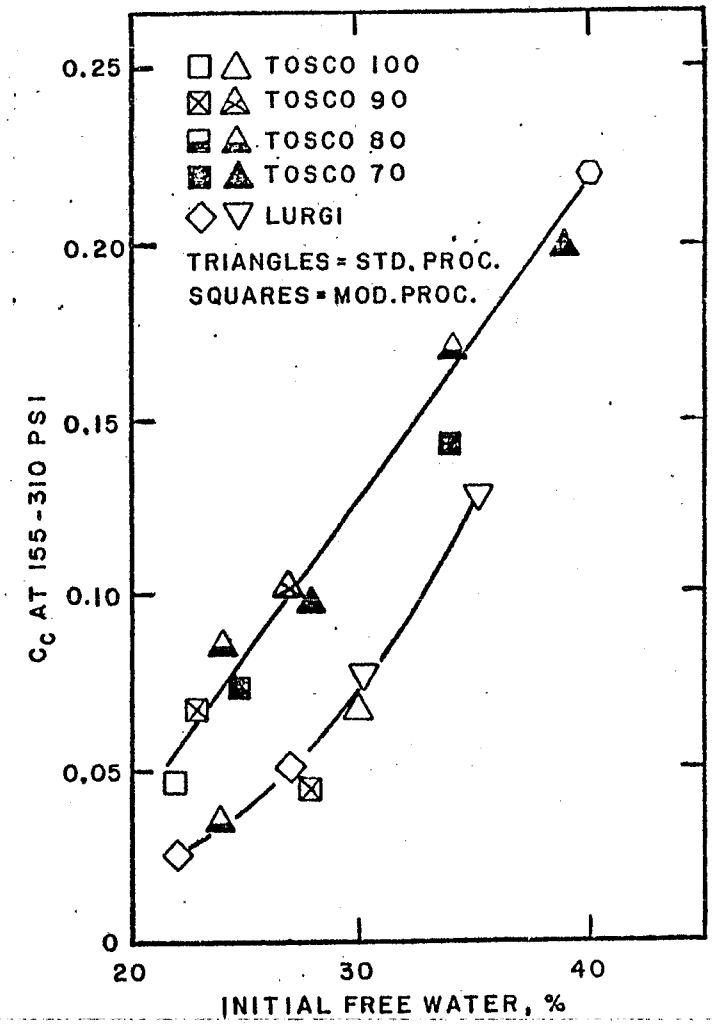

Figure VI 38. Compression Index of Fresh Specimens for Loading Increment 155 to 310 PSI

VII. CONCLUSIONS AND RECOMMENDATIONS

1. A softer less brittle material after placement seems desirable for most of the specimens tested. Apparently the angularity and harshness of silt and sand sized particles in most mixes is the cause of a relatively high angle of internal friction for the peak shear strengths and residual shear strengths found after yielding. Such high strengths do not seem necessary nor desirable and should be traded off for lower angles of friction through less compaction, some heap mellowing time which will allow more particle surface roughening and floculation and looser compaction while retaining some measure of swelling and shrinkage stability, and/or addition or generation of some quantity of clayish material. The latter can apparently be made from certain spent oil shales by autoclave mellowing but it may be more economical to add clay from other sources. Trial of further autoclave mellowed or other mellowed materials seems desirable.

2. Trial of addition of clay or other similar fines to reduce permeability in the case of the TOSCO II spent shale or the average Lurgi spent shale is desirable. This could be an added component or could be generated from autoclaving an especially active burned spent shale such as the burned TOSCO material.

3. Ring shear tests should be made to get τ_R at large displacements for several examples of candidate liner material.

4. The cementing characteristics of burned spent shale seem to be a detriment to self healing as any shear movement needed for closure of a vertical tension crack by "caving in" of liner material would produce shear plane separated fragments. The planes may be possible water channels. Moreover the depth into the liner away from the tension crack for a source of fill material will be less for high shear strength liner material. Extrusion of a non brittle plastic liner material, into a tension crack, on the other hand, should not produce such distinct planes. Autoclave mellowing inhibits cementation of materials.

5. The high friction angles observed in most of the liner specimens tested are useful in that there will be less tendency for a pile of spent oil shale founded on a liner to slip down a valley. Silty sandy materials producing high friction angles are generally rather permeable and uncemented specimens of the materials here tested are no exception. To reduce permeability clay sized material can be mixed in or a non strength producing fine precipitate or colloid within the interstitial spaces of the silt grains might conceivably be internally generated. In this way a synthetic boulder clay having both low permeability yet a reasonably high friction angle might be produced.

6. Quick clay inadvertently made in any of the above ways should be avoided. Even a material that has only a little above critical void volume should be suspect until proven unlikely to soften or liquify when subjected to slip or earthquake produced shear. Even though a liner material in unsaturated condition may not soften or liquify the same material when saturated may soften under shear strains. This must be predictable and eventually probably must be studied for any candidate liner material.

7. The "final" secondary compression rates or C_α for none of the materials, when measurements ceased just before torsion testing, was excessive. Rates below 2% settlement at 10,000 years by extrapolation were about as large as observed. Much lower rates were more typical. However since the settlement vs log time curves plotted were often concave downward specimens should be followed for longer periods and chemistry of the apparent softening with age ascertained.

8. The effect of additives on spent shale should be further studied in a more methodical experimental design. Gradations of mixes between silty spent shale and clayish material should be tested for the following:

1. Permeability
2. Shear strength by a quick method relative to the permeability so any softening due to reduction of soil skeleton volume during shear is observable.
3. Shear strength of both saturated and unsaturated material should be studied.

Well mixed or pugged materials should be used or fines should be generated internally.

9. Possible methods for in situ fines generation include the following:

a. Mix two slow precipitating liquid intereactants in with the spent shale.
b. Mix in one liquid reactant which reacts with the spent shale itself.
c. Mix in a solid reactant which reacts with the spent shale.

The spent shale base for the mixture should not be burned spent shale to avoid the cementation already demonstrated but one such as TOSCO II material. Perhaps mildly autoclave mellowed burned spent shale would not cement even though much ettringite may be initially formed.

10. Periodic non destructive resonant measurement of shear modulus G may be valuable for following development of any cementation in a given specimen as curing or aging procedes. EGA and to a lessor degree x-ray diffraction may also be done on the same specimen without affecting G since such small samples are required.

11. Experiments with physical models of liner materials should be made in which a tension crack is induced in brittle containment strata and the ability of liner material to suppress water flow as the crack opens is measured. It is desirable to be able to perform meaningful experiments of this sort without the need for continuous high vertical pressures during aging of the liner. Strong forces at the time of, say, flexing or stretching a model to generate a tension crack would, of course be necessary however. Proof is desirable that proctor or other compacted liner material in such a model approximates a real liner aged with considerable overburden pressure.

VIII. QUALITY ASSURANCE AND QUALITY CONTROL

A. Objective

The overall objective of the quality control and quality assurance program was to assure that the data obtained were of known quality and integrity that would permit valid scientific conclusions to be made regarding the potential for using retorted oil shale as liners below retorted shale disposal sites. This study was exploratory in nature and intended to provide a general assessment of the potential for using new materials (mellowed and burned retorted oil shales blended with standard retorted shales) in a unique new manner (liners below several hundred feet of retorted shale) for long term stability (centuries). No standard methods exist to perform such as assessment. Therefore, some of the methods used, as well as much of the equipment and test procedures, were developed under, and are original to, this effort. Therefore an important QA objective was to assure internally consistent and reproducible results permitting valid conclusions to be made.

B. Activities

Since the experiments described in this report are of an exploratory and unique nature, the general QA/QC procedures involved internal correlation, cross-checking and duplicate testing as required to provide internally self consistent results. This was accomplished to the degree required to assure that the trends were internally consistent thus indicating reproducible results. Table VIII-I provides a summary of the most significant QA objectives, methods, and results. The following discussion provides an overview of some additional, QA activities.

1. Compaction and Dry Density Measurements

Due to the somewhat "non standard" diameter of the test speciments, a miniature proctor hammer was constructed for sample compaction. Compacting efforts were conducted at 656 kV/m^3 for the standard proctor and 2929 kV/m^3 for the modified proctor as described in section IV-A. Since specimens used were of non standard size they were checked against specimens of standard size to assure that they were comparable.

The apparent dry density was obtained by weighing all the damp mixed material added in lifts for proctoring. Care was taken to avoid evaporation of the moisture. The volume was calculated from the internal diameter of the specimen sheath and the measured specimen height. Linear measurements were made to the nearest 0.025 mm and weights were determined to the nearest 0.1 gram.

2. Mineralogical Species Identification

Mineral species were determined by X-ray analysis using spiked standards of known quantities of known mineral species to provide diffraction peaks for calibratrion. Cross correlation was established through differential thermal analysis and evolved gas analysis (DTA-EGA) as appropriate. Finally, as an internal check, a material balance was performed.

3. Soil Mechanics

Soil mechanics tests of consolidation, zone shear strength, cohesive intercept, and brittleness index were made on molded compacted specimens of fine-grained spent shales in specially designed and built zone shear cells. During the consolidation period the movement of the anvils were measured using linear variable differential transformers. The transformers were calibrated against displacements produced by a micrometer to the nearest 0.025 mm. Consolidation time was measured in days. After various periods of ageing time samples were zone sheared to obtain the zone shear strength, cohesive intercept, and brittleness index. The proving ring of the shear fixture was calibrated with the load cell of the Instron testing machine. The load cell of the Instron testing machine was calibrated with dead weights.

C. Accomplishment of the Quality Assurance and Quality Control Objectives

The quality assurance and quality control objectives were achieved as evidenced by the internal consistency of results. Further, the data is consistent with the anticipated behavior of the materials based on their physical and chemical properties. Based on the QA/QC procedures used herein, this data is valid for making initial assessments regarding the utility, design, and potential for using retorted oil shale as a liner below retorted shale piles. However the results are not intended for use in regulatory decisions, litigation, or design of specific retorted shale liners.

TABLE VIII I. QUALITY ASSURANCE OBJECTIVES AND PERFORMANCE

QA OBJECTIVE	QA/QC METHOD	RESULTS
1. Assure that each raw material used was of known and consistent composition.	Duplicate analyses on selected specimens.	Results were consistent within ± 10% Reference Table III-I, III-2.
2. Assure that preparation of liner specimens was consistent and did not introduce additional variables.	Prepare duplicate specimens for testing.	Results were very similar-Reference Tables V-1, V-2 and V-3.
3. Assure that the non standard size proctor compactions correlate with full size (standard) methods.	Prepare selected specimens by both systems and compare results.	Results were very similar as shown in Figure III-7 and III-8.
4. Assure that results and conclusions are in reasonable agreement with the accepted scientific data base.	Compare to similar evaluations reported by other researchers.	General results and conclusions are similar though specific values vary slightly due to different raw materials and methods. See Section VIII for references and specific citations such as Townsend & Peterson (1979) on page 17.
5. Assure that changes in specimen strength are not caused by sample disturbance when moving and loading the cured specimens for torsion triaxial testing.	Use the SHANSEP method of Ladd & Foott (1974) to evaluate shear strength at known over-consolidation ratios of unity or above. Figure IV-I illustrates apparatus used for transfer.	Dimensional and strength changes in specimens during transfer were avoided. See discussion in Section IV-D
6. Assure that data obtained for material strength (resistence to shear and compressions) are reasonably accurate even though there is no single standard accepted method for determining this property for these materials and applications.	Use several different test methods and check to see that results between them are comparible. Methods employed were triaxial torsion shear tests, Brazil tensile strength tests, and pneumatic loaded arm oedometers. Duplicate and triplicate samples were also run.	Table V-I and V-2 present results from the spring oedometers and the triaxial torsion tests. Table V-3 presents results of the Brazil strength tests. Table V-4 presents results from the pneumatic arm oedometers. Duplicate analyses are included on these Tables. The duplicate analyses and the cross check between test methods show minor variation in test results but close overall agreement on material properties.
7. Assure that the results are internally consistent and reproducible.	Use of a statistically designed experimental plan to produce intermediate date points to verify that the patterns and trends observed are consistent.	Table II-I presents the overall experimental design including intermediate values for % of burned shale mixed with unburned shale, curing (ageing) times, moisture content, and amount of mellowed shale used in the blend. The extensive use of graphs to illustrate experimental results demonstrates that results are consistent and reproducible.

IX REFERENCES

Culbertson, W.J., Jr., C. Habenicht, R. Nye, F. Bonomo, E. Barrow and C. Ruff. Fifth Progress Report: Development of Liner Materials from Spent Oil Shale. Some Spent Oil Shale Properties and Development of a "Torsion Triaxial" Testing Procedure. Under Cooperative Agreement CR 809233 by Denver Research Institute, Chemical and Materials Science Divisio-, Univ. of Denver, Nov. 22, 1983, unpublished.

Ingles, O.G., "Soil Chemistry Relevant to the Engineering Behavior of Soils" in I.K. Lee, Editor, Soil Mechanics Selected Topics, American Elsevier Publishing Co., Inc., New York 1968.

Krishnayya, A.V.G., Eisenstein, Z., and Morgenstern, N.R. "Behavior of Compacted Soil in Tension." Journal of the Geotechnical Division, Am. Soc. of Civil. Engrs. 100, No. GT 9, pp 1051 -1061. Spet. 1974. Discussions: Fang, H-Y and W. Deutsch, Same Journal GT5, pp. 569-573, May 1976, Moore, R.K., Same Journal. GT9, p. 985, Sept. 1975. Closure: Same Journal GT9, p. 1020-22, Sept. 1976

Ladd, C.C. and R. Foott, "New Design Procedure for Stability of Soft Clays", Geotechnical Engineering Division Journal, Am. Soc. of Civil Engrs. No. GT7, pp. 763-86, (1974).

Narain, J. and Rawat, P., "Tensile Strength of Compacted Soils," Soil Mechanics and Foundations Division Journal, Am. Soc. of Civil Engrs. 96, No. SM6, Nov. 1975

Townsend, F.C. and R.W. Peterson, Geotechnical Properties of Oil Shale Retorted by the Paraho and TOSCO Processes, Tech. Rept. GL-79-22, Geotechnical Laboratory, U.S. Army Engineer Waterways Experiment Station. Vicksburg Miss. For U.S. Dept. of Interior, Bur. of Mines, Spokane Mining Research Center, Spokane Wash. Under Contract No. H0262064.